OAK RIDGE NATIONAL LABORATORY
OPERATED BY UNION CARBIDE CORPORATION · FOR THE DEPARTMENT OF ENERGY

ORNL/RSIC-41

A Review of
MULTIGROUP NUCLEAR CROSS-SECTION PROCESSING PROCEEDINGS
OF A
SEMINAR-WORKSHOP, OAK RIDGE, TENNESSEE
March 14–16, 1978

Note:
This Work Partially Supported by
U.S. DEFENSE NUCLEAR AGENCY
and
U.S. NUCLEAR REGULATORY COMMISSION

RADIATION SHIELDING INFORMATION CENTER

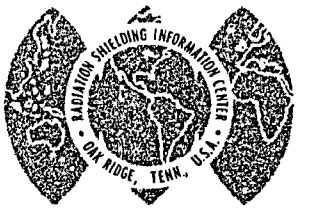

ORNL/RSIC-41

Contract No. W-7405-eng 26

Engineering Physics Division

A REVIEW OF MULTIGROUP NUCLEAR CROSS-SECTION PROCESSING, PROCEEDINGS OF A SEMINAR-WORKSHOP, OAK RIDGE, TENNESSEE March 14–16, 1978

Compiled by:
D. K. Trubey and H. R. Hendrickson

Note:

This work partially supported by
U.S. DEFENSE NUCLEAR AGENCY
and
U.S. NUCLEAR REGULATORY COMMISSION

Date Published: October 1978

OAK RIDGE NATIONAL LABORATORY
Oak Ridge, Tennessee 37830
operated by
UNION CARBIDE CORPORATION
for the
DEPARTMENT OF ENERGY

TABLE OF CONTENTS

PAGE

Abstract v

Foreword vii

Acknowledgments ix

1. "Characteristics of ENDF/B-V," S. Pearlstein, R. Kinsey, and C. Dunford, National Nuclear Data Center (Brookhaven National Laboratory)..... 1

2. "AMPX: A Modular System for Multigroup Cross-Section Generation and Manipulation," N.M. Greene, W.E. Ford, III, L.M. Petrie, B.R. Diggs, C.C. Webster, J.L. Lucius, J.E. White, R.Q. Wright, and R.M. Westfall (Oak Ridge National Laboratory)..... 9

3. "NJOY: A Comprehensive ENDF/B Processing System," R.E. MacFarlane, R. J. Barrett, D. W. Muir, and R. M. Boicourt (Los Alamos Scientific Laboratory)..... 23

4. "ETOE-2/MC^2-2/SDX Multigroup Neutron Cross-Section Processing," B. J. Toppel, H. Henryson II, and C.G. Stenberg (Argonne National Laboratory)..... 39

5. "Production of Multigroup Data at Livermore," P.C. Giles (Lawrence Livermore Laboratory)..... 55

6. "New Resonance Cross Section Calculational Algorithms," D. Mathews (General Atomic Co.)..... 59

7. "The Shielding Factor Method for Producing Effective Cross Sections: MINX/SPHINX and the CCCC Interface System," R.E. MacFarlane (Los Alamos Scientific Laboratory), C.R. Weisbin (Oak Ridge National Laboratory), and N.C. Paik (Westinghouse Advanced Reactor Division)..... 83

8. "Implementation of the Rapid Cross Section Adjustment Approach at General Electric," C.L. Cowan, E. Kujawski, and R. Protsik (General Electric Co., Fast Breeder Reactor Department)..... 97

BLANK PAGE

9. "Experience in Developing and Using the VITAMIN-C 171-Neutron, 36-Gamma-Ray Multigroup Coupled Cross-Section Library," R.W. Roussin, C.R. Weisbin, J.E. White, R.Q. Wright, N.M. Greene, W.E. Ford,III, J.B. Wright, and B.R. Diggs (Oak Ridge National Laboratory). 107

10. "Design Criteria for the 218-Group Criticality Safety Reference Library," R.M. Westfall, W.E. Ford, III, and C.C. Webster (Union Carbide Corp. Nuclear Division, Computer Sciences Division). 121

11. "The MACK/MACKLIB System for Nuclear Response Functions," M.A. Abdou and Y. Gohar (Argonne National Laboratory). 131

12. "Resolved Resonance Processing in the AMPX Modular Code System," R.M. Westfall (Union Carbide Corp. Nuclear Division, Computer Sciences Division). 147

13. "Cross Section Probability Tables in Multigroup Transport Calculations," D.E. Cullen, E.F. Plechaty, and R.J. Doyas (Lawrence Livermore Laboratory), and C.R. Weisbin and J.E. White (Oak Ridge National Laboratory). 155

14. "Comparison of VITAMIN-C Master Library Reaction Cross Sections for Iron with Multigroup Cross Sections Generated by the VIM Monte Carlo Code," N. Hertel and B. Wehring (University of Illinois), and R.H. Johnson (Purdue University). 181

15. "Experience with the DLC-37/EPR Cross Section Library for Preliminary Gamma-Ray Heating Analysis of the Purdue University Fast Breeder Blanket Facility," R.H. Johnson and J.H. Paczolt (Purdue University). 191

16. "An Analytic Angular Integration Technique for Generating Multigroup Transfer Matrices," J.A. Bucholz (Oak Ridge National Laboratory). 205

17. "Code Implementation of Partial-Range Angular Scattering Cross Sections: GAMMAR and MORSE," J.T. Ward, Jr. (University of Virginia). 215

18. "Analytical Inequalities Satisfied by the Cross-Section Self-Shielding Factors: Best Upper and Lower Bounds," D.G. Cacuci and M. A. Bjerke (Oak Ridge National Laboratory). 227

ABSTRACT

These proceedings consist of 18 papers given at a seminar-workshop on "Multigroup Nuclear Cross-Section Processing" held at Oak Ridge, Tennessee, March 14–16, 1978. The papers describe various computer code systems and computing algorithms for producing multigroup neutron and gamma-ray cross sections from evaluated data and experience with several reference data libraries.

FOREWORD

The Radiation Shielding Information Center (RSIC) has developed and used the seminar-workshop format on a number of occasions to disseminate in a few days considerable technical information on newly-available computing technology. The seminar portion, with speakers from all the leading laboratories developing or using similar technology, provides a comprehensive review of the state of the art. These proceedings document that review of the technology for generating and processing multigroup nuclear cross sections. The workshop, held over a period of several days, provided in-depth training in the use of several computer code and data packages which have become available.

The March 1978 seminar-workshop attracted nearly 100 persons from approximately 49 institutions (four foreign) to Oak Ridge to review the subject of multigroup nuclear cross-section preparation and processing. Papers presented in the seminar portion have been assembled for these proceedings. Taken together, they document the current state of the art. The workshop, led by Oak Ridge National Laboratory (ORNL) and Union Carbide Corporation Nuclear Division, Computer Sciences Division (UCND-CSD) personnel, concentrated for two days on the AMPX-II modular code system and related data interface formats, processing schemes, and data libraries. The packages studied included: PSR-63/AMPX-II, PSR-117/MARS (codes to manipulate data libraries in AMPX or CCCC formats), DLC-41/VITAMIN-C (171n–36γ, i.e., coupled 171-group neutron, 36-group gamma-ray), DLC-42/CLEAR (126n–36γ), and DLC-43/CSRL (218n).

The data libraries DLC-41, -42, and -43 represent a significant change from the more usual transport-code input-format type of library heretofore available from RSIC. Such data libraries, providing data for ANISN, DTF-IV, DOT, TWOTRAN, MORSE, and other codes, have been available from RSIC since the first version of DLC-2/100G was generated from ENDF/B-I by SUPERTOG in 1969. The newer libraries are characterized by greater energy detail (more groups) with energy boundaries placed to represent important cross-section structure and, of equal importance, by information which can be used to apply self-shielding and Doppler broadening as functions of temperature and nuclide composition. DLC-41 and -42 utilize the Bondarenko method, and DLC-43 the Nordheim integral treatment. These are relatively easily applied for self-shielding using AMPX modules BONAMI and NITAWL, respectively.

The great increase in sophistication to make the data libraries less problem-dependent has resulted in a great increase in data bulk (the DLC-41 and -42 libraries require 4 9-track tapes), an increase in complexity of retrieval/processing codes (a new PSR-117/MARS code library was packaged), and an increased requirement for user skills (hence the seminar-workshop). Not all users of multigroup data will find it practicable to implement a full AMPX capability, and therefore, various modules can be selected for particular limited purposes. Also, the simpler, more problem-dependent libraries in ANISN format will continue to be available. These are likely to be based on the more detailed libraries. An example is DLC-47/BUGLE (45n–16γ) developed for the LWR shielding community in cooperation with the American Nuclear Society working group on cross sections, ANS-6.1. Further information, of course, on all these code and data libraries is available from RSIC upon request.

BLANK PAGE

The previous RSIC seminar-workshop on multigroup cross sections was held in 1969. In examining the proceedings of that meeting[1], one is impressed with the progress since that time. In 1969 ENDF/B had become available, and newly developed processing codes such as ETOM, ETOE, ETOX, MC^2, ETOG, or SUPERTOG could produce multigroup cross sections, but there were no gamma-ray production or interaction cross sections in ENDF. The state of the art in producing gamma-ray production cross sections was represented by POPOP4 and for producing gamma-ray interaction cross sections by GAMLEG or MUG. Coupling was still by *ad hoc* procedures. Codes such as GGC-5, XSDRN, and MC^2 could produce self-shielded cross sections, but these data were not usually used in shielding calculations. The paper on ETOX-1DX referred to a Bondarenko treatment, but again the results were given in terms of reactor analysis parameters such as k_{eff}.

In conclusion, the seminar-workshop showed a great advance in the state of the art of multigroup cross-section processing and preparation since 1969.

D. K. Trubey
Radiation Shielding Information Center
Oak Ridge National Laboratory

March 29, 1978

---

1. D. K. Trubey and Jane Gurney, "A Review of Multigroup nuclear Cross-Section Preparation—Theory, Techniques, and Computer Codes," ORNL-RSIC-27 (Jan. 1970).

ACKNOWLEDGMENTS

In addition to the authors whose papers appear here, we are grateful to W. E. (Eddy) Ford, III, N. M. (Maurice) Greene, R. Q. (Dick) Wright, J. E. (John) White, R. M. (Mike) Westfall, J. L. (Jim) Lucius, and L. M. (Les) Petrie of the UCND-CSD staff at ORNL and D. B. (Dave) Simpson who willingly expended much time and effort in preparing for and conducting the workshops. C. R. (Chuck) Weisbin and D. K. (Dave) Trubey were chairmen of the seminar sessions. The effective guidance, leadership, and hard work of R. W. (Bob) Roussin of the RSIC staff was evident throughout the entire three days. Bob had overall responsibility for organizing the seminar-workshop.

We are also grateful for the effective and conscientious efforts of the entire RSIC staff, especially Eddie Bryant who had responsibility for publications and registration.

BLANK PAGE

CHARACTERISTICS OF ENDF/B-V

S. Pearlstein, R. Kinsey, and C. Dunford
National Nuclear Data Center
Brookhaven National Laboratory
Upton, NY 11973

ABSTRACT

A primary source of microscopic nuclear data for processing into multi-group cross sections is the Evaluated Nuclear Data File (ENDF/B). This data file is maintained and distributed by the National Nuclear Data Center (NNDC) of Brookhaven National Laboratory. The File is based on nuclear data evaluations provided by members of the Cross Section Evaluation Working Group (CSEWG). A new version of the ENDF/B (ENDF/B-V) is in preparation for release in the first half of 1978.

In order to improve the accuracy and reliability of ENDF/B-V, extensive improvements were made in the checking programs and the review kits. New evaluations are processed through three levels of checking codes that detect errors in formats, consistency, and physical information, in that order. Kits consisting of the results of checking codes, documentation and plots are presented to designated reviewers for comments. Upon receiving CSEWG approval, evaluations are included in ENDF/B. The major materials in the General Purpose File are being revised for ENDF/B-V where new measurements indicate improvements are required. The number of materials containing photon production data have been increased. A revision of the Photon Interaction File is planned for the end of 1978.

An extensive set of integral experiments have been adopted as CSEWG Benchmarks to test ENDF/B data. Benchmark experiments have been selected to test data for thermal and fast reactor, shielding and dosimetry applications and additional benchmark candidates are reviewed on a regular basis. CSEWG performs interlaboratory comparisons of the benchmark results.

A primary source of microscopic nuclear data for processing into multi-group cross sections is the Evaluated Nuclear Data File (ENDF/B).[1-3] This data file is maintained and distributed by the National Nuclear Data Center (NNDC) of Brookhaven National Laboratory. The file is based on nuclear data evaluations provided by members of the Cross Section Evaluation Working Group (CSEWG).

The characteristics of ENDF/B are described in Figure 1. Useful features of ENDF/B are its completeness, gaps in critically evaluated experimental data are filled in by theory; and its integration into current methodology, interfacing of the data base to major application codes has been provided. Revised versions of ENDF/B have appeared in 1967, 1970, 1972, and 1974 with a new version planned for early 1978.

The CSEWG laboratories contributing to the development of ENDF/B are shown in Figure 2. The chairman of CSEWG is Sol Pearlstein of BNL. The committee has several technical subcommittees whose responsibilities lie in the areas of data content, data testing, formats and procedures and special applications. Figure 3 lists the present committees and their chairmen. The Data Testing Subcommittee organizes the review of each ENDF evaluation first by arranging for a review of each evaluation by an independent measurer, evaluator or user. Secondly, they organize the testing of evaluated data using well documented integral benchmark experiments. All evaluations must be approved by Data Testing before release. The Codes and Formats Subcommittee is responsible for approving all changes to the ENDF formats and recommended procedures. In addition, it coordinates the computer code development activities for programs which process ENDF data files. The Normalization and Standards Subcommittee is responsible for the consistent evaluation of the neutron reaction standards and for thermal cross sections.

The CSEWG-ENDF system was initiated approximately twelve years ago with the support of the USAEC's Division of Reactor Development. Originally proposed some two years earlier, it was conceived to be a common data base to be used in the nuclear design of neutron reactors. The development of such a data base had obvious advantages when comparing the nuclear performance of competing reactor designs. Brookhaven National Laboratory was asked to organize the development of this nuclear data base, hence the formation of CSEWG. All AEC contractors interested in nuclear data were invited to participate.

In the beginning, two data files, ENDF/A and ENDF/B were conceived. ENDF/B was the designation of the data file containing the recommended complete material evaluations whereas, ENDF/A was to contain other evaluations and various small partial evaluations. The initial contents of ENDF/B were heavily oriented toward thermal and fast reactor core physics design and covered the energy range from 10^{-5} eV to 10 MeV. ENDF/B-I consisted primarily of existing evaluations converted to the ENDF format. ENDF/B-II represented an attempt to remove the deficiencies found when comparing ENDF/B-I with both differential neutron data and integral experiments. The development of data checking codes and data processing codes such as CHECKER and MC2 were carried on to promote quality and general availability to the user community.

CHARACTERISTICS OF ENDF/B

- COMPLETE INFORMATION BASE
- DOCUMENTED
- DEVELOPED COOPERATIVELY
- INTEGRATED INTO METHODOLOGY
- APPLICATION INDEPENDENT
- REVISED PERIODICALLY

Fig. 1.

CROSS SECTION EVALUATION WORKING GROUP

FEDERAL

- ARGONNE
- ATOMIC ENERGY OF CANADA LTD.
- BATTELLE NORTHWEST
- BETTIS ATOMIC POWER
- BROOKHAVEN
- HANFORD ENGINEERING
- IDAHO
- KNOLLS ATOMIC POWER
- LIVERMORE
- LOS ALAMOS
- NATIONAL BUREAU OF STANDARDS
- OAK RIDGE
- SAVANNAH RIVER

INDUSTRIAL

- BABCOCK AND WILCOX
- COMBUSTION ENGINEERING
- ELECTRIC POWER RESEARCH INSTITUTE
- GENERAL ATOMIC
- GENERAL ELECTRIC
- MATHEMATICS APPLICATIONS GROUP INC.
- NUCLEAR ASSOCIATES INTERNATIONAL
- SCIENCE APPLICATIONS INC.
- WESTINGHOUSE

UNIVERSITY

- COLUMBIA
- MICHIGAN
- RENSSELAER POLYTECHNIC
- STANFORD
- WISCONSIN

Fig. 2.

CSEWG COMMITTEE ORGANIZATION

COMMITTEE	CHAIRMAN	LAB
CSEWG	SOL PEARLSTEIN	BNL
DATA TESTING	CHUCK WEISBIN	ORNL
CODES AND FORMATS	RAPHE LABAUVE	LASL
NORMALIZATION & STDS.	BO LEONARD	BNWL
SHIELDING	BOB ROUSSIN	ORNL
RESONANCE REGION	CECE LUBITZ	KAPL
FISSION PRODUCTS & DECAY DATA	BOB SCHENTER	HEDL
NUCLEAR MODEL CODES	GUS PRINCE	BNL
DATA COVARIANCE	FRANCIS PEREY	ORNL
SPECIAL APPLICATION FILES	BEN MAGURNO	BNL

Fig. 3

ENDF PROCESSING CODES

- RIGEL
- CHECKR
- FIZCON
- STNDRD
- INTER
- CRECT
- SUMRIZ
- INTEND
- RESEND

Fig. 4

Production of ENDF/B-III represented an attempt to improve the higher energy data especially for shielding calculations. The energy range was extended to 15 MeV and photon production data added to the ENDF system. Uniform coverage of the energy range 10^{-5} eV to 20 MeV was a goal of ENDF/B-IV. The desire to calculate long term burn up effects and decay heat properties of reactor systems led to the introduction of formats to handle nuclear decay and radioactivity data. Decay data for over 800 nuclides was added to ENDF for Version IV. Care was taken to attempt to resolve continuing neutron data inconsistencies by taking special care of the neutron standard reactions and insuring that evaluations of the heavy element fission and capture cross sections were in agreement with experimentally measured ratios. Finally, a special data file of single reaction evaluations for important in-core dosimetry applications was made.

ENDF/B consists of a General Purpose File and several Special Applications Files. Evaluations in the General Purpose File contain most all nuclear data needed for a variety of applications. Evaluations in Special Application Files will generally contain only nuclear data of special interest. Special Application Files exist for photon-interaction, fission product cross sections and radioactive decay, and neutron cross-section standards data. New Special Application Files are being developed for actinide, gas production, and activation data.

Based on the experiences with the creation of ENDF/B-IV, the checking codes for ENDF/B-V have been greatly improved and extended. Briefly the checking codes and their functions are:

1) CHECKR - this code checks the compliance of the ENDF file with the format requirements of the file. With the hollerith read option, this program is impervious even to incorrect variable types in the input fields. In addition, other simple consistency checks are also made.

2) FIZCON - this code checks the physical consistency of the data represented in the file. For example, one option is to check that partial cross section sum correctly to their total. Also, that angular distributions do not go negative and that probability distributions are normalized to unity.

3) PSYCHE - this code provides further physics checking of the data files. It calculates resonance integrals and checks the energy balance of the various reactions specified in the file. This code uses physics information not contained in the file to check the reasonableness of the data given.

A list of codes[4] available from the NNDC to users for the checking or manipulation of data in the ENDF format is shown in Figure 4. The list includes those codes mentioned above as well as RIGEL, STNDRD, and SUMRIZ, to perform accounting or merge and rewrite ENDF data into alternate forms; CRECT, to alter ENDF data; and INTEND, INTER and RESEND, to convert data to a standard form and integrate over specified energy ranges.

The review of an ENDF/B material proceeds in two steps as illustrated in Figure 5. In the first step called Phase I, the data evaluations are given an independent review by other evaluators. In the second step called Phase II, the library is tested against integral benchmarks.

Once an evaluation has been processed by the checking codes, one of two things can happen. If any errors uncovered are only of a clerical nature and the nature of the corrections is clear, the file is corrected and a Phase I review kit is prepared. Otherwise, the results of the checking codes are returned to the evaluator and he is asked to make the necessary corrections and resubmit the evaluation.

The Phase I review kits, when they have been assembled, are sent to the designated CSEWG reviewer. The Phase I review kit consists of the Evaluators Summary Sheet, a listing of the file, the output of the checking codes, a summary of the contents of the file, an expanded listing of the data file, and plots of the data in the file. The Evaluators Summary Sheet gives the evaluator an opportunity to tell the reviewer upon what this evaluation is based and what data was considered in producing the evaluation. If the evaluation is an upgrade of a previous evaluation, then changes and improvements are also noted.

The reviewer then reports to the Data Testing Subcommittee of CSEWG, via the Phase I Review Sheet, the results of his review. He attempts to answer questions concerning the completeness and correctness of the evaluation. More than one reviewer may be asked to review a material especially if it is used in a variety of applications.

In conclusion, we would like to mention that changes and improvements can be expected in future versions of ENDF/B. These changes can be separated into two categories, namely those needed to correct problems existing in ENDF/B-V and those needed to meet expected new demands for data.

In the area of new demands, we would expect to find an increasing need for evaluated data between 10 and 40 MeV as evidenced during a recent symposium[5] sponsored by the National Nuclear Data Center. The need relates primarily to the intense neutron sources being planned for the study of radiation damage in fusion devices. The solution of this problem will come from improved measurement techniques and nuclear theory code improvements.

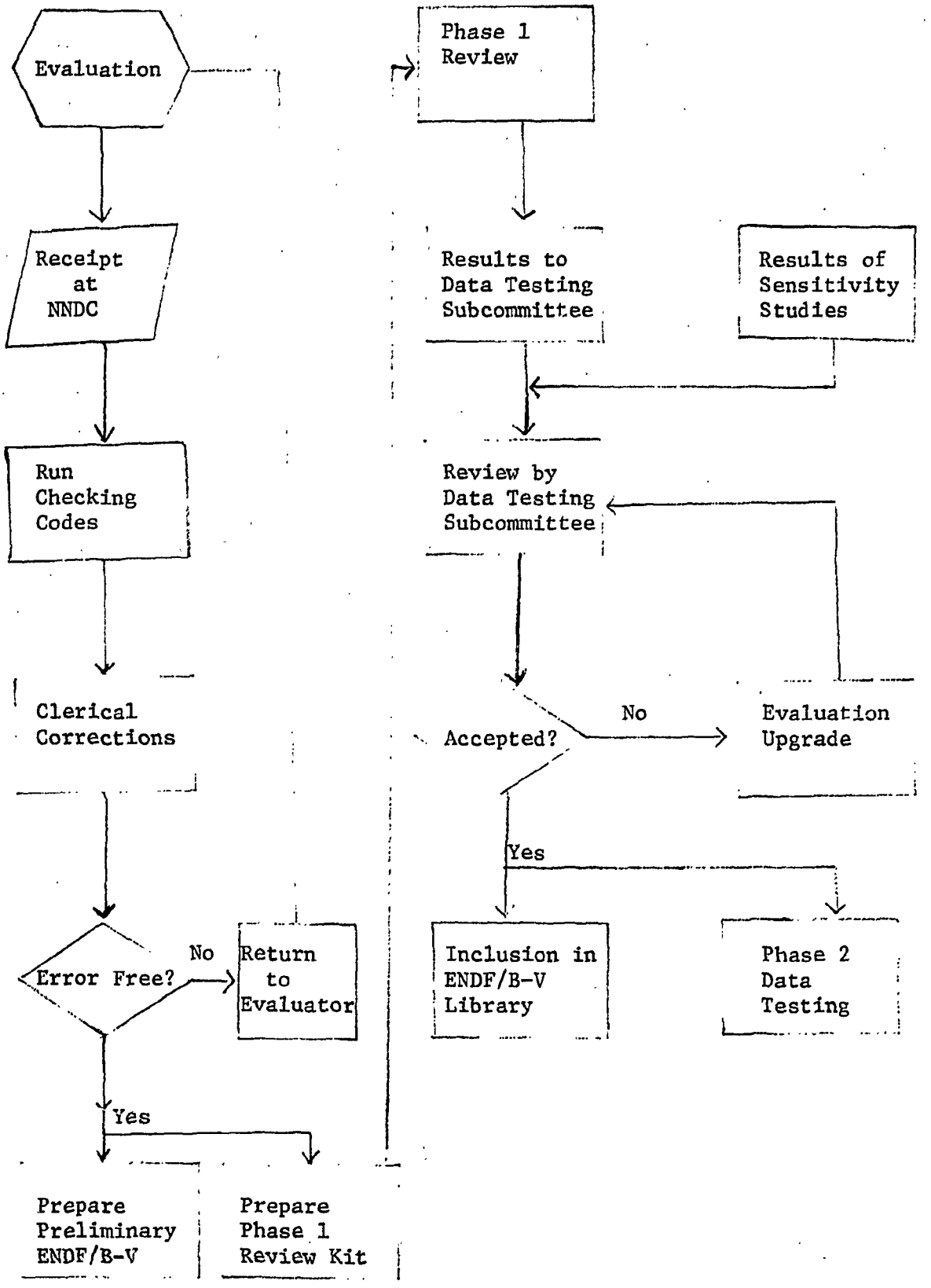
Evaluation
Receipt at NNDC
Run Checking Codes
Clerical Corrections
Error Free?
No
Return to Evaluator
Yes
Prepare Preliminary ENDF/B-V
Prepare Phase 1 Review Kit
Phase 1 Review
Results to Data Testing Subcommittee
Results of Sensitivity Studies
Review by Data Testing Subcommittee
Accepted?
No
Evaluation Upgrade
Yes
Inclusion in ENDF/B-V Library
Phase 2 Data Testing

Fig. 5

We also see an increased need for nuclear recoil data from nuclear reactions to aid in damage model analysis. There will also be additional needs for covariance information for secondary energy-angle distributions.

In the area of charged particle reaction data, we expect increased use of evaluated charged particle data via inverse reactions, neutron source reaction and isotope production reactions. Such data cannot be generally included in the present ENDF structure which was originally designed with only incident neutrons considered. Therefore, we will be looking at a possible restructuring of the ENDF format to provide a better ability for the system to respond to the varied demands discussed above and others not yet anticipated.

REFERENCES

1. Data Formats and Procedures for the Evaluated Nuclear Data File, ENDF. BNL-NCS-50496 (ENDF 102) revised by D. Garber, C. Dunford, and S. Pearlstein. October 1975.

2. D. I. Garber, ENDF/B Summary Documentation. BNL-17541 (ENDF-201), 2nd Edition, October 1975.

3. CSEWG, Benchmark Specifications. BNL-19302 (ENDF-202),

4. Description of the ENDF Processing Codes and Retrieval Subroutines.

5. Symposium on Neutron Cross-Sections from 10 to 40 MeV. BNL-NCS 50681, Edited by M. Bhat and S. Pearlstein, July 1977.

AMPX: A MODULAR SYSTEM FOR MULTIGROUP CROSS-SECTION GENERATION AND MANIPULATION

N. M. Greene, W. E. Ford, III, L. M. Petrie, B. R. Diggs, C. C. Webster, J. L. Lucius, J. E. White, R. Q. Wright, and R. M. Westfall
Computer Sciences Division
Union Carbide Corporation, Nuclear Division
Oak Ridge National Laboratory
Oak Ridge, Tennessee, U.S.A.

ABSTRACT

The AMPX system, developed at the Oak Ridge National Laboratory over the past seven years, is a collection of computer programs in a modular arrangement. Starting with ENDF-formatted nuclear data files, the system includes a full range of features needed to produce and use multigroup neutron, gamma-ray production, and gamma-ray interaction cross-section data. The balance between production and analysis is roughly even; thus, the system serves a wide variety of needs. The modularity is particularly attractive, since it allows the user to choose an arbitrary execution sequence from the approximately 40-50 modules available in the system. The modularity also allows selection from different treatments; e.g., the Nordheim method, a full blown integral transport calculation, the Bondarenko method, or other alternatives can be selected for resonance shielding.

INTRODUCTION

In early 1971, an effort was initiated to build a system of computer programs capable of producing multigroup cross sections. This work was funded by the Defense Nuclear Agency which had a particular interest in producing "coupled neutron-gamma cross sections" for use in weapons shielding and effects studies. The system was named AMPX which is an acronym for Automation of MUG[1], POPOP4[2] and XSDRN[3], three codes which were then in use at the Oak Ridge National Laboratory (ORNL) to generate multigroup gamma-ray interaction, gamma-ray production, and neutron cross sections, respectively.

The production of multigroup cross sections has always been (and still is) a particularly distasteful process involving the execution of many programs in transforming point data into multigroup form. To further complicate matters, this field is wrapped in its own mysterious jargon, e.g., ENDF/B, self-shielding, $S_{\alpha,\beta}$, P_{ℓ} matrices, transport corrections, etc. The selection of the most appropriate treatment from the vast collection of algorithms available for producing multigroup cross sections is a challenge even for the experienced analyst.

The standard procedures for making cross sections involve the execution of several codes in sequence. Many of these executions are large, long running computer jobs. Consider Figure 1 which aptly describes the 1971 ORNL procedure for producing coupled neutron-gamma cross sections.

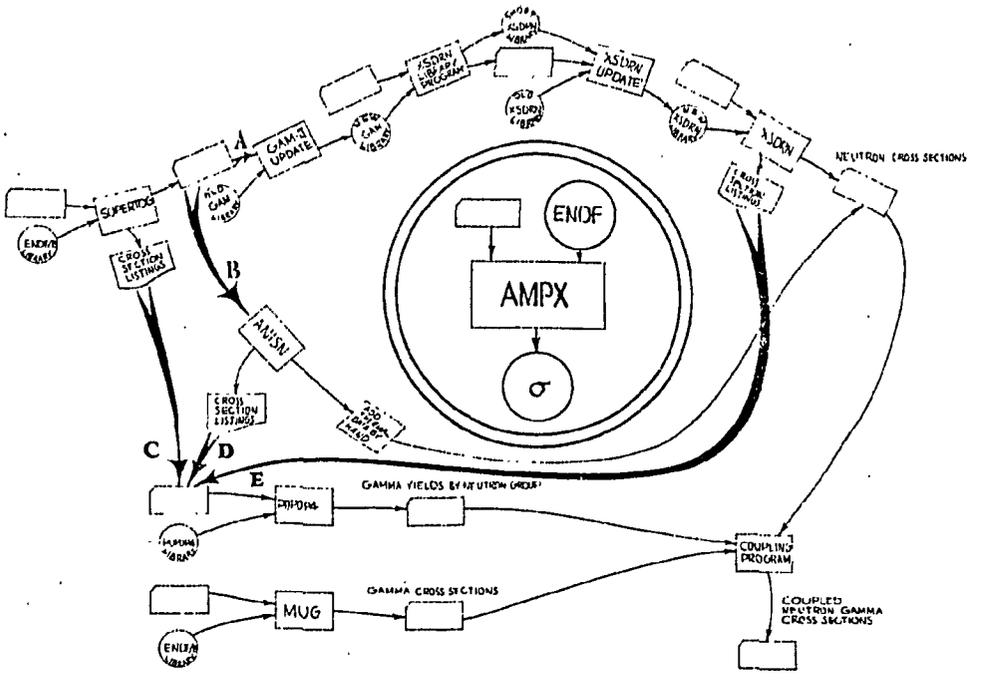

Figure 1.

The procedure was as follows:

Using ENDF/B data for neutrons, the SUPERTOG code was run to produce multigroup data in a reasonably fine group structure (approximately 100 groups). Depending on the option selected, SUPERTOG output was available in two formats: 1) a GAM-II[4] "update" stream and 2) ANISN[5] format. Option 1 was commonly used because it allowed for the eventual self-shielding of resonance nuclides. In cases involving non-resonance nuclides, the second option was used. For option 1, the GAM-II Update Code was run to produce a library in GAM-II format. After this run, a code which merged the GAM-II data with THERMOS[6] thermal data was executed. This produced a short XSDRN library which was coupled with existing neutron data through yet another updating run. At this point, an XSDRN run self-shielded resonance nuclides using the Nordheim Integral Treatment[7] and performed a discrete ordinates spectral calculation for collapsing to a few-group structure. Output was on cards for the ANISN code. For the ANISN option, one made an ANISN collapsing run analagous to the XSDRN run after first adding thermal values by hand into the ANISN cross sections.

Another part of this procedure required the execution of the POPOP4 program to calculate the coefficients used to determine gamma sources from neutron interactions. This code had its own "gamma yield" library

and required multigroup cross sections for specific reactions from the neutron averaging runs. Thus, its start depended on all the aforementioned codes having been run.

- A completely independent path used the MUG code to generate gamma-ray interaction cross sections.

- After all other steps were completed, a "COUPLING CODE" was run to combine the cross sections for all three sequences into a coupled neutron-gamma set. At this point the user was able to perform the calculation he wanted to make in the first place, e.g., a Monte Carlo or an S_n calculation, etc.

This was a very time consuming procedure. Many of the codes required input from previous codes which had to be laboriously transferred from computer printout to a card input form. An error in some of the initial codes could invalidate almost all runs in the procedure, requiring practically all of the codes to be rerun. These schemes literally took weeks to produce a few sets of cross sections.

AMPX DEVELOPMENT

A more palatable way of attacking a problem involving the execution of multiple codes in a loosely defined sequence is to build a modular system which encompasses the complete collection of codes.

Modular System

A modular system is a collection of codes which can be run in either a preassigned and/or an arbitrary sequence and which communicate to each other through external interfaces. This external communication is the key to a true modular system and is accomplished through the use of tapes, drums, disks, etc. (Many large programs lay claim to the word "modular" in a description of the programming techniques employed, but a close scrutiny reveals them to be "FORTRAN programs" which communicate through COMMON's and argument lists, just like any other program!)

In a true modular system, the module many times is a program which has a clearly defined function, e.g., to calculate multigroup neutron cross sections or to calculate neutron fluxes. Since communication to other modules is through external interfaces, it is convenient to substitute modules in execution sequences, e.g., to substitute a diffusion theory code for a transport theory code.

The modular approach is fairly widely supported with notable examples being: the ARC[8] system at Argonne National Laboratory, the NOVA[9] system at Knolls Atomic Power Laboratory, the JOSHUA[10] system at Savannah River

Laboratory, and the CCCC[11] effort developed for use in several computer code development areas supported by the Department of Energy (DOE).

The means for accomplishing the linking together and communication between programs varies from a simple to a very complicated level: 1) the simplest approach provides no module for driving computer codes at all. Standard communication interfaces are rigidly defined, and a user still has to make independent submissions for each code he runs or he ties codes together using job control procedures. This type of system is represented by the CCCC modules. 2) The next level of sophistication is to define the rigid interfaces with a "driver" module which allows the user to run several modules back-to-back during a single execution. The AMPX system is characteristic of this type. A FORTRAN driver serves for the CDC versions of the system while a very flexible assembler language driver serves on IBM systems. 3) A variation of the second approach produces yet another increase in convenience. This is the case wherein the user supplies input for a complete module execution sequence to a control program which both creates all input files for the various modules and selects those modules in the proper order. In this scheme individual modules generally don't read card input streams, except for the control program. This type of system is characterized by the ARC, SCALE[12] (an extension of AMPX), and VENTURE[13] systems. (VENTURE is a major "module" in the CCCC array of codes.) 4) Another level is reached when the "driver" module dynamically decides which modules are to be run based on results obtained during an execution sequence. The JOSHUA and the NOVA systems use a central data base management system (DBMS) for communication links between modules.

AMPX Design Considerations

The major design features for AMPX are shown in Figure 2. Because of the obvious advantages for an area that requires a very loose and variable sequence of codes to be run, the modular system approach was chosen for AMPX. Many cross-section applications do not require both neutron and gamma-ray data. The modular approach is a convenient vehicle for supporting both areas (and others) in a manner which allows any improvement or modification to be universally available.

Basic Data Source

Evaluated Nuclear Data Files[14] (ENDF) are the standard means for distributing current basic neutron and gamma-ray cross sections in the United States. Basic processing modules in AMPX were to exclusively rely on ENDF-formatted libraries as their data source.

Variable Dimensioning

A technique widely used in reactor physics codes, e.g., ANISN and XSDRN, is to maximize the use of data array space by having all arrays a code uses stacked into one large container array. The size of this

ORNL-DWG 72-7329

Figure 2

array is that amount left over from the core region assigned a program after one accounts for the program space (load module size) and possible buffer regions required for input/output. The program itself keeps an internal set of pointers which locate the various arrays in the large array. These pointers are set to the actual size needed by the problem being run. This kind of flexibility is highly desirable for a cross-section processing system as there are many arrays whose lengths vary significantly from case to case as a function of the number of neutron groups, number of gamma-ray groups, order of P_n, weighting spectrum, etc. Each increase in computing capacity (time-and space-wise) has always been matched by a corresponding increase in the degree of complexity which goes into a "typical job." The variable dimensioning approach minimizes and ideally eliminates the amount of reprogramming needed to accommodate these demands. In IBM versions of AMPX (and some CDC versions), special routines are available which will look at the core areas available and automatically assign the maximum available amount of data storage to the container array for a module. This is a particularly attractive feature as it allows varying the amount of data storage by merely varying the region of core assigned to a job without having to recompile a small control program.

Multipath Flexibility

The principal advantage of having a system where one can select an arbitrary set of modules and tie them together is that it reduces duplication. A module can be inserted at any point in an execution sequence that the module's function is required. A modular system permits simpler modules since modules have fewer options. It is a positive approach because the user never has to "turn off" options he doesn't want. He selects only those pieces needed. Examples of features which can easily serve at several points in a sequence are: conversion of cross-section library formats, data editing, data checking, data collapsing, etc.

General Library Formats and Communication Interfaces

In systems tailored for producing and using multigroup data, communication between codes is primarily made with cross-section data in multigroup or basic (point, resonance parameter, etc.) forms. An examination of the 1971 ORNL procedure shown in Figure 1 supports this. In each case it was a block of neutron data, gamma-ray interaction data, or gamma-ray production data which formed a communication link. A more careful examination reveals that the different blocks had several different formats (in fact, some of the codes served for little more than format converters).

Since formats are restrictive and the addition of new schemes might require modifications in many places in different ways, the use of different formats for different types of cross-section data is a very undesirable situation. Many of the cross-section blocks are not self-describing and require many descriptors to augment them (for example,

ANISN blocks require a user to specify number of energy groups, total cross section location, etc.). To circumvent many of these difficulties, one of the first steps in AMPX development was to design a reasonably general and flexible format for passing multigroup data. It would have many features, including the following:

1. including the neutron and/or gamma-ray energy group structures in the library,
2. the ability to serve for neutron, gamma-ray interaction, gamma-ray production or coupled neutron-gamma data libraries where the different types of data are well identified,
3. a capability for accommodating any number of separate processes represented in angle to a completely arbitrary and variable order (elastic neutron data might be represented to order 8, while discrete inelastic levels were all given to order 3, other neutron processes to order 0, gamma-ray data to order 10, etc.),
4. the ability to carry all data needed in typical multigroup operations, including resonance parameters for self-shielding via the Nordheim treatment and/or Bondarenko[15] factor data for self-shielding,
5. options to specify a temperature dependence on cross sections,
6. provisions for truncating the "zeroes" in cross-section scattering matrices so as to both keep from wasting space and to allow codes which use the data to consider only the "real" data (for example, the calculation of an inscattering source term would only consider those transfers which are nonzero).

This general format, called an AMPX Master Interface, covers most of the interfacing requirements for AMPX. In retrospect, the generality in the format has never been regreted and the modifications considered desirable would be to expand it to allow more generality.

Another standard interface for AMPX is the Working Interface, which is a library with individual processes summed together into "total matrices" and which is ready for use in a nuclear calculation. This also implies that a resonance calculation has been made for resonance nuclides.

Free Form Input Data

In a system of several codes, many applications can require a considerable amount of card input data for the different modules. To reduce the tedium of preparing this input, AMPX modules use an input system called FIDO which has evolved over the years from input routines developed for the predecessors of ANISN. These routines presently allow a formidable array of convenience options, in addition to free form provisions, making the preparation of input less of a chore. As examples, provisions are allowed to repeat entries, to interpolate between entries, to initialize arrays, etc.

Comprehensive Processing

AMPX attempts to span the full range of cross-section processing needed at ORNL. This requires a large number of capabilities, many of which are listed in the next section of this paper.

AMPX CAPABILITIES

The capabilities of AMPX modules can be loosely categorized into the following areas:

1) Basic data processing

2) Resonance self shielding

3) Spectral collapsing

4) Format conversion

5) Service functions

6) Miscellaneous

Basic Data Processing

AMPX has several modules which start with ENDF/B data and use it to obtain multigroup values. XLACS is a module to process neutron data. It is unique among processors of this type in that it produces a set of cross sections containing both fast and epithermal data merged together with thermal data. The thermal data is based on $S_{\alpha,\beta}$ data on special ENDF/B thermal libraries. (This is somewhat contrary to the "modular" philosophy where such distinctly separate areas would be separated into different modules.) LAPHNGAS is a module which processes gamma-ray yield information, i.e., the data which allows one to determine the gamma sources caused from different neutron interactions. SMUG is analogous to XLACS except that it processes gamma-gamma interaction data. Scattering matrices from this code are based on the Klein-Nishina formula. JFC is a newer gamma-gamma processor which treats gamma-ray form factor data given in newer ENDF/B evaluations. This code is capable of generating proper data for photons at x-ray energies. Though not in the system, the MINX[17] code at ORNL produces an AMPX Master Interface allowing its output to be accessed by other AMPX modules.

Resonance Self-Shielding

The NITAWL module contains an upgraded version of the Nordheim Integral Treatment[7] which has been widely used at ORNL, especially in

thermal reactor and in criticality safety calculational studies. Among improvements in the AMPX version are: an ability to self-shield elastic scattering, compliance with the Breit-Wigner equations expected by ENDF/B, the ability to treat "Multi-isotope" ENDF/B evaluations, and inclusion of a capability of self-shielding p-wave resonances. The BONAMI module provides for a Bonarenko iterative self-shielding treatment. Indicative of this module's generality is the ability to perform the BONARENKO calculation over energy ranges that vary nuclide by nuclide and process by process. The ROLAIDS module gives a one dimensional integral transport solution to a system with an arbitrary number of spatial zones, each of which contain an arbitrary mixture. The fluxes from this solution are used to produce self-shielded cross sections which include self-shielded elastic transfer matrices.

Spectral Collapsing

Modules that spectrally collapse use a calculated or a previously prepared multigroup spectrum to flux weight cross sections. This generally involves a reduction in the number of energy groups, though, in the case of cell weighting, this may not be the case. The simplest AMPX module of this type is COMAND, which will accept an ANISN library on cards or binary tape along with a spectrum and will collapse to another ANISN library on cards or on binary tape. (This module is sometimes used just for its ability to convert ANISN data on cards to a tape, or vice versa.) ARID is an obsolete (and retired) AMPX module that accomplished the same thing to a very specific ANISN library, e.g., one with 37 neutron and 21 gamma groups. The MALOCS module is analogous to COMAND, except that the input and output libraries are in AMPX Master Interface form. This module collapses cross sections, Bonarenko factors, etc., in a manner which retains the full capability for subsequent self-shielding calculations. In the case of both MALOCS and COMAND, all sets of data on the original library are treated without the user selecting specific data. A more prevalent kind of weighting, however, comes in the use of the XSDRNPM module. This module accepts an AMPX working library as input along with a description of a spectral calculation to be performed (one dimensional discrete ordinates, one dimensional diffusion theory, or infinite medium theories are available) and uses the results of the calculation to weight cross sections. A user has a variety of options available including zone and cell weighting. The output cross sections are written in AMPX Working Interface form, and can also be requested in ANISN form (on cards or tape) or in CCCC[11] ISOTXS form. XSDRNPM is also used many times just for its one dimensional calculation capability. A particularly attractive feature of the code is its built-in routines for calculating S_n quadrature sets, thereby relieving the user of having to maintain files of these data. Different quadratures are used for spherical, slab, and cylindrical geometries.

Format Conversion

Several major codes and code systems are used at ORNL and elsewhere for neutron and gamma-ray calculations. Unfortunately, these different systems generally require different and sometimes unique formats for cross-section libraries. AMPX provides several modules for converting to and from these formats. As previously mentioned, the XSDRNPM module can convert from AMPX Working Interface format to ANISN or CCCC[11] ISOTXS format. NITAWL can convert from AMPX Master or Working Interface formats to the ANISN format. The CONVERT module converts a library written for the stand-alone XSDRN[3] code to AMPX Master Interface format. REVERT accomplished the same mapping in the other direction. The OCTAGN module converts AMPX working formats to CITATION[16] libraries. LAVA is a module for converting ANISN libraries to AMPX working formats. The CONTAC module takes an AMPX working format and converts it to either a CCCC ISOTXS file or into an ANISN library.

Service Functions

There are a myraid of operations needed to maintain multigroup libraries. Historically these functions were provided in the module needing the operation (e.g., XLACS, NITAWL, XSDRNPM, have fairly complete data editing options); but, as AMPX has evolved, more and more of these functions are relegated to independent service modules. This is very desirable in that it makes modules more compact and easier to maintain. The CHOX and CHOXM modules serve to create an AMPX Master Interface containing coupled neutron-gamma data starting with data separated on a neutron only, a gamma-ray interaction only, and a gamma-ray production only library. CHOX uses all AMPX Master Interfaces as input, while CHOXM uses CCCC interfaces for the neutron only interface. UNITAB is a more general module of this type. It allows constructing an AMPX Master Interface where individual parts of the cross-section data are selected from any AMPX Master Interface. For example, one can create a set consisting of the Bonarenko data from one library, the averaged neutron data by group and process from another library, the elastic neutron matrices from one library, the (n,2n) matrices from another, etc. The final set can be a coupled library or a neutron only library, etc. UNITAB can split a coupled library back into its neutron, gamma-ray production components. DIAL is a module to edit Master or Working Interfaces. PAL will punch data from a Master or Working Interface. The ICE module accepts a Working Interface, creates mixtures and outputs these mixtures onto another Working Interface or onto ANISN libraries. For those embarrassing cases where one finds a library which is improperly normalized (e.g., the total cross sections are not the sums of all partial values, or the averaged inelastic value does not agree with the sum of all P_0 transfers, etc.), the COMET module is provided. This module accepts a Master Interface and can be made to force normalizations; it can modify resonance data; it can create new cross section vectors according to a user specified set of directions. For those cases where the error on a Master Interface is a bad number, the CLAROL module is provided. This module can replace group averaged values or can replace

terms or add to transfer matrices on the library. (This module has a direct coupling to the ROLAIDS module wherein ROLAIDS does a self-shielding calculation and prepares an input stream for CLAROL which then modifies the library.) The module allows a user to easily introduce a change to many processes without having to explicitly make the changes. As an example, the user may change the (n,γ) cross section and have CLAROL automatically include the change in the capture, absorption, and total cross sections. AJAX is a module which allows a very general capability for merging sets of data from different libraries onto a single master library. Or it can be used to select a part of a large library, etc. A reasonably general capability for plotting cross section data is given by the VASELINE module. This code allows a user to plot group averaged data by process taken from a Master or Working Interface. It also provides for plotting point data from ENDF/B libraries or from AMPX Point Interfaces. Point-versus-multigroup plots can be made in a procedure which will allow an arbitrary number of curves to be put on a single graph.

Miscellaneous

This section covers those modules which don't easily fit under one of the headings listed above. Many applications require just the point data for selected processes. The NPTXS module accesses an ENDF/B library and calculates point values of the elastic scattering, fission, capture, and total cross sections for resonance nuclides. These are written on an AMPX Point Interface. Provisions are given for (ψ,χ) Doppler broadening or for a numerical treatment taken from the MINX code. The JERGENS code can take the point strings from NPTXS or elsewhere and perform mathematical operations based on the input strings to form other point strings. The mathematical operations are all performed to a user specified accuracy. For example, many operations could use the product of cross section times flux in a single array, or other applications need $1/E\Sigma_t$ values where Σ_t is a macroscopic point function consisting of a combination of many point functions. JERGENS also allows for the generation of several commonly needed functions on a point mesh, e.g., a Maxwellian or a fission spectrum. AIM is a module which converts an AMPX Master Interface (in binary form) into an equivalent BCD form. It also serves to convert the BCD form back to binary form and, in this roll, is used to pass data between different types of computers. An added advantage of the code is that the BCD form was designed as a normal FIDO card input stream, so that the user can create a Master Interface starting with cards. For an automatic checking of any AMPX Master or Working Interface, RADE is available. This module makes many simple checks, including summing group averaged values to check against "total" averaged values, summing transfer matrices to compare with averaged values for the process, checking higher order Legendre coefficients for reasonableness, looking for suspicious negative numbers, checking record counters in directories, etc. (In retrospect, this is one of the more valuable modules in AMPX in that it has many times caught

improperly processed results before they were included in any calculational study.) In addition to the AMPX Master or Working Interface checking, this module has options to check ANISN libraries.

FUTURE DEVELOPMENT

A successful modular system is probably never through its development stage. The features of an existing modular system can be used as a starting point for code development in new areas. The modularity makes it easy to substitute or upgrade specific operations without affecting the total system. The modular system makes it as easy (and efficient time and space-wise) to execute a code as it is to execute the code in a stand-alone mode. Except for maintenance, new development will only involve the new areas. With a little instruction, non-AMPX personnel write modules which can efficiently interact with other modules in the system.

Trends

Over the course of the development of AMPX, modules have tended to become more compact and specific in their functions. This trend has minimized effort that was being expended doing redundant programming. Another trend is the move toward a variation on AMPX wherein the control programs create input streams for other modules and select module execution sequences. Since the user only makes input to the control program, this eliminates redundant input. The need for this type of operation has intensified as the modularity of the system has increased and the typical operation involves more and smaller modules.

Present and Future Modules Under Development

At least 10–15 new modules are in varying stages of development. These include four small modules which perform service function on AMPX point interfaces. Another module can recover data from a Master Interface when a portion of tape becomes unreadable. Another module processes ENDF/B unresolved data and creates point files which are fed to another module which produces Bondarenko factors from these data. A new thermal processor has been written which converts $S_{\alpha,\beta}$ data to ENDF/B File 6 form and processes it. A code has been written to produce "sensitivity" Working Interfaces from Master Interfaces. A new generalized cross section weighting module has been planned, etc. These new modules will be added to the RSIC AMPX collection as they become fully operational.

REFERENCES

1. J. R. Knight and F. R. Mynatt, MUG: A Program for Generating Multigroup Photon Cross Sections, CTC-17 (January 1970).

2. W. E. Ford, III, and D. H. Wallace, POPOP4 - A Code for Converting Gamma-Ray Spectra to Secondary Gamma-Ray Production Cross Sections, CTC-12, (May 1969).

3. N. M. Greene and C. W. Craven, Jr., XSDRN; A Discrete Ordinates Spectral Averaging Code, ORNL-TM-2500 (July 1969).

4. G. D. Joanou and J. S. Dudek, GAM-II A B_3 Code for the Calculation of Fast-Neutron Spectra and Associated Multigroup Constants, GA-4265 (September 1963).

5. W. W. Engle, Jr., A Users Manual for ANISN, K-1693, (March 1967).

6. H. C. Honeck, THERMOS: A Thermalization Transport Theory Code for Reactor Lattice Calculations, BNL-5826 (September 1961).

7. L. W. Nordheim, "The Theory of Resonance Absorption," Proceedings of Symposia in Applied Mathematics, American Mathematical Soc. Vol. XI, p. 58, Garrett Birkhoff and Eugene P. Wigner, Eds., (1961).

8. C. N. Kelber, G. Jensen, L. Just, and B. J. Toppel, The Argonne Reactor Computation System, ARC, Proceedings of the International Conference on the Utilization of Research Reactors and Reactor Mathematics and Computation, Mexico City, pp. 1428–1445. (1967). See also:

   B. J. Toppel, The Argonne Reactor Computation System, ARC, ANL-7332, (1968). See also:

   B. J. Toppel, The Argonne Reactor Computation (ARC) System, Reactor Physics Division Annual Report, July 1, 1966 to June 30, 1967, ANL-7310, pp. 433–436. See also:

   L. Just, and S. G. Sparck, The ARC System, Applied Mathematics Division Internal Technical Memorandum No. 157 (1968) (unpublished).

9. E. D. Reilly and W. H. Turner, "The Automation of Reactor Design Calculations at the Knolls Atomic Power Laboratory." Proc. Conf. Application of Computing Methods to Reactor Problems, Argonne, Ill., May 27–29, 1965. USAEC Report ANL-7050, Argonne National Laboratory, pp. 251–63 (1965).

10. H. C. Honeck, The JOSHUA System, DP-1380, (April 1975).

11. B. M. Carmichael, Standard Interface Files and Procedures for Reactor Physics Codes, Version III, LA-5486-MS (February 1974).

12. R. M. Westfall, Private Communication.

13. D. R. Vondy, T. B. Fowler, and G. W. Cunningham, VENTURE: A Code Block for Solving Multigroup Neutronics Problems Applying the Finite-Difference Diffusion-Theory Approximation to Neutron Transport, Version II, ORNL-5062/R1, (November 1977).

14. ENDF-102-Data Formats and Procedures for the Evaluate Nuclear Data File, ENDF, Edited by D. Garber, C. Dunford and S. Pearlstein, BNL-NCS-50496 (END 102), (October 1975).

15. I. I. Bondarenko (Ed.) Group Constants for Nuclear Reactor Calculations, (Consultants Bureau, New York 1964).

16. T. B. Fowler, and D. R. Vondy, Nuclear Reactor Depletion and Dynamics Code: CITATION, ORNL-TM-2496, (July 1969).

17. C. R. Weisbin et.al, MINX: A Multigroup Interpretation of Nuclear X-Sections from ENDF/B, LA-6486-MS, (September 1976).

18. N. M. Greene and F. R. Mynatt, "The AMPX Modular Code System for Generating Coupled Neutron-Gamma Multigroup Cross-Section Sets," Trans. Am. Nucl. Soc.. 15, 568 (1972); see also N. M. Greene et al., AMPX: A Modular Code System for Generating Coupled Multigroup Neutron-Gamma Libraries from ENDF/B, ORNL-TM-3706 (March 1976).

Dup
-4

LA-UR

TITLE: NJOY: A COMPREHENSIVE ENDF/B PROCESSING SYSTEM

AUTHOR(S): R. E. MacFarlane, R. J. Barrett, D. W. Muir and. R. M. Boicourt

SUBMITTED TO: RSIC Multigroup Cross Section Seminar
Oak Ridge, Tennessee
March 14-16, 1978

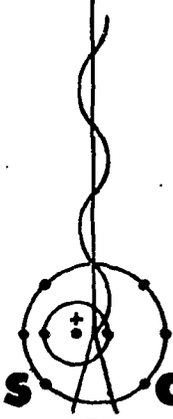

NJOY: A COMPREHENSIVE ENDF/B PROCESSING SYSTEM

R. E. MacFarlane, R. J. Barrett, D. W. Muir, and R. M. Boicourt
Los Alamos Scientific Laboratory, University of California
Theoretical Division
P. O. Box 1663, Los Alamos, NM 87545

ABSTRACT

NJOY is the successor to the MINX code. It provides an efficient and accurate capability for processing ENDF/B-IV and V data for use in fast reactor, thermal reactor, fusion reactor, shielding, and weapons analysis. NJOY produces neutron cross sections and group-to-group scattering matrices, heat production cross sections, photon production matrices, photon interaction cross sections and group-to-group matrices, delayed neutron spectra, thermal scattering cross sections and matrices, and cross-section covariances. Detailed pointwise cross sections, heating KERMA factors, thermal cross sections, and energy-to-energy thermal matrices are also available for plotting and Monte Carlo applications. NJOY currently processess all types of data on ENDF/B except for the decay chain and fission product yield files. NJOY provides output in the CCCC ISOTXS, BRKOXS, and DLAYXS formats, in DTF/ANISN format, and in a new comprehensive format called MATXS. Other important features of NJOY include free-format input, efficient binary I/O, dynamic storage allocation, an extremely modular structure, an accurate center-of-mass Gaussian integration for two-body scattering, and a flux calculator that makes it possible to compute accurate self-shielded cross sections when wide and intermediate-width resonance effects are important. NJOY is a single, integrated, efficient system that produces almost all of the basic cross sections required for multigroup methods of nuclear analysis.

INTRODUCTION

As data requirements for nuclear analysis grow steadily more complex, the analyst is faced with a bewildering variety of acronymic codes and libraries, each fulfilling only part of his needs, and each using a different format. Assembling the data he needs is full of annoyances, and incompatibilities are a constant danger. The goal of the NJOY development program has been to create a single self-consistent easy-to-use system which will process all data types in the ENDF/B evaluated nuclear data files[1] and output it in the form the designer needs.

BLANK PAGE

NJOY is a child of MINX[2] and the name stands for "MINX-plus." It is a modular system where each module is an essentially free-standing code devoted to one particular processing task (see Table 1 for a list of the current modules). The following sections discuss the structure of NJOY and describe the functions and interesting features of each module.

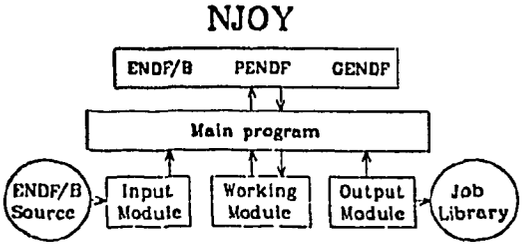

Fig. 1. Overall structure of the NJOY system.

Table 1. The Modules of NJOY

Name	Function
MODER	Mode conversion
RECONR	X-sec reconstruction
BROADR	Doppler broadening
UNRESR	Unresolved x-secs
HEATR	Heating pointwise data
THERMR	Thermal pointwise data
GROUPR	Group neutron and nγ x-secs
GAMINR	Gamma interaction x-secs
ERRORR	X-sec covariances
DTFR	DTF format output
CCCCR	CCCC format output
MATXSR	MATXS format output

STRUCTURE AND UTILITIES

The overall structure of the NJOY system is shown in Fig. 1. All working modules communicate with each other using disk files (loosely "tapes") in ENDF/B format. These files are the original ENDF/B tape, a completely pointwise ENDF tape (PENDF), and a groupwise ENDF tape (GENDF). Modules can be run in many different orders and these internal tapes are useful for restarts. For example, a single saved GENDF tape can be reformatted into DTF, CCCC, and MATXS formats without rerunning the expensive group-averaging process. Similarly, multigroup constants for several different group structure and weighting function combinations can be run from one preprocessed PENDF tape.

The function of the main program is to specify the order of execution of these modules. In OVERLAY versions of the code, it also contains the library of utility systems available to all modules: free format input, variable-dimensioned dynamic storage, and ENDF/B input/output and computation.

NJOY contains its own machine-independent free format input processor with very simple rules of context. This input routine is especially useful with terminal-oriented computer systems. Variable-dimensioned storage and dynamic storage allocation are handled by a set of simple subroutines called the STORAG package. It allows space to be reserved, released, or located by name in a large container array. As a result, computer memory is used very efficiently.

The ENDF/B I/O routines in NJOY use either the BCD mode or a new blocked binary mode. The new mode allows large tabulations to be broken up into small logical records which can be "paged" through calculations efficiently without using excessive memory. Significant time savings are achieved by avoiding repeated "coding" and "cracking" of BCD records as shown in Table 2. MODER is used to convert back and forth between ENDF/B BCD and blocked binary modes.

Table 2. Comparison of BCD and Binary I/O Modes

Test	BCD	Binary
^{235}U Doppler broadening	169.0	72.1
^{235}U P_3 elastic matrix	10.9	4.99
^{235}U(n,2n) matrix	4.31	0.84
Fe Doppler broadening	139.	46.5

RECONR

This module reconstructs ENDF/B cross sections on a union energy grid such that all partial cross sections can be represented to within a stated accuracy using linear interpolation. The total cross section and any other summation cross sections (i.e., inelastic, sometimes fission, sometimes n,2n) are then recomputed to equal the sum of their parts. Linearization uses the method developed for MINX and resonance reconstruction uses the methods of RESEND[3] with several additions. A more efficient multilevel Breit-Wigner resonance calculation has been added based on the work of C. Lubitz.[4] The accurate Hwang and Henryson unresolved quadrature set[5] has been added. Finally, an option has been added to the single-level Breit-Wigner calculation to allow reconstruction at a specified temperature using the ψ and χ functions. The input to RECONR is a standard ENDF tape; the output is a PENDF tape.

BROADR

This module broadens tabulated cross sections at some input temperature to specified output temperatures. The results can be thinned to a specified accuracy. In the "bootstrap" mode, the starting temperature for final temperature 2 is final temperature 1. Due to the thinning, this mode is faster. Restart from a previously broadened PENDF tape is possible to add temperatures or to recover from an error in a previous attempt such as time limit.

The method of the SIGMA-1 code[6] is used with two major modifications. First, storage and indexing of data is changed to allow for broadening of several reactions on the union grid simultaneously. The summation cross

sections are recomputed after broadening. Second, a new method for computing broadening integrals at low energies and high temperatures is used which eliminates a numerical instability in the original code. Table 3 compares processing times for NJOY and the original SIGMA-1 method as used in MINX.

The broadened cross sections are written on a new PENDF tape as a series of materials, all with the same MAT number, but each with a different temperature.

Table 3. Comparison of Doppler Broadening in NJOY and MINX

Nuclide	CP seconds (0 to 300 K) MINX	NJOY
^{12}C	5.83	0.73
Fe	104.7	31.9
^{235}U	171.1	42.1
^{240}Pu	2239.6	570.1

UNRESR

This module prepares effective self-shielded cross sections versus energy, temperature, and background cross section. The methods used were borrowed from ETOX[7] and are almost identical to those used in MINX except that the accurate Hwang and Henryson quadrature scheme[5] is used. The results are added to the input PENDF tape using a special ENDF/B format (MF=2, MT=152) for use by subsequent modules.

HEATR

The HEATR module computes pointwise prompt heat production cross sections (KERMA factors) and adds them to the PENDF tape using the 300 series of reaction numbers (e.g., MT301 is total heating). The calculation is similar to the MACK code[8] except that photon production is accounted for consistently using an energy-balance method.

Prompt, local heating is a result of the slowing down of charged particles including the recoil nucleus itself. However, ENDF/B does not contain the charged particle spectrum data necessary for the direct calculation. By energy conservation, the energy available for local heating is equal to the total available energy minus the energy carried away by secondary neutrons minus the energy carried away by photons. This approach has the advantage of giving the correct heating for large systems (i.e., few photons escape) when the partition between neutron and photon events is severely misevaluated, or even when photon production is absent.

HEATR computes the average neutron energies directly from ENDF/B angular distributions (MF4) and energy distributions (MF5). Average photon energies are computed from the energies of discrete photons (MF12 and/or MF13) and the energy distributions for continuum photons (MF15). Cross sections are obtained from the PENDF tape.

As shown in Fig. 2, the data produced by HEATR is only one component of the data required for a complete heating calculation. Once the neutron flux has been computed, the heat production cross section from HEATR is used to compute the "prompt local heating," the photon production matrix (see GROUPR) is used to compute the prompt part of the photon source, and the activation cross sections are used to produce the delayed photon precursors. The total photon source is used in a transport calculation to determine the photon flux. This flux is then used with the photon heat production cross section (see GAMINR) to compute the "non-local heating." The last component is the "delayed local heating" due to particle decay of the activation products or fission products. A future NJOY module will provide the data for the decay branch in Fig. 2 directly from ENDF/B-V file 8.

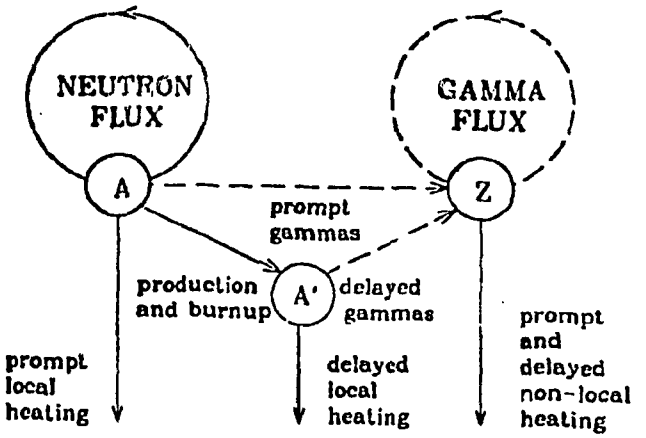

Fig. 2. Procedure for a complete nuclear heating calculation.

THERMR

THERMR is used to generate pointwise cross sections and energy-to-energy scattering matrices in the thermal range. The results are added to the PENDF tape for use by subsequent modules.

Incoherent energy-to-energy P_n or angular scattering matrices can be generated for free scatterers or for bound scatterers when ENDF/B scattering functions are available.[9] The secondary energy grid is determined adaptively for each incident energy and angle or Legendre moment so that linear interpolation is accurate to with a specified tolerance. The incident energy grid is fixed. The incoherent cross section is determined by integrating over these distributions and transferring them onto the grid of the PENDF tape by Langrangian interpolation. Finally, the energy-and-angle distributions are normalized and written onto the PENDF tape

using a modified version of File 6. This approach is more direct than that of FLANGE-II,[10] and it permits multigroup averages to be taken (see GROUPR).

Coherent scattering for hexagonal lattices is handled as in the HEXSCAT code[11] except that more Legendre orders are allowed, and a new approximation is used at high energies where reciprocal lattice shells become closely spaced. In addition, the energy grid is determined adaptively so as to represent the P_n cross sections to within a specified tolerance using linear interpolation. The results are written on File 3 using special MT numbers.

GROUPR

GROUPR is used to produce multigroup cross sections, anisotropic group-to-group neutron scattering matrices, and anisotropic photon production matrices. Special features are provided for ratio quantities (e.g., ν, $\bar{\mu}$, ξ, or photon yields), delayed neutron spectra by time group, and anisotropic thermal neutron scattering. Fission is represented as group-to-group matrices for full generality. All cross sections and matrices can be temperature dependent and self-shielded.

It has been found that all these varied types of data can be processed efficiently and compactly using the following generalized integral over incident energy in group g:

$$\sigma_g = \frac{\int_g F\,\sigma\,\phi\,dE}{\int_g \phi\,dE} \quad , \tag{1}$$

where ϕ is the model neutron flux, σ is a particular cross section, and F is a function which varies for different data types. For example, $\sigma = \sigma_f$ and $F = \nu$ gives the fission neutron production cross section. Matrices for two-body scattering reactions are obtained with

$$F = \int_{g'} f^{CM}(E,\omega)\; P_n\,[\mu(\omega)]\,d\omega \quad , \tag{2}$$

where f is the angular distribution in the center-of-mass frame, P_n is a Legendre polynomial, μ is the LAB cosine, ω is the CM cosine, and the integration is over all ω that lead to secondary energies in group g'. (GROUPR uses an accurate Gaussian quadrature for this integral). Similarly, continuum scattering uses

$$F = f_n^{LAB}(E) \int_{g'} g(E'\rightarrow E)\,dE' \quad , \tag{3}$$

where g is the secondary energy distribution for the reaction (g may be a delta function for discrete photons).

Thermal coherent reactions are processed as cross sections but incoherent scattering requires special methods because of the relatively coarse incident energy grid. The feature of this reaction is a peak which moves in the (E,E') plane but whose shape changes slowly. Straightforward interpolation along E and E' would lead to double-humped shapes. Therefore, when E is between E_i and E_{i+1}, GROUPR projects up from E_i and down from E_{i+1} along the lines E=E' and adds to get the effective shape at E. Then

$$F = \int_{g'} g_n(E \leftarrow E')dE' \quad , \tag{4}$$

where g_n is the projected distribution.

The incident energy integrals of Eq. (1) are particularly simple. Because of the linearization of the point cross sections on the PENDF tape (see RECONR) trapazoidal integration can be used for all cases except Eq. (2). In that case, the additional structure in F(E) is approximately an oscillatory polynomial of known order which can be accurately integrated by a Gaussian quadrature.

The use of such simple quadrature schemes lends itself to doing many integrations in parallel, thus saving the time required to page the complex cross-section tabulations through memory. NJOY does the incident energy integrations for all secondary groups, all Legendre orders, and all σ_0 values simultaneously. The savings of computing time are illustrated in Table 4.

Table 4. Comparison of Multigroup Calculations Using MINX and NJOY

Test	MINX	NJOY
^{235}U selected cross sections	25.0	5.75
^{235}U P_3 elastic matrix	33.4	4.99
^{235}U P_3 total matrix	567.	21.4
Fe P_3 elastic matrix	58.5	13.8

This parallel processing also insures that all neutron induced cross sections are consistent in precision, weight function, and content, thereby avoiding many of the problems encountered when building coupled sets with neutron data from MINX, photon production from LAPHANO,[12] and heating from MACK.

GROUPR normally uses a model flux appropriate for large systems in the narrow resonance approximation

$$\phi(E) = \frac{W(E)}{\sigma_0 + \sigma_t(E)} \quad , \tag{5}$$

where W is a smooth weight function selected by the user, σ_t is the total cross section, and σ_0 is the background cross section parameter. For thermal reactor problems, where the narrow resonance approximation breaks down, GROUPR can compute the flux appropriate to a heaby absorber mixed with a light scatterer using

$$[\sigma_0 + \sigma_t(E)]\phi(E) = \sigma_0 W(E) + \int_E^{E/\alpha} \frac{\sigma_s(E')\phi(E')}{(1-\alpha)E'}\, dE' \quad , \tag{6}$$

where σ_s is the scattering cross section of the absorber and α is the maximum lethargy change in scattering. The integral equation is solved by iteration using the PENDF cross sections. The result is a very accurate accounting of all wide and intermediate resonance effects on self-shielding.

The GROUPR results are written onto the ENDF-like GENDF tape for eventual use by the formatting modules (DTFR, CCCCR, MATXSR).

GAMINR

GAMINR produces photon interaction multigroup cross sections and group-to-group photon scattering matrices from ENDF/B data. Total, coherent, incoherent, pair production, and photoelectric cross sections can be averaged using specified group structure and weight function. The Legendre components of the coherent and incoherent scattering cross sections are calculated using the form factors[13] now available in ENDF/B-IV. These form factors account for the binding of the electron in its atom. Consequently, the cross sections are accurate for energies as low as 1 keV. GAMINR also computes the photon heat production cross section. The resulting multigroup constants are written on a GENDF tape for use by the formatting modules (see MATXSR).

Calculational methods are very similar to those in GROUPR except that special methods had to be developed for doing the integrals required to define the F functions for coherent and incoherent scattering.

GAMINR has many advantages over the older GAMLEG code[14] including P_n coherent matrices, the form factors, and the heat production cross sections. Variable-dimensioning allows very large problems to be run. However, GAMINR is slower than GAMLEG.

ERRORR

This module produces cross section covariances from ENDF/B error files.[15] The current version processes only File 33 (cross sections). This is sufficient to compute covariance between the cross section of group g for reaction x and group g' for reaction x' when resonances are not important. The necessary multigroup cross sections can be obtained from a preprocessed supergroup library or generated internally in ERRORR using the methods of GROUPR. The code also has a very general method for constructing covariance matrices for reactions which are linear combinations of other reactions.

As with the other multigroup modules of NJOY, ERRORR writes its results on a GENDF tape for later use by the formatting modules.

The capabilities of ERRORR are very similar to those of PUFF[16] which is based on MINX.

DTFR

This is a formatting module which converts multigroup data from a GENDF tape into a form compatible with transport codes such as DTF[17] and ANISN.[18] Tables can be produced for nn, nγ, and γγ data with as many Legendre orders as desired and with up to 100 groups. Thermal data (see THERMR) can be substituted for the normal static data in the low energy groups. Upscatter is allowed, and consistent table truncation is performed for both upscatter and downscatter groups which lie outside the limits of the table. Activity edits can be added to the P_0 tables. Since the edits can be any linear combination of cross sections on the GOUT tape, complex things like gas production are easy to construct. In addition, DTFR makes plots of the multigroup cross sections overlaid on the pointwise data, and it makes isometric plots of the group-to-group matrices (see Fig. 3).

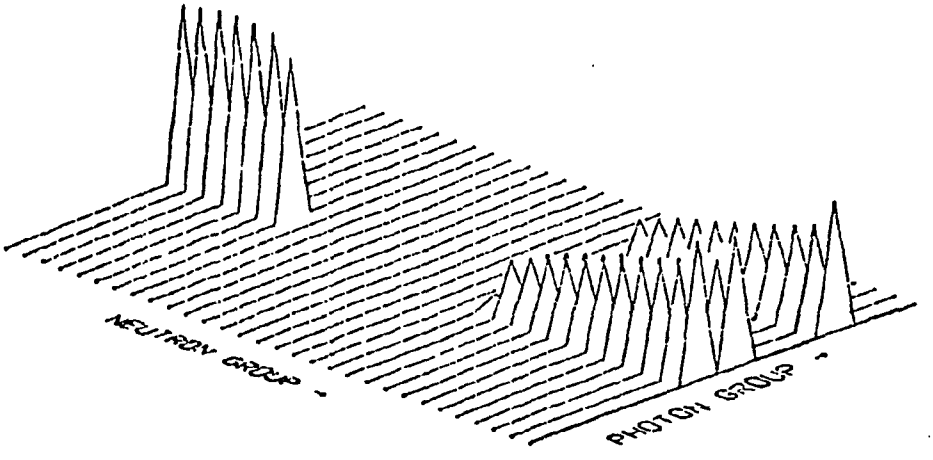

Fig. 3. Photon production matrix for ^{12}C from ENDF/B-IV (30 neutron and 12 photon groups).

CCCCR

The CCCCR module formats GOUT cross sections into interface formats developed by the Committee for Computer Code Coordination (CCCC). Three CCCC-III files[19] are supported.

ISOTXS is a material-ordered file containing cross sections (total, transport, n2n, nα, nd, nt) and P_n scattering matrices (total, elastic, inelastic, n2n).

BRKOXS is a file of shielding factors by temperature and σ_0 (total, transport, capture, fission) and a few auxiliary cross sections used in shielding calculations (e.g., elastic, inelastic, σ_p, ξ).

DLAYXS is a file of delayed neutron yields and spectra by time group. ENDF/B uses the traditional six groups.

Complex data management schemes are used that make it possible to use very large group structures. The conventions used to load these files are the same as those used for the MINX libraries[20] except for a more sophisticated definition for the transport cross section and the treatment of fission. The average fission χ vector is computed by collapsing the GROUPR fission matrix with the multigroup model flux and including delayed contributions.

MATXSR

This module reformats multigroup constants from the GENDF tape into the MATXS interface format. MATXS is a new flexible and comprehensive CCCC-type format designed to hold all the data types which can be produced by NJOY.

The current CCCC cross section files (ISOTXS, BRKOXS, DLAYXS, ISONGX) are rather inflexible. For example, there is no place in ISOTXS for heat production, gas production, or important high threshold reactions like n3n and nαt. Sensitivity studies require partial matrices which are not allowed for. There is no provisions for self-shielding of elastic removal, heat production, or photon production, Furthermore, every data type has a different format, leading to complex and bulky utilities.

MATXS, on the otherhand, has a very general organization designed to hold arbitrary vectors and matrices. The file is first divided into "data types" such as neutron scattering, photon production, gamma scattering, and neutron thermal data. Each type is assigned a name (NSCAT, NGAMA, GSCAT, NTHERM) and new types are easily added. Data types are distinguished by the choice of incident and secondary group structures. In addition to simple cases like n→n or n→γ, MATXS allows for complex coupled sets such as nγ→nγ or n→nγβ.

Each data type is divided into materials specified by nuclide, temperature, and background cross section. Each material is further subdivided

into "vector partials" and "matrix partials." These reaction partials are labeled with Hollerith names so there is no limit on the quantities that can be stored. Vectors are packed with leading and trailing zeroes removed, and matrices are banded as in ISOTXS.

MATXSR reads reactions from the GENDF tape, assigns the Hollerith names, and packs the cross sections into MATXS format. A readable listing of the file is produced if desired, and an index of all the data types, materials, and reactions on the file is printed.

Codes that use MATXS are under development at both Los Alamos and Oak Ridge. One example is TRANSX, an interface to transport codes such as ANISN. TRANSX constructs tables in various formats for $n \rightarrow n$, $\gamma \rightarrow \gamma$, or $n\gamma \rightarrow n\gamma$ coupled sets. The results can be direct or adjoint, material-ordered or group-ordered, prompt or infinite-time, and transport corrected if desired. The code will collapse to a subset group structure, form mixes, and form activity edits which are any linear combination of vectors from MATXS. Upscatter is allowed and thermal cross sections can be used at low energies. Temperature and σ_0 interpolation are included for self-shielding.

CONCLUSIONS

NJOY is a single nuclear cross-section processing system which performs all the functions of MINX, LAPHANO, GAMLEG, MACK, PUFF, FLANGE-II, and HEXSCAT simply and conveniently. It currently processes all ENDF/B-IV and V data types except MF8 (decay data) and MF32 (resonance covariances) and makes the results available to subsequent codes using comprehensive and efficient formats.

REFERENCES

1. D. Garber, C. Dunford, and S. Pearlstein, "Data Formats and Procedures for the Evaluated Nuclear Data File, ENDF," Brookhaven National Laboratory report BNL-NCS-50496 (ENDF 102) (1975).

2. C. R. Weisbin, P. D. Soran, R. E. MacFarlane, D. R. Harris, R. J. LaBauve, J. S. Hendricks, J. E. White, and R. B. Kidman, "MINX: A Multigroup Interpretation of Nuclear X-Sections from ENDF/B," Los Alamos Scientific Laboratory report LA-6486-MS (1974).

3. O. Ozer, "RESEND: A Program to Preprocess ENDF/B Materials with Resonance Files into a Pointwise Form," Brookhaven National Laboratory report BNL-17134 (1972).

4. P. Rose, Brookhaven National Laboratory, private communication (1975).

5. R. N. Hwang and H. Henryson, II, "Critical Examination of Low-Order Quadratures for Statistical Integrations," Trans. Am. Nucl. Soc. 22, 712 (1975).

6. D. E. Cullen and C. R. Weisbin,"Exact Doppler Broadening of Tabulated Cross Sections," Nucl. Sci. Eng. 60, 199 (1976).

7. R. E. Schenter, J. L. Baker, and R. B. Kidman, "ETOX, A Code to Calculate Group Constants for Nuclear Reactor Calculations," Battelle Northwest Laboratory report BNWL-1002 (ENDF-127) (1969).

8. M. A. Abdou, C. W. Maynard, and R. Q. Wright, "MACK: A Computer Program to Calculate Neutron Energy Release Parameters (Fluence-to-Kerma Factors) and Multigroup Neutron Reaction Cross Sections from Nuclear Data in ENDF Format," Oak Ridge National Laboratory report ORNL-TM-3994 (1973).

9. J. U. Koppel and D. H. Houston, "Reference Manual for ENDF Thermal Neutron Scattering Data," General Atomic Co. report GA-8774 (1968).

10. H. C. Honeck and D. R. Finch, "FLANGE-II (Version 71-1), A Code to Process Thermal Neutron Data from an ENDF/B Tape," E. I. DuPont de Nemours and Co. Savannah River Laboratory report DP-1278 (1971).

11. Y. D. Naliboff and J. U. Koppel, "HEXSCAT, Coherent Elastic Scattering of Neutrons by Hexagonal Lattices," General Atomic Co. report GA-6026 (1964).

12. D. J. Dudziak, R. E. Seamon, and D. V. Susco, "LAPHANO: A Multigroup Photon-Production Matrix and Source Code for ENDF," Los Alamos Scientific Laboratory report LA-4750-MS (ENDF-156) (1967).

13. J. H. Hubbell, W. J. Veigele, E. A. Briggs, R. T. Brown, D. T. Cromer, and R. J. Howerton, "Atomic Form Factors, Incoherent Scattering Functions, and Photon Scattering Cross Sections," J. Phys. Chem. Ref. Data 4, 471 (1975).

14. K. D. Lathrop, "GAMLEG - A FORTRAN Code to Produce Multigroup Cross Sections for Photon Transport Calculations," Los Alamos Scientific Laboratory report LA-3267 (1965).

15. F. G. Perey, "The Data Covariance Files for ENDF/B-V," Oak Ridge National Laboratory report ORNL-TM-5938 (ENDF-249) (1977).

16. C. R. Weisbin, E. M. Oblow, J. Ching, J. E. White, R. Q. Wright, and J. Drischler, "Cross Section and Method Uncertainties: The Application of Sensitivity Analysis to Study Their Relationship in Radiation Transport Benchmark Problem," Oak Ridge National Laboratory report ORNL-TM-4847 (ENDF-218) (1975).

17. K. D. Lathrop, "DTF-IV, A FORTRAN Program for Solving the Multigroup Transport Equation with Anisotropic Scattering," Los Alamos Scientific Laboratory report LA-3373 (1965).

18. W. W. Engle, Jr., "A User's Manual for ANISN: A One Dimension Discrete Ordinates Transport Code with Anisotropic Scattering," Union Carbide Corporation report K-1693 (1967).

19. B. M. Carmichael, "Standard Interface Files and Procedures for Reactor Physics Codes, Version III," Los Alamos Scientific Laboratory report LA-5486-MS (1974).

20. R. B. Kidman and R. E. MacFarlane, "LIB-IV, A Library of Group Constants for Nuclear Reactor Calculations," Los Alamos Scientific Laboratory report LA-6260-MS (1976).

ETOE-2/MC^2-2/SDX MULTIGROUP CROSS-SECTION PROCESSING*

B. J. Toppel, H. Henryson II, and C. G. Stenberg
Argonne National Laboratory
Argonne, Illinois, U.S.A. 60439

ABSTRACT

The ETOE-2/MC^2-2/SDX multigroup cross-section processing codes have been designed to provide a comprehensive neutron cross-section processing capability for a wide range of applications including critical experiment analysis and core design calculations. Fundamental nuclear data from ENDF/B provide the primary input to the code system and the output consists of a user-specified CCCC ISOTXS multigroup cross-section data file. Great flexibility has been provided to the user in specifying the rigor of the calculation so that a unified cross-section processing system with a single data base is available which may be used for both preliminary survey scoping studies and rigorous design calculations.

The principal program blocks of the code system include: a library processor and format converter between ENDF/B data and the MC^2-2/SDX library; an ultra-fine-group fundamental mode calculation (MC^2-2) which provides a composition dependent spectrum calculation and broad-group collapsing capability; a rigorous hyper-fine-group spatially heterogeneous resolved resonance calculation (RABANL) to supplement the more approximate NR approximation used in the ultra-fine-group treatement; and an intermediate group space-dependent capability (SDX).

INTRODUCTION

The ETOE-2/MC^2-2/SDX multigroup cross-section processing codes have been designed to provide a comprehensive neutron cross-section generation capability for a wide range of applications including critical experiment analysis and core calculations. Fundamental nuclear data (ENDF/B) provide the primary input to the code system and the output consists of a user-specified multigroup cross-section data file (ISOTXS). Great flexibility is provided to the user in specifying the rigor of a calculation, thus providing a unified cross-section processing system with a single data base which may be used for both preliminary survey scoping and design calculations.

Work performed under the auspices of the U.S. Department of Energy.

BLANK PAGE

The principal program blocks of the code system include a library processor (ETOE-2), an ultra-fine-group (ufg) fundamental mode calculation (MC^2-2), a rigorous hyper-fine-group (hfg) spatially heterogeneous resolved resonance capability (RABANL) and an intermediate-group space-dependent capability (SDX). A block diagram indicating the general program flow is given in Fig. 1. Brief descriptions of the physics methods and models incorporated in the ETOE-2/MC^2-2/SDX code system are presented below.

ETOE-2

The ETOE-2 program processes the fundamental nuclear data from an ENDF/B[1] data file and prepares eight binary library files for use by the computational modules of MC^2-2/SDX. Neither MC^2-2, RABANL, nor SDX reads the ENDF/B data directly. Thus, one could prepare MC^2-2/SDX library files from an alternative input data base (e.g., UKNDL, KEDAK) by either conversion of the basic data to the ENDF/B formats or by the replacement of the ETOE-2 code with a new processing code which generates the MC^2-2/SDX libraries.

The ETOE-2 program performs six basic functions: (1) reformat data; (2) preprocess "light" element ($A \approx 100$) resonance cross sections; (3) screen and preprocess "wide" and "weak" resolved resonances; (4) generate ultra-fine-group "floor" cross sections; (5) calculate function tables; and (6) convert all ENDF/B formats to laws which are allowed by MC^2-2/SDX.

The ENDF/B data files provide all data for a given material, whereas the MC^2-2/SDX computational modules require that the data be ordered by reaction type (e.g., resolved resonance parameters, scattering coefficients, etc.). The MC^2-2/SDX library structure has been designed to permit efficient access to data by the computational modules. The eight data files in the MC^2-2/SDX library include resolved resonance parameters, unresolved resonance parameters, ufg nonresonance cross sections, inelastic and (n,2n) scattering data, fission spectrum parameters, and elastic scattering distributions, as well as function tables and an administrative file.

At user option the ETOE-2 code calculates resonance cross sections from ENDF/B resonance parameters for all materials of mass less than an input value. Generally a mass of 100 is used. These "light" element resonance cross sections are then combined with the ENDF/B "floor" cross sections and integrated over ufg energy boundaries ($\Delta u \approx 0.008$) to provide the ufg cross sections required by MC^2-2/SDX. It is assumed that "light" element resonance cross sections are composition-independent on the ultra-fine-group level.

With recent increasing emphasis on the use of the rigorous RABANL capability, much attention has been given to improving the computational efficiency of RABANL. One of the approaches taken has been to have

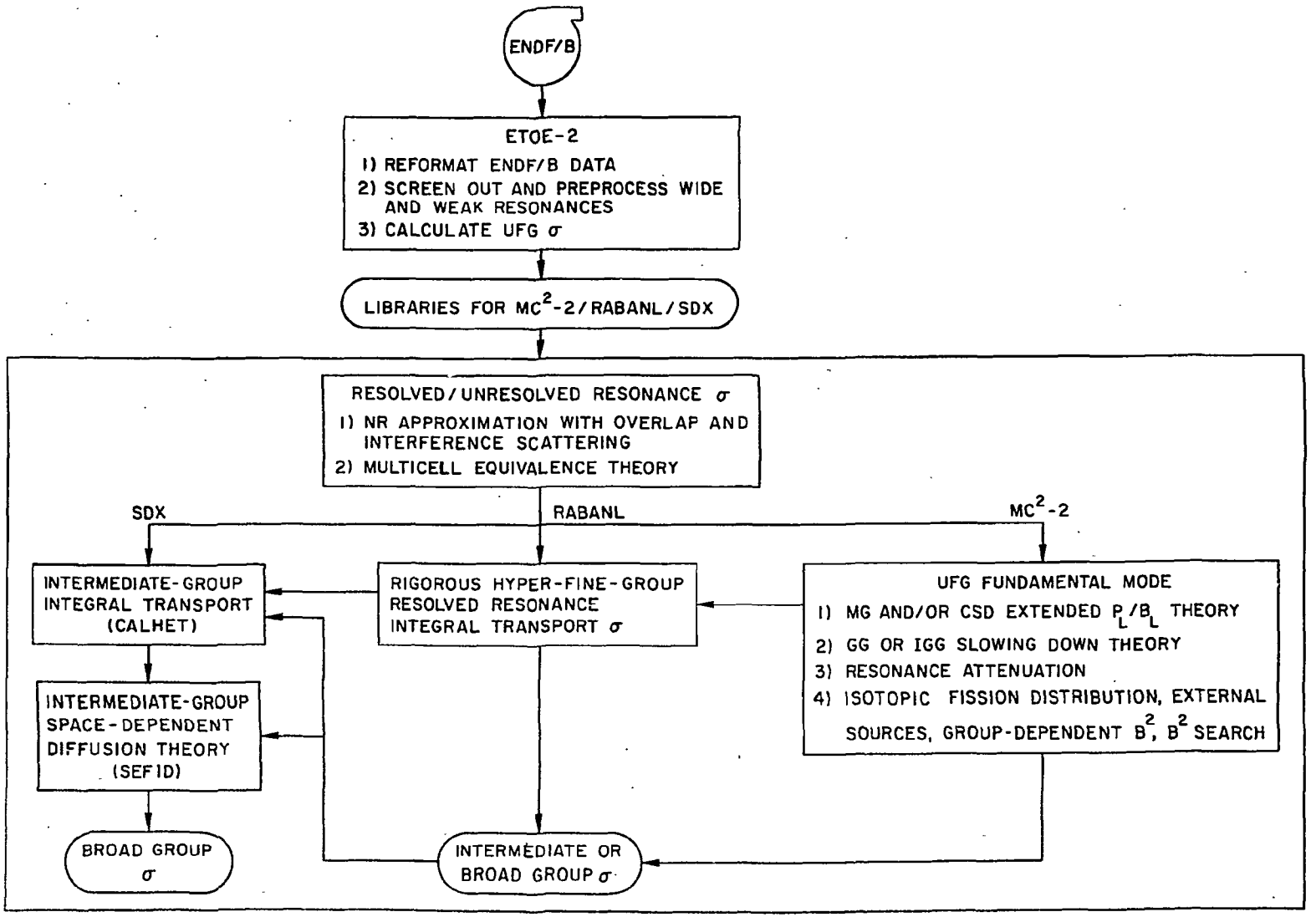

Fig. 1. ETOE-2/MC²-2/SDX

ETOE-2 screen out and preprocess a significant number of the resolved resonances into composition and temperature independent ufg "smooth" cross sections. Resolved resonances suitable for such screening can be characterized as belonging to one of two types. The first are the extremely wide resonances with natural widths much larger than both the corresponding Doppler width and the ufg width. The second type of resonance is typified by the extremely weak resonances belonging to the medium weight nuclei of low natural abundance, or the p-wave resonances of the heavy nuclei. This preprocessing by ETOE-2 has provided significant reductions in RABANL execution times, especially for problems involving structural material resonances.[2]

The ENDF/B formats permit a large number of options in describing the fundamental data. Many of these options have not been used in the four releases of ENDF/B to date and only a subset of the allowed ENDF/B laws are processed by MC^2-2/SDX. It is, therefore, necessary for the ETOE-2 code to process data given by any of the other laws and prepare these data in a format permitted by MC^2-2/SDX. The MC^2-2/SDX resolved resonance algorithms assume a single or multilevel Breit-Wigner or a multilevel Adler-Adler description whereas ENDF/B also permits R-Matrix (Reich-Moore) parameters. It is well known that equivalent multilevel Adler-Adler parameters may be derived from these models[3] and these equivalent parameters are calculated by ETOE-2. Similarly, ENDF/B permits six secondary energy distribution laws for inelastic and (n,2n) scattering, whereas MC^2-2 permits only three. The ETOE-2 code generates a tabulated function if data are provided for any of the three laws not processed by MC^2-2. Similar examples may be cited in the processing of elastic scattering distributions and fission spectrum data. In general, the format conversions performed by ETOE-2 do not alter the basic data input on the ENDF/B files. The unresolved parameters in ENDF/B may include data for the average competitive reaction width. These data have been ignored by ETOE-2 up to the present time. With the release of ENDF/B-V the ETOE-2 and MC^2-2/SDX codes will be modified to process the competitive width reaction data and the MC^2-2/SDX library files will be changed to include these data.

The ETOE-2 program thus provides an automated capability for the generation of MC^2-2/SDX library files from ENDF/B data. It performs the same functions for MC^2-2/SDX as the ETOE[4] and MERMC2[5] codes performed for the MC^2 cross-section preparation program.[6] Since the library files generated by ETOE-2 are not composition dependent, the program need be executed only when new fundamental data become available (e.g., each release of ENDF/B). A limited capability is also available to modify the data in the MC^2-2/SDX libraries, thus obviating the need to rerun ETOE-2 in order to study the sensitivity of multigroup cross sections to changes in fundamental data.

MC^2-2

Since its introduction in 1967 and up to the present time, the MC^2 code has been used extensively for the preparation of multigroup cross sections. However, a number of recognized limitations and inconsistencies in the code pointed out the need for a new capability which could serve as a standard for fast reactor calculations. The MC^2-2 code[7] has been developed to satisfy this need and represents a significant departure from the earlier MC^2 code. Recent advances in neutron slowing-down theory, resonance theory, and numerical methods have been incorporated into the ultra-fine-group fundamental mode MC^2-2 calculation. The code algorithms and implementation strategy which are described in detail in Ref. 7 are briefly summarized below. A block diagram indicating the flow through the computational modules of MC^2-2 is given in Fig. 2.

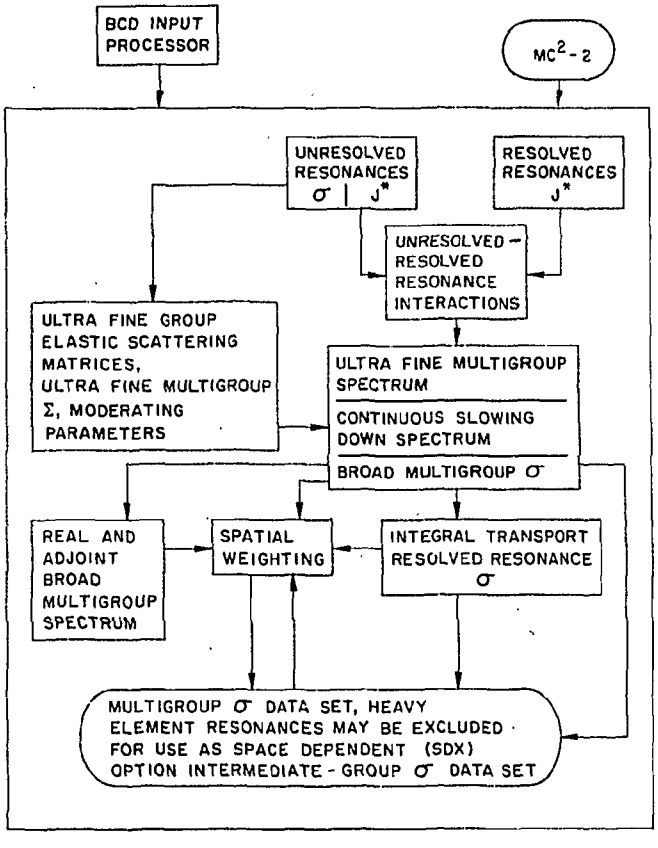

Fig. 2
MC^2-2 Program Flow

The MC^2-2 code solves the neutron slowing-down equations in the P_1, B_1, consistent P_1, and consistent B_1 approximations and makes use of the extended transport approximation to account for high-order transport and anisotropic scattering effects.[8,9] Both the continuous slowing down and multigroup forms of the slowing-down equations are solved using an ufg lethargy structure as depicted in Fig. 3.

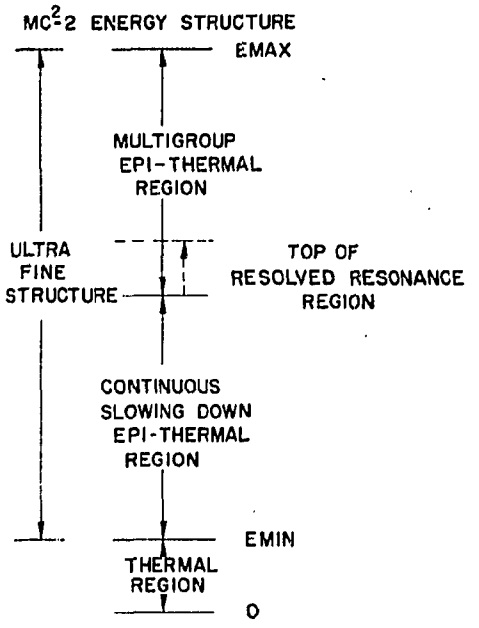

Fig. 3. MC^2-2 Energy Structure

The energy boundary between the multigroup and continuous slowing-down formulations is user-specified but must lie above the top of the resolved resonance energy region. This is a consequence of the resonance treatment discussed below. The moderating parameters, in the continuous slowing-down formulation may be calculated using either Greuling-Goertzel[10] or Improved Greuling-Goertzel[8] algorithms. Only elastic scattering is treated continuously in the continuous slowing-down formulation. Inhomogeneous sources along with fission, inelastic and (n,2n) sources are represented in the ufg multigroup form.

The resolved and unresolved resonance calculations of MC^2-2 are modeled after the work of Hwang[11] and represent a marked improvement in accuracy and a dramatic improvement in efficiency over the methods incorporated in the MC^2 code. The resonance algorithms make use of a generalized J*-integral formulation based on the narrow resonance approximation including overlap effects. The characteristics of these algorithms may be summarized briefly as follows:

(1) The integration procedure was optimized by utilizing the asymptotic properties of the integrands and the general characteristics of the Gauss-Jacobi quadrature. This was achieved by introducing a rational transformation of the variable of integration.

(2) For the relatively weak resonances which represent a significant portion in practical calculations, the J*-integral is evaluated analytically.

(3) For the resolved energy range, the new algorithms allow the use of the multilevel formalism in Adler-Adler form[12] and the multilevel and single level Breit-Wigner[13] forms.

(4) For the unresolved energy range, the algorithms provide an accurate estimate of the in-sequence overlap effect which accounts for the long-range correlation of levels described by Dyson[14] and include the influence of interference scattering.

As shown in Ref. 15, the J*-integral method provides an efficient means of accounting for resonance effects in the continuous slowing-down formulation. In particular, the continuous slowing-down equations are solved for the "asymptotic" neutron slowing-down density ignoring narrow resonances. Then the resonance reaction rates are computed using the flux resulting from the asymptotic slowing-down density

attentuated by absorption in higher energy resonances. The ultra-fine-group flux derived from the attentuated slowing-down is then used in the generation of broad-group cross sections by standard group-collapsing methods.

As noted above, the entire MC^2-2 calculation is performed on an ultra-fine-group mesh. Inelastic and (n,2n) secondary energy distributions may be described by discrete levels, evaporation spectra and/or tabulated functions according to the ENDF/B specifications. Detailed angular distributions are used in calculating ultra-fine-group P_0 and P_1 elastic transfer matrices for all materials. For light elements, an analytic integration over the sink group is combined with a detailed numerical integration over the source group.[16] Heavy element transfer matrices are calculated semi-analytically according to the methods described in Ref. 17.

Options available to the user of MC^2-2 include inhomogeneous group-dependent sources, group-dependent buckling, buckling search to critical, and isotope-dependent fission spectrum distributions. The user-specified cross-section file generated by MC^2-2 is appropriate for neutronics calculations ($\lesssim$50 groups) or for use in intermediate group ($\approx$50-300 groups) spectrum calculations. In particular, the intermediate group cross-section file may be used in the SDX capability described below.

A hyper-fine-group integral transport capability RABANL is also available at user option. The hfg width is defined to be small compared to the maximum lethargy gain on scattering by the heaviest isotope in the problem. RABANL was modeled after the RABID[18] and RABBLE[19] codes although significant modifications have been made to: (1) eliminate precision difficulties; (2) make use of the MC^2-2/SDX library data; (3) link the hyper-fine-group calculation to the ultra-fine-group calculations through the slowing-down souce; and (4) increase the overall efficiency of the codes.

Since hundreds of thousands of hfg may be involved, especially when including resonances of the structural materials which occur at tens or hundreds of keV, attention to algorithm efficiency was essential in order to permit RABANL to be used for routine calculations. The ETOE-2 screening mentioned above represents one such efficiency. Even more significant was recognizing and taking advantage of the asymptotic shape of the Doppler broadened resonance line shape functions to minimize calculations of these functions during the hfg sweep.[2]

An example of the improvement in accuracy of RABANL compared to the previous codes is the calculation of cylindrical transmission probabilities. By recognition of the asymptotic nature and analytic representation of the integrals involved, Hwang[20] has been able to eliminate the tabular interpolations required by earlier brute force methods with consequent improvements in storage requirements as well as accuracy.

Whereas initially RABANL was thought of as an option intended for use only in the low energy region (≲300 eV) where the narrow resonance approximation assumed in the J*-integral formulation is known to be deficient, the algorithm improvements in RABANL have resulted in a code which is now used routinely for design and analysis activities with users frequently specifying a RABANL upper energy well above the heavy element resolved resonance range.

Figure 4 shows an example of the spectral detail provided by the MC^2-2 ufg capability for an inner core composition of ZPPR. The spectral detail below 4 keV is provided by the resolved resonance treatment described above, whereas the detail above 1 MeV is due primarily to the ufg treatment of the inelastic and (n,2n) scattering.

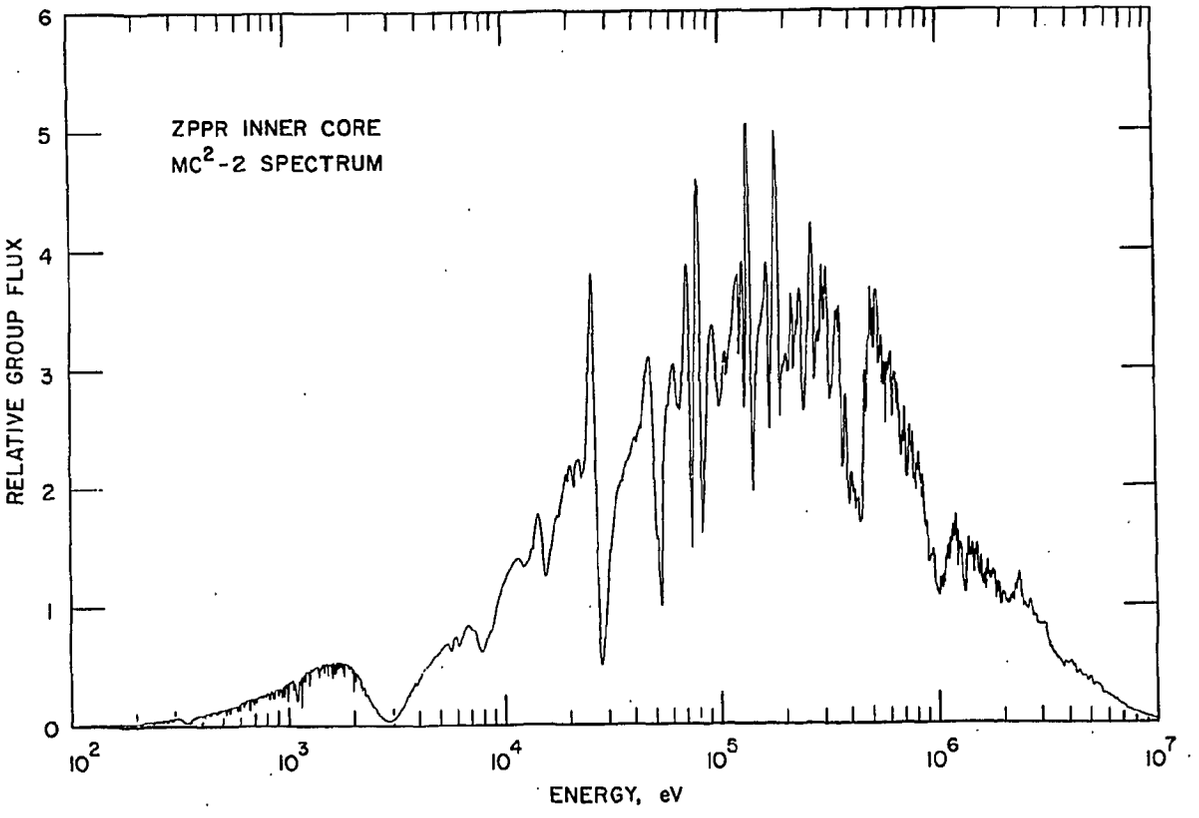

Fig. 4. MC^2-2 Spectrum, 0.0001-10 MeV

In order to illustrate the MC^2-2 execution times and compare IBM and CDC versions of the code, a sample problem as specified in Table 1 was run at ANL on the IBM/370-195 computer and at LRL Berkeley on the CDC 7600 computer. Table 2 compares the CPU execution times on the two machines for different areas of the code. The peripheral processor time is not available on the CDC 7600.

Table 1. MC^2-2 Sample Problem Specifications

Mixture:	^{239}Pu, ^{240}Pu, ^{241}Pu, ^{235}U, ^{238}U, ^{12}C, ^{16}O. ^{23}Na, ^{27}Al, Fe, Cr, Ni, Mn, Cu, Mo, Si
Options:	Δu^{ufg} = 1/120, 27 epi-thermal broad groups; inconsistent P_1 homogeneous spectrum; buckling iteration; 1740 ultra-fine groups; single fission spectrum; continuous slowing down below ∿4 keV; improved Greuling-Goertzel moderating parameters; unresolved resonance self-overlap; four nearest resolved resonances; RABANL treatment below ∿1.234 keV.

Table 2. MC^2-2 Sample Problem Timing

Code Area	IBM/370-195 CPU, sec	IBM/370-195 CPU + PP, sec	CDC-7600 CPU, sec
Input	0.5	4.1(0.5%)	0.1
NR Unresolved Resonance σ	42.7	66.8	24.3
NR Resolved Resonance σ	17.0	22.7	19.0
NR Interaction	0.3	2.8	0.1
NR Resonance Calculation	60.0	92.3(11.0%)	43.4
Tabulated σ	1.4	15.6	0.1
Elastic Matrices	36.0	136.6	19.4
Moderating Parameters	2.3	4.9	1.3
Macroscopic Data Processing	39.7	157.1(18.8%)	21.5
Ultra-fine Group Spectrum	143.8[a]	279.8[a]	106.7[a]
Broad Group σ Management	31.3	83.0	13.8
Inelastic σ Management	10.9	71.6	5.0
Ufg Spectrum and Broad Group σ	186.9[a]	448.8[a](53.6%)	148.2[a]
Broad Group Spectrum	0.6	1.5(0.2%)	0.2
RABANL Resolved Resonance σ	74.6	-	85.5
RABANL Slowing Down	15.1	-	11.6
RABANL Collision Rates	2.0	-	4.7
RABANL	111.3	130.4(15.6%)	113.0
TOTAL	401.4	836.7	327.6
Total CPU/Total	0.48		

[a]Three passes to obtain critical buckling.

SDX

A space-dependent cross-section generation capability is provided by the SDX option of the ETOE-2/MC^2-2/SDX code system. The SDX option may be characterized by three salient features:

(1) the use of an intermediate-group microscopic cross-section library for all cross sections except those represented by resonance formalisms;

(2) run time computation of intermediate-group resonance cross sections appropriate to the composition, cell structure, and temperature of the problem; and

(3) explicit treatment of all heterogeneity and multiregion spatial effects in one dimension.

The SDX option has been designed to provide the user great latitude in the rigor, complexity, and computational effort associated with a given problem. For example, it is possible, for each region in a multiregion problem, to obtain the intermediate-group cross sections, perform the resonance cross section and integral transport calculation for a heterogeneous cell model, and homogenize the intermediate-group cross sections. The homogenized cross sections for each region would then be used in a multiregion, intermediate-group diffusion theory calculation, and the resulting flux used to calculate broad-group spatially averaged cross sections on a cell-averaged and plate (pin)-wise basis. The rigor, and computational effort, of such a calculation could be relaxed by using a single set of intermediate-group cross sections for all regions, but still generating the resonance cross sections for each different region. The integral transport calculation could be omitted and volume-averaging used in the cell homogenization with or without the use of equivalence theory to account for heterogeneous effects in the calculation of resonance cross sections. A block diagram indicating the major program modules of SDX is given in Fig. 5.

At its most rigorous the SDX calculation is more rigorous, yet significantly more economical, than the most rigorous previously existing fast neutron multigroup cross-section preparation capability. On the other end of the spectrum, the simplest SDX calculation provides in less than 2 min a broad-group cross-section set which should be adequate for many analyses. In particular, the latter option is an improvement upon the self-shielding factor schemes because of the more accurate resonance cross-section and elastic removal treatments.

Broad-group microscopic cross sections are composition-dependent because of the composition-dependence of the neutron flux (and current) weighting spectrum. Elastic removal and heavy element resonance cross sections are generally the most sensitive to composition due to intermediate element scattering resonances and heavy element resonances. In the SDX option the resonance cross sections are calculated on an

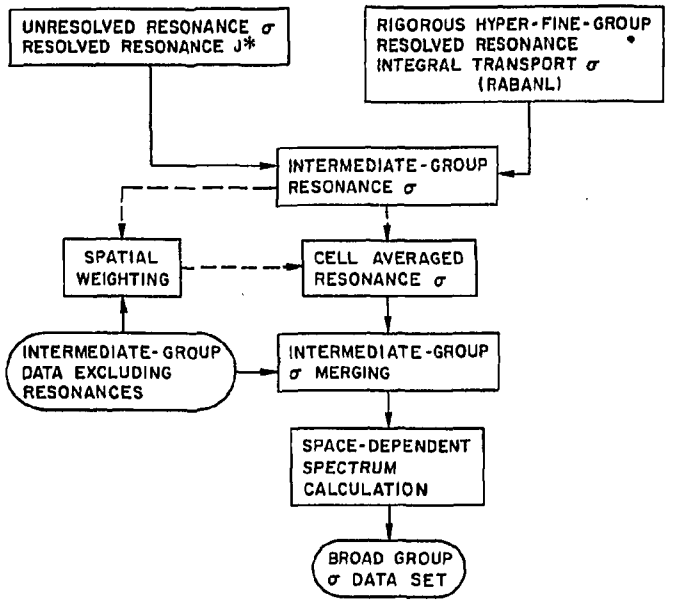

Fig. 5

SDX Program Flow

intermediate-group level for each plate or pin type (using equivalence theory) or homogeneous mixture in each region of a multiregion problem. As Fig. 1 indicates, the resonance calculation in SDX uses the same program modules as MC^2-2. In particular, either the narrow resonance J*-integral treatment or the rigorous RABANL treatment may be used to provide the composition and temperature dependent resonance cross sections. Intermediate-group resonance cross- sections are calculated assuming a constant collision density per unit lethargy in SDX rather than by use of the attenuation treatment described earlier in MC^2-2. Thus the resonance algorithms employed in the SDX calculation combine a high degree of accuracy with modest computational time. It is assumed in the SDX option that all the remaining cross sections are composition independent on the intermediate-group level and that the intermediate-group spectrum will adequately reflect the composition-dependence for the purpose of obtaining broad-group cross sections. For current applications, intermediate-group cross-section libraries on the order of 150 to 200 groups have been generated. These libraries adequately "trace out" the higher energy scattering resonances in intermediate mass nuclei. The intermediate-group cross-section libraries may be constructed from MC^2-2 ultra-fine group calculations as indicated in Fig. 1 or any other code which creates a cross-section file in the proper format.

Three options exist in SDX with respect to unit cell homogenization:

(1) A homogeneous mixture may be specified in which case resonance cross sections are computed for a homogeneous mixture and simply combined with the intermediate-group library data (i.e., no unit cell homogenization).

(2) If a heterogeneous unit cell is specified, heterogeneous resonance cross sections are computed for selected isotopes in the specified plate/pin types using equivalence theory or the rigorous RABANL heterogeneous treatment. These resonance cross sections are combined with the intermediate-group library data and an infinite slab or cylinder integral transport calculation is performed for the unit cell. Spatial self-shielding factors and cell-averaged intermediate-group cross sections are calculated. The integral transport calculation is based on a modified version of the code CALHET[21] which makes use of the collision probability methods developed for RABANL.

(3) The integral transport calculation described in item (2) may be omitted and volume averaging used to obtain all cross sections.

The intermediate-group library data and cell-averaged resonance cross sections are input to a one-dimensional diffusion theory calculation. The space-dependent calculation employs the space-energy factorization[22] approximation optionally as a final solution or as a means for accelerating the direct intermediate-group solution, and employs power iteration with Chebyshev acceleration. A fundamental mode option is available for space-independent solutions. A modified version of the SEF1D code[22] is used for the space-dependent calculation. Broad-group microscopic cross sections are averaged over the intermediate-group spectrum and over user-specified spatial regions with cross sections appropriate to individual plates/pins available on option.

SDX has also been extended to provide a γ-processing capability by interfacing AMPX[24] generated files with SDX and providing a γ-source module. Use of this capability permits a consistent calculation of γ-production data accounting for the resonance and spatial self-shielding of the capture and fission cross sections.

The computing time required for an SDX calculation is dependent upon the user options as discussed above. Three sample problems have been run on the IBM-370/195 at Argonne National Laboratory to provide an indication of time requirements. All problems were run with a single 156-group cross-section library. Both the unit cell calculation and the diffusion theory spectrum calculation depend upon the number of intermediate groups. In Table 3 timing results are presented for a single-region problem in both a homogeneous and heterogeneous (12-plate) representation. The computation times for the resolved and unresolved resonance calculations increase in the heterogeneous problem since the calculation must be performed for the homogeneous mixture as well as for each resonance material in each plate. In Table 4 timings are presented for a multiregion space-dependent calculation in which each region was treated homogeneously. The simplest SDX calculation is represented by the homogeneous problem of Table 3. The most detailed calculation would include multiregion effects as in Table 4 along with a heterogeneous cell model as in Table 3.

Table 3. Fundamental Mode SDX, 12 Isotopes (time in sec)

Code Area	Homogeneous		Heterogeneous[a]	
	CPU	PP	CPU	PP
Input processor	<1	2	<1	2
Unresolved resonances	18	14	28	32
Resolved resonances	13	4	22	6
Interaction and cross-section preparation	2	9	3	13
Unit cell	-	-	36	9
Spectrum	8	7	8	7
Total	43	50	98	81

[a]Twelve plates of which seven contained resonance isotopes.

Table 4. Homogeneous, Space-Dependent SDX - 16 Isotopes, 4 Regions (time in sec)

SEF1D		Remainder		Total	
CPU	PP	CPU	PP	CPU	PP
73	23	92	126	165	149

PROGRAMMING METHODS

The ETOE-2/MC^2-2/SDX code system was developed at Argonne National Laboratory on an IBM-370/195. All programming has been done in FORTRAN and has rigorously adhered to the standards established by the Committee on Computer Code Coordination (CCCC).[25] In addition, considerable effort was expended to produce a code which may be implemented as simply as possible on other computers.

The entire code is variably dimensioned through use of the subprogram package BPOINTER.[26] All binary I/O is performed by subroutine calls to the standard CCCC routines REED/RITE[25] so that great flexibility is provided in specifying installation-dependent data management strategies. The standard CCCC routine TIMER[25] has been used for installation-dependent timing function. Extensive use has been made of comment cards in order to make the codes as self-documenting as possible (approximately one-third of the more than 50,000 source cards of MC^2-2 are comments).

As ponted out above, the input to the code system is an ENDF/B data file. Broad-group cross-section files are output by the code system in either the ARC System XS.ISO format[25] or the ISOTXS format[24] specified by the CCCC. BCD input is prepared according to standard ARC System conventions.[26]

The code system is operational at ANL (IBM), SLAC (IBM), LRL Berkeley (CDC), BNL (CDC), and is available from the Argonne Code Center and the NEA ISPRA Code Center. The program package includes ETOE-2 processed data for the ENDF/B Version IV data. Modifications to ETOE-2 and MC^2-2 are underway to permit processing of ENDF/B Version V data which is scheduled for release during CY 1978. The modified code and data will be made available through the ANL and ISPRA Code Centers.

REFERENCES

1. D. Garber, C. Dunford, and S. Pearlstein, ENDF-102 Data Formats and Procedures for the Evaluated Nuclear Data File, ENDF, BNL-NCS-50496 (ENDF 102) (October 1975).

2. B. J. Toppel and R. N. Hwang, "Considerations Pertinent to Rigorous and Efficient Structural Doppler Effect Calculations," Trans. Am. Nucl. Soc. 26, 540 (1977).

3. G. DeSaussure and R. B. Perez, POLLA, A Fortran Program to Convert R-Matrix-Type Multilevel Resonance Parameters for Fissile Nuclei into Equivalent Kupur-Peierls-Type Parameters, ORNL-TM-2599 (1969).

4. D. M. Green and T. A. Pitterle, ETOE, A Program for ENDF/B to MC^2, APDA-219 (ENDF-120) (1968).

5. E. M. Pennington, J. C. Gajniak, A. B. Cohen, and W. Bohl, Service Routines for the Multigroup Code MC^2, ANL-7654 (April 1970).

6. B. J. Toppel, A. L. Rago, and D. M. O'Shea, MC^2 - A Code to Calculate Multigroup Cross Sections, ANL-7318 (June 1967).

7. H. Henryson II, B. J. Toppel, and C. G. Stenberg, MC^2-2: A Code to Calculate Fast Neutron Spectra and Multigroup Cross Sections, ANL-8144 (ENDF 239) (June 1976).

8. W. M. Stacey, Jr., "Continuous Slowing-Down Theory for Anisotropic Elastic Neutron Moderation in the P_N and B_N Representations," Nucl. Sci. Eng. 41, 381 (1970).

9. W. M. Stacey, Jr., "Continuous Slowing-Down Theory Applied to Fast Reactor Assemblies," Nucl. Sci. Eng. 41, 381 (1970).

10. G. Goertzel and E. Grueling, "An Approximate Method for Treating Slowing Down," Nucl. Sci. Eng. 7, 69 (1960).

11. R. N. Hwang, "Efficient Methods for the Treatment of Resonance Cross Sections," Nucl. Sci. Eng. 52, 157 (1973).

12. D. B. Adler and F. T. Adler, Neutron Cross Sections in Fissile Elements, Proc. Conf. on Breeding and Economics in Large Fast Reactors, ANL-6792, 695 (1963).

13. K. Gregson, M. F. James, and D. S. Norton, MLBW - A Multilevel Breit-Wigner Computer Programme, AEEW-M-517 (March 1965).

14. F. J. Dyson, "Statistical Theory Levels of Complex Systems, III," J. Math. Phys. 3, 166 (1962).

15. W. M. Stacey, Jr. "Resolved Narrow Resonance Reaction Rates in Fast Reactor Mixtures," Nucl. Sci. Eng. 41, 455 (1970).

16. H. Henryson II, C. G. Stenberg, and B. J. Toppel, Calculation of Elastic Scattering Matrices, ANL-7710, 395 (1971).

17. H. Henryson II, "Multigroup Elastic Scattering Cross Sections for Heavy Elements," Nucl. Sci. Eng. 43, 235 (1971).

18. A. P. Olson, RABID: An Integral Transport-Theory Code for Neutron Slowing Down in Slab Cells, ANL-7645 (1970).

19. P. H. Kier and A. A. Robba, RABBLE, A Program for Computation of Resonance Absorption in Multigroup Reactor Cells, ANL-7326 (1967).

20. R. N. Hwang and B. J. Toppel, "Asymptotic Behavior of Transmission Probabilities for Annular Regions, Trans. Am. Nucl. Soc. 23, 525 (1976).

21. F. L. Fillmore, The CALHET-2 Heterogeneous Perturbation Theory Code and Application to ZPR-3-48, AI-69-13 (1969).

22. W. M. Stacey, Jr. and H. Henryson II, Applications of Space-Energy Factorization to the Solution of Static Fast Reactor Neutronics Problems, Proc. Conf. New Developments in Reactor Mathematics and Applications, Idaho Falls, CONF-710302, Vol. 2, 953 (1971).

23. W. M. Stacey, Jr. and H. Henryson II, "Application of Space-Energy Factorization to LMFBR Diffusion Theory Calculations," Trans. Am. Nucl. Soc. 14, 205 (1971).

24. N. M. Greene, J. L. Lucius, L. M. Petrie, W. E. Ford, III, J. E. White, and R. Q. Wright, AMPX: A Modular Code System for Generating Coupled Multigroup Neutron-Gamma Libraries from ENDF/B ORNL-TM-3706 (March 1976).

25. R. Douglas O'Dell, Standard Interface Files for Reactor Physics Codes, Version IV, LA-6941-MS, UC-32 (September 1977).

26. L. C. Just, H. Henryson II, A. S. Kennedy, S. D. Sparck, B. J. Toppel, and P. M. Walker, The System Aspects and Interface Data Sets of the Argonne Reactor Computation (ARC) System, ANL-7711 (April 1971).

Dup

-2

PRODUCTION OF MULTI-GROUP DATA AT LIVERMORE*

Peter C. Giles
Lawrence Livermore Laboratory
Livermore, California, U.S.A.

ABSTRACT

The Livermore evaluated nuclear data library (ENDL) is used at Livermore as a source of data from which multi-group parameters are derived for use in a variety of transport codes which in terms of methods span the gamut from Monte Carlo to S_n to diffusion and in terms of particles considered includes neutrons, photons and/or charged particles.

In order to service all of these application areas a system of computer codes have been in operation for some time. This paper will discuss the initial design philosophy and goals of this system, its present status and future projected features.

The CLYDE code has been developed to handle a broad range of cross section processing requirements. These run the gamut of data tables for Monte Carlo to S_n to Diffusion codes. The present version processes neutron and gamma interactions from neutron-induced reactions. The code is operable on the CDC-7600, and occupies about 155k (octal) of SCM; 460k (octal) words of LCM are available for storage and working arrays.

The evaluated cross sections that are input to CLYDE may appear on either cards, tape, or disk, but they must be in the format of the Evaluated Nuclear Data Library (ENDL). ENDL is described in LLL report UCRL-50400, Vol. 4 (1971). Furthermore, the user must specify group boundaries, weighting fluxes, and the isotopes for which the processed data are required. The atomic mass for each isotope is carried with the isotope in the evaluated library. Standard sets of group boundaries and weighting fluxes are also maintained. There is, incidentally, a preprocessor (ENDFLLL) available to translate ENDF/B library data into the ENDL input format, and vice versa.

The output from CLYDE is flux-averaged group cross sections, transfer probabilities, energy depositions, particle and isotope cross sections, isotope destruction cross sections, and appropriate averages of collateral quantities such as the average number of neutrons per fission. The code

---

* Work performed under the auspices of the U.S. Department of Energy by the Lawrence Livermore Laboratory under contract number W-7405-ENG-48.

processes data for transport theory, diffusion theory or Monte Carlo applications to neutronic systems, shielding, and fusion research.

The design philosophy behind the CLYDE code encompasses these points:

a) It is designed to be unlimited in the amount of data it can handle, and in the number of groups and order of transfer matrices that it can generate.

b) It is designed to calculate the group constants for any isotope with a standard group structure and scattering order in a reasonable amount of computer time.

c) Built-in rigidity with regard to particular models or parameters is not allowed.

d) Redundancy in input information is allowed in the evaluated library, but is not processed in CLYDE.

e) Output is provided in two general formats for the S_n/Dn (deterministic) codes. CTART produces Monte Carlo output. Card, disc, or tape output are all available, and with each option printouts are produced that include all pertinent information in a convenient form.

Conditions (b) and (c) are satisfied by transferring certain specific model calculations to preprocessor codes. These codes perform appropriate operations to produce basic microscopic data from models and/or recipes. Their results are stored in ENDL. Or these results may be used as card input to CLYDE if it is undesirable to place them in the library. Some of these preprocessor functions are:

a) To convert angular distributions to Legendre coefficients, incorporating fitting and thinning procedures (UPDATE).

b) To process scattering kernels for the more time-consuming multibody transfer processes (e.g., n,2n); and, to generate the correlated energy-angle Legendre expansions of the kernels (FIRST and DECAY).

c) To generate thermal scattering kernels from $S(\alpha,\beta)$ data (FLANGELLL).

d) To generate differential angular probability data from Legendre expansion coefficients (UPDATE).

e) To generate energy tables for the emitted neutrons from fission (FISPEC).

f) To calculate average energy depositions from neutron induced reactions (ENDEP).

g) To generate "cold" cross section data from resonance parameters (resolved or unresolved) (ENDFLLL).

Where is CLYDE going? We will be elaborating our charged particle interaction file (presently an addendum to ENDL). Part of the user community at LLL is interested in charged particle scattering matrices for both scattered particle and knockon, and for other appropriate group constants (e.g., reaction cross sections). EGDL is the gamma analogue to the ENDL file. We intend that CLYDE be able to operate on EGDL and ENDL files to produce a complete set of nuclear group constants, whether neutron, gamma, or charged particle initiated. It now handles neutron and photon data. For charged particles, our initial efforts include data for the hydrogen and helium isotopes. We may proceed in Z beyond that, thinking, for example, of potential medical physics requirements.

Plans for CLYDE also include an abbreviated operation which would provide activation group constants; essentially the usual reaction and destruction cross sections, but without transfer matrices. The base data file (ACTL) presently exists.

Other improvements include an improved Doppler broadening subroutine (SIGMA1). We may try to include some kind of Bonderenko self-shielding.

Finally, there are some almost "cosmetic" improvements which need to be made. We expect to realize some timing improvement, especially with higher order output. We now use double, even triple precision routines for some of our integrals. We have available some more sophisticated algorithms which require only single precision, and which should be implemented soon. Lastly, CLYDE is a user code. Unless program proprietors want to become involved in every users dalliance with their code, it is essential that simple instructions, complete diagnostic and error comments, and reasonable drop-through options be provided. We intend to put considerable effort into these last items.

NEW RESONANCE CROSS SECTION CALCULATIONAL ALGORITHMS *

by
Donald R. Mathews
General Atomic Co.
P.O. Box 81608
San Diego, Calif. 92138

Improved resonance cross section calculational algorithms have been developed and tested for inclusion in a fast reactor version of the MICROX code[1]. The resonance energy portion of the MICROX code solves the neutron slowing down equations for a two region lattice cell on a very detailed energy grid (about 14500 energies). In the MICROX algorithms, the exact P_0 elastic scattering kernels are replaced by synthetic (approximate) elastic scattering kernels which permit the use of an efficient and numerically stable recursion relation solution of the slowing down equations. In the work described here, the MICROX algorithms have been modified to include:

1. An additional delta function term in the P_0 synthetic scattering kernel per a suggestion by Turinsky and Roman [2]. The additional delta function term allows one more moment of the exact elastic scattering kernel to be preserved without much extra computational effort. With the improved synthetic scattering kernel, the flux returns more closely to the exact flux below a resonance than with the original MICROX kernel.

2. The slowing down calculation has been extended to a true B_1 hyper-fine energy grid calculation in each region using P_1 synthetic scattering kernels and transport-corrected P_0 collision probabilities to couple the two regions.

* Work Supported by the Department of Energy, Contract EY-76-C-03-0167.

BLANK PAGE

1. INTRODUCTION:

The algorithms described here have been incorporated into a new code called SKM2. The SKM2 code is effectively a modernized GAROL code[3].

The original version of the SKM code was written by P. Walti as part of the development of the MICROX code[1]. The SKM code solved the neutron slowing down equations for a two-region lattice cell on a very detailed energy grid in the resonance energy region. Spatially flat and isotropic neutron emission densities in each region were assumed for evaluating the P_0 collision probabilities used to couple the fluxes in the two region cell. A second level of heterogeneity was also treated, i.e., one region could have imbedded grains(particles). The effect of neutron leakage was approximated by the addition of a DB^2 absorption term. The input cross sections were read from a 9000 energy ($\Delta u = 0.001$) GAR data tape[4] prepared by the GAND code[5]. Isotropic in the center of mass coordinate system P_0 elastic scattering was assumed for the neutron slowing down process. The exact elastic scattering kernels were replaced by synthetic (approximate) elastic scattering kernels which permitted a very rapid evaluation of the slowing down integrals via an efficient and numerically stable recursion relation.

The development of a more accurate synthetic scattering kernel, extension to true B_1 calculation in each region, and results for an HTGR test problem follow.

2. NEW SYNTHETIC SCATTERING KERNEL ALGORITHMS

2.1 Exact Elastic Scattering Kernels

The $\ell=0(P_o)$ Legendre moment of the exact isotropic in the center-of-the mass coordinate system elastic scattering kernel is

$$P_o(u\to u') = \frac{\theta(u'-u)\theta(q-u'+u)}{1-\alpha} e^{-(u'-u)} \tag{2.1}$$

where

$$\alpha \equiv \left(\frac{A-1}{A+1}\right)^2 \tag{2.2}$$

$$q \equiv -\ell n\ \alpha \tag{2.3}$$

$$\theta(x) \equiv \begin{cases} 1 \text{ for } x \geq 0 \\ 0 \text{ for } x < 0 \end{cases} \tag{2.4}$$

and A is the atomic mass of the nuclide in question (in units of the mass of the neutron). Equation (2.1) is identifiable as isotropic in the center-of-mass system neutron scatter from a zero temperature free gas. The $\ell=1(P_1)$ Legendre moment of the exact kernel is

$$P_1(u\to u') = \frac{\theta(u'-u)\theta(q-u'+u)}{2(1-\alpha)} \left[(A+1)e^{-(3/2)(u'-u)} - (A-1)e^{-(1/2)(u'-u)}\right] \tag{2.5}$$

2.2 Lethargy Moments of the Exact Kernels

The n^{th} lethargy moment of a scattering kernel will be defined here as

$$I_\ell^{(n)} \equiv \int_u^\infty (u'-u)^n P_\ell(u\to u')du'. \tag{2.6}$$

Analytic expressions for the n = 0, 1, 2 lethargy moments of the exact P_o and P_1 elastic scattering kernels are given in Table 1.

TABLE 1

Lethargy Moments of the Exact Elastic Scattering Kernels

QUANTITY	$A \neq 1$	$A = 1$	$A \gg 1$
$I_0^{(0)}$	1	1	1
$I_0^{(1)}$	$1 + \frac{\alpha}{1-\alpha}\ell n\alpha$	1	$\frac{2}{A}$
$I_0^{(2)}$	$2 + \frac{\alpha}{1-\alpha}\ell n\alpha(2-\ell n\alpha)$	2	$\frac{16}{3A^2}$
$I_1^{(0)}$	$\frac{2}{3A}$	$\frac{2}{3}$	$\frac{2}{3A}$
$I_1^{(1)}$	$-\frac{(A-1)^2(A+2)}{6 \cdot A}\ell n\alpha + \frac{10}{9 \cdot A} - \frac{2 \cdot A}{3}$	$\frac{4}{9}$	$-\frac{2}{3A}$
$I_1^{(2)}$	$\frac{(A-1)^2(A+2)}{6 \cdot A}(\ell n\alpha)^2 - \frac{2(A-1)^2(4A+5)}{9 \cdot A}\ell n\alpha - \frac{32 \cdot A}{9} + \frac{112}{27 \cdot A}$	$\frac{16}{27}$	$-\frac{8}{3A^2}$

2.3 Revised Synthetic Scattering Kernels

The Turinsky-Roman synthetic scattering kernel is[2]

$$p(u\to u') = \theta(u'-u)\left[f\cdot\delta(u'-u) + \text{Real}\left\{ghe^{-g(u'-u)}\right\}\right] \qquad (2.7)$$

where the constants f, g and h depend upon the nuclide mass A but not upon lethargy. Note that g and h are complex.

Wälti's synthetic scattering kernel has the same form as the Turinsky-Roman kernel except that the real constant f in Eq. (2.6) is taken to be zero (no delta function term).

In the SKM2 code, the P_o and P_1 synthetic scattering kernels are both assumed to be of the functional form of Eq. (2.6). Only the numerical values of the constants differ between the P_o and P_1 kernels. The subscript denoting the Legendre moment index will be omitted in the following discussion to simplify the notation.

The values of the constants appearing in Eq. (2.6) are determined in the same manner as in the original Wälti derivation[1] except that one more lethargy moment of the exact scattering kernel may now be matched by the synthetic kernel because of the extra delta function term.

Using Eq. (2.7) in Eq. (2.6) yields the following expression for the lethargy moments of the Turinsky-Roman synthetic scattering kernel

$$I^{(o)} = f + h_r \qquad (2.8)$$

$$I^{(1)} = \frac{h_r g_r + h_i g_i}{g_r^2 + g_i^2} \qquad (2.9)$$

$$I^{(2)} = \frac{2h_r(g_r^2 - g_i^2) + 4h_i g_r g_i}{(g_r^2 + g_i^2)^2} \qquad (2.10)$$

where the r and i subscripts denote the real and imaginary parts of g and h, respectively.

After equating Eqs. (2.8) through (2.10) to the expressions for the lethargy moments of the exact kernels given previously, we now have three equations for the determination of 5 unknowns (f, g_r, g_i, h_r and h_i).

Following Wälti, the values of g_r and g_i are obtained from a least squares fit of the synthetic kernel to the exact kernel. This means that

$$\varepsilon^2(u) = \int_u^\infty \left\{ \text{Real}\left[g h e^{-g(u'-u)} \right] - p^{\text{exact}}(u \to u') \right\}^2 du' \qquad (2.11)$$

should be minimized with respect to g. The P_o results obtained by Wälti for this minimization problem were expressed in the approximate forms

$$g_r = \begin{cases} 1 & \text{for } A=1 \\ (1.10 - 0.50/A)/I_o^{(1)} & \text{for } A \geq 2 \end{cases} \qquad (2.12)$$

$$g_i = \begin{cases} 0 & \text{for } A=1 \\ (1.64 - 0.24/(A-1.2))/q & \text{for } A \geq 2. \end{cases} \qquad (2.13)$$

The P_1 results obtained by Wälti were that the P_1 values of g_r and g_i may be assumed to be the same as the P_o values for $A \geq 2$ and that $g_r = 3/2$, $g_i = 0$ for $A=1$. Note that the P_o and P_1 synthetic kernels are exact for $A=1$ (hydrogen).

For given values of g_r and g_i obtained from the least squares fitting process, Eqs. (2.9) and (2.10) may be solved for h_r and h_i in the forms

$$h_r = 2g_r I^{(1)} - (1/2)(g_r^2 + g_i^2) I^{(2)} \qquad (2.14)$$

$$h_i = \begin{cases} 0 & \text{for } A=1 \\ \left[-(g_r^2 - g_i^2) I^{(1)} + (1/2) g_r (g_r^2 + g_i^2) I^{(2)} \right] / g_i & \text{for } A \geq 2 \end{cases} \qquad (2.15)$$

following which Eq. (2.8) yields

$$f = I^{(o)} - h_r. \qquad (2.16)$$

Turinsky and Roman chose to perform the minimization of Eq. (2.11) with respect to h rather than g. This approach leads to somewhat more complicated expressions for the various constants which they solved by

an iterative scheme. Wälti's approach seems preferable on physical grounds. The constant g appears in an exponential and contains the main information about the shape of the synthetic kernel whereas the constant h is primarily a normalization factor. It therefore seems more appropriate to perform the least squares fit to the exact kernel in terms of the "shape" parameter g rather than the "amplitude" parameter h.

Results obtained with the SKM2 code are thus not precisely comparable to those obtained by Turinsky and Roman because of differences in the method of choosing the synthetic kernel parameters even though in both schemes the 0^{th} through 2^{nd} lethargy moments of the exact kernel are preserved along with a least squares fit to the exact kernel.

2.4 Revised Slowing Down Source Recursion

Let the Turinsky-Roman synthetic scattering kernel be represented by

$$p(u) = f\cdot\delta(u) + \theta(u)\ \text{Real}\left[ghe^{-gu}\right] \tag{2.17}$$

where

$$\theta(u) = \begin{cases} 1 \text{ for } u\geq 0 \\ 0 \text{ for } u<0 \ . \end{cases} \tag{2.18}$$

The complex slowing down source to a given lethargy u is

$$H(u) = \int_{-\infty}^{u} F(u') \left[f\cdot\delta(u-u') + ghe^{-g(u-u')}\right] du' \tag{2.19}$$

or

$$H(u) = f\cdot F(u) + \int_{-\infty}^{u} F(u')\ ghe^{-g(u-u')}du' \tag{2.20}$$

where

$$F(u') \equiv \phi(u')\Sigma_s(u') \ . \tag{2.21}$$

Similarly

$$H(u+\Delta) = f\cdot F(u+\Delta) + \int_{-\infty}^{u+\Delta} F(u')ghe^{-g(u+\Delta-u')}du' \tag{2.22}$$

or

$$H(u+\Delta)=f\cdot F(u+\Delta)+e^{-g\Delta}\int_{-\infty}^{u} F(u')ghe^{-g(u-u')}du'+\int_{0}^{\Delta}F(u+\Delta-v)ghe^{-gv}dv \tag{2.23}$$

where

$$v \equiv u+\Delta-u' . \tag{2.24}$$

Using Eq. (2.20) in Eq. (2.23) yields

$$H(u+\Delta) = f\cdot F(u+\Delta) + e^{-g\Delta}\left[H(u)-f\cdot F(u)\right] + \int_0^{\Delta} F(u+\Delta-v)\,ghe^{-gv}dv \tag{2.25}$$

Let the scattering density F(u) be represented by a linear function of u in the interval of u to u+Δ, i.e., let

$$F(u') = a + bu' \tag{2.26}$$

or

$$F(u+\Delta-v) = F(u+\Delta) + \left[F(u) - F(u+\Delta)\right]\left(\frac{v}{\Delta}\right) \tag{2.27}$$

With this assumption the last integral in Eq. (2.25) becomes

$$\int_0^{\Delta} F(u+\Delta-v)\,ghe^{-gv}dv = F(u+\Delta)h\left[1-\left(\frac{1-e^{-g\Delta}}{g\Delta}\right)\right] + F(u)\,h\left[\left(\frac{1-e^{-g\Delta}}{g\Delta}\right)-e^{-g\Delta}\right] \tag{2.28}$$

Now define

$$A(g\Delta) \equiv 1-\left(\frac{1-e^{-g\Delta}}{g\Delta}\right) \tag{2.29}$$

and

$$B(g\Delta) \equiv \left(\frac{1-e^{-g\Delta}}{g\Delta}\right)-e^{-g\Delta} \tag{2.30}$$

so that Eq. (2.28) becomes

$$H(u+\Delta)=e^{-g\Delta}\cdot H(u)+F(u)\left[B(g\Delta)h-f\cdot e^{-g\Delta}\right] + F(u+\Delta)\left[A(g\Delta)h+f\right] . \tag{2.31}$$

To obtain a recursion similar to Wälti's, set

$$\hat{A}(g\Delta)\equiv A(g\Delta)h+f \tag{2.32}$$

and

$$\hat{B}(g\Delta) \equiv B(g\Delta)h - f\cdot e^{-g\Delta} \tag{2.33}$$

to obtain

$$H(u+\Delta)=e^{-g\Delta}H(u) + \hat{B}(g\Delta)\cdot F(u) + \hat{A}(g\Delta)\cdot F(u+\Delta). \tag{2.34}$$

For the real part of $(q\Delta) < 0.05$, the following series expansions are used in the SKIP code

$$e^{-g\Delta} \cong 1-g\Delta(1-g\Delta((1/2) - g\Delta((1/6) - (1/24)\,g\Delta))) \tag{2.35}$$

$$A(g\Delta) \cong g\Delta(1/2) - g\Delta((1/6) - g\Delta((1/24) - (1/120)\,g\Delta))) \tag{2.36}$$

$$B(g\Delta) \cong g\Delta((1/2) - g\Delta((1/3) - g\Delta((1/8) - (1/30)\,g\Delta))) \tag{2.37}$$

3. POINTWISE B_1 EQUATIONS

3.1 N-Region B_1 Equations

The B_1 equations used by the SKM2 Code were derived from the B_1 equations for a single region given in Ref. 4 by assuming P_o collision probability coupling* between regions as in the MICROX code[1]. The B_1 equations for the j^{th} of N regions may then be written in the form

$$|B|\varphi_{1j}(u) + \Sigma_{tj}(u)\varphi_{oj}(u) = \frac{1}{V_j}\sum_{i=1}^{N} V_i P_{ij}(u)\, S_{oi}(u) \qquad (3.1.a)$$

$$3\gamma_j(u)\,\Sigma_{tj}(u)\varphi_{1j}(u) - \frac{B^2}{|B|}\,\varphi_{oj}(u) = 3S_{1j}(u) \qquad (3.1.b)$$

where

$$S_{\ell j}(u) \equiv \int_{-\infty}^{u} \varphi_{\ell j}(u')\,\Sigma_{sj}(u')P_{\ell j}(u-u')du' + S^{ex}_{\ell j}(u) \qquad (3.2)$$

$$\gamma_j(u) \equiv \frac{X_j}{3\left[R(X_j)-1\right]} \qquad (3.3)$$

$$X_j \equiv \frac{B^2(u)}{\Sigma^2_{tj}(u)} \qquad (3.4)$$

$$y_j \equiv \sqrt{|X_j|} \qquad (3.5)$$

---

* The effect of anisotropic (P_1) scattering effects on the region couplings are approximated by replacing the total cross section by the transport cross section during the evaluation of the collision probabilities.[6,7,8] This refinement was used only in the thermal section of the MICROX code[1]. Except for this change, the SKM2 code uses the collision probability calculational algorithms described in Ref. 1.

$$R(X_j) \equiv \begin{cases} \dfrac{y_j}{\tan^{-1} y_j} & \text{for } X_j > 0 \\ \dfrac{y}{\tanh^{-1} y_j} & \text{for } X_j < 0 \end{cases} \tag{3.6}$$

For $|X_j| < 0.25$

$$\gamma_j(u) = 1 + \frac{\frac{4}{15} X_j - \frac{8}{35} X_j^2 + \frac{4}{21} X_j^3}{1 - \frac{3}{5} X_j + \frac{3}{7} X_j^2 - \frac{1}{3} X_j^3} \tag{3.7}$$

Using (3.2) in (3.1.a) and (3.1.b) and dropping references to the lethargy u at which the fluxes are being computed yields

$$|B|\phi_{1j} + \Sigma_{tj}\phi_{oj} = \sum_{i=1}^{N} \frac{V_i}{V_j} P_{ij} \left\{ \int_{-\infty}^{u} \phi_{oi}(u')\Sigma_{si}(u')p_{oi}(u-u')du' + S_{oi}^{ex} \right\} \tag{3.8.a}$$

$$\gamma_j \Sigma_{tj}\phi_{1j} - \frac{1}{3}\frac{B^2}{|B|}\phi_{oj} = \int_{-\infty}^{u} \phi_{1j}(u')\Sigma_{sj}(u')P_{1j}(u-u')du' + S_{1j}^{ex} \tag{3.8.b}$$

Now define the scattering kernels to be approximate (synthetic) kernels of the Turinsky-Roman form discussed previously, i.e.,

$$P_{\ell j}(u) \equiv f_{\ell j}\cdot\delta(u) + \vartheta(u)\cdot \text{Real}\left[g_{\ell j} h_{\ell j} e^{-g_{\ell j}\cdot u}\right] \tag{3.9}$$

where the $f_{\ell j}$ are real constants, $\delta(u)$ is the Dirac delta function, $\vartheta(u)$ is the Heaviside function defined by

$$\vartheta(u) = \begin{cases} 1 \text{ for } u > 0 \\ 0 \text{ for } u < 0 \end{cases} \tag{3.10}$$

and the $g_{\ell j}$ and $h_{\ell j}$ are complex constants. Further define the complex slowing down sources

$$H_{\ell j}(u) \equiv \phi_{\ell j}(u)\Sigma_{sj}(u)f_{\ell j} + g_{\ell j}h_{\ell j}\int_{-\infty}^{u}\phi_{\ell j}(u')\Sigma_{sj}(u')e^{-g_{\ell j}(u-u')}du' \tag{3.11}$$

and now that

$$S_{\ell j}(u) = \text{Real}\left[H_{\ell j}(u)\right] + S^{ex}_{\ell j}(u) \tag{3.12}$$

As shown in the previous section, the $H_{\ell j}(u)$ obey the following recursion relation

$$H_{\ell j}(u+\Delta) = e^{-g_{\ell j}\Delta}H_{\ell j}(u) + D_{\ell j}\phi_{\ell j}(u) + A_{\ell j}\phi_{\ell j}(u+\Delta) \tag{3.13}$$

where

$$D_{\ell j} \equiv \Sigma_{sj}(u)\left\{h_{\ell j}\left[\frac{1-e^{-g_{\ell j}\Delta}}{g_{\ell j}\Delta} - e^{-g_{\ell j}\Delta}\right] - f_{\ell j}e^{-g_{\ell j}\Delta}\right\} \tag{3.14}$$

$$A_{\ell j} \equiv \Sigma_{sj}(u+\Delta)\left\{h_{\ell j}\left[1 - \frac{1-e^{-g_{\ell j}\Delta}}{g_{\ell j}\Delta}\right] + f_{\ell j}\right\} \tag{3.15}$$

If we further define

$$C_{\ell j} \equiv D_{\ell j}\phi_{\ell j}(u) + e^{-g_{\ell j}\Delta}H_{\ell j}(u) \tag{3.16}$$

then Eq. (3.13) becomes

$$H_{\ell j}(u+\Delta) = A_{\ell j}\phi_{\ell j}(u+\Delta) + C_{\ell j} \tag{3.17}$$

Using the above definitions in Eqs. (3.8.a) and (3.8.b) yields

$$|B|\phi_{1j} + \Sigma_{tj}\phi_{oj} = \sum_{i=1}^{N}\frac{V_i}{V_j}P_{ij}\left\{\text{Real}\left[H_{oi}(u)\right] + S^{ex}_{oi}\right\} \tag{3.18.a}$$

$$\gamma_j\Sigma_{tj}\phi_{1j} - \frac{1}{3}\frac{B^2}{|B|}\phi_{oj} = \text{Real}\left[H_{1j}(u)\right] + S^{ex}_{1j} \tag{3.18.b}$$

Rewriting Eqs. (3.18.a) and (3.18.b) at $u+\Delta$ and using Eq. (3.17) yields

$$|B(u+\Delta)|\phi_{ij}(u+\Delta)+\Sigma_{tj}(u+\Delta)\phi_{oj}(u+\Delta) = \sum_{i=1}^{N}\frac{V_i}{V_j}P_{ij}\left\{\phi_{oi}(u+\Delta)\text{Real}\left[A_{oi}\right] + \text{Real}\left[C_{oi}\right] + S^{ex}_{oi}(u+\Delta)\right\} \tag{3.19.a}$$

$$\gamma_j(u+\Delta)\Sigma_{tj}(u+\Delta)\phi_{1j}(u+\Delta) - \frac{1}{3}\frac{B^2(u+\Delta)}{|B(u+\Delta)|}\phi_{oj}(u+\Delta)=\phi_{1j}(u+\Delta)\text{Real}\left[A_{1j}\right]$$
$$+\text{Real}\left[C_{1j}\right]+ S_{1j}^{ex}(u+\Delta) \qquad (3.19.b)$$

Collecting terms and dropping references to u+Δ

$$|B|\phi_{1j} + \left\{\Sigma_{tj} - P_{jj}\text{Re}\ (A_{oj})\right\}\phi_{oj} - \sum_{i\neq j}\frac{V_i}{V_j}P_{ij}\phi_{oi}\text{Re}(A_{oi}) =$$

$$\sum_{i=1}^{N}\frac{V_i}{V_j}P_{ij}\left\{\text{Re}(C_{oi}) + S_{oi}^{ex}\right\} \qquad (3.20.a)$$

$$\left\{\gamma_j\Sigma_{tj} - \text{Re}(A_{1j})\right\}\phi_{1j} - \frac{1}{3}\frac{B^2}{|B|}\phi_{oj} = \text{Re}(C_{1j}) + S_{1j}^{ex} \qquad (3.20.b)$$

From Eq. (3.20.b) we have

$$|B|\phi_{1j} = \frac{\frac{B^2}{3}\phi_{oj} + |B|\left[\text{Re}(C_{1j}) + S_{1j}^{ex}\right]}{\gamma_j\Sigma_{tj} - \text{Re}\ (A_{1j})} \qquad (3.21)$$

Using Eq. (3.21) in Eq. (3.20.a) yields

$$\left\{\frac{B^2}{3\left[\gamma_j\Sigma_{tj} - \text{Re}(A_{1j})\right]} + \Sigma_{tj} - P_{jj}\text{Re}(A_{oj})\right\}\phi_{oj}$$

$$-\sum_{i\neq j}\frac{V_i}{V_j}P_{ij}\phi_{oi}\text{Re}(A_{oi}) = \qquad (3.22)$$

$$\sum_{i=1}^{N}\frac{V_i}{V_j}P_{ij}\left\{\text{Re}(C_{oi}) + S_{oi}^{ex}\right\} - \frac{|B|\left[\text{Re}(C_{1j})+S_{1j}^{ex}\right]}{\gamma_j\Sigma_{tj} - \text{Re}(A_{1j})}$$

Eq. (3.22) and then (3.21) are the B_1 equations for N regions (j=1, ..., N) coupled by P_o collision probabilities (P_{ij}'s) and using a slowing down source recursion (Eq. 3.16) made possible by assuming approximate separable (synthetic) scattering kernels.

3.2 Two-Region B_1 Equations

Specializing to 2 regions, we have

$$\left\{\frac{B^2}{3[\gamma_1\Sigma_{t1}-\mathrm{Re}(A_{11})]}+\Sigma_{t1}-P_{11}\mathrm{Re}(A_{01})\right\}\phi_{01}-\frac{V_2}{V_1}P_{21}\phi_{02}\mathrm{Re}(A_{02})=Q_{01} \qquad (3.23.a)$$

$$\left\{\frac{B^2}{3[\gamma_2\Sigma_{t2}-\mathrm{Re}(A_{12})]}+\Sigma_{t2}-P_{22}\mathrm{Re}(A_{02})\right\}\phi_{02}-\frac{V_1}{V_2}P_{12}\phi_{01}\mathrm{Re}(A_{01})=Q_{02} \qquad (3.23.b)$$

where

$$Q_{oj}\equiv\sum_{i=1}^{2}\frac{V_i}{V_j}P_{ij}\left\{\mathrm{Re}(C_{oi})+S_{oi}^{ex}\right\}-\frac{|B|\left[\mathrm{Re}(C_{1j})+S_{1j}^{ex}\right]}{\gamma_j\Sigma_{tj}-\mathrm{Re}(A_{1j})} \qquad (3.24)$$

Solving Eqs. (3.23.a) and (3.23.b) for ϕ_{01} and ϕ_{02} yields

$$\phi_{01}=\frac{\left\{\frac{B^2}{3[\gamma_2\Sigma_{t2}-\mathrm{Re}(A_{12})]}+\Sigma_{t2}-P_{22}\mathrm{Re}(A_{02})\right\}Q_{01}+\frac{V_2}{V_1}P_{21}\mathrm{Re}(A_{02})Q_{02}}{E} \qquad (3.25.a)$$

$$\phi_{02}=\frac{\left\{\frac{B^2}{3[\gamma_1\Sigma_{t1}-\mathrm{Re}(A_{11})]}+\Sigma_{t1}-P_{11}\mathrm{Re}(A_{01})\right\}Q_{02}+\frac{V_1}{V_2}P_{12}\mathrm{Re}(A_{01})Q_{01}}{E} \qquad (3.25.b)$$

where

$$E\equiv\left\{\frac{B^2}{3[\gamma_1\Sigma_{t1}-\mathrm{Re}(A_{11})]}+\Sigma_1-P_{11}\mathrm{Re}(A_{01})\right\}\left\{\frac{B^2}{3[\gamma_2\Sigma_{t2}-\mathrm{Re}(A_{12})]}+\Sigma_{t2}-P_{22}\mathrm{Re}(A_{02})\right\}$$

$$-P_{21}\mathrm{Re}(A_{02})P_{12}\mathrm{Re}(A_{01}) \qquad (3.26)$$

4. TEST PROBLEM RESULTS

4.1 Fort St. Vrain HTGR Test Problem

The test problem results presented in this section represent a comparison of selected results from the MICROX code[8], the GGC-5 code[9], the original SKM code and the SKM2 code.

The four-nuclide test problem, which is a simplification of typical Fort St. Vrain reactor problems, is defined by the following data.

Geometry	Cylinder
Diameter of the fuel grains	400 microns
Volume fraction of grains in the rods	0.1027
Diameter of the fuel rods	1.27 cm
Volume fraction of the rods	0.20
Dancoff correction factor	0.42
Buckling	0.0 cm^{-2}
Fission source	U-235
Temperature	1100°K

The broad group energy structure and core composition used for the problem are given in Tables 4.1 and 4.2 respectively.

GGC-5 included a GANDY unresolved resonance calculation for thorium in fine groups 53-63. The value of $\sigma_{m_{eff}}$ was 734 barns and the resonance parameters were chosen so as to reproduce the GAM infinite dilution cross sections.

The GAROL resolved resonance calculation for thorium in GGC-5 (fine groups 64-92) was modified to include the grain-shielding method used in MICROX (Reference *10*) in lieu of the Dyos-Pomraning treatment (Reference *11*).

TABLE 4.1

BROAD GROUP ENERGY STRUCTURE FOR THE
FORT ST. VRAIN HTGR TEST PROBLEM

Broad Group	GAM-II Fine Groups	Lower Energy (eV)
1	1-44	1.832×10^5
2	45-63	3.355×10^3
3	64-68	961.1
4	69-84	17.6
5	85-90	3.928
6	91-92	2.382

TABLE 4.2

CORE COMPOSITION FOR THE FORT ST. VRAIN
HTGR TEST PROBLEM

Nuclide	Density in the Grains [a]	Homogenized Density in the Rod	Homogenized Density in the Moderator	Cell Averaged Density
C	4.41300-2	5.78-2	6.28-2	6.180-2
Th-232	1.94742-2	2.00-3	--	4.000-4
U-235	8.18890-4	8.41-5	--	1.682-5
U-238	4.40117-5	4.52-6	--	9.040-7

a) All densities are in atoms/b-cm.

The MICROX calculation used a reference value of $\Sigma_{tot,2} = 0.2983$ cm^{-1} (macroscopic total cross section in region 2) to correspond to the Dancoff factor of 0.42.

A buckling of 0.0 cm^{-2} was chosen in order to compare GGC-5 and MICROX as closely as possible. In addition, MICROX was run with zero-temperature slowing down in the fast energy range and no thermal upscatter to the fast range was allowed. (The restriction on the thermal upscatter was made because the present version of MICROX always performs a complete calculation including both fast and thermal spectrum computations.)

The cell-averaged microscopic results for the thorium absorption cross sections and the carbon and thorium out-scattering cross sections are compared in Tables 4.3, 4.4, and 4.5, respectively. The GGC-5, GAROL and MICROX results are from Ref. 1.

The major thorium resonances are located in broad group 4 in these calculations. The group 4 thorium absorption cross section is 0.72% higher than the SKM or MICROX results. The change in the group 4 thorium absorption cross section between the SKM and SKM2 codes is due to the following effects:

1. A 1.05% decrease due to the improved synthetic scattering kernel in the SKM2 code.
2. A 1.49% increase due to the use of the transport cross section instead of the total cross section in the computation of the regionwise collision probabilities in the SKM2 code.
3. A 0.18% increase due to the use of the transport cross section in the computation of the grain shielding.

TABLE 4.3

THORIUM ABSORPTION CROSS SECTIONS FOR THE FORT ST. VRAIN HTGR TEST PROBLEM

Group	GGC-5	GAROL	MICROX	SKM	SKM2
1	0.1712	--	0.1712	--	--
2	0.6332	--	0.6357	--	--
3	1.7730	1.7731	1.7986	1.7727	1.7723
4	7.8354	7.8664	7.8556	7.8555*	7.9120
5	0.1393	0.1393	0.1393	0.1393	0.1393
6	0.2963	0.2962	0.2962	0.2962	0.2962

* 7.8636 with built-in point skipping criteria.

TABLE 4.4

Carbon P_0 Outscattering Cross Sections For The Fort St. Vrain HTGR Test Problem

Group	GGC-5	MICROX	SKM2
1	0.1986	0.1986	--
2	0.1789	0.1789	--
3	0.5964	0.5953	0.5962
4	0.1511	0.1508	0.1505
5	0.4954	0.4946	0.4948
6	1.5083	1.5046	1.5395

TABLE 4.5

Thorium P_0 Outscatter Cross Sections For the Fort St. Vrain HTGR Test Problem

Group	GGC-5	MICROX	SKM2
1	0.1827	0.1827	--
2	0.0306	0.0306	--
3	0.1148	0.0608	0.0669
4	0.0282	0.0151	0.0151
5	0.0673	0.0618	0.0618
6	0.2072	0.1923	0.1923

It should be noted that item 3 above is included in the present production version of the MICROX code. The results given in Tables 4.3, 4.4, and 4.5 are from the original version of the MICROX code. It is planned to re-run this test problem with the present production version of the MICROX code in the near future. More rigorous tests against the GAROL code with special GAR data tapes using a finer lethargy spacing are also planned.

The effect of the new delta function synthetic scattering kernel on the computed neutron fluxes in the neighborhood of the first two major resonances of thorium is given in Fig. 4.1. As expected, the original Wälti synthetic scattering kernel slightly underestimates the fluxes below the resonances. Insignificant differences in U-235 fission and U-238 capture cross sections were obtained between the SKM and SKM2 codes.

The difference in the results for the carbon out-scattering cross sections between GGC-5 and MICROX is due to the fact that GGC-5 overestimates the effect of out-scattering. The evaluation of GAM cross section data for fine-group out-scattering is based on the assumption that the flux shape within each GAM fine group is flat (constant lethargy flux). In reality, the mean flux at the upper GAM group boundary is greater than the flux at the lower group boundary. A neutron suffering a scattering collision near the lower group boundary is more likely to end up in the next lower GAM group than is a neutron which is scattered near the upper group boundary. Therefore, the GAM out-scattering cross sections are too high. MICROX does not use the constant flux approximation for primary nuclides. The GAROL section of GGC-5 does not suffer from that limitation either; however, the scattering cross sections from GAROL are not presently used by GGC-5 for broad-group averaging.

The reason for the large differences in the results for the thorium out-scattering cross sections is that resonance scattering cross sections are self-shielded in MICROX and SKM2 and unshielded

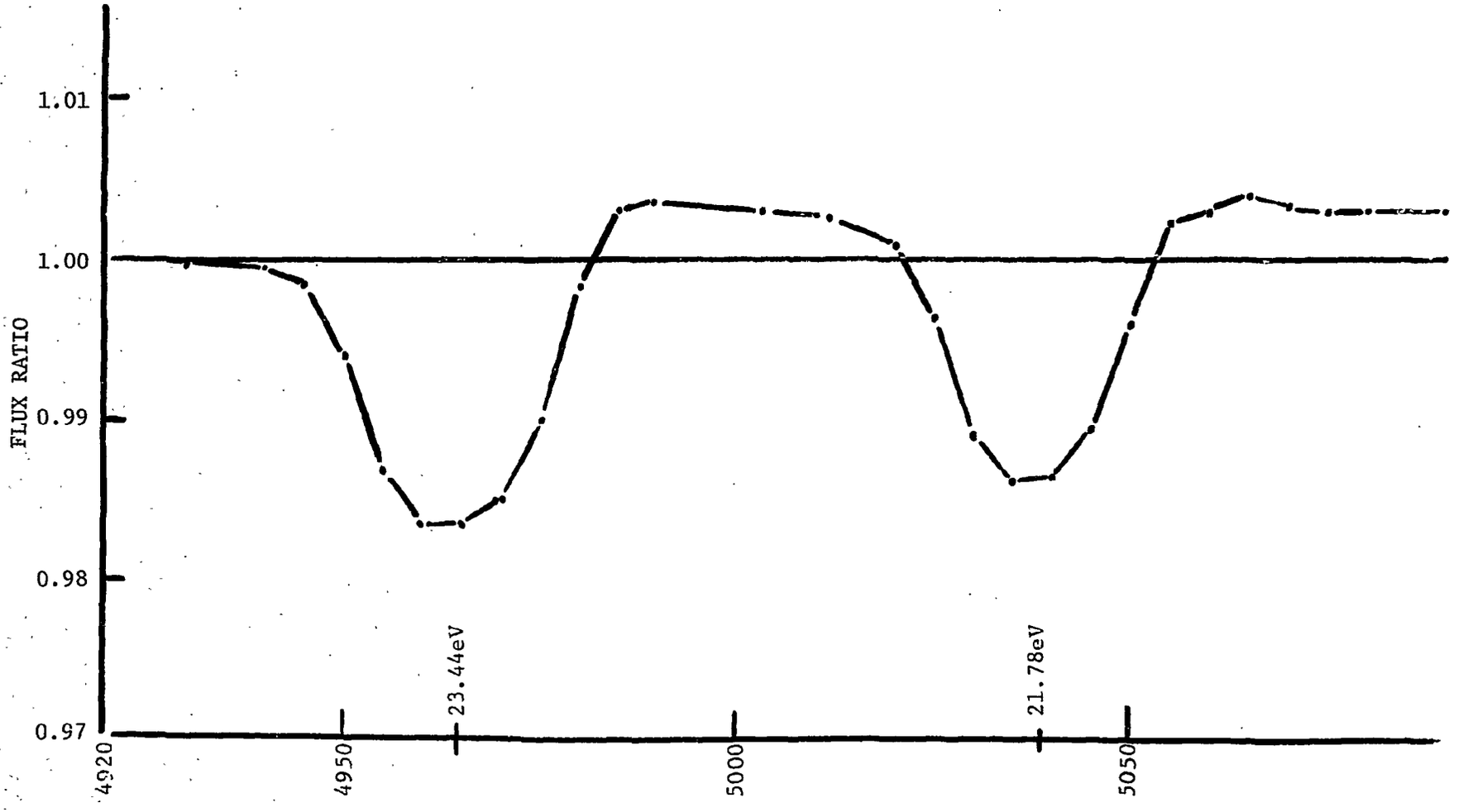

FIG. 4.1 DELTA FUNCTION KERNEL FLUX DIVIDED BY WALTI KERNEL FLUX IN THE THORIUM DOUBLET REGION FOR THE FORT ST. VRAIN HTGR TEST PROBLEM

in GGC-5 except in the internal calculations of the GAROL section. (The thorium out-scattering cross sections are, of course, relatively unimportant in HTGR analysis, but are of considerable importance in fast breeder reactor analyses.)

The SKM code did not compute transfer matrices. The SKM2 code results compare well with the MICROX code results except for the group 6 carbon outscatter. The MICROX code assumption of very wide broad groups breaks down for the relatively narrow group 6.

ACKNOWLEDGEMENTS

R. Moore and W. Davison encouraged this work and provided many helpful comments. P. Koch who worked with P. Wälti on the development of the MICROX code was quite helpful in helping me determine how the original SKM code worked and also contributed many helpful comments on the improvements described here. C. Hamilton provided invaluable moral and financial support.

REFERENCES

1. Walti, P., and P. Koch, "MICROX, A Two-Region Flux Spectrum Code for the Efficient Calculation of Group Cross Sections," Gulf General Atomic Co. Report Gulf-GA-A10827, 1972.

2. Roman, Charles P., "Comparison of Separable Scattering Kernels for Neutron Elastic Slowing Down Theory," M.S. Thesis, Rensselaer Polytechnic Institute, June, 1973.

3. Stevens, C. A., and C. V. Smith, "GAROL, A Computer Program for Evaluating Resonance Absorption Including Resonance Overlap," Gulf General Atomic Report GA-6637, 1965.

4. Archibald, R. J., and D. R. Mathews, "GAFGAR, A Program for the Calculation of Neutron Spectra and Group-Averaged Cross Sections," Gulf General Atomic Inc. Report GA-7542 (vol. I), 1968.

5. Archibald, R. J., and D. R. Mathews, "GAND2 and GFE2, Computer Codes for Preparing Input Data for the GAFGAR, GGC, and MICROX Codes from an ENDF/B Format Nuclear Data File," Gulf General Atomic Co. Report GA-7542 (Vol. II), 1973.

6. Honeck, H. C., "The Calculation of the Thermal Utilization and Disadvantage Factor in Uranium/Water Lattices," Nucl. Sci. & Eng. 18, 49(1969) (see particularly pp. 55-56).

7. Takahashi, H., "The Generalized First-Flight Collision Probability in The Cylindricalized System," Nucl. Sci. & Eng. 24, 69(1966) (see particularly pp. 70-71).

8. Carvik, I., "Calculations of Neutron Flux Distributions by Means of Integral Transport Methods," Report AE-279, 1967 (see particularly pp. 26-27).

9. Mathews, D. R., P. K. Koch, J. Adir, and P. Walti, "GGC-5, A Computer Program for Calculating Neutron Spectra and Group Constants," Gulf General Atomic Co. Report GA-8871, 1971.

10. Walti, P., "Evaluation of Grain Shielding Factors for Coated Fuel Particles," Nucl. Sci. & Eng. 45, 321(1971).

11. Dyos, M. W., and G. C. Pomraning, "Effective Thermal-Neutron Cross Sections for Materials with Grain Structure," Nucl. Sci. & Eng. 25, 8(1966).

Dup
-3

LA-UR

TITLE:
THE SHIELDING FACTOR METHOD FOR PRODUCING EFFECTIVE CROSS SECTIONS: MINX/SPHINX AND THE CCCC INTERFACE SYSTEM

AUTHOR(S):
R. E. MacFarlane, C. R. Weisbin and N. C. Paik

SUBMITTED TO:
RSIC Multigroup Cross Section Seminar
Oak Ridge, Tennessee
March 14-16, 1978

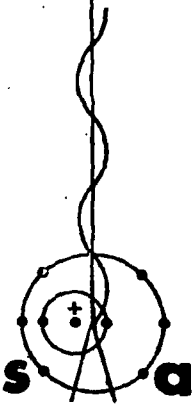

los alamos
scientific laboratory
of the University of California
LOS ALAMOS, NEW MEXICO 87545

Form No. 836
St. No. 2629
1/75

UNITED STATES
ENERGY RESEARCH AND
DEVELOPMENT ADMINISTRATION
CONTRACT W-7405-ENG. 36

BLANK PAGE

THE SHIELDING FACTOR METHOD FOR PRODUCING EFFECTIVE CROSS SECTIONS: MINX/SPHINX AND THE CCCC INTERFACE SYSTEM

R. E. MacFarlane
Los Alamos Scientific Laboratory, University of California
Theoretical Division
P O Box 1663, Los Alamos, NM 87545

C. R. Weisbin
Oak Ridge National Laboratory
P O Box X, Oak Ridge, TN 37830

N. C. Paik
Westinghouse Advanced Reactor Division
P O Box 158, Madison, PA 15663

ABSTRACT

The Shielding Factor Method is an economical designer-oriented method for producing the coarse-group space and energy self-shielded cross sections needed for reactor-core analysis. Extensive experience with the ETOX/1DX and ENDRUN/TDOWN systems has made the SFM the method of choice for most US fast-reactor design activities. The MINX/SPHINX system was designed to expand upon the capabilities of the older SFM codes and to incorporate the new standard interfaces for fast reactor cross sections specified by the Committee for Computer Code Coordination. MINX is the cross-section processor. It generates multigroup cross sections, shielding factors, and group-to-group transfer matrices from ENDF/B-IV and writes them out as CCCC ISOTXS and BRKOXS files. It features detailed pointwise resonance reconstruction, accurate Doppler broadening, and an efficient treatment of anisotropic scattering. SPHINX is the space-and-energy shielding code. It uses specific mixture and geometry information together with equivalence principles to construct shielded macroscopic multigroup cross sections in as many as 240 groups. It then makes a flux calculation by diffusion or transport methods and collapses to an appropriate set of cell-averaged coarse-group effective cross sections. The integration of MINX and SPHINX with the CCCC interface system provides an efficient, accurate, and convenient system for producing effective cross sections for use in fast-reactor problems. The system has also proved useful in shielding and CTR applications.

INTRODUCTION

The complexity of a typical reactor core makes it impractical to solve the neutron transport problem with full space and energy detail. For this reason designers normally use effective cross sections averaged over relatively coarse energy groups and space regions. The Shielding Factor Method (SFM) is an economical method for producing these effective cross section that was originally developed in Russia.[1] Development of the SFM in the US has been chiefly for the fast-reactor program, and extensive experience has been accumulated with the ETOX[2]/1DX[3] and ENDRUN[4]/TDOWN[5] code systems. More recently the SFM has received increased attention for thermal power reactor analysis with the development of EPRI-CELL and EPRI-CPM for the electric utility industry.[6] SFM code systems are traditionally divided into two parts: the cross section processor (e.g., ETOX) and the space-energy collapse code (e.g., 1DX). The MINX/SPHINX system follows this pattern. It was designed to expand upon the capabilities of the older SFM codes and to incorporate the standard interface formats for fast reactor codes specified by the Committee for Computer Code Coordination (CCCC).[7] The MINX[8] cross section processor generates a library of multigroup cross sections, shielding factors, and group-to-group transfer matrices from ENDF/B-IV[9] evaluated nuclear data and writes it out as CCCC ISOTXS and BRKOXS files. The SPHINX[10] space-energy code uses specific mixture and geometry information together with equivalence principles and a diffusion or transport flux calculation to construct effective coarse-group cell-averaged macroscopic cross sections in CCCC format.

The MINX/SPHINX system is in routine use on both IBM and CDC equipment. Comparisons with the older SFM codes show generally good agreement. Comparisons with independent codes such as ETOE-2[11]/MC^2-2,[12] VIM,[13] and GGC-5[14] give confidence that the MINX/SPHINX system is suitable for the routine analysis of large fast-reactor cores.

THEORY OF THE SHIELDING FACTOR METHOD

The goal of the SFM is to define effective cross sections for some range of energy (E in group g) and some region of space ($\underline{r}$ in volume v) that preserve macroscopic overservables such as reaction rate. Clearly,

$$\sigma^i_{xgv} = \frac{\int_g dE \int_v d\underline{r}\ \sigma^i_x(E,\underline{r})\ \phi\ (E,\underline{r})}{\int_g dE \int_v d\underline{r}\ \phi\ (E,\underline{r})}\ , \qquad (1)$$

where σ^i_x is the cross section for isotope i and reaction x at E and $\underline{r}$, and ϕ is the neutron scalar flux at that energy and position. Similar expressions can be constructed to preserve the group-to-group scattering rates and the transport cross section.

Unfortunately, the flux needed for Eq. (1) is not known before the fact; in fact, it is one of the quantities being sought in the analysis. In addition it is very complex, being full of sharp dips and peaks caused by resonances in the cross sections. However, experience has shown that it is possible to separate the variation of the flux into a part that is relatively smooth with respect to energy group and spatial zone size and a remaining resonance part. The variations in the smooth part can be determined by a multigroup flux calculation, but the intra-group flux must be selected by model.

The class of codes represented by MC^2 and GGC-5 determines this model flux by making a detailed flux calculation for a simplified homogeneous system. This is an expensive procedure. The SFM codes, on the other hand, assume that the intragroup flux can be modeled as

$$\phi(E) = \frac{W(E)}{\Sigma_t(E)} \quad , \tag{2}$$

where W is a smooth function of energy reflecting the fission and scattering sources into E and Σ_t is the total macroscopic cross section. Formally, Eq. (2) gives the flux for an infinite homogeneous system satisfying the narrow resonance approximation. However, heterogeneous systems can be included using equivalence princples.[15] Extension to wide and intermediate-width resonances is also possible.[16]

Furthermore, in evaluating the numerator of Eq. (1), it is assumed that the important effect is the interaction between a resonance in σ_x and the dip in the flux caused by that resonance (self-shielding). The reaction rate becomes

$$\int_g \frac{\sigma_x^i(E)}{\sigma_0^i + \sigma_t^i(E)} W(E)dE \quad , \tag{3}$$

where

$$\sigma_0^i = \frac{1}{\rho_i} \sum_{j \neq i} \rho_j \sigma_t^j \quad , \tag{4}$$

and where ρ_i is the number density for isotope i in the homogeneous mixture. The simplification comes from assuming that σ_0 is constant in g. The result is a single parameter, the "background cross section per atom," which can be used to characterize self-shielding. The cross sections produced by MINX are computed using

$$\sigma^i_{xg} = \frac{\int_g \frac{\sigma^i_x}{\sigma_0 + \sigma^i_t} \, WdE}{\int_g \frac{1}{\sigma_0 + \sigma^i_t} \, WdE} \quad . \tag{5}$$

The results are tabulated as cross sections for $\sigma_0 = \infty$ and shielding factors

$$f^i_{xg} = \frac{\sigma^i_{xg}(\sigma_0)}{\sigma^i_{xg}(\infty)} \quad , \tag{6}$$

for several values of σ_0. SPHINX then computes σ^i_0 using Eq. (4). In heterogeneous systems an additional "escape cross section per atom" is added. The corresponding shielded cross section is then obtained by interpolating the f-factors for this σ_0. Temperature is handled in the same way.

This approach makes a composition-independent cross-section library possible. The economy of the SFM results from being able to use this library many times.

THE MINX PROCESSING CODE

MINX was designed to combine and improve upon the resonance capabilities of ETOX[2] and ENDRUN[4] and the anisotropic scattering capabilities of ETOG[17] and SUPERTOG.[18] It is a modular code that uses paging techniques and variable dimensioning to make it possible to process the complex evaluations found in ENDF/B-IV.[9] The normal flow through the code is pictured in Fig. 1.

First, detailed pointwise cross sections are generated from ENDF/B resonance parameters and cross sections using the method of RESEND.[19] The energy grid is suitable for linear interpolation to within a user specified accuracy. The results are written out as a "pointwise-ENDF" (PENDF) tape suitable for printing, plotting, or further processing.

These pointwise cross sections are then accurately Doppler broadened to any desired temperatures using the method of SIGMA-1.[20] This approach has the advantage of correctly broadening smooth cross sections, backgrounds, and multi-level representations. Since broadening is a smoothing process, the results are thinned to a user specified accuracy and written out as PENDF tapes. Examples of the number of points produced in reconstruction and Doppler thinning are given in Table 1. Although this highly accurate process is expensive, it only has to be done once for a particular evaluation. Many subsequent averaging runs with different parameters can be made using the one temperature-dependent PENDF

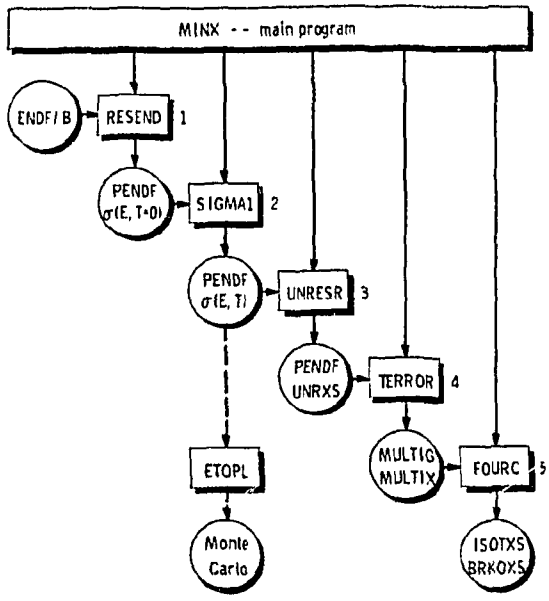

Fig. 1. Structure of MINX code illustrating functional blocks and data flow. ETOPL is not a part of MINX.

Table 1. Results of MINX Resonance Reconstruction and Doppler Broadening

Nuclide	Points at 0 K[a]	Points at 2100 K[b]	CP Seconds (CDC7600)
^{12}C	404	404	68.1
Fe	8798	5033	302.8
^{235}U	7209	2660	492.3
^{238}U	50372	6683	3483

[a] 0.5% reconstruction except 1.0% for ^{238}U.
[b] 0.1% thinning tolerance.

tape. The tape can also be reworked for use by continuous-energy Monte Carlo codes.[21]

This procedure will not work in the unresolved energy range where only statistical knowledge of the resonances is available. Effective pointwise cross sections vs T and σ_0 are produced by averaging over the ENDF/B distributions of resonance widths using methods based on ETOX.[2]

Multigroup cross sections are computed using Eq. (5) and appropriate generalizations. The group structure and smooth weight function are chosen by the user. The energy integrations are performed by adaptive quadrature starting from the union grid of the functions in the integrands. The nature of the PENDF cross section grid assures that all features are well-represented. Fission yields are averaged to preserve $\nu\sigma_f$ and slowing-down parameters are averaged to preserve $\bar{\mu}\sigma_e$ and $\xi\sigma_e$. The transport cross section is computed as $\sigma_t - \bar{\mu}\sigma_e$ where ^{e}current-weighting is used for the total cross section.

Elastic and discrete-inelastic scattering both obey two-body kinematics. MINX usually performs the resulting complex integrals over energy and angle with a semi-analytic method[22] based on an expansion in the laboratory system. The analytic integrals are obtained by a recursion relation, and the single energy integral is performed adaptively to a user specified tolerance. When this is not appropriate (e.g., light isotopes and near thresholds) MINX automatically changes to a direct numerical integration in the center-of-mass frame.

Group-to-group cross sections for continuum reactions are evaluated using analytic integrations over secondary energy and the standard adaptive quadrature for initial energy. Fission chi vectors by isotope are

produced by averaging the ENDF/B spectrum appropriate to a specified incident energy.

The final step is to format the results of the multigroup averaging module into the CCCC-III[7] ISOTXS (cross sections and matrices) and BRKOXS (shielding factors) files.

THE SPHINX SPACE-ENERGY CODE

SPHINX combines an extended version of the resonance treatment of 1DX[3] with the one-dimensional diffusion theory flux calculation of 1DX or the one-dimensional transport flux transport of ANISN.[23] It is modular in structure and uses the flexible POINTR system[24] of dynamic storage allocation. The entire code was assembled in accordance with the CCCC specifications for code compatibility.[7,25] The use of CCCC interface files makes communication with other CCCC-compatible codes such as TWOTRAN[26] and VENTURE[27] straightforward.

The basic structure of SPHINX is shown in Fig. 2. The various execution paths through the code are administered by the ZEUS CONTROL module using input data from the CCCC standard and code-dependent interfaces listed in Table 2. The fundamental cross-section data, intermediate results, and final answers are transmitted using the CCCC files described in Table 3.

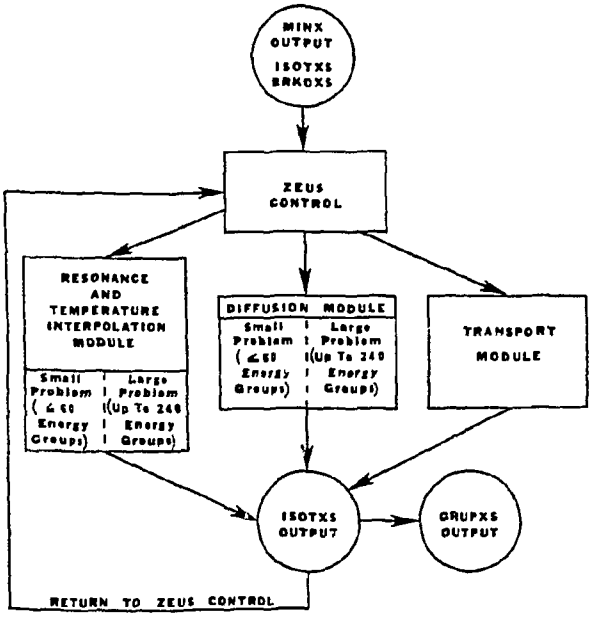

Fig. 2. Execution paths through SPHINX.

Table 2. SPHINX Control Files

Name	Standard	Description
ZEUS1A	no[a]	Modular control input
XSRINP	no	Resonance module input
SKODXI	no	Diffusion module input
ANISIN	no	Transport module input
ZNBTDN	no	Zone atomic densities
FPRINT	no	Print control
GEODST	yes[b]	Geometry description
NDXSRF	yes	Nuclide density and cross section parameters
ZNATON	yes	Zone nuclide atomic densities
SEARCH	yes	Criticality search parameters
SNCONS	yes	S_n constants
FIXSRC	yes	Volume and surface sources

[a] See Ref. 10 for detailed specifications.

[b] See Ref. 7 for detailed specifications.

Table 3. SPHINX Standard[a] Interface Files

Name	Description
ISOTXS	Nuclide-ordered cross section data
GRUPXS	Group-ordered cross section data
BRKOXS	Resonance self-shielding data
RTFLUX	Regular scalar flux
ATFLUX	Adjoint scalar flux
RCURNT	Regular current
ACURNT	Adjoint current
RAFLUX	Regular angular flux
AAFLUX	Adjoint angular flux
RZFLUX	Regular zone-averaged flux
PWDINT	Power densities

[a] See Ref. 7 for detailed specifications.

The first step in most problems is to use the resonance module to prepare effective self-shielded cross sections appropriate to the specified composition and geometry. The background cross section σ_0 is computed for each group and nuclide using Eq. (4). An additional escape term can be added for one of the seven options: (1) cylindrical cell using Sauer's approximation[28] for the Dancoff factor in a hexagonal lattice, (2) cylindrical cell using Sauer's approximation to the Dancoff factor in a square lattice, (3) symmetric slab cell, (4) asymmetric slab cell, (5) isolated rod, (6) cylindrical cell with the Bell approximation[29] to the Dancoff factor, and (7) symmetric slab cell with the Bell approximation. Self-shielding factors are then computed at σ_0 by Langranian interpolation. Effective cross sections are defined as in 1DX except that provision is made for an elastic group-to-group matrix. The results are written in ISOTXS format for communication with the flux modules.

On option, the code then branches to the diffusion module. The calculation is identical to that in 1DX except that input is in ISOTXS format and cross-section storage has been modified to allow for up to 240 groups and for several additional partial reaction types (i.e, n2n, nα, nd, ...). The cross sections are then collapsed to a subset group structure using the computed flux and written out in ISOTXS format.

The optional transport module uses the S_n method to obtain the flux. The method is identical to ANISN except for the ISOTXS interface capability. When the flux has been obtained, cross sections are collapsed to a subset group structure and zone-averaged using either volume or flux weighting. This provides a capability for cell homogenization.

The use of standard files provides many possible paths. For example, the flux from a diffusion calculation is easily available as an input guess for a subsequent transport calculation using already shielded cross sections.

LIBRARIES AND UTILITIES

SPHINX is normally used with one of the existing multigroup libraries generated by MINX. LIB-IV[30] is a 50-group 101-isotope library generated from ENDF/B-IV. The library includes all the general purpose evaluations from ENDF/B-IV plus the two copper isotopes and the nine lumped fission products from ENDF/B-III. All materials were run at 300, 900, and 2100 K using 4 to 6 σ_0 values with decade steps. Scattering matrices are given to P_3. The weight function consists of a 1.4 MeV fission spectrum joined at 820.8 keV to a 1/E shape which, in turn, joins to a 0.025 eV Maxwellian at 0.10 eV. The library also contains delayed neutron yields and spectra for seven isotopes generated in CCCC DLAYXS format using NJOY.[31]

VITAMIN-C[32] is a 171-group library with 36 isotopes chosen for importance in fusion and fast-reactor calculations. The specifications

for temperature, σ_0, Legendre order, and weight function are similar to LIB-IV, except that a velocity exponential fusion peak has been attached in the 14 MeV range.

These libraries require several utility codes in order to knit them into a system with MINX and SPHINX. First, BINX[33] is a code for converting back-and-forth between binary and BCD modes for transmission of ISOTXS, BRKOXS, and DLAYXS files between laboratories. LINX[33] is a code for adding new isotopes to an existing CCCC cross-section library. Finally, CINX[34] is a collapse code that can be used to generate a subset library tailored to a particular set of problems. As an example, CINX has been used to produce a 126-group subset of VITAMIN-C especially designed for LMFBR core and shield analysis.[35] Figure 3 illustrates how these codes and libraries combine to form a complete system.

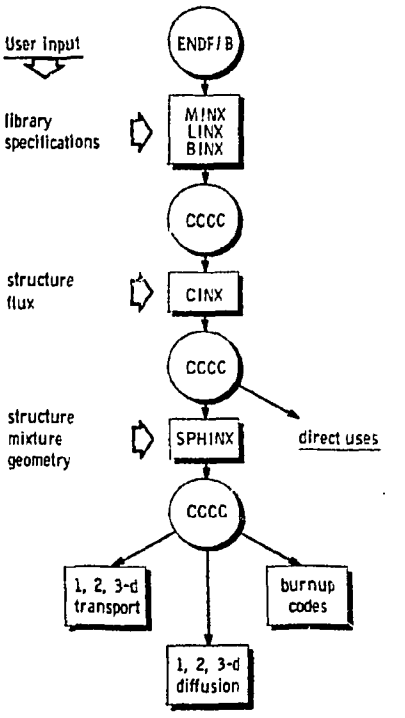

Fig. 3. Outline of CCCC interface system for generating multigroup constants for fast reactor analysis.

CODE VALIDATION

The MINX/SPHINX system has been tested in a variety of ways.[32,35] One ongoing project is a comparison of various processing codes being carried on by a committee of industrial and national laboratories (the DOE Code Evaluation Working Group). In order to minimize confusing complications, this group has analyzed a simple homogeneous composition typical of a large fast-breeder reactor core. The current results for some important parameters are given in Table 4. Larger differences exist between the fluxes and various cross sections. At the present time, for this type of problem, the chief causes of these differences seem to be: (1) group structure and weight function, (2) elastic removal treatment and (3) unresolved self-shielding. In any case, the numbers in Table 4 are less than the uncertainties associated with the basic evaluated data and with other design conservatisms. They imply that the MINX/SPHINX system is accurate for routine fast-reactor design.

Table 4. Comparison of Various Codes for a Buckled Homogeneous Fast Reactor Model

Parameter	ANL MC^2-2 Value	ARD 50g/SPHINX % diff	ORNL 126g/SPHINX % diff	LASL 50g/1DX % diff	LASL ETOX/1DX % diff	GE 50g/TDOWN % diff
k_{eff}	1.0040	0.10	0.31	0.19	0.13	0.17
C28/F49	0.1585	-0.06	-0.88	-0.26	-0.32	0.00
C28/F25	0.1447	-0.35	-0.76	-0.35	-0.48	0.28
F49/F25	0.9132	-0.33	0.12	-0.12	-0.23	0.22
F28/F25	0.0206	0.44	1.12	0.68	-0.44	4.27
F40/F25	0.1806	0.17	0.55	0.33	-0.44	1.55
F41/F25	1.294	0.29	0.36	0.33	-0.15	0.30

REFERENCES

1. I. I. Bondarenko, Ed., Group Constants for Nuclear Reactor Calculations (Consultants Bureau, New York, 1964).

2. R. E. Schenter, J. L. Baker, and R. B. Kidman, "ETOX, A Code to Calculate Group Constants for Nuclear Reactor Calculations," Battelle Northwest Laboratory report BNWL-1002 (ENDF-127) (1969).

3. R. W. Hardie and W. W. Little, Jr., "1DX, A One-Dimensional Diffusion Code for Generating Effective Nuclear Cross Sections," Battelle Northwest Laboratory report BNWL-954 (1969).

4. B. A. Hutchins, C. L. Cowan, M. D. Kelley, and J. E. Turner, "ENDRUN II, A computer Code to generate a Generalized Multigroup Data File for ENDF/B," General Electric Co. report GEAP-13703 (ENDF-145) (1971).

5. C. L. Cowan, B. A. Hutchins, and J. E. Turner, "TDOWN - A Code to Generate Composition and Spatially Dependent Cross Sections," General Electric Co. report GEAP-13740 (1971).

6. EPRI-CELL and EPRI-CPM are parts of the proprietary Advanced Recycle Methods Package developed for the Electric Power Research Institute (EPRI) by Nuclear Associates International.

7. B. M. Carmichael, "Standard Interface Files and Procedures for Reactor Physics Codes, Version III," Los Alamos Scientific Laboratory report LA-5486-MS (1974).

8. C. R. Weisbin, P. D. Soran, R. E. MacFarlane, D. R. Harris, R. J. LaBauve, J. S. Hendricks, J. E. White, and R. B. Kidman, "MINX: A Multigroup Interpretation of Nuclear X-Sections from ENDF/B," Los Alamos Scientific Laboratory report LA-6486-MS (1974).

9. D. Garber, C. Dunford, and S. Pearlstein, "Data Formats and Procedures for the Evaluated Nuclear Data File, ENDF," Brookhaven National Laboratory report BNL-NCS-50496 (ENDF-102) (1975).

10. W. J. Davis, M. B. Yarbrough, and A. B. Bortz, "SPHINX, A One Dimensional Diffusion and Transport Nuclear Cross Section Processing Code," Westinghouse Electric Corp. report WARD-XS-3045-17 (1977).

11. C. G. Stenberg, "ETOE-2, A Program for Data Conversion of ENDF/B to MC^2-2/SDX," Argonne National Laboratory report, to be published.

12. H. Henryson, II, B. J. Toppel, and C. G. Stenberg, "MC^2-2: A Code to Calculate Fast Neutron Spectra and Multigroup Cross Sections," Argonne National Laboratory report ANL-8144 (ENDF 239) (1976).

13. R. E. Prael and L. J. Milton, "A User's Manual for the Monte Carlo Code VIM," Argonne National Laboratory report FRA-TM-84 (1976).

14. D. R. Mathews et al., "GGC-5, A Computer Program for Calculating Neutron Spectra and Group Constants," General Atomic Co. report GA-8871 (1971).

15. L. Dresner, Resonance Absorption in Nuclear Reactors (Pergamon Press, New York, 1960).

16. R. Goldstein and E. R. Cohen, Nucl. Sci. Eng. 13, 132 (1962).

17. D. E. Kusner and R. A. Dannels, "ETOG-1, A FORTRAN-IV Program to Process Data from the ENDF/B File to the MUFT, GAM, and ANISN Formats," Westinghouse Electric Corp. report WCAP-3845-1 (ENDF 114) (1969).

18. R. Q. Wright, N. M. Greene, J. L. Lucius, and C. W. Craven, "SUPERTOG: A Program to Generate Fine Group Constants and Pn Scattering Matrices from ENDF/B," Oak Ridge National Laboratory report ORNL-TM-2679 (1969).

19. O. Ozer, "RESEND: A Program to Preprocess ENDF/B Materials with Resonance Files into a Pointwise Form," Brookhaven National Laboratory report BNL-17134 (1972).

20. D. E. Cullen and C. R. Weisbin, Exact Doppler Broadening of Tabulated Cross Sections," Nucl. Sci. Eng. 60, 199 (1976).

21. R. J. LaBauve, C. R. Weisbin, R. E. Seamon, M. E. Battat, D. R. Harris, P. G. Young, and M. M. Klein, "PENDF: A Library of Nuclear Data for Monte Carlo Calculations Derived from Data in ENDF/B Format," Los Alamos Scientific Laboratory report LA-5686 (1974).

22. C. R. Weisbin, P. D. Soran, and J. S. Hendricks, "A New Procedure for the Determination of Neutron Multigroup Transfer Matrices," Nucl. Sci. Eng. 55, 329 (1974).

23. W. W. Engle, Jr., "A User's Manual for ANISN: A One Dimension Discrete Ordinates Transport Code with Anisotropic Scattering,' Union Carbide Corporation report K-1693 (1967).

24. A. S. Kennedy, "POINTR, A Dynamic Storage Allocation Program," Argonne National Laboratory Technical Memorandum No. 98 (1967).

25. B. M. Carmichael, D. A. Meneley, and D. R. Vondy, "Report of the Subcommittee of Standard Interface Files," Los Alamos Scientific Laboratory report LA-5324-MS (1973).

26. K. D. Lathrop and F. W. Brinkley, "TWOTRAN-II: An Interfaced, Exportable Version of the TWOTRAN Code for Two-Dimensional Transport," Los Alamos Scientific Laboratory report LA-4848-MS (1973).

27. D. R. Vondy, T. B. Fowler, and G. W. Cunningham, "VENTURE: A Code for Solving Multigroup Neutronics Problems Applying the Finite-Difference Diffusion-Theory Approximation to Neutron Transport," Oak Ridge National Laboratory report ORNL-TM-4259.

28. A. Sauer, "Approximate Escape Probabilities," Nucl. Sci. Eng. 16, 329 (1963).

29. G. I. Bell, "A Simple Treatment for Effective Resonance Absorption Cross Sections in Dense Lattices," Nucl. Sci. Eng. 5, 138 (1959).

30. R. B. Kidman and R. E. MacFarlane, "LIB-IV, A Library of Group Constants for Nuclear Reactor Calculations," Los Alamos Scientific Laboratory report LA-6260-MS (1976).

31. R. E. MacFarlane and R. M. Boicourt, "NJOY: A Neutron and Photon Cross Section Processing System," Trans. Am. Nucl. Soc. 22, 720 (1975).

32. C. R. Weisbin, R. W. Roussin, E. M. Oblow, D. E. Cullen, J. E. White, and R. Q. Wright, "The Role of 'Standard' Fine-Group Cross Section Libraries in Shielding Analysis," in Proceeding of the Fifth International Conference on Reactor Shielding (Science Press, 1977) p. 472.

33. R. E. MacFarlane and R. B. Kidman, "LINX and BINX: CCCC Utility Codes for the MINX Multigroup Processing Code," Los Alamos Scientific Laboratory report LA-6219-MS (1976).

34. R. B. Kidman and R. E. MacFarlane, "CINX, Collapsed Interpretation of Nuclear X-Sections," Los Alamos Scientific Laboratory report LA-6287-MS (1976).

35. J. E. White, R. Q. Wright, L. R. Williams, and C. R. Weisbin, "Data Testing of the 126/36 Neutron-Gamma ENDF/B-IV Coupled Library for LMFBR Core and Shield Analysis," Trans. Am. Nucl. Soc. 23, 507 (1976).

IMPLEMENTATION OF THE RAPID CROSS SECTION ADJUSTMENT APPROACH AT GENERAL ELECTRIC

C. L. Cowan, E. Kujawski and R. Protsik
General Electric Co. - Fast Breeder Reactor Department
Sunnyvale, California

ABSTRACT

The General Electric rapid cross section adjustment approach was developed to use the shielding factor method for formulating multigroup cross sections. In this approach, spatial and composition dependent cross sections for a particular reactor or shield design are prepared from a generalized cross section library by the use of resonance self-shielding factors, and by the adjustment of elastic scattering cross sections for the local neutron flux spectra. The principal tool in the cross section adjustment package is the data processing code TDOWN. This code was specified to give the user a high degree of flexibility in the analysis of advanced reactor designs. Of particular interest in the analysis of critical experiments is the ability to carry out cell heterogeneity self-shielding calculations using a multiregion equivalence relationship, and the homogenization of the cross sections over the specified cell with the flux weighting obtained from transport theory calculations. Extensive testing of the rapid cross section adjustment approach, including comparisons with Monte Carlo methods, has indicated that this approach can be utilized with a high degree of confidence in the design analysis of complex fast reactor systems.

INTRODUCTION AND REVIEW

The generation of multigroup cross sections for the analysis of fast reactors at General Electric is based upon a rapid cross section adjustment approach. This approach was specified to utilize the shielding factor method for processing basic nuclear data, and has undergone extensive development since the middle 1960s. Many of the early underlying theories for this approach are described in the compilations of group constants by I.I. Bondarenko.(1)

The shielding factor method is basically a two-step process. In the first step, a generalized composition independent cross section library is created from the pointwise ENDF/B data. The generalized

library includes fine-group infinitely dilute cross sections, self-shielding factors and group-to-group transfer matrices for all materials of interest. This library serves as a preprocessed data base for generating the energy group constants for a specific fast reactor system. The self-shielding factors are peculiar to this approach and are given in tabular form in the generalized file for different values of the parameter σ_o, where for a given material, σ_o is designated as the ratio of the sum of the total cross sections for all other materials in a given composition to the atom density of the material in question.

The second step in the shielding factor approach involves the calculations of spatial and composition dependent cross sections for a particular reactor or shield design. The group constants are determined by interpolating on the self-shielding factors for the specific σ_o values which are computed for the given compositions. In addition, the elastic removal cross sections on the generalized file are corrected for the actual neutron flux distribution.

The early techniques for treating the shielding factor approach were incorporated into the ENDRUN - TDOWN code packages[2,3] at GE and the ETOX - 1DX code packages at HEDL.[4,5] The successful application of these techniques in the design analysis of fast reactor systems, has led to the development of a second generation of data processing codes, as characterized by the MINX[6] and SPHINX[7] systems. A significant development effort has also gone into the present version of TDOWN, and a number of these features are presented in the material which follows. TDOWN was specified to give the user maximum flexibility in using the rapid cross section adjustment approach for performing advanced design and critical experiments analysis. Problem descriptions can vary from a single composition with fluxes input, to a two-dimensional multiregion problem requiring several one-dimensional diffusion or transport theory flux solutions and resulting in a set of microscopic cross sections for each material in each region.

GENERAL FEATURES OF THE TDOWN CODE

The TDOWN code performs the following modifications to a generalized data library to generate composition and spatially dependent neutron cross sections for a specific fast reactor system:

1) Self-shielding factors (f-factors) are used to modify the infinitely-dilute cross sections for fission, capture, elastic-scattering, transport and total reactions. The f-factors are dependent upon the temperature of the material, the composition in which the material is found, and (optionally) on the cell configuration.

2) Eigenvalue and fixed source flux calculations may be carried out in fundamental mode, or in one-dimensional diffusion or

transport theory.

3) The elastic-removal cross sections are corrected for the energy distribution of the actual neutron flux. The neutron flux spectra may be input or taken as calculated in step (2) above.

4) The fission spectrum for a given composition is determined by weighting the flux averaged fission spectra for each isotope in accordance with its contribution to the neutron source.

5) The cross sections may be homogenized over all or a portion of specified cells, with flux-weighting obtained from transport theory calculations.

6) The cross sections may be condensed to one or more few group libraries, using any of the computed or input flux spectra.

A generalized flow diagram outlining the TDOWN procedures and operations is given in Figure 1. The computations for a given composition begin with the calculations of the self-shielding parameter for the i-th group and m-th material, $(\sigma_o)_{im}$. This parameter is calculated in an iterative process with the maximum number of iterations specified by the user. Following the determination of the $(\sigma_o)_{im}$ values, resonance self-shielding correction factors are computed by interpolating between the f-factors which are tabulated for discrete values of the temperature and σ_o. The f-factor interpolation on σ_o is carried out by means of a Taylor series expansion about neighboring values whereas the interpolation on the temperature is based upon the logarithmic proportionality between the tabulated values.

The technique for carrying out the spectral adjustment to the elastic removal cross section in TDOWN is based upon a Taylor series expansion of the ratio of the neutron fluxes for the ℓth and 0th flux spectrum iterations about some average lethargy $\bar{u}$. In this expansion, only the first two terms are retained to give,

$$R_{im}^{(\ell)}(u) \equiv \frac{\phi^{(\ell)}(u)}{\phi_{im}^{(0)}(u)} \simeq R_{im}^{(\ell)}(\bar{u}) + (u-\bar{u})\, R_{im}'^{(\ell)}(\bar{u}) \qquad (1)$$

Here $\phi_{im}^{(0)}$ is the intragroup flux weighting spectrum used to generate the group constants for material m in the generalized data library. Ideally, this term can be expressed as a function of lethargy as follows:

$$\phi_{im}^{(0)}(u) = \left[\frac{(\sigma_o)_{im} + (\sigma_t)_{im}}{(\sigma_o)_{im} + \sigma_{t,m}(u)}\right] \psi(u), \qquad (2)$$

FIGURE 1 GENERALIZED FLOW DIAGRAM OF TDOWN COMPUTATIONS

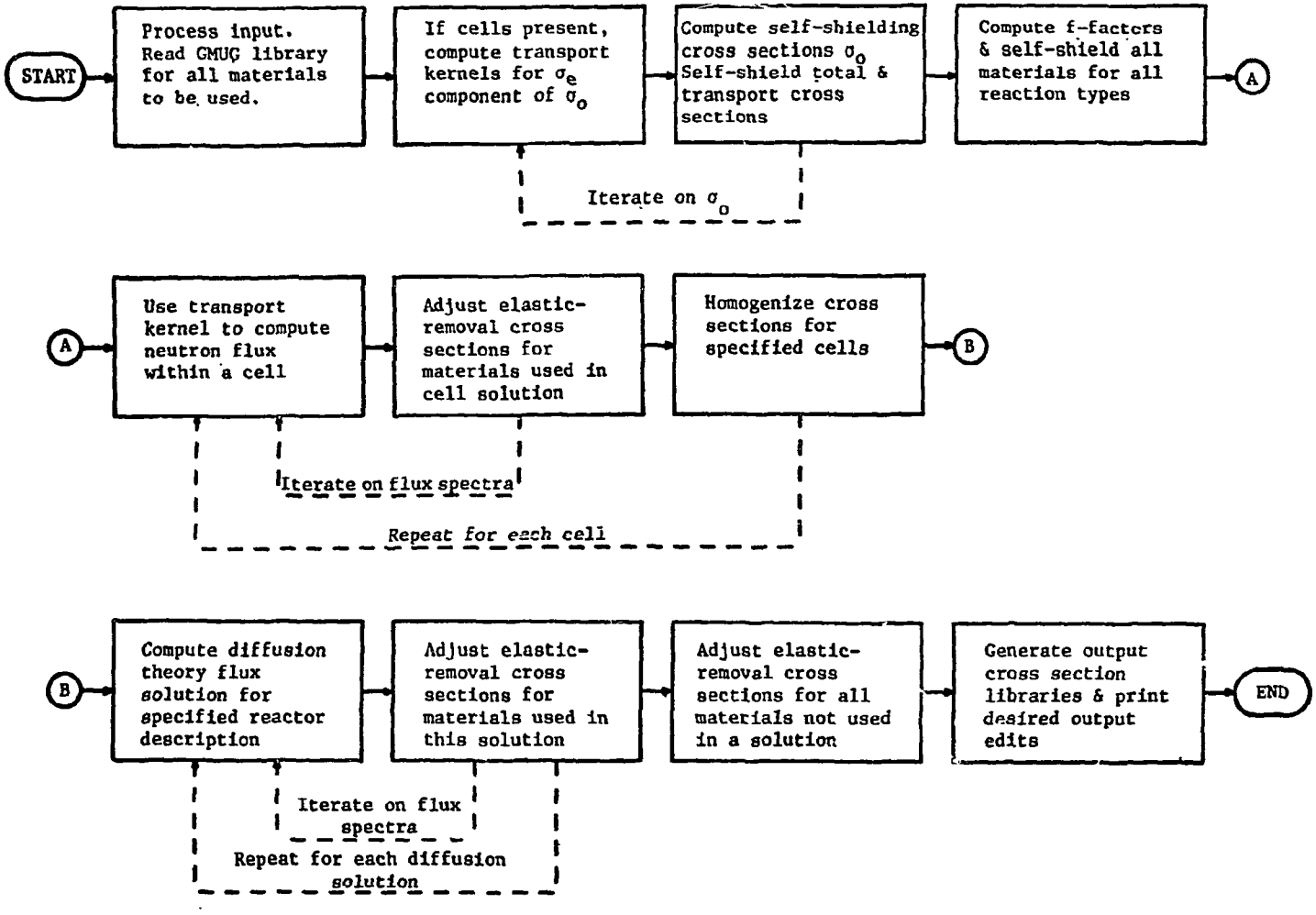

where (σ_o) is the standard self-shielding parameter, and $\psi(u)$ corresponds to the fission spectrum or a constant, depending on whether the lethargy is above or below some specified cutoff point.

Using Equation (1) it can be shown that the elastic removal cross section after the ℓth iteration is approximately given by

$$(\sigma_{er})_{im}^{(\ell)} \sim (\sigma_{er})_{im}^{(0)} \frac{R_{im}^{(\ell)}(\bar{u} + \delta\bar{u})}{R_{im}^{(\ell)}(\bar{u})} \tag{3a}$$

where

$$\bar{u} + \delta\bar{u} = u_i - \gamma_{im} \tag{3b}$$

$$\gamma_{im} = \frac{\int_{u_i - u_{i-1}}^{u_i} du(u_i - u)\, P_m(u \rightarrow > u_i)}{\int_{u_i - u_{i-1}}^{u_i} du\, P_m(u \rightarrow > u_i)} \tag{3c}$$

u_i = Upper lethargy for group i, and

$P_m(u \rightarrow > u_i)$ = Probability of scattering from lethargy u to a lethargy greater than u_i

It is noted that the probability term P_m includes an expression for anisotropic scattering.

Using Equation (2) the elastic removal adjustment factor can be rewritten in a form which readily lends itself to a physical interpretation:

$$\frac{R_{im}^{(\ell)}(\bar{u} + \delta\bar{u})}{R_{im}^{(\ell)}(\bar{u})} = \left[\frac{\Sigma_t(u_i - \gamma_{im})\ \phi^{(\ell)}(u_i - \gamma_{im})}{\Sigma_{t,i}\ \phi_i^{(\ell)}/\Delta u_i}\right]\left[\frac{\psi_i/\Delta u_i}{\psi(u_i - \gamma_{im})}\right], \tag{4}$$

where

$\Sigma_{t,i}$ and ϕ_i = ith group total macroscopic cross section and flux corresponding to $\Sigma_t(u)$ and $\phi^{\ell}(u)$, respectively

ψ_i = group flux corresponding to $\psi(u)$

Δu_i = width of group i

To evaluate the adjustment factor in Equation (4), the reaction rate and original flux spectrum are approximated by continuous linear functions which conserve the integrals of the reaction rates and $\psi(u)$ in the neighborhood of each group and over the entire lethargy span. It should be noted that this requires a break at the boundary between adjacent groups of unequal lethargy width. By rearranging Equation (4) and substituting into Equation (3a), the elastic removal correction in TDOWN is expressed as follows:

$$(\sigma_{er})_{im}^{(\ell)} = (\sigma_{er})_{im}^{(o)} \left[\frac{1 + \left(\frac{\Delta u_i - 2\gamma_{im}}{\Delta u_i + \Delta u_{i+1}} \right) \left(\frac{\Sigma_{t,i+1}\, \phi_{i+1}^{(\ell)}}{\Sigma_{t,i}\, \phi_i^{(\ell)}} - \frac{\Delta u_{i+1}}{\Delta u_i} \right)}{1 + \left(\frac{\Delta u_i - 2\gamma_{im}}{\Delta u_i + \Delta u_{i+1}} \right) \left(\frac{\psi_{i+1}}{\psi_i} - \frac{\Delta u_{i+1}}{\Delta u_i} \right)} \right], \quad (5)$$

Heterogeneity is treated in TDOWN by using an optional procedure for calculating the σ_o's based upon multiregion equivalence theory. The optional treatment is limited to one-dimensional slab, cylindrical or spherical cell geometries as supplied by the user. The multiregion equivalence relationship permits the computation of "self-shielded" cross sections in a complex multiregion cell. This formulation is especially important for the ZPPR plate cells, where the use of a "two-region equivalence relation" is at best ambiguous. The geometry is properly accounted for through the use of the transport coefficients or first flight collision probabilities $T_{zz'}$ between regions z and z'. In this approach, a generalized equivalence relationship is derived with the self-shielding parameter given as follows:

$$(\sigma_o)_m = (\sigma_o)_{mz} + (\sigma_e)_{mz} \quad (6)$$

Here $(\sigma_e)_{mz}$ is defined as an escape cross section which is material and region dependent (the group indicators have been omitted for convenience). The escape cross section is expressed in terms of the collision probabilities as,

$$(\sigma_e)_{mz} = \frac{(\Sigma_t)_z}{N_{mz}} \left(\frac{1 - T_{zz}}{T'_{zz}} \right), \quad (7)$$

where

$$T'_{zz} = T_{zz} + \sum_{z' \neq z} T_{zz'} \frac{N_{mz'}\, \sigma_{mz'}}{(\Sigma_t)_{z'}} \frac{(\Sigma_t)_z}{N_{mz}\, \sigma_{mz}} \quad (8)$$

The coefficients, $T_{zz'}$, may be conveniently computed using S_N-transport theory by considering unit sources. The problem of choosing an appropriate "modified Bell approximation" is thereby avoided. This transport kernel may then be used to generate a flux solution for use in homogenizing the cross sections in the cell.

The broad range of computations available in TDOWN provide a high degree of flexibility in specifying the cross sections for the analysis of a particular fast reactor design. Thus, the cross sections for each material on the output library from TDOWN are determined by 1) the source material on the generalized file, 2) the composition set and material temperature which were specified for carrying out the self-shielding calculations, 3) the spectral set which was utilized in the elastic-removal correction, 4) the heterogeneity description, and 5) the spectral set which was utilized in the condensation of the fine-group data library. A two-dimensional reactor description is input to aid the user in setting up several one-dimensional diffusion theory flux solutions through specified zones in the two-dimensional model. Specific cell descriptions may also be input for multizone self-shielding and for transport theory flux solutions. Composition sets may, or may not, correspond to the compositions in either the two-dimensional or cell models. Thus, a single TDOWN problem can be utilized to provide output data sets for the same material in the same composition at different temperatures, or even cross section sets for different neutronics problems. The flux spectra sets may be obtained from any of the zero or one-dimensional flux solutions which are carried out by TDOWN, or may be input.

TESTING THE RAPID CROSS SECTION ADJUSTMENT APPROACH

The shielding factor methods have undergone an extensive validation. Detailed comparisons with the Monte Carlo code VIM[8] and the direct data processing code MC^2-2[9] have been carried out as part of the activities of the Data Processing Subcommittee of the Code Evaluation Working Group. The differences between the results of calculations using the shielding factor approach and the more accurate methods were found to be small for the important integral parameters. The multiregion heterogeneity treatment incorporated in TDOWN has also been tested against the VIM computations for the ZPPR inner core normal cell. The results of the reaction rate calculations within the individual plates are summarized in Table I. The agreement between the results of the shielding factor heterogeneity calculations and the Monte Carlo calculations were found to be excellent. These studies have also indicated some limitations in the applicability of the two-region equivalence relationships. In particular, the shielding effects for the structural materials have been found to be significant for certain cell configurations.

Based upon the testing results described above and the successful application of the shielding factor method in the analysis of critical experiments it is concluded that the TDOWN code can be used with a high degree of confidence in the analysis of fast reactor systems.

TABLE I

COMPARISON OF TDOWN AND VIM HETEROGENEITY FACTORS[a]
FOR PLATEWISE ONE-GROUP CROSS SECTIONS

One-Group Cross Section[b]	TDOWN Heterogeneity	TDOWN/VIM[c]
$^{238}U(n,\gamma)$ (U_3O_8 Plate)	1.0057	0.997 ± 0.28%
$^{238}U(n,\gamma)$ (Pu-U-Mo Plate)	0.9509	1.001 ± 0.27%
$^{238}U(n,f)$ (U_3O_8 Plate)	0.9293	0.986 ± 0.39%
$^{238}U(n,f)$ (Pu-U-Mo Plate)	1.1283	0.981 ± 0.34%
$^{235}U(n,f)$ (Pu-U-Mo Plate)	1.0022	1.002 ± 0.26%
$^{239}Pu(n,\gamma)$ (Pu-U-Mo Plate)	0.9527	1.004 ± 0.37%
$^{239}Pu(n,f)$ (Pu-U-Mo Plate)	0.9968	1.002 ± 0.20%
Fe(n,γ) (Can Zone 1)	0.9962	1.009 ± 1.02%
Fe(n,γ) (Can Zone 3)	1.0320	1.018 ± 1.31%
Fe(n,γ) (Na Plate)	1.0215	0.999 ± 1.06%
Fe(n,γ) (FeO_3 Plate)	0.9897	0.998 ± 0.98%
Fe(n,γ) (Can Zone 7)	0.9992	0.968 ± 1.61%

a) The heterogeneity factors are defined as the ratio of the one-group platewise cross sections for the normal inner core ZPPR cell divided by the corresponding one-group cross sections for the homogeneous cell.

b) The plate layout for the ZPPR cell is shown as follows:

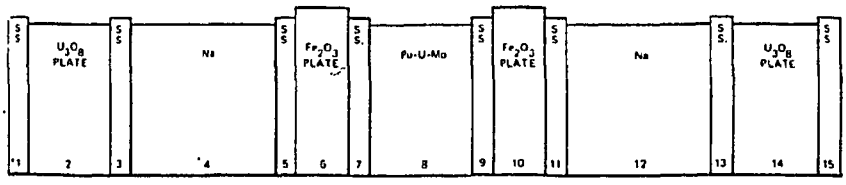

c) The assigned uncertainty is simply the uncertainty in the individual isotopic reaction rate for the heterogeneous cell given by VIM using track length estimators after 200,000 histories.

REFERENCES

1. Group Constants for Nuclear Reactor Calculations, Edited by I.I. Bondarenko, Consultants Bureau, New York, 1964.

2. B.A. Hutchins, C.L. Cowan, M.D. Kelley and J.E. Turner, "ENDRUN-II - A Computer Code to Generate a Generalized Multigroup Data File from ENDF/B," GEAP-13704, March 1971.

3. C.L. Cowan, B.A. Hutchins and J.E. Turner, "TDOWN - A Code to Generate Composition and Spatially Dependent Cross Sections", GEAP-13740, August 1971.

4. R.E. Schenter, J.L. Baker and R.B. Kidman, "ETOX - A Code to Calculate Group Constants for Nuclear Reactor Calculations", BNWL-1002, May 1969.

5. R.W. Hardie and W.W. Little, Jr., "1DX - A One-Dimensional Diffusion Code for Generating Effective Nuclear Cross Sections," BNWL-954, March 1969.

6. C.R. Weisbin, et al., "MINX - A Multigroup Interpretation of Nuclear X-Sections from ENDF/B," UC-34 and UC-80, September 1976.

7. W.J. Davis, M.B. Yarbrough and A.B. Bortz, "SPHINX - A One Dimensional Diffusion and Transport Nuclear Cross Section Processing Code," WARD-XS-3045-17 (UC-79d), August 1977.

8. R.E. Prael and L.J. Milton, "A User's Manual for the Monte Carlo Code VIM," FRA-TM-84, February 20, 1976.

9. C.G. Stenberg and A. Lindeman, "The ARC System Cross-Section Generation Capabilities, ARC-MC^2," ANL-7722, June 1973.

BLANK PAGE

EXPERIENCE IN DEVELOPING AND USING THE VITAMIN-C 171-NEUTRON, 36-GAMMA-RAY GROUP CROSS-SECTION LIBRARY

R. W. Roussin, C. R. Weisbin, J. E. White, R. Q. Wright, N. M. Greene, W. E. Ford, III, J. B. Wright, and B. R. Diggs

Oak Ridge National Laboratory
Oak Ridge, Tennessee, USA

ABSTRACT

The Department of Energy (DOE) Divisions of Magnetic Fusion Energy (DMFE) and Reactor Research and Technology (DRRT) jointly sponsored the development of a coupled, fine-group cross-section library. The 171-neutron, 36-gamma-ray group library is intended to be applicable to fusion reactor neutronics and LMFBR core and shield analysis.

Versions of the library are available from the Radiation Shielding Information Center (RSIC) at Oak Ridge National Laboratory in both AMPX and CCCC formats. Computer codes for energy group collapsing, interpolation on Bondarenko factors for resonance self-shielding and temperature corrections, and various other useful data manipulations are available.

The experience gained in the utilization of this library is discussed. Indications are that this venture, which is designed to allow users to derive problem-dependent cross sections from a fine-group master library, has been a success.

ACKNOWLEDGMENT

The authors are grateful to Eddie Bryant for her excellent effort in the preparation of this manuscript.

INTRODUCTION

The idea of producing a fine-group cross-section library designed to satisfy jointly the needs of fusion technology and breeder reactor core and shield physics is an attractive one since there is much overlap in the energy range and materials of interest to both communities. It is obvious that savings in costs (manpower and computing) can be realized if users can rely on a processed fine-group cross-section library rather than generating their own. However, there are possible drawbacks to developing, maintaining and distributing such a library. First, the cost in terms of dollars is large. Second, errors in the fine-group data are propagated to derived libraries (i.e., common mode failure). Third, such a library is voluminous and cumbersome to handle.

The library which was developed contains P_3, 171-neutron, 36-gamma-ray group cross sections for 61 materials. Resonance self-shielding and temperature effects are accounted for by means of interpolation on self-shielding factors. The library is available in very flexible formats which allow the user access to individual reaction cross sections and scattering transfer arrays.

After two years of experience in generating, distributing, maintaining, and using the VITAMIN-C library, it appears that the benefits from the project are substantial and are increasing with time. First, the effort provides a compilation of cumulative experience which helps improve the existing version of VITAMIN-C and provides important insights in the development of future versions. Second, a fine-group library provides a norm by which other techniques can be judged (e.g., broad group results). Third, it provides a vehicle for collaboration in the interpretation of integral benchmarks. Fourth, the data and retrieval capability provided by VITAMIN-C provide an effective and economical means of carrying out design studies. Fifth, its wide applicability and utilization allows a broad range of user feedback. Finally, since it is distributed as part of the Radiation Shielding Information Center's (RSIC) Data Library Collection (DLC)[1] a monthly status report is provided to users via the RSIC Newsletter.

Supporting evidence for the benefits listed above is given in the remaining sections. The sponsorship for and characteristics of VITAMIN-C are described in the next section. There follows a section on validation which lists various applications to which the library has been applied. The development and testing of some broad-group libraries based on VITAMIN-C are then described. Conclusions about the success of the effort are provided and a summary of plans for future work is given.

CHARACTERISTICS OF VITAMIN-C

Sponsorship

The joint sponsorship of VITAMIN-C by the Divisions of Magnetic Fusion Energy (DMFE) and Reactor Research and Technology (DRRT) is the result of a collaboration between RSIC and the Reactor Methods and Data Development Group (RMDDG) organizations within the Neutron Physics Division at Oak Ridge National Laboratory (ORNL). RSIC had a task to provide a fine-group cross-section library for fusion neutronics while RMDDG had a similar task to develop[2] a coupled cross-section library for LMFBR core and shield analysis. A poll of fusion contractor needs indicated that the specifications for both libraries could be combined to produce a single fine-group library which would meet the needs of both communities.

Characteristics

The resulting library[3] contains 171-neutron and 36-gamma-ray groups and utilizes Bondarenko factors[4] for interpolation to provide resonance self-shielding and temperature corrections. The multigroup neutron cross sections and Bondarenko factors were generated with MINX[5] while the gamma-ray production and interaction cross sections were generated with the LAPHNGAS and SMUG modules, respectively, of the AMPX system.[6,7] Most of the evaluated data from which the multigroup data were derived was ENDF/B-IV[8]. For materials not found in ENDF/B-IV, evaluated data from the Livermore Evaluated Nuclear Library[9] were used.

A detailed discussion of the characteristics of the library is found in Ref. 3.

Group Structure and Weighting Function

The 171-neutron and 36-gamma-ray group structures and the weighting function for the library were selected carefully. The neutron group structure includes as subsets those used in past design studies in various fields.[10,11,12] It includes detailed representation of specific features including total cross-section minima in Na, Fe, Al, O, N, Si, and C and threshold reactions for energies above 1 MeV. Some group boundaries are included that are not found in the 239-neutron-group ANSI Standard[13], but it is believed that the 171-group structure offers improvements due to better representation of the 300 KeV minimum in Na and of the 24 and 80 KeV minima in Fe.

The neutron weighting spectrum includes a thermal Maxwellian region, a fission spectrum and a fusion peak with 1/E slowing down regions joining these features.

Formats and Designation

The version of MINX used at ORNL (MINX-I.3) produces libraries in both AMPX and CCCC[14] master library formats. The version of the library in AMPX master format is called DLC-41/VITAMIN-C. The CCCC formatted library is called DLC-53/VITAMIN-4C ("4C" is a common way of pronouncing "CCCC"). The materials included in the libraries are listed in Table 1.

Table 1. Materials Available in DLC-41/VITAMIN-C and DLC-53/VITAMIN-4C.

H-1	K	Eu-153
H-2	Ca	Ta-181
H-3	Ti	W-182
He-3	V	W-183
He-4	Cr	W-184
Li-6	Mn-55	W-186
Li-7	Fe	Pb
Be-9	Co-59	Th-232
B-10	Ni	U-233
B-11	Cu	U-234
C-12	Zr	U-235
N-14	Zirc-2	U-236
O-16	Nb-93	U-238
F	Mo	Np-237
Na-23	Ag-107	Pu-238
Mg	Ag-109	Pu-239
Al-27	Cd	Pu-240
Si	Sn	Pu-241
P-31	Ba	Pu-242
S-32	Eu-151	Am-241
Cl		

It should be noted that DLC-53/VITAMIN-4C includes only neutron cross sections (ISOTXS format) and Bondarenko factors (BRKOXS format). DLC-41/VITAMIN-C contains neutron cross sections, gamma-ray production cross sections, and gamma-ray interaction cross sections.

Handling Codes for the Libraries

A variety of computer codes exists for retrieving, manipulating, converting, editing, collapsing, self-shielding, etc., the libraries. Those which can be used in conjunction with DLC-41/VITAMIN-C are modules from the AMPX[6,7] system. Those which are compatible with DLC-53/VITAMIN-4C have been developed primarily at Los Alamos Scientific Laboratory and at Westinghouse Advanced Reactor Division. All these processing codes

have been assembled into a single computer code package, PSR-117/MARS, which is available from RSIC. Various programs and their function are listed in Table 2.

Table 2. Selected Computer Codes from PSR-117/MARS Which Can Be Used in Conjunction with DLC-41 and DLC-53.

AMPX Module	CCCC Computer Code	Function
AIM	BINX[15], LASIP-III[16]	BCD-to-binary conversion.
AJAX	LINX[15], I2I[17], B2B[18]	Merging and deleting operations.
CHOX	CHOXM	Combining neutron and gamma-ray files.
MALOCS	CINX[19]	Energy group collapsing.
BONAMI	SPHINX[20]	Perform interpolation on bondarenko factors.
NITAWL	I2D[21]	Prepare working libraries for use in transport calculations.
RADE	---	Perform tests on multigroup libraries.

It should be noted that only a selected number of codes from MARS are listed in Table 2. In addition, the function of the codes may be more comprehensive than is indicated in the table, which is mainly a guide to codes which have shown corresponding functions for AMPX and CCCC formatted libraries.

All the codes in MARS are operational on the IBM-360/91. The CCCC codes were written for the CDC-7600 and were converted for IBM-360/91 use at ORNL. Some AMPX modules useful for handling DLC-41 have been converted to CDC and UNIVAC machines by the user community and are available from RSIC in PSR-112/MAME.

APPLICATION AND VALIDATION OF THE DATA PACKAGES

The VITAMIN-C (and -4C) library has been used for integral experiment analysis for a broad range of problems. Discrete ordinates results have been compared against MONTE CARLO results as an independent calculational

check against the procedure for multigroup data generation. A collective validation effort continues by volunteers from about twenty laboratories throughout the country.

Integral Experiment Analysis

The VITAMIN-C library has been used for the analysis of LMFBR core and shielding integral experiments with reasonable success as indicated below. It will also be applied to DMFE integral experiment analysis and to the Gas Cooled Fast Reactor shielding experiment in the near future.

LMFBR Core

Results have been published[22] of the analysis of the ZPPR-5 source level flux monitor experiment. Count rate ratios were calculated within 20% of experimental values using broad group cross sections based on VITAMIN-C. Calculated-to-experimental reactivity ratios near unity were calculated for a U-235 fission counter and a BF_3 detector.

Fast reactor data testing results for the Cross Section Evaluation Working Group (CSEWG) of ENDF/B-IV data show consistency[23] with results obtained at other laboratories. The ORNL calculations were obtained using a 126-group library collapsed from the 171-group master. Some typical results are summarized in Table 3.

Table 3. CSEWG Fast Reactor Benchmark Data Testing Results Using ENDF/B-IV. k-eff for Plutonium Fueled Assemblies

Benchmark Experiment	Argonne National Laboratory	Hanford Engineering Development Laboratory	Los Alamos Scientific Laboratory	Oak Ridge National Laboratory
JEZEBEL			0.9956	0.9920
ZPR3-56B		0.9901		0.9919
ZPR6-7	0.9850	0.9938	0.9892	0.9885
ZPR-2	0.9877	0.9973		0.991 (±0.0025)

LMFBR Shielding

Tests of the gamma-ray production data in VITAMIN-C[24] showed good agreement with CSEWG Shielding Data Testing Results[23] on ENDF/B-IV data.

A considerable improvement resulted (see Table 4) when VITMAIN-C was applied to the analysis[25] of a steel/sodium/iron experiment with attenuation of the order 10^{12}. The 51-group results were obtained with a library[26] commonly used at ORNL for the analysis of FFTF and CRBR design studies. Table 4 summarizes some comparative results.

Table 4. Comparison of 51-Group and VITAMIN-C Results (Calculation/Experiment) for the Steel/Sodium/Iron Experiment (46 cm Stainless Steel, 460 cm Sodium, and Varying Thickness of Iron).

Thickness of Iron (cm)	C/E Ratio (51-Group)	C/E Ratio (171-Group)
0	0.84	0.73
15	1.54	0.95
31	1.82	1.38
41	0.46	0.80
51	0.30	0.72
62	0.30	0.75

Independent Calculational Verification Efforts

VITAMIN-C was used to calculate the so-called CTR Standard Blanket[27] problems with the ANISN[28] discrete ordinates code. Another calculation[29] using cross sections processed at Lawrence Livermore Laboratory by a different method and the TART Monte Carlo technique served as an independent check of VITAMIN-C library for the CTR Standard Blanket Problem. Results are tabulated in Table 5.

Table 5. Comparison of LLL TART Monte Carlo and ORNL VITAMIN-C/ANISN Discrete Ordinates Calculations of Tritium Production for the CTR Standard Blanket Model.

Tritium Production Reaction	LLL TART Monte Carlo Results	ORNL VITAMIN-C/ANISN Results
$^{6}Li(n,\alpha)T$	0.956±0.013	0.969
$^{7}Li(n,n'\alpha)T$	0.579±0.006	0.575
TOTAL	1.535±0.013	1.544

Validation Efforts

Fast Reactor Physics Codes

A reactor physics Code Evaluation Working Group (CEWG) methods comparison effort is underway. The program compares results obtained by several laboratories on well defined problems.[30] The ORNL participation includes calculations using multigroup cross sections derived from VITAMIN-C. Participation in this effort has provided feedback which has resulted in improvements to multigroup processing schemes and to calculational techniques.

Fusion Neutronics

A group of about ten laboratories involved in fusion neutronics studies have participated in a voluntary effort to help validate[31] the VITAMIN-C libraries and associated computer codes. All the participants have successfully operated the VITAMIN-C package on sample problems and are now using it for other neutronics problems at their installations.

CSEWG Fast Reactor Data Testing

The CSEWG data testing of fast reactor benchmarks at both ORNL and General Electric Breeder Reactor Division is being performed using cross sections derived from VITAMIN-C.

ANS Shielding Standards

The American Nuclear Society (ANS) standards effort for shielding is attempting to develop a standard for multigroup cross sections for use in concrete and light water reactor shielding. The ANS-6.1.2 Working Group on Shielding Cross Sections is considering, among others, the VITAMIN-C library and a 45-neutron, 16-gamma-ray group library derived from it as possible candidates for designation as libraries conforming to its definition of a "Standard" cross-section library. The applicability of VITAMIN-C with relation to such standards has previously been discussed.[32] The effort involves six laboratories and corporations interested in the ANS-6.1.2 project.

All the above efforts have provided useful feedback which has and will continue to improve the VITAMIN-C multigroup cross sections.

DEVELOPMENT AND APPLICATION OF DERIVED LIBRARIES

The VITAMIN-C library has provided a basis for the development and application of derived libraries to a broad range of design and scoping analyses. The requirements for a variety of applications are being met by deriving broad group libraries that are tailored to solve the particular problem at hand. Some of these applications have been mentioned above. Table 6 offers a summary of some of the projects and resulting broad group libraries.

Table 6. Problem Dependent Broad-Group Libraries Derived from VITAMIN-C.

APPLICATION	LIBRARY (Neutron Groups/Gamma-Ray Groups)	REFERENCE
Concrete and Light Water Reactor Shielding Studies	(45/16)	DLC-47/BUGLE[33]
LMFBR and CRBR Core and Shield	44	ORNL-5314[22]
Proliferation Resistant Design Studies	9	ORNL-5389[34]
Gas Cooled Fast Reactor Shielding Studies	(60/17)	Private Communication[35]
DMFE Integral Experiment Analysis	(45/16)	Trans. ANS (June 1978)[36]
CSEWG Data and CEWG Methods Testing	(126/36)	DLC-42/CLEAR[2]
DMFE Design Analysis	(35/21)	Private Communication[37]

FUTURE WORK AND ADDITIONS

Work is continuing in the development of VITAMIN-C. Additional materials are to be added to the library based on ENDF/B-IV. These will include neutron cross sections for Pa-233, Gd, and Sm.

As indicated in the presentation[38] on MACKLIB at this meeting, kerma factors, damage energy cross sections and other response functions in the 171-group structure will be added to basic cross section library. Delayed γ-ray production spectra from fission are also available[39] in the 36-group structure and will be added to VITAMIN-C.

With the release of ENDF/B-V in 1978, it is expected that a new version of VITAMIN-C will be processed. Because of the expanded nature of ENDF/B-V, it is likely that the new VITAMIN-C will include not only cross sections for radiation transport but also actinide, fission product and activation cross sections as well as multigroup covariance matrices.

It is expected that the relevant computer codes needed for handling the libraries will be upgraded. For example, a checking code for CCCC interfaces is planned. (See the paper by Cacuci and Bjerke[40] in these proceedings).

CONCLUSIONS

A considerable amount of experience has been gained by this venture aimed at providing a master multigroup library from which the user can derive his own problem dependent cross sections. It is expensive to produce a comprehensive multigroup library such as VITAMIN-C. There are numerous handling problems due to the quantity of data in the resulting libraries (several tapes are required to transmit the DLC-41 or -53 to another installation). The variety and complexity of the retrieval programs which are required for conversion, editing, group collapsing, resonance self-shielding and other manipulations requires good communications and cooperation.

It is evident, however, that the benefits of such a project are substantial. Application of the libraries to a wide variety of problems offers many channels of communication for feedback which results in improvements to both cross-section data and computer codes. The voluntary efforts of interested parties at many installations provide an important part of this feedback. The successful results obtained in integral experiment and data testing analyses and the verification of the multigroup processing methods against independent calculations are encouraging signs of adequate validation. The variety of design and scoping studies to which libraries derived from DLC-41/VITAMIN-C and/ or DLC-53/VITAMIN-4C have been applied are evidence of the true economy and success of the project.

REFERENCES

1. R. W. Roussin, "Abstracts of the Data Library Packages Assembled by the Radiation Shielding Information Center," ORNL-RSIC-30 (1972).

2. C. R. Weisbin, R. W. Roussin, J. E. White, and R. Q. Wright, "Specification for Pseudo-Composition-Independent Fine-Group and Composition Dependent Fine- and Broad-Group LMFBR Neutron-Gamma Libraries at ORNL," ORNL-TM-5142 (ENDF-224), 1975.

3. R. W. Roussin, C. R. Weisbin, J. E. White, N. M. Greene, R. Q. Wright, and J. B. Wright, "The CTR Processed Multigroup Cross-Section Library for Neutronics Studies," ORNL-RSIC-37 (1978).

4. I. I. Bondarenko, Ed., "Group Constants for Nuclear Reactor Calculations," Consultants Bureau, New York (1964).

5. C. R. Weisbin, P. D. Soran, R. E. MacFarlane, D. R. Harris, R. J. LaBauve, J. S. Hendricks, J. E. White, and R. B. Kidman, "MINX, A Multigroup Interpretation of Nuclear Cross Sections," LA-6486-MS (1976).

6. N. M. Greene, J. L. Lucius, L. M. Petrie, W. E. Ford, III, J. E. White, and R. Q. Wright, "AMPX: A Modular Code System for Generating Coupled Multigroup Neutron-Gamma Libraries from ENDF/B," ORNL/TM-3706 (1976).

7. N. M. Greene, W. E. Ford, III, and M. Petrie, B. R. Diggs, C. C. Webster, J. L. Lucius, J. E. White, R. Q. Wright, and R. M. Westfall, "AMPX: A Modular System for Multigroup Cross-Section Generation and Manipulation," these proceedings.

8. D. Garber, Compiler, "ENDF/B Summary Documentation," BNL 17541 (ENDF-201) (1975).

9. R. J. Howerton, "The LLL Evaluated Nuclear Data Library (ENDF): Translation of ENDL Neutron-Induced Interaction Data into the ENDF/B Format," UCRL-50400, Vol. 15, Part C (1976).

10. W. E. Ford, III, R. T. Santoro, R. W. Roussin, and D. M. Plaster, "Modification Number One to the Coupled 100n-21γ Cross-Section Library for EPR Calculations," ORNL/TM-5249 (1976). Available from RSIC as DLC-37/EPR.

11. J. T. Kriese, "Coupled Neutron and Gamma-Ray Cross-Section Sets for Fusion Reactor Calculations," ORNL-TM-4277 (1973) Available from RSIC as DLC-28/CTR.

12. D. E. Bartine, J. R. Knight, J. V. Pace, III, and R. W. Roussin, "Production and Testing of the DNA Few-Group Coupled Neutron-Gamma Cross-Section Library," ORNL/TM-4840 (1977). Available from RSIC as DLC-31/(DPL-1/FEWG1).

13. C. R. Weisbin and R. J. LaBauve, "Specification of a Generally Useful Multigroup Structure for Neutron Transport," LA-5277-MS (1973).

14. B. M. Carmichael, "Standard Interface Files and Procedures for Reactor Physics Codes, Version III," LA-5486-MS (1974).

15. R. E. MacFarlane and R. B. Kidman, "LINX and BINX: CCCC Utility Codes for the MINX Multigroup Processing Code," LA-6219-MS (1976).

16. G. E. Bosler, R. D. O'Dell, and W. M. Resnick, II, "LASIP-III, A Generalized Processor for Standard Interface Files," LA-6280-MS (1976).

17. G. E. Bosler, Los Alamos Scientific Laboratory, informal notes on I2I (1976).

18. G. E. Bosler, Los Alamos Scientific Laboratory, informal notes on B2B (1976).

19. R. B. Kidman and R. E. MacFarlane, "CINX, Collapsed Interpretation of Nuclear X sections," LA-6287-MS (1976).

20. W. J. Davis, M. B. Yarbrough, and A. B. Bortz, "SPHINX: A One-Dimensional Diffusion and Transport Nuclear Cross-Section Processing Code," WARD-XS-3045-17 (1977).

21. W. M. Resnick, II, "I2D: Code for Conversion of ISOTXS Structured Data to DTF and ANISN Structured Tables," LA-6857-MS (1977).

22. D. L. Selby and G. F. Flanagan, " Analysis of ZPPR-5 Source Level Flux Monitor Experiments," ORNL-5314 (1973).

23. E. M. Bohn et al., Editors, "Benchmark Testing of ENDF/B-IV," BNL-NCS-21118 (Vol. I and II) (1976).

24. J. E. White, R. Q. Wright, L. R. Williams, and C. R. Weisbin, "Data Testing of the 126/36 Neutron-Gamma ENDF/B-IV Coupled Library for LMFBR Core and Shield Analysis," Trans. Amer. Nucl. Soc. 23, 507-508 (1976).

25. R. E. Maerker, F. J. Muckenthaler, and C. E. Clifford, "SB4. Measurements and Calculations of the ORNL CRBR Upper Axial Shield Experiment," ORNL-5259(ENDF-258) (1977).

26. C. C. Webster to F. R. Mynatt, "Modification No. 20 to 51n-25γ Cross-Section Library," UCCND IC (Aug. 5, 1976).

27. D. Steiner, "Analysis of a Bench-Mark Calculation of Tritium Breeding in a Fusion Reactor Blanket: The United States Contribution," ORNL-TM-4177 (1973).

28. W. W. Engle, Jr., "A User's Manual for ANISN, A One-Dimensional Discrete Ordinates Transport Code With Anisotropic Scattering," K-1693 (1967).

29. R. C. Haight, Lawrence Livermore Laboratory, to R. W. Roussin, ORNL, private communication.

30. R. E. MacFarlane to Processing Code Subcommittee of the Code Evaluation Working Group," Homogeneous Test Problems," LASL Memo T-2-L-2515 (Oct. 3, 1977).

31. R. W. Roussin, C. R. Weisbin, J. E. White, N. M. Greene, R. Q. Wright, and J. B. Wright, "Progress on the Validation of the CTR Multigroup Data Package," Trans. Amer. Nucl. Soc. 28, 14-15 (1976).

32. C. R. Weisbin, R. W. Roussin, E. M. Oblow, J. E. White, and R. Q. Wright, Oak Ridge National Laboratory, and D. E. Cullen, Lawrence Livermore Laboratory, "The Role of "Standard" Fine-Group Cross-Section Libraries in Shielding Analysis," Proc. of the 5th International Conference on Reactor Shielding, Science Press, Princeton (1977).

33. J. T. West, G. P. DeBeer, B. Nakhai, and R. W. Roussin, "Development of an ANS Coupled Cross-Section Standard for Concrete Shielding," to be presented at the San Diego American Nuclear Society Meeting, June 1978.

34. T. J. Burns and J. R. White, "Preliminary Evaluation of Alternative LMFBR Fuel Cycle Options," ORNL-5389, in preparation.

35. D. T. Ingersoll, Oak Ridge National Laboratory, Private Communication (1978).

36. Y. Seki, R. T. Santoro, E. M. Oblow, J. L. Lucius, "Macroscopic Cross-Section Sensitivity Study for the TNS Integral Experiment," to be presented at the San Diego American Nuclear Society Meeting, June 1978.

37. R. T. Santoro, Oak Ridge National Laboratory, Private Communication (1978).

38. M. A. Abdou and Y. Gohar, "The MACK/MACKLIB System for Nuclear Response Functions," these proceedings.

39. O. W. Hermann and G. W. Morrison, Union Carbide Nuclear Computer Sciences Division at Oak Ridge National Laboratory to C. R. Weisbin, private communication (1976).

40. D. G. Cacuci and M. A. Bjerke, "Analytical Inequalities Satisfied by the Cross-Section Self-Shielding Factors: Best Upper and Lower Bounds," these proceedings.

DESIGN CRITERIA FOR THE 218-GROUP CRITICALITY SAFETY REFERENCE LIBRARY

R. M. Westfall, W. E. Ford, III, C. C. Webster
Computer Sciences Division,
Union Carbide Corporation, Nuclear Division
Oak Ridge National Laboratory
Oak Ridge, Tennessee, U.S.A.

ABSTRACT

The generation of a 218-group neutron cross-section library from ENDF/B-IV data is described. Experience in selecting broad-group subsets and applying them in the analysis of critical experiments is related. Recommendations on the use of the 218-group library are made.

INTRODUCTION

The 218-group AMPX[1] master neutron cross-section library was developed to serve as an analytical reference and data source in the development of an ENDF/B-IV broad-group library for criticality safety studies. The primary purpose of this paper is to present the criteria for the selection of the 218-energy group boundaries and to discuss the proce-dures followed in processing the ENDF/B-IV data into the multigroup library. Included in the paper is a brief review of an effort to determine a broad-energy-group subset of the 218-group library which is suitable for the analysis of systems containing selected fuel, structural, and neutron moderating and absorbing nuclides. Also discussed is the effectiveness of the 218-group library and its broad-group derivatives in the analysis of uranium, plutonium and mixed-oxide fueled systems. Finally, recommendations are made on various approaches to applying the 218-group library in performing criticality safety analyses.

Master Library Generation From ENDF/B-IV

The initial criteria established for the 218-group criticality safety reference library were that it should

1. be in AMPX master interface format[1] with provision for problem-dependent resolved resonance processing,
2. be suitable for the analysis of thermal systems,
3. contain data for the fuel, neutron-absorbing and structural materials found in shipping casks and other equipment associated with the fule cycle, and

BLANK PAGE

4. be sufficiently detailed so as to provide reference results for trial broad-group libraries.

These criteria determined the bases for the selection of the 218-group energy boundaries which are summarized in Figure 1. Reference 2 contains a listing of the 140 epithermal boundaries including their function in terms of nuclides and reaction types. The 78 boundaries below 3.05 eV provide sharp definition of the thermal resonances in U-233, U-235, Pu-239, Pu-240, Pu-241, and Pu-242.

The weighting functions used to process the ENDF/B-IV point data into the 218-multigroup data are given in Figure 2. The essential features of the weighting functions are the high energy $1/E\sigma_T$ treatment of the cross-section structure in the nonresonance nuclides and the 1/E "infinite dilution" weighting for the resonance nuclides. Under this weighting, provision is made for carrying the resolved resonance parameters in the AMPX master interface for problem-dependent processing with the Nordheim integral method in the NITAWL module.[1] If problem-dependent data is not specified by the user, the "infinite dilution" values are used in producing the working cross-section library.

Fig. 1. 218 ENERGY GROUP BOUNDARIES

1. Nuclides considered: Be, B-10, C, N, O, F, Na, Mg, Al, Si, K, Ca, Cr, Mn, Fe, Ni, Cu, Zr, Mo, Ag, Cd, In, Sn, Ba, Gd, Hf, Pb, Th-232, U-233, U-234, U-235, U-236, U-238, Pu-239, Pu-240, Pu-241, Pu-242.
2. 20 MeV $\leq$ 51 Groups $\leq$ 8.03 keV; Boundaries chosen to fit structure and reaction thresholds of light and intermediate mass nuclides.
3. 8.03 keV $\leq$ 89 Groups $\leq$ 3.05 eV; Boundaries chosen to bracket major resonance levels in the intermediate-mass and heavy nuclides.
4. 3.05 eV < 78 Groups $\leq 10^{-5}$ eV; Boundaries chosen to "march-over" thermal resonances in fuel nuclides.
5. Hansen-Roach 16-group boundaries.

Fig. 2. POINT-TO-FINE GROUP WEIGHTING FUNCTIONS

1. Nonresonance Materials (fission - $1/E\sigma_T$ - Maxwellian)

Energy Range	Weighting
20-1.4 MeV	Fission
1.4 MeV-0.1264 eV	$1/E\sigma_T$
0.1264-10^{-5} eV	Maxwellian (293°K)

2. Resonance Materials (fission - 1/E - Maxwellian)

Energy Range	Weighting
20-0.1 MeV	Fission
100 keV-0.1264 eV	1/E
0.1264-10^{-5} eV	Maxwellian (293°K)

3. Selected Structural Materials (Fe, Ni, Cr)

Energy Range	Weighting
20 MeV-0.1264 eV	$(1/E\Sigma_T)$ Inconel or
	$(1/E\Sigma_T)$ SS-304
0.1264-10^{-5} eV	Maxwellian (293°K)

Since the principal application envisioned for this library was the analysis of thermal systems, the unresolved resonance data was processed at a temperature at 293°K and a background cross section of 50,000 bn. Thermal transfer arrays were calculated with free gas kernels at 293°K for all nuclides with the exception of multithermal bound kernels for hydrogen, deuterium, boron-10, boron-11, and carbon.

Broad Energy Group Determination

An extensive series of model calculations were performed to determine a broad energy group structure suitable for the analysis of commonly encountered criticality safety problems. The procedure followed in determining the broad-group structure is described in reference 3. The Hansen-Roach 16-group structure[4] was the initial trial group structure for this determination. The final 27-group structure resulting from the determination is given in Figure 3. Group boundaries were added to the base 16-group structure for the following reasons.

1. 6.434 and 1.85 MeV to match fast leakage.
2. 1.77, 1.3, 1.13 and 0.8 eV to fit the large Pu-240 resonance at 1.056 eV.
3. 0.325 and 0.225 to fit the thermal resonances in U-235 (0.29 Ev), Pu-239 (0.296 eV) and Pu-241 (0.258 eV).
4. 0.05, 0.03 and 0.01 eV to calculate the thermal flux shape.

Fig. 3. 27 BROAD ENERGY GROUP STRUCTURE

Group No.	Upper Boundary	Group No.	Upper Boundary
1	20 MeV	15	3.05 eV
2	6.434	16	1.77
3	3	17	1.3
4	1.85	18	1.13
5	1.4	19	1
6	900 keV	20	0.8
7	400	21	0.4
8	100	22	0.325
9	17	23	0.225
10	3	24	0.1
11	550 eV	25	0.05
12	100	26	0.03
13	30	27	0.01
14	10		0.00001

This group structure was found to be adequate through the broad-group-determination procedure for the nuclides: U-238, U-235, Pu-239, Pu-240, Pu-241, Pu-242, B-10, SS-304, (Ni, Fe, Cr), Cd, Al, Cu, H_2O, Zircalloy-2.

The "nuclides of interest" for which the model calculations were performed are listed in Figure 3. During the broad-group determination process for U-238, it was found to be necessary to relax the acceptance criterion from a 0.3% Δk to a 1% Δk difference between 218 and broad-group results. The relaxed criterion was applied to the models with median fission energies between 1 and 100 eV. The initial, more stringent criterion was retained for the thermal and fast spectrum testing.

Library Performance on Water-Moderated Systems

Analyses of uranium-fueled critical experiments with the ENDF/B-IV data applied in the 218-group library, a 19-group subset of the 218-group library, and as point cross sections in a continuous energy version of KENO are summarized in Tables 1 and 2. Results for the high-enriched uranium solutions are 0.5 to 1.5% Δk high, depending on

group structure and the H/U-235 atom ratio. The well-thermalized systems are predicted quite closely. Results for the low-enriched fuel lattice experiments are seen to be 1.5% Δk low for lattice pitches of 0.6 inch to near critical for the more highly moderated configurations. The agreement between the multigroup and point cross-section results is very close. This agreement indicates that the calculated biases from critical are due to the ENDF/B-IV data and do not depend on the processing of the data into the 218-group library.

Analyses of plutonium fueled critical experiments are given in Tables 3 and 4. Here the calculated bias is 0.5 to 3% Δk high depending on the H/Pu atom ratio and the percentage of Pu-240 in the fuel. Again, the close agreement between the multigroup and point cross-section results indicates that the problem lies in the ENDF/B-IV data.

Results from the analysis of 2 wt.% Pu(8% Pu-240)O_2-UO_2 rod lattices are given in Table 5. The close agreement with critical is apparently due to offsetting negative and positive reactivity biases due to the uranium and plutonium, respectively. Here again, the trend toward higher multiplication factors at wider lattice pitches is clearly evident.

Table 1. Calculated Results for Uranium Solution Critical Experiments

Experiment Description	Designation	H/U-235 Atom Ratio	Calculated K-eff: XSDRNPM, S_8 Hansen-Roach 16 Group, P_1	XSDRNPM, S_8 ENDF/B-IV, AMPX 218 Group, P_3	XSDRNPM, S_8 ENDF/B-IV, AMPX 19 Group, P_3	PX KENO ENDF/B-IV, P_{17}
93.2% enriched uranyl fluoride solution spheres. Infinite water reflector	CS1	76.1	1.0000	1.0088	1.0159	0.990 ± 0.005
	CS2	269.8	0.9963	1.0033	1.0096	0.989 ± 0.006
4.98% enriched uranyl fluoride solution spheres	CS4	490	0.988	0.9984	0.9973	0.983 ± 00.005
93.2% enriched uranyl nitrate solution spheres	CS5	425.1	0.9921	1.0057	1.0063	0.999 ± 0.003
	CS6	1377.8	1.0083	0.9995	1.0010	0.993 ± 0.005
Borated 93.2% enriched uranyl nitrate solution sphere	CS7	971.6	1.0055	0.9973	1.0003	0.992 ± 0.004

Table 2. Calculated Results for Critical Uranium Metal and Uranium Oxide Lattices with Clean and Borated Water Moderators

Critical Experiment	Water/Fuel Volume Ratio	Pitch (inches)	ENDF/B-IV Data		
			Point XSECS	218 Group	19 Group
WCAP[a] A water moderated 23 x 23 array of 2.72% enriched UO_2 rods	1.49	0.6	0.9869 ± 0.0063	0.9848 ± 0.0068	0.9867 ± 0.0044
EPRI[b] Clean water moderated lattice of 2.35% enriched UO_2 rods	1.20	0.615	0.9900 ± 0.0060	0.9864 ± 0.0042	0.9849 ± 0.0037
	2.41	0.750	---	0.9922 ± 0.0050	0.9934 ± 0.0039
	3.68	0.87	0.9984 ± 0.0061	0.9932 ± 0.0047	0.9934 ± 0.0039
EPRI[b] Borated water moderated lattice of 2.35% enriched UO_2 rods		0.615	---	---	0.9837 ± 0.0035
		0.75	---	---	0.9983 ± 0.0036
		0.87	---	---	1.0007 ± 0.0034
4.98% enriched metal rod[c], water moderated lattices in a basic 21 x 21 array from which rods were removed	3.09	0.512	---	---	0.9878 ± 0.005
	3.48	0.512	---	---	0.9952 ± 0.0050
	3.58	0.512	---	---	0.9965 ± 0.0050
	6.66	0.512	---	---	0.9967 ± 0.0050
	9.40	0.81	---	---	0.9913 ± 0.0053
	10.15	0.81	---	---	0.9908 ± 0.0044
	10.38	0.81	---	---	0.9962 ± 0.0051

[a] R. D. Leamer, et al., "Critical Experiments Performed With Clustered and Uniform Arrays of Rodded Absorbers, WCAP-3269-39 (November 1965).

[b] R. I. Smith and G. J. Konzek, "Clean Critical Experiment Benchmarks for Plutonium Recycle in LWR's," EPRI NP-196 (April 1976).

[c] E. B. Johnson, "Critical Lattices of U(4.98) Rods in Water and in Aquecus Boron Solution," ORNL-4280 (October 1968).

Table 3. Analysis of Plutonium Solution Critical Experiments

Benchmark Experiment No.[a]	Geometry	H/Pu[b] Atom Ratio	WT % Pu-240 in Plutonium	25 Group K-eff[c]
2	38.6 cm sphere	125	5	1.0197
4	38.6 cm sphere[d]	758	5	1.0194
7	45.4 cm cylinder	110	14	1.0043±0.004
9	61 cm cylinder[e]	210	8	1.0086±0.006
13	61 cm cylinder[e]	623	43	1.0145±0.003
14	38.6 cm sphere[c]	1067	4.6	1.0210

[a] U.P. Jenquin and S. R. Bierman, "Benchmark Experiments to Test Plutonium and Stainless Steel Cross Sections," Battelle Pacific Northwest Laboratories, to be published.

[b] The plutonium isotopes were given resolved resonance processing throughout the specified ENDF/B-IV range, e.g., down to 0.5eV for Pu-240.

[c] XSDRNPM analysis of spheres, KENO-IV analysis of cylinders.

[d] 6.604 mm thick stainless steel reflector.

[e] Water reflected.

Table 4. Analysis of Pu-Al Rod Lattices[a]

Lattice Spacing (in)	H/Pu Atom Ratio	ENDF/B-IV PX KENO, K-eff	25 Group KENO-IV, k-eff
	Al-1.8 wt% Pu (5.58 wt% Pu-240) Rods		
0.75	630	1.0189 ± 0.0051	1.0232 ± 0.0053
0.80	810	1.0138 ± 0.0062	1.0169 ± 0.0084
0.85	1000	1.0092 ± 0.0051	1.0214 ± 0.0093
0.90	1204	1.0116 ± 0.0040	1.0214 ± 0.0076
0.95	1418	1.0022 ± 0.0051	1.0223 ± 0.0064
	Al-2 wt% Pu (16.46 wt% Pu-240) Rods		
0.75	578	1.0311 ± 0.0059	1.0272 ± 0.0058
0.80	743	1.0267 ± 0.0062	1.0328 ± 0.0056
0.85	918	1.0314 ± 0.0050	1.0268 ± 0.0072
0.90	1104	1.0308 ± 0.0045	1.0210 ± 0.0061
0.95	1300	1.0327 ± 0.0050	1.0276 ± 0.0055

[a] V. O. Uotinen, et al., "Lattices of Plutonium-Enriched Rods in Light Water - Part I: Experimental Results," Nuclear Technology 15, 257 (August 1972).

Table 5. Analysis of EPRI[a] Mixed-Oxide Lattices

Benchmark Experiment No.	Lattice Spacing (cm)	H/Pu[b] Atom Ratio	Critical No. of Rods	Boron (wppm)	25 Group KENO-V K-eff
1	1.0031	185	469	3.5	0.9920 ± 0.0042
2	1.003	185	761	688.5	0.9972 ± 0.0037
3	1.2464	391	195	4.1	1.0073 ± 0.0041
4	1.2464	391	761	1093.5	1.0070 ± 0.0036
5	1.4186	564	160	6.0	1.0089 ± 0.0045
6	1.4186	564	689	768.0	1.0056 ± 0.0033

[a] R. I. Smith and G. J. Konzek, "Clean Critical Experiment Benchmarks for Plutonium Recycle in LWR's," NP-196, Vol. 1., Battelle Pacific Northwest Laboratories, April 1976.

[b] The plutonium isotopes were given resolved resonance processing throughout the specified ENDF/B-IV range, e.g., down to 0.5 eV for Pu-240.

Recommended Procedures For Applying the 218-Group Library

The 218-group library is too large to be effectively used in systems analysis. However, there are three procedures for applying the library in a practical manner to achieve reliable results.

1. If the system to be analyzed principally consists of the nuclides studied in the determination of the 27-group structure given in Figure 3, the AMPX module MALOCS[1] can be used to weight-function collapse to this group structure for problem-dependent resonance processing and systems analysis.

2. Lattice cell calculations can be performed with the 218-group library in the AMPX module XSDRNPM[1] in a reasonable amount of CPU time. Therefore, a very effective procedure is to perform problem-dependent resonance processing and lattice cell analyses in 218 groups, followed by a flux collapse to a broad-group structure for the systems analysis.

3. Finally, if the system to be analyzed contains nuclides appearing in Figure 1 but not in Figure 3, the opportunity exists for the user to develop his own broad-group structure. As noted before, the nuclide- dependent criteria to be considered in selecting a broad-group structure are tabulated in reference 2.

This work was funded under a task supported by the Transportation Branch, Office of Nuclear Material Safety and Safeguards, U.S. Nuclear Regulatory Commission.

REFERENCES

1. N. M. Greene, et al., "AMPX, A Modular Code System for Generating Coupled Multigroup Neutron-Gamma Libraries from ENDF/B," ORNL-TM-3706 (March 1976).

2. W. E. Ford, III, et al., "A 218 Neutron-Group Master Cross-Section Library for Criticality Safety Studies," ORNL/CSD/TM-4 (July 1976).

3. R. M. Westfall, et al., "Procedure for Determining Broad-Group Energy Structure for Criticality Safety Calculations," Trans. Am. Nucl. Soc., 22, 291 (1975).

4. G. E. Hansen and W. H. Roach, "Six and Sixteen Group Cross Sections for Fast and Intermediate Critical Assemblies," LAMS-2543, (1961).

Paper for presentation at *The RSIC Seminar-Workshop on Multigroup Cross-Section Preparation*, March 14-16, 1978, Oak Ridge National Laboratory, Oak Ridge, Tennessee; and for publication in the *Proceedings*.

THE MACK/MACKLIB SYSTEM FOR NUCLEAR RESPONSE FUNCTIONS*

M. A. Abdou and Y. Gohar

Applied Physics Division
Argonne National Laboratory
Argonne, Illinois 60439, U.S.A.

*Work supported by the U. S. Department of Energy.

THE MACK/MACKLIB SYSTEM FOR NUCLEAR RESPONSE FUNCTIONS*

M. A. Abdou and Y. Gohar
Applied Physics Division
Argonne National Laboratory
Argonne, Illinois 60439, U.S.A.

ABSTRACT

The MACK computer program calculates energy pointwise and multigroup nuclear response functions from basic nuclear data in ENDF/B format. The new version of the program MACK-IV, incorporates major developments and improvements aimed at maximizing the utilization of available nuclear data and ensuring energy conservation in nuclear heating calculations. A new library, MACKLIB-IV, of nuclear response functions was generated in the CTR energy group structure of 171 neutron groups and 36 gamma groups. The library was prepared using MACK-IV and ENDF/B-IV and is suitable for fusion, fusion-fission hybrids, and fission applications.

I. INTRODUCTION

A primary function of the neutronics and photonics analyses of a nuclear system is to estimate a set of nuclear response rates. The calculation of a nuclear response involves an integration over the appropriate phase space of the product of the neutron (or gamma) flux and a nuclear response function. The MACK/MACKLIB system is concerned with the computation and data management of the nuclear response functions. MACK is a computer program that calculates nuclear response functions such as neutron kerma factors, gas production, and tritium production cross sections from basic nuclear data in ENDF/B format. MACKLIB is a library of nuclear response functions in multigroup format, generated with MACK and is directly usable with most transport codes.

The MACK/MACKLIB system has evolved from a strong need in the nuclear fusion field for such a capability. The first versions of MACK[1] and MACKLIB[2] were released in 1973. These early versions have been used extensively with great success in many practical applications; the most noticeable of these is the area of the neutronics analysis for "pure" fusion reactor designs. Over the past two years, major developments have been made in the calculational algorithms and new capabilities have been added into the MACK code. The new version of the code has been released recently as MACK-IV.[3] This new version maximizes the utilization of available

*Work supported by the U. S. Department of Energy.

BLANK PAGE

nuclear data and is intended to be usable in more practical applications such as fission reactors, fission-fusion hybrids in addition to pure fusion and others. A new version of MACKLIB has also been produced and released as MACKLIB-IV.[4] The library was generated with MACK-IV and the primary source of basic nuclear data was ENDF/B-IV.[5] The library includes response functions for a large number of materials and has a new versatile format. The response functions are given in a fine-energy group structure (171 for neutrons and 36 for gammas). A retrieval routine is available to prepare data from MACKLIB-IV in a broader group structure.

The purpose of this paper is to present an overview of the MACK/MACKLIB system. The most important part of the MACK program concerns the calculation of the neutron kerma factors. The basic theory and the calculational algorithms for kerma factors in MACK-IV are discussed briefly in Sec. II. Consistency in preserving the energy and the relationship between the kerma factors and gamma production cross sections are delineated in this section. The general features of MACK-IV are discussed in Sec. III. A description of the important characteristics of MACKLIB-IV is the subject of Sec. IV. A summary is given in Sec. V.

II. NUCLEAR HEATING CALCULATIONAL ALGORITHMS AND MACK-IV

Calculation of the response function for nuclear heating is the central part of the program MACK. The basic theory for these calculations is summarized in this section. The major differences in the calculational algorithms between the earlier version of MACK and the present MACK-IV are also pointed out.

The nuclear heating $H_t(\vec{r})$, at any spatial point $\vec{r}$, is the sum of the neutron heating, $H_n(\vec{r})$, and the gamma heating, $H_\gamma(\vec{r})$, where[6,7]

$$H_n(\vec{r}) = \sum_j N_j(\vec{r}) \int \phi_n(\vec{r},E_n) k_{nj}(E_n)\, dE_n \tag{1}$$

$$H_\gamma(\vec{r}) = \sum_j N_j(\vec{r}) \int \phi_\gamma(\vec{r},E_\gamma) k_{\gamma j}(E_\gamma)\, dE_\gamma \,, \tag{2}$$

and where $N_j(\vec{r})$ is the number density of nuclide j at $\vec{r}$; $k_{nj}(E_n)$ is the response function for nuclear heating which is more commonly known as the neutron kerma factor for nuclide j at neutron energy, E_n; $k_{\gamma j}(E_\gamma)$ is the gamma-ray kerma factor for nuclide j at photon energy, E_γ; and $\phi_n(E_n)$ is the neutron flux for neutrons of energy E_n. The gamma flux, ϕ_γ, is obtained by solving the transport equation with a secondary photon production source,

$$S_\gamma\left(\vec{r},E_\gamma\right) = \sum_j N_j(\vec{r}) \int \phi_n\left(\vec{r},E_n\right)\sigma_{pj}\left(E_n,E_\gamma\right)\, dE_n \ , \tag{3}$$

where σ_{pj} is the photon production cross section in nuclide j for neutrons of energy E_n and photons of energy E_γ. The summation over j includes all nuclides in the mixture present at $\vec{r}$. The neutron kerma factor can be written as

$$k_{nj}(E) = \sigma_{tj}(E)\left(E + \sum_i \frac{\sigma_{ij}}{\sigma_{tj}} Q_{ij} + \sum_{i'} \frac{\sigma_{i'j}}{\sigma_{tj}} E_{Di'j} - \sum_m \frac{\sigma_{mj}}{\sigma_{tj}} \bar{E}_{n',mj} - \frac{1}{\sigma_{tj}} S^*_{E\gamma,j}\right), \tag{4}$$

where σ_t is the total microscopic collision cross section, and the terms in parentheses are the energies contributed or taken by a particular reaction weighted by the relative probability of the reaction. The first term is the energy of the incident neutron times the probability that a collision occurred which is certain; Q_i is the energy resulting from mass conversion in reaction i; $E_{Di'}$ is the average decay energy per reaction i'; $E_{n',m}$ is the average secondary neutron energy per reaction m, and

$$S^*_{E\gamma,j}\left(E_n\right) = \int \sigma_{pj}\left(E_n,E_\gamma\right)E_\gamma \, dE_\gamma \ , \tag{5}$$

$$k_{\gamma j}(E) = \sigma_{pe,j}E + \sigma_{ca,j}E + \sigma_{pp,j}\left(E - a_{pp}\right) , \tag{6}$$

where σ_{pe}, σ_{ca}, and σ_{pp} are the gamma-interaction cross sections for photoelectric, compton absorption, and pair-production processes, respectively; and a_{pp} is equal to 1.02 MeV. The kerma factors are flux and density independent. The heating rate can therefore be calculated from neutron and photon transport results for any system if these factors are predetermined for all materials in the system. The evaluation of $k_{\gamma j}$ is straightforward and is normally performed by the codes which generate photon-interaction multigroup cross sections such as MUG.[8] Calculation of neutron kerma factors is complicated by the variety of reactions that a neutron can undergo, the kinematics for reactions in which more than one particle is emitted, and the demand for extensive nuclear data information.

All the terms in Eq. (4) except $S^*_{E\gamma}$ are calculated in MACK from basic nuclear data in files 1 through 5 of ENDF/B. The calculation of these

terms is somewhat straightforward and is similar in many respects to the methodologies employed in other multigroup cross-section processing codes. The calculation of $S^*_{E\gamma}$, however, is more involved and has been the subject of a large part of the developments in MACK-IV. This term can be calculated by the new version of the program, MACK-IV, via one of two paths as selected by the user:

Path I. The Nuclear Kinematics Path: In this path the solutions of the kinematics equations of all nuclear reactions are used to calculate $S^*_{E\gamma}$. In this methodology no direct information on gamma production is required. One needs the individual neutron reaction cross sections and the provided in files 1-5 of ENDF/B. If charged particles are emitted in a reaction [e.g. (n,α) reaction], one needs the partial cross sections for this reaction to individual excited levels (i.e. the 700's MT series) or the energy distribution of the charged particles emitted. This type of information is scarce in ENDF/B and this leads to difficulties in calculating neutron kerma factors for charged-particle-producing reactions associated with strong gamma-ray emission.

Path II. The Gamma Production Path: In this path, $S^*_{E\gamma}$ is calculated directly from the gamma production data (files 12-15 in ENDF/B) as

$$S^*_{E\gamma}(E_n) = \int \sigma_p(E_n, E_\gamma) E_\gamma \, dE_\gamma ,$$

where $\sigma_p(E_n, E_\gamma)$ is the production cross section for a photon of energy E_γ at an incident neutron energy E_n.

When energy-conserving gamma production data are given in ENDF/B the gamma-production path provides a more reliable and straightforward methodology to calculating the neutron kerma factors. This path was not provided in the earlier version of MACK because of the lack of most gamma production data at that time. These data have been provided for a large number of materials in ENDF/B-IV to warrant the new development. The nuclear kinematics path has been retained and improved in MACK-IV because: (1) gamma-production data are still lacking for some important materials (e.g. ^{11}B, ^{232}Th, etc.); (2) the gamma-production data provided in ENDF/B for some materials are not consistent with the neutronics data content as to energy conservation; and (3) the kinematics path provides a convenient way for calculating the contribution to heating from each individual reaction, which is of interest in specialized nuclear and chemonuclear applications.

III. GENERAL FEATURES OF MACK-IV

The purpose of this section is to briefly describe the general features of MACK-IV. A simplified flow diagram of the calculations in MACK-IV is given in Fig. 1. The program calculates pointwise and/or multigroup nuclear response functions. The pointwise energy mesh, group structure, and weighting functions can be provided by input or selected from several

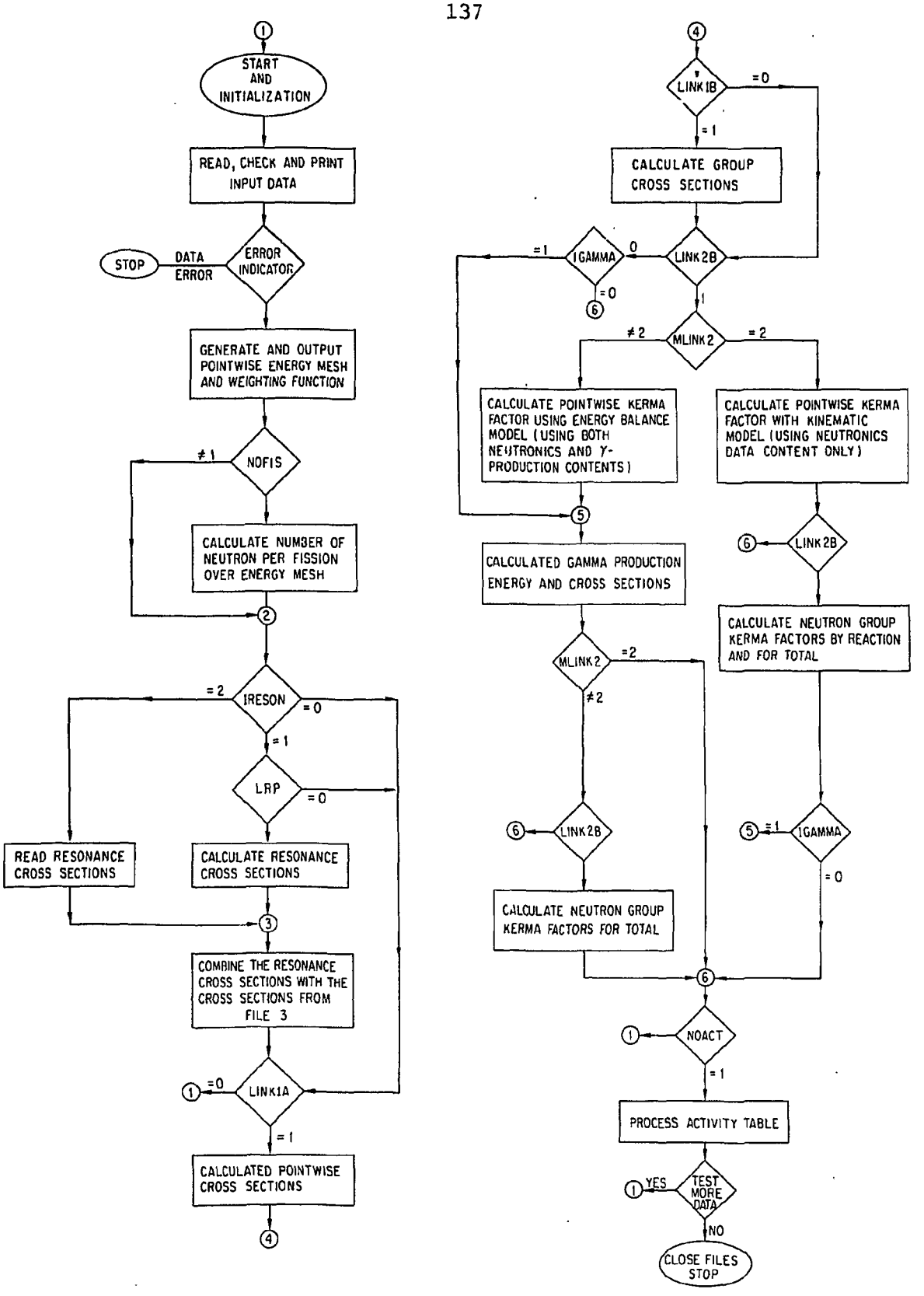

Fig. 1. A flow diagram for MACK-IV.

built-in procedures. The program has the capability to calculate the neutron cross sections in the resonance region from resonance parameters given in file 2 of ENDF/B. The program also permits reading the resonance region cross sections as input.

There is a large number of user's selected options to control the flow and methodology of computations as well as the type and format of the output. These are described in Ref. 3. All materials including fissionable isotopes can be processed by MACK-IV. Among the types of information that can be generated with MACK-IV are:

(1) Pointwise and multigroup neutron kerma factors.

(2) Pointwise and multigroup reaction cross sections.

(3) Multigroup response functions for specific nuclear processes. An example is the helium-production cross section which is calculated in MACK-IV by summing the appropriate reactions such as (n,α); $(n,n'\alpha)$ and $(n,3\alpha)$ with the multiplicities of the alpha generation accounted for.

(4) Gamma-production cross sections and the gamma-production energy matrix.

MACK-IV has a new processor that enables the user to produce the nuclear response functions for each material in the "MACK-Activity-Table" format. The format of the table is similar to that used for multigroup (transport) cross sections commonly employed in transport codes such as ANISN, DØT, and MØRSE. The data are arranged by groups (group 1, 2 . . . through group IGM) and the data for each group are given in IHM positions as illustrated in Table I. As shown in this table, the type of information given in positions 1 through 34 is fixed. For example, the neutron kerma factor is always given in position 2 and the tritium-production cross section is given in position 7. The advantage of this format is that it provides a versatile capability for mixing the activity tables for different materials to obtain a response function table for any mixture.

One convenient way to employ the MACK-Activity-Tables is to mix them (explicitly) with the "regular transport" multigroup cross sections. The number density for each activity table should be the appropriate number density for the material multiplied by a small (e.g. 10^{-15}) fixed number, f. This multiplication factor ensures that the transport cross sections are not significantly altered. The reaction rates and other integrated responses calculated by the transport codes will be the true values multiplied by f. For this procedure to be successful the value of IHM provided as input to MACK must be equal to that employed in the regular transport multigroup cross sections (generally IHM $\geq$ IGM + 3).

The MACK-Activity-Tables can be produced in neutron-gamma-coupled format for use with coupled neutron-gamma multigroup cross sections. In this case, the gamma kerma factors have to be provided as input to MACK-IV. The data given in positions 1, 2, and 3 are such that the integrated responses

for these positions are the total, neutron, and gamma heating, respectively. The atomic displacements cross sections are not calculated in MACK-IV at present but they are accepted as input to fill positions 4 and 5 of the activity table.

Table 1. MACK-Activity-Table

Position	Content
1	Neutron and gamma kerma factors
2	Neutron kerma factor
3	Gamma kerma factor
4	Displacement cross section - A
5	Displacement cross section - B
6	Total hydrogen production cross section
7	Total tritium production cross section
8	Total helium production cross section
9	Total cross section
10	Elastic cross section
11	Total inelastic cross section
12	Total (n,2n) cross section
13	(n,3n) cross section
14	Total fission cross section
15	(n,n't) cross section
16	(n,n') continuum cross section
17	(n,γ) cross section
18	(n,p) cross section
19	(n,D) cross section
20	(n,t) cross section
21	(n,^{3}He) cross section
22	(n,α) cross section
23	Elastic scattering kerma factor
24	(n,n') charged particles kerma factor
25	Inelastic-level scattering kerma factor
26	(n, charged particles) kerma factor
27	(n,2n) kerma factor
28	(n,3n) kerma factor
29	Fission kerma factor
30	Inelastic continuum kerma factor
31	Radiative capture kerma factor
32	Group mid-energy for neutron and gamma
33	Group mid-energy for neutron only
34	Group mid-energy for gamma only
35	Positions 35 through IHM are filled with cross sections for the MT reactions not given in the fixed positions 1 through 34.
.	
.	
.	
IHM	

The computational time varies significantly from isotope to isotope. The CPU time is most sensitive to the requirement of cross section calculations in the resolved resonance region and Doppler broadening. Table 2 shows a sample of the CPU time on the IBM-370 Model 195 to completely process all types of data for several materials with one-thousand energy points and 171 neutron energy groups. The machine core storage requirements vary typically from ∿400 to 900 k bytes on the IBM-370 Model 195 computer.

IV. MACKLIB-IV LIBRARY

A new library, MACKLIB-IV, of nuclear response functions has recently been generated. The library was prepared using MACK-IV and basic nuclear data from ENDF/B-IV. Nuclear response functions are provided in the library for all materials listed in Table 3. These materials are of great interest in fusion, fusion-fission hybrids, and fission application.

The library is in the new format of "MACK-Activity-Table" described earlier in this paper and shown in Table 1. The response functions included in the library are neutron kerma factors, gamma kerma factors, atomic displacements, gas-production and tritium-breeding functions, and all important reaction cross sections. The gamma kerma factors were generated with MUG[8] and the atomic displacements were taken from Doran's work.[9]

MACKLIB-IV employs the CTR energy group structure[10] of 171 neutron groups and 36 gamma groups. A retrieval program is included with the library to perform the following functions: (1) collapse the data into a broader group structure; (2) modify (add, delete, replace) parts of the library; (3) prepare activity tables for mixtures of materials in the library; and (4) output the data in printed, punched, and/or magnetic tape format.

As discussed in the previous section, one of the significant improvements in MACK-IV is the provision for two different calculational techniques for neutron kerma factors: (1) the nuclear kinematics path which utilizes only the neutron data files in ENDF/B; and (2) the gamma-production path which employs the gamma-production files as well as the neutron files. While the basic formalisms of the two methods are exact, the accuracy of the kerma factors calculated differs for the two methods depending on the type and accuracy of information provided in the ENDF files. The ENDF/B-IV evaluations were reviewed for each material and an appropriate calculational technique was selected to ensure the relative validity of the results.

As an example, the neutron kerma factor, k_n, for beryllium is plotted in Fig. 2 for three cases: (1) k_n based on ENDF/B-III data using the nuclear kinematics path; (2) k_n based on ENDF/B-IV data calculated with the nuclear knematics path; and (3) k_n based on ENDF/B-IV data using the gamma-production path. Comparing (1) and (2), one notes that the changes in the basic data from Version III to IV is very small. The neutron kerma factor

Table 2. Sample of CPU time (s) for MACK-IV

	Path I[a]	Path II[a]
^{6}Li	18	45
^{7}Li	18	46
Na[b]	66	286
Cr[b]	145	237
^{238}U[b]	243	387

[a] Path I: kerma factors from nuclear kinematics.
Path II: kerma factors from gamma production path.

[b] Includes resonance calculations.

Table 3. List of Materials in MACKLIB-IV

	ENDF/B MAT No.		ENDF/B MAT No.
Hydrogen	1269	Copper	1295
Helium	1146	Niobium	1189
Lithium-6	1271	Molybdenum	1287
Lithium-7	1272	Tantalum	1285
Beryllium	1289	Tungsten-182	1128
Boron-10	1273	Tungsten-183	1129
Boron-11	1160	Tungsten-184	1130
Carbon	1274	Tungsten-186	1131
Nitrogen	1275	Lead	1288
Oxygen	1276	Thorium-232	1296
Flourine	1277	Protactinium	1297
Sodium	1156	Uranium-233	1260
Magnesium	1280	Uranium-234	1043
Aluminum	1193	Uranium-235	1261
Silicon	1194	Uranium-236	1163
Chlorine	1149	Uranium-238	1262
Potassium	1150	Neptunium	1263
Calcium	1195	Plutonium-238	1050
Titanium	1286	Plutonium-239	1264
Vanadium	1196	Plutonium-240	1265
Chromium	1191	Plutonium-241	1266
Manganese	1197	Plutonium-242	1161
Iron	1192	Americium-241	1056
Cobalt	1199	Americium-243	1057
Nickel	1190		

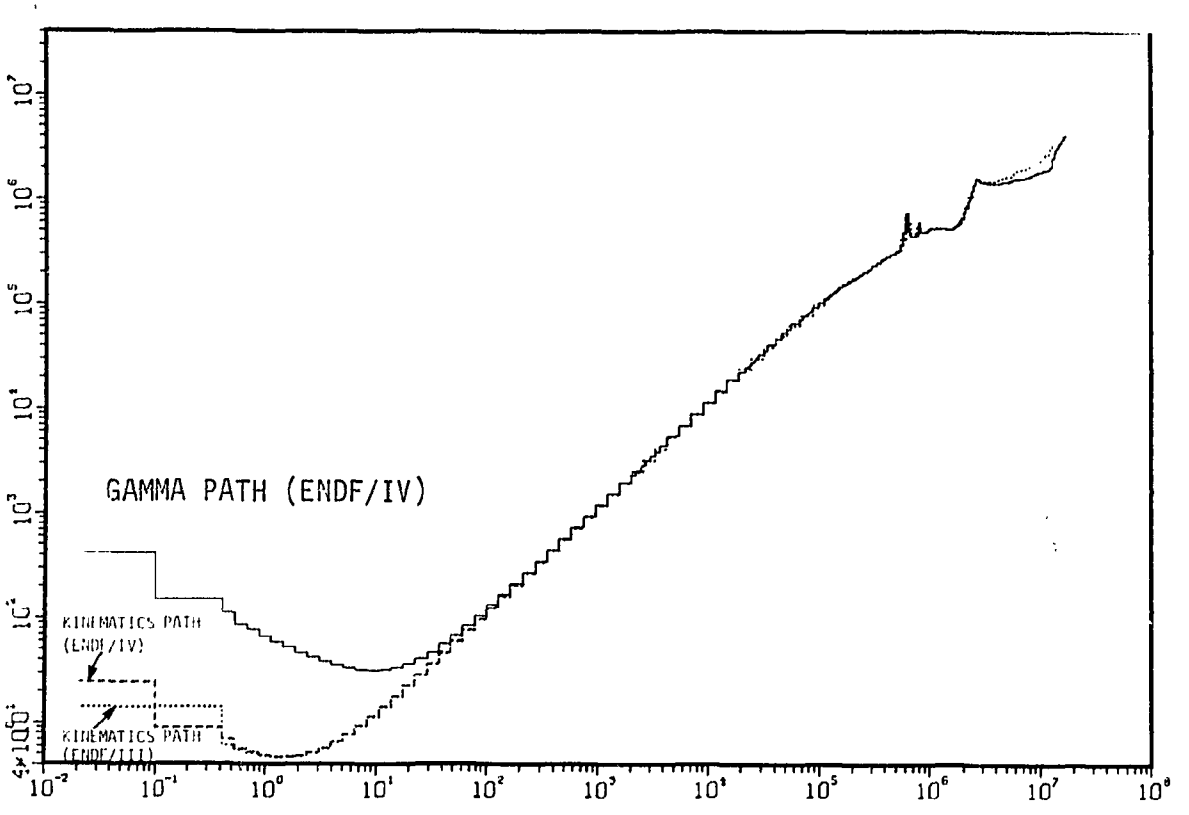

Fig. 2. Neutron kerma factors for beryllium.

calculated in Case 2 is higher than that in Case 3 at high energies (>10 MeV). The reason is that no information on the individual levels (partial level cross sections) are given in the neutron files for the (n, charged particles) reactions. In this case it is clear that the results from Case 3 are more accurate than those of Case 2 and hence the kerma factors calculated from the gamma-production path are adopted for inclusion in MACKLIB-IV.

The library also includes response functions for fissionable materials. The neutron kerma factors for ^{235}U, ^{232}Th, and ^{238}U are displayed in Fig. 3. Using the kerma factor methodology for calculation of nuclear heating in nuclear systems with fissionable materials should provide a significant improvement over the approximate methods commonly used at present. Table 4 compares the neutron kerma factors in MACKLIB-IV[4] to those in the earlier version of MACKLIB[2] for several materials. The comparison is shown for selected energy ranges where large differences occur. These differences reflect a combination of effects due to changes in basic nuclear data between Versions III and IV of ENDF/B as well as differences in calculational methods.

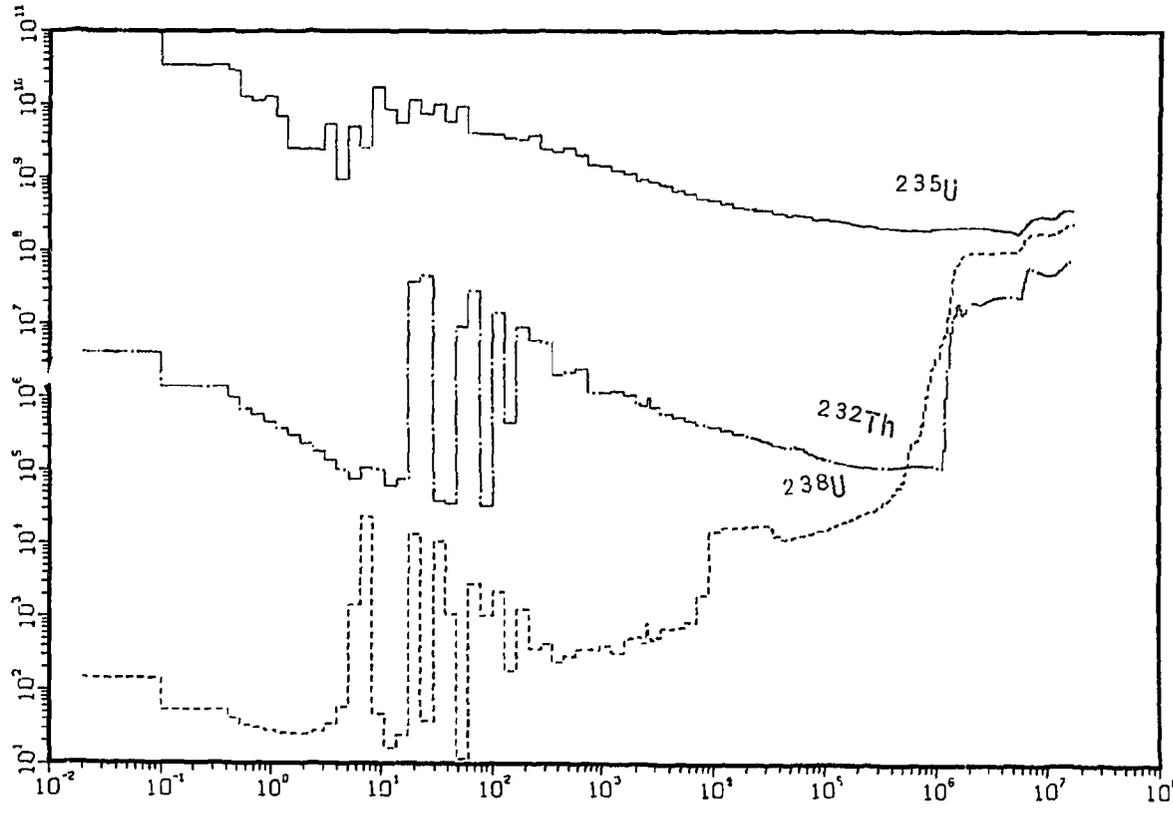

Fig. 3. Neutron kerma factors for ^{232}Th, ^{235}U, and ^{238}U

Table 4. Comparison of Neutron Kerma Factors in MACKLIB-IV[a] and MACKLIB[b] for Several Materials in Selected Energy Groups[c,d]

	13.499-14.918		10.0-11.052		1.0026-1.102	
Mat.	MACKLIB/IV	MACKLIB	MACKLIB/IV	MACKLIB	MACKLIB/IV	MACKLIB
Be	3.018	3.473	1.848	2.738	0.516	0.521
^{6}Li	4.901	4.400	4.760	4.154	1.684	1.782
^{7}Li	4.185	3.313	3.785	2.952	0.408	0.416
^{10}B	6.260	3.686	5.002	3.433	1.118	1.518
^{12}C	4.618	3.244	1.980	2.407	0.350	0.364
Al	6.252	4.010	2.852	2.893	0.148	0.206
Nb	1.207	1.045	0.764	0.792	0.082	0.093
Cu	3.517	2.712	1.898	1.994	0.096	0.101
Pb	0.282	0.266	0.232	0.252	0.041	0.047

[a]See Ref. 4.

[b]See Ref. 2.

[c]All MACKLIB kerma factors are based on ENDF/B-III data but those of MACKLIB-IV are based on ENDF/B-IV.

[d]All neutron kerma factors in units of MeV-barn/atom.

V. SUMMARY

Major developments have been made in the calculational aogirthms and new capabilities have been added into the MACK computer program. The new version of the program, MACK-IV, is available for distribution. The program generates important nuclear response functions such as neutron kerma factors and tritium breeding and gas production functions as well as the gamma production cross sections. The new developments in MACK-IV represent a major step in ensuring energy conservation in nuclear heating calculations. The program is useful in almost all practical nuclear applications.

A new library, MACKLIB-IV, of nuclear response functions was generated using MACK-IV and basic nuclear data from ENDF/B-IV. The library includes data for a large number of materials of great interest in fusion, fusion-fission hybrids, and fission applications. The library and a retrieval routine are readily available from major nuclear information centers.

REFERENCES

1. M. A. ABDOU, C. W. MAYNARD and R. Q. WRIGHT, "MACK: A Computer Program to Calculate Neutron Energy Release Parameter (Fluence-to-Kerma Factors) and Multigroup Neutron Reaction Cross Sections from Nuclear Data in ENDF Format," ORNL-TM-3994, Oak Ridge National Laboratory (1973); also UWFDM-37.

2. M. A. ABDOU and R. W. ROUSSIN, "MACKLIB 100-Group Neutron Fluence-to-Kerma Factors and Reaction Cross Sections Generated by the MACK Computer Program from ENDF Format," ORNL-TM-3995, Oak Ridge National Laboratory (1973).

3. M. A. ABDOU, Y. GOHAR and R. Q. WRIGHT, "MACK-IV, A New Version of MACK: A Program to Calculate Nuclear Response Functions from Data in ENDF/B Format," ANL/FPP-77-5, Argonne National Laboratory (1978).

4. Y. GOHAR and M. A. ABDOU, "MACKLIB-IV, A Multigroup Library of Nuclear Response Functions," ANL/FPP/TM-106, Argonne National Laboratory (1978).

5. D. GARBER, C. DUNFORD and S. PEARLSTEIN, "Data Formats and Procedures for the Evaluated Nuclear Data File, ENDF," BNL-NCS-50496, Brookhaven National Laboratory (1975).

6. M. A. ABDOU and C. W. MAYNARD, "Calculational Methods for Nuclear Heating. Part I. Theoretical and Computational Algorithms," Nucl. Sci. Eng. 56, 360 (1975).

7. M. A. ABDOU and C. W. MAYNARD, "Calculational Methods for Nuclear Heating. Part II. Applications to Fusion Reactor Blanket and Shields," Nucl. Sci. Eng. 56, 381 (1975).

8. J. R. WRIGHT and F. R. Mynatt, "MUG: A Program for Generating Multigroup Photon Cross Sections," CTC-17 (1970).

9. D. G. DORAN and N. J. GRAVES, "Displacement Cross Sections and PNA Spectra: Tables and Applications," HEDL-TMG-76-70, Hanford Engineering Development Laboratory (1976).

10. R. W. ROUSSIN, ET AL., "The CTR Processed Multigroup Cross Section Library for Neutronics Studies," ORNL/RSIC-37, Oak Ridge National Laboratory (1977).

BLANK PAGE

RESOLVED RESONANCE PROCESSING IN THE AMPX MODULAR CODE SYSTEM

R. M. Westfall
Computer Sciences Division,
Union Carbide Corporation, Nuclear Division
Oak Ridge National Laboratory
Oak Ridge, Tennessee, U.S.A.

ABSTRACT

The energy and spatial treatments employed in the AMPX modules BONAMI, NITAWL and ROLAIDS are described. Recommendations are made on the suitability of the various analytical models for particular applications.

INTRODUCTION

The initial problem-dependent resolved resonance processing capability in AMPX[1] was the Nordheim[2] integral treatment as applied in the NITAWL module. Recently, two new resonance processing modules, BONAMI and ROLAIDS, have been developed for application in AMPX. The BONAMI module employs the BONDARENKO[3] or shielding factor method. The ROLAIDS module performs an interface-currents, integral transport solution for energy-pointwise, slowing down flux distributions in multiregion, one-dimensional geometries.

The purpose of this paper is to describe the analytical models employed in these three modules from the viewpoint of the assumptions inherent in the energy and spatial treatments applied therein. Hopefully, through a comparison of the similarities and differences between the three methods, the potential user will gain an appreciation of which approach might be most suitable for his particular application.

Energy Treatments

NITAWL, BONAMI and ROLAIDS each shield resonance cross sections through an integral weighting using some approximation for the slowing-down flux interacting with the resonance nuclides. Ignoring, for the time being, the spatial dependence of the slowing-down flux, the collision density at energy E due to isotropic elastic scattering at higher energies E' is written as

$$\sigma(E)\phi(E) = \int_E^{E/\alpha_m} \frac{\sigma_m \phi(E')dE'}{(1-\alpha_m)E'} + \int_E^{E/\alpha_a} \frac{\sigma_s(E')\phi(E')dE'}{(1-\alpha_a)E'} \quad , \qquad (1)$$

where

$$\sigma(E) = \sigma_m(E) + \sigma_s(E) + \sum_x \sigma_x(E),$$

$$\alpha = \left(\frac{A - 1}{A + 1}\right)^2 \equiv \text{the minimum fractional energy after collision, and}$$

subscripts m and a refer to moderator and absorber materials, respectively.

The three modules employ substantially different approximations in obtaining the slowing-down flux $\phi(E')$. These approximations are listed in Fig. 1. The narrow resonance approximation applies when the practical width of the resonance, Γ_p, is much less than the energy interval over which the absorber down-scatters. In effect, the resonance does not perturb the slowing-down flux available to it. The isolated resonance approximation applies when the resonances are spaced sufficiently wide apart so that the slowing-down flux can recover its asymptotic form between resonances. The infinite absorber mass approximation applies when the slowing-down is dominated by nuclides other than the absorber. Effectively, it justifies the neglect of slowing-down sources from resonance nuclides. The assumption of a linear variation of the scattering density ($\sigma_s(E')\phi(E')$) is applicable over very small energy ranges or when these two functions are varying slowing with energy.

1. Narrow Resonances, i.e., $\Gamma_p = << (1-\alpha_a)E_0$
2. Isolated Resonances
3. Infinite Absorber Mass, i.e., $\alpha_a = 1$
4. Linear Variation of Scattering-Density with Energy

Fig. 1. Approximations to Obtain Slowing-Down Flux

The Bondarenko method assumes narrow, isolated resonances which permit the expression of the slowing-down flux in an asymptotic form, i.e., $\sigma(E') = 1/E'$. Substitution of $\phi(E')$ into Eq. (1) and integration over the slowing-down intervals yields:

$$\phi(E) = \frac{\sigma_m + \sigma_{pot}}{E[\sigma_m + \sigma_s(E) + \sum_x \sigma_x(E)]}, \qquad (2)$$

where the moderator cross section is assumed constant and only potential scattering is considered for the absorber. The various reaction types represented by σ_x are temperature dependent. The expression for $\phi(E)$ given in Eq. (2) (or a similar form) is used to weight the cross sections over the group structure and develop shielding factors as a function of

σ_m and temperature. On a problem-dependent basis, BONAMI develops the background cross sections, selects the appropriate shielding factors and produces the shielded library.

The Nordheim integral treatment assumes isolated resonances and treats each resonance independently. For each resonance, the flux in the absorber region is obtained by numerical integration over a fine group (450 lethargy intervals) mesh with slowing-down sources due to the absorber and two moderators explicitly calculated as in Eq. (1). In the NITAWL module, faster procedures for obtaining the slowing-down sources based on the narrow resonance and infinite mass approximations are available as options. Resonance wing corrections and resonance-independent background (ENDF/B File 3 data) are add-in on a multigroup basis.

The ROLAIDS module sets up a variable energy mesh chosen to fit the cross section structure of all the nuclides present in the problem. With an assumed 1/E shaped source scattering down from above the maximum energy, ROLAIDS performs an interface-currents, integral transport solution for the flux at each energy point. The solution is similar to that employed in the RABBLE program.[4] The calculated flux at each energy point is used with the assumption of a linear variation of the scattering density between points to analytically integrate the slowing-down sources due to each nuclide to all lower energy points.

Spatial Treatments

The BONAMI and NITAWL modules employ the same two-region model in which the absorber region can be adjacent to a moderator region containing a 1/E shaped flux. In BONAMI, the homogeneous medium background cross section is modified with an escape cross section to account for neutron sources due to the external moderator. In NITAWL, the fine-group fluxes calculated across each resonance are augmented by the external 1/E shaped source. In both modules, the major effort in calculating heterogeneity effects is in the determination of how much of the 1/E shaped source penetrates the absorber region.

The ROLAIDS module contains the true multiregion calculation based on the interface-currents technique. The geometry capabilities were designed to be compatible with the one-dimensional discrete-ordinates program XSDRNPM.[1] Thus the user has options of any number of zones in slab, cylindrical or spherical geometries with reflected (white), vacuum or periodic boundary conditions, as appropriate. Scattering is assumed to be isotropic. Furthermore, the interface-currents integral transport technique employs escape and transmission probabilities which are similar to those used by NITAWL. Various approximations applied to the spatial models are summarized in Fig. 2.

Considerations on Application

The applicability of the three models is highly system-dependent. However, for a wide range of applications, the difference between the models is in the capability to calculate second order effects. Assuming

the system to be analyzed can be adequately represented with a two-region model, the user should consider the importance of other effects such as the treatment of resonance scattering or resonance overlap. Procedures followed in shielding transfer arrays are summarized in Fig. 3. The analytical technique of Bucholz[5] is applied in ROLAIDS to generate transfer arrays which account for the relative location of resonance scattering in each source group term. Mathews[6] has shown this to be important in systems with intermediate levels of moderation.

Both NITAWL and BONAMI employ the monoenergetic, two-region reciprocity theorem in determining the penetration of the external source into the absorber region. This approach involves the escape probability from the fuel and a Dancoff factor to account for neighboring fuel regions.

NITAWL - 1. Constant Dancoff factor supplied by user.

2. Escape probabilities from Case, de Hoffman and Placzek.

BONAMI - 1. Groupwise Dancoff factor calculated with Sauer's approximations.

2. Escape probabilities from the Levine-modified, Wigner rational approximation.

ROLAIDS - 1. Multiregion geometries with reflective boundary conditions precludes the need for a Dancoff factor.

2. Escape and transmission probabilities assume uniform, isotropic sources in each region and isotropic fluxes at each boundary.

Fig. 2. Spatial Approximations.

1. BONAMI shields the multigroup values (MT=2) and renormalizes the transfer arrays.

2. NITAWL shields the scattering with fine-group fluxes and renormalizes the transfer arrays with the multigroup values.

3. ROLAIDS generates transfer arrays weighted by the pointwise fluxes, applying the point-to-group analytic technique of Bucholz.

Fig. 3. Resonance Scattering.

The calculation of resonance overlap effects should be considered for systems which contain substantial quantities of the various actinides. The base energies of several large resonances subject to overlap effects are listed in Table 1. Again, the overlap effect is most important in systems with significant reactivity generated in the epithermal energy range.

Table 1. Potential Resonance Overlap

Nuclide	Resonance Energy, E_0			
U-238	6.67	21.0	36.7	66.2
Th-232		21.78		69.13
U-233	6.82			
Pu-239				66.0
Pu-240			38.1	

A very common application of these modules is in the analysis of light-water moderated, pin-fuel lattice cells. Multigroup cross sections generated by ROLAIDS and by NITAWL using both the Nordheim method and the narrow resonance approximation for a 0.615 inch pitch, low-enriched fuel cell are given in Table 2. Compared to the 1/E weighted values of the cross sections, the shielded values are in reasonably good agreement. However, assuming the ROLAIDS values to be correct, the Nordheim integral method and the narrow resonance approximation are seen to over-shield the ^{238}U resonances. This effect leads to the range in infinite lattice multiplication factors listed below.

Resonance Processing:	NITAWL (Narrow Resonance)	NITAWL (Nordheim)	ROLAIDS
k_∞	1.3143	1.3002	1.2889

The spread in the effective multiplication factors for finite systems would probably be somewhat less.

Finally, a practical consideration in selecting which of these modules should be used in a particular application is the relative investment in computational resources. Typical running times for the three modules are given in Table 3. The running times indicate that, where applicable, NITAWL and BONAMI should be used for production work. At the present time, the primary interest in ROLAIDS is in benchmarking heterogeneity and overlaps effects.

Table 2. U-238 Cross Sections Shielded for the 0.615 Inch Pitch Cell[a] of Smith and Konzek[b]

Upper Energy	σ_c (NR)	σ_c (Nordheim)	σ_c (ROLAIDS)	σ_c (1/E)
3 KeV	1.03	1.06	1.12	2.29
550 eV	1.42	1.73	1.76	11.84
100	2.43	3.10	3.15	46.35
30	2.81	3.02	3.16	57.15
10	6.31	5.82	6.35	110.75
3.05 eV				

σ_s (NR)	σ_s (Nordheim)	σ_s (ROLAIDS)	σ_s (1/E)
12.67	12.36	12.67	19.69
11.86	12.64	12.69	40.25
10.52	11.70	11.85	61.98
8.72	9.05	9.18	28.88
8.65	8.79	8.87	14.94

[a] 2.35 wt % enriched UO_2 fuel, Al clad, no boron in H_2O.

[b] R. I. Smith and G. J. Konzek, "Clean Critical Experiment Benchmarks for Plutonium Recycle in LWR's," NP-196, Vol. 1, Battelle Pacific Northwest Laboraotires, April 1976.

Table 3. Relative Running Times

Problem	BONAMI	NITAWL	ROLAIDS
Homogeneous Absorber-Moderator	Few Seconds	Tens of Seconds	Few Minutes
Several Absorbers, External Moderators	Few Seconds	Few Minutes	∿Ten Minutes
Ten Absorbers, Ten Regions	--	--	Tens of Minutes

This work was funded under a task supported by the Transportation Branch, Office of Nuclear Material Safety and Safeguards, U.S. Nuclear Regulatory Commission.

REFERENCES

1. N. M. Greene, et al., AMPX: A Modular Code System for Generating Coupled Multigroup Neutron-Gamma Libraries from ENDF/B, ORNL/TM-3706 (March 1976).

2. L. W. Nordheim, "The Theory of Resonance Absorption," Proceedings of Symposia in Applied Mathematics, Vol. XI, p. 58, Garret Birkhoff and Eugene P. Wigner, Eds., Am. Math. Soc. (1961).

3. I. I. Bondarenko, et al., "Group Constants for Nuclear Reactor Calculations," Consultants Bureau, N.Y. (1964).

4. P. H. Kier and A. A. Robba, RABBLE, A Program for Computation of Resonance Absorption in Multiregion Reactor Cells, ANL-7326 (1967).

5. J. A. Bucholz, "An Analytic Angular Integration Technique for Generating Multigroup Transfer Matrices," Proceedings of RSIC Seminar-Workshop on Multigroup Nuclear Cross-Section Preparation (1978).

6. D. R. Mathews, "Self-Shielded Scattering Transfer Array Effects," Trans. Am. Nucl. Soc., 13, 324 (1970).

CROSS SECTION PROBABILITY TABLES IN MULTI-GROUP TRANSPORT CALCULATIONS*

Dermott E. Cullen, Ernest F. Plechaty and Richard J. Doyas
Lawrence Livermore Laboratory, Livermore, California, U.S.A.

and

Charles R. Weisbin and John E. White
Oak Ridge National Laboratory, Oak Ridge, Tennessee, U.S.A.

ABSTRACT

The use of cross section probability tables in multi-group transport calculations is presented. Emphasis is placed on how probability table parameters are generated in a multi-group cross section processor and how existing transport codes must be modified to use them. In order to illustrate the accuracy obtained using probability tables, results will be presented for a variety of neutron and photon transport problems.

INTRODUCTION

The probability table method was developed in order to account for spatially dependent self-shielding-effects as applied to Monte Carlo neutron transport calculations in the unresolved resonance region.[1] More recently the probability table method has been extended for use in multi-group calculations.[2,3] In addition, the method has been extended to apply to all energy ranges[4] and to both neutron and photon transport problems.[5]

At Livermore the probability table method has been applied in the neutron multi-group transport code TARTNP[6] and the photon multi-group transport code LASNEX.[7] At Oak Ridge the method has been applied in the neutron multi-group transport code ANISN.[8]

In the case of neutron transport the accuracy of the method has been compared to the Los Alamos continuous energy Monte Carlo code MCN.[9] In the case of photon transport convergence has been studied as a function of the number of groups.

This paper will first discuss how the probability table parameters are generated in a multi-group cross section processor and how existing

*Work performed under the auspices of the U.S. Department of Energy by the Lawrence Livermore Laboratory under contract number W-7405-ENG-48.

BLANK PAGE

transport codes must be modified to use them. Then results will be presented for various neutron and photon transport problems, in order to illustrate the accuracy of the method.

DEFINITION OF THE TOTAL CROSS SECTION PROBABILITY (TCP) DENSITY

An important concept to understand in dealing with so-called probability tables is that any integral over an energy interval is exactly equivalent to an integral over the range of the total cross section within that energy interval. In order to illustrate this equivalence consider the integral,

$$\int_{E_g}^{E_{g+1}} \Sigma_i(E) N(\bar{r},\bar{\Omega},E,t)dE \Big/ \int_{E_g}^{E_{g+1}} N(\bar{r},\bar{\Omega},E,t)dE \qquad (1)$$

where,

$\Sigma_i(E)$ - cross section for reaction i (i = total, elastic, capture, etc.)

$N(\bar{r},\bar{\Omega},E,t)$ - angular flux or weighting function

(E_g,E_{g+1}) - energy range of group g

The weighting function used in neutron and photon transport calculations is usually written as a product of two terms,

$$N(\bar{r},\bar{\Omega}, E,t) = S(E)W(\Sigma_t) \qquad (2)$$

where,

$S(E)$ - energy dependent weighting spectrum

$w(\Sigma_t)$ - cross section dependent self-shielding factor.

Specifically, for neutrons and photons the weighting functions most often used are,

	unshielded/Planckian	self-shielded/ Rosseland
neutrons	$M(E)$	$\dfrac{M(E)}{[\Sigma_t(E) + \Sigma_0]^N}$
photons	$B_\nu(T)$	$\dfrac{1}{\Sigma_t} \dfrac{\partial B_\nu}{\partial T}(T)$

where,

$M(E)$ - neutron energy dependent weighting spectrum; composite Maxwellian, 1/E, fission and fusion spectra.[10]

$B_\nu(E)$ - photon energy dependent weighting spectrum; blackbody function.[11]

Σ_t - total cross section.

Σ_0 - cross section representing effect of all other materials as well as spatial leakage.

N - integer that varies for each Legendre component of the angular flux.

From this table it may be seen that unshielded neutron cross sections are analogous to Planckian mean cross sections for photons, in the sense that both use the same self-shielding factor ($W(\Sigma_t) \equiv 1$). Similarly, the totally self-shielded neutron cross sections ($\Sigma_0 \simeq 0$, $N = 1$) are analogous to Rosseland mean cross sections for photons, in the sense that both use the same self-shielding factor ($W(\Sigma_t) = 1/\Sigma_t$). Without introducing the concept of self-shielding the extremes of unshielded/Planckian on the one hand or totally shielded/Rosseland cross sections on the other hand may be shown to be equivalent to conserving either reaction rates or distance to collision, respectively.

Since all cases described above for either photon or neutron cross section averaging all use weighting functions of the form $S(E)W(\Sigma_t)$ the following results apply to all of these cases. Indeed it is fairly straight forward to show that the following results apply to any weighting function; the separable weighting function is introduced at this point merely to simplify the following derivations and to illustrate how this approach directly applies to the weighting functions normally used to define neutron and photon multi-group cross sections.

The definition of the multi-group cross section, Eq. (1) may be written in the equivalent form,

$$\frac{\int_{E_g}^{E_{g+1}} \int_{\Sigma_t^*}^{} \delta[\Sigma_t^* - \Sigma_t(E)]\Sigma_i(E)S(E)W(\Sigma_t^*)d\Sigma_t^* dE}{\int_{E_g}^{E_{g+1}} \int_{\Sigma_t^*}^{} \delta[\Sigma_t^* - \Sigma_t(E)]S(E)W(\Sigma_t^*)d\Sigma_t^* dE} \tag{3}$$

where

$\delta(x)$ - Dirac's delta function

$\Sigma_t(E)$ - total cross section

If the integration over Σ_t^* is performed first we return to the normal definition of the group averaged cross section (Eq. 1). However, if the integration over E is performed first we obtain the equivalent equation,

$$\frac{\int_{\Sigma_t^*} \Sigma_i(\Sigma_t^*) w(\Sigma_t^*) p(\Sigma_t^*) d\Sigma_t^*}{\int_{\Sigma_t^*} w(\Sigma_t^*) p(\Sigma_t^*) d\Sigma_t^*} \tag{4}$$

where,

$$p(\Sigma_t^*) = \int_{E_g}^{E_{g+1}} \delta[\Sigma_t^* - \Sigma_t(E)] S(E) dE \Big/ \int_{E_g}^{E_{g+1}} S(E) dE \tag{5}$$

$$\Sigma_i(\Sigma_t^*) p(\Sigma_t^*) = \int_{E_g}^{E_{g+1}} \delta[\Sigma_t^* - \Sigma_t(E)] \Sigma_i(E) S(E) dE \tag{6}$$

Equations (5) and (6) serve to define the total cross section probability density, $p(\Sigma_t^*)$, and cross section for each reaction i as a function of the total cross section, $\Sigma_i(\Sigma_t^*)$. From its definition it may be seen that $p(\Sigma_t^*)d\Sigma_t^*$ is a normalized probability distribution that defines the probability of the total cross section being within $d\Sigma_t^*$ of Σ_t^* within the energy interval (E_g, E_{g+1}).

It is important to realize that since the definition of the group averaged cross section as an integral over total cross section (Eq. 4) has been derived from the normal definition as an integral over energy (Eq. 1) merely by introducing definitions, but no approximations, the two forms are exactly equivalent.

The advantage of using the cross section dependent form to define group averaged cross sections (Eq. 4) may be demonstrated by comparing the relative difficulty of evaluating the two integrals,

$$\int_{E_g}^{E_{g+1}} \frac{1}{\Sigma_t(E) + \Sigma_0} \frac{dE}{E} \tag{7}$$

or

$$\int_{\Sigma_{tmin}}^{\Sigma_{tmax}} \frac{p(\Sigma_t^*) d\Sigma_t}{\Sigma_t^* + \Sigma_0} = \int_0^1 \frac{dP}{\Sigma_t^*(P) + \Sigma_0} \tag{8}$$

where,

$$p(\Sigma_t^*) = \int_{E_g}^{E_{g+1}} \delta[\Sigma_t^* - \Sigma_t(E)] \frac{dE}{E} \Big/ \int_{E_g}^{E_{g+1}} \frac{dE}{E} \qquad (9)$$

If we consider the ^{239}Pu cross sections between 40 and 300 eV we see in Fig. 1 that in the energy vs cross section plane $\Sigma_t(E) + \Sigma_0$ is a rapidly varying, fairly complicated function represented by thousands of data points. By contrast in Fig. 2 we see that in the probability vs cross section plane $\Sigma_t^* + \Sigma_0$ is a simple monotonically increasing function of P. Therefore, once the total cross section probability density is known, integrals in the probability vs cross section plane may be performed very efficiently for a variety of weighting functions, $W(\Sigma_t^*)$.

Another advantage of using the probability vs cross section plane is the increased physical insight that is obtained by allowing one to examine the importance of specific cross section ranges (see Fig. 2) instead of having to deal with hundreds of cross section minima and maxima (see Fig. 1). For example the effect of the iron 26 keV minima on shielding problems is known. What is the collective effect of the many minima in the iron cross section in the 0.5 to 2 MeV energy range?[3]

DETERMINATION OF THE TOTAL CROSS SECTION PROBABILITY (TCP) DENSITY

Levitt formulated the probability table method[1] for use with Monte Carlo calculations in the neutron unresolved resonance region in order to account for spatially dependent self-shielding effects. Unresolved resonance parameters were sampled to define ladders of resonances from which energy dependent cross sections were reconstructed. Instead of using the energy dependent cross sections directly in the Monte Carlo calculation, in the probability table method, the cross sections are first pre-processed to define the probability density. In Levitt's approach[12] within successive energy intervals of the unresolved resonance energy range the total cross section range is divided into a number of logarithmically spaced cross section intervals. A direct analogy of the definition of the probability density (Eq. 5) was then used to determine the probability of the total cross section being in each cross section interval. For example between 10 and 20 eV if the combined energy widths of the many energy intervals over which the total cross section is between 50 and 100 barns is 2.3 eV, then in this energy range the probability of the total cross section being between 50 and 100 barns is simply 0.23 (2.3/(20-10)). This approach automatically conserves the unshielded average cross section for the resonance ladder and greatly reduces the computer storage and time requirements for Monte Carlo calculations.[13] Compared to using the energy dependent cross sections directly in the Monte Carlo calculations the core savings using probability tables in the calculation were so large that there was no incentive to optimize the size of the probability tables.[14]

There are two obvious problems with the probability table method. One problem is that although even short resonance ladders can accurately

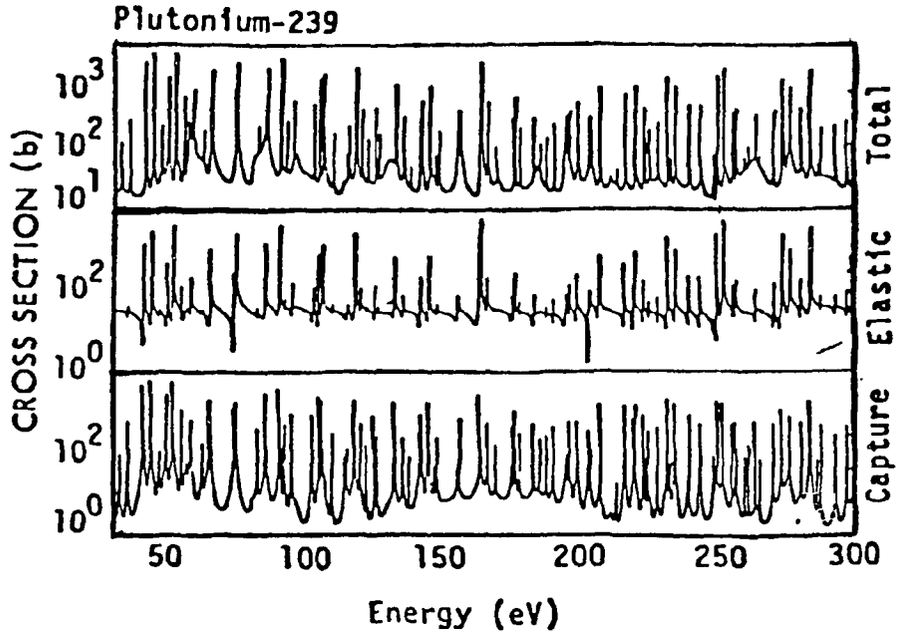

Fig. 1 ^{239}Pu neutron cross sections in the resonance region.

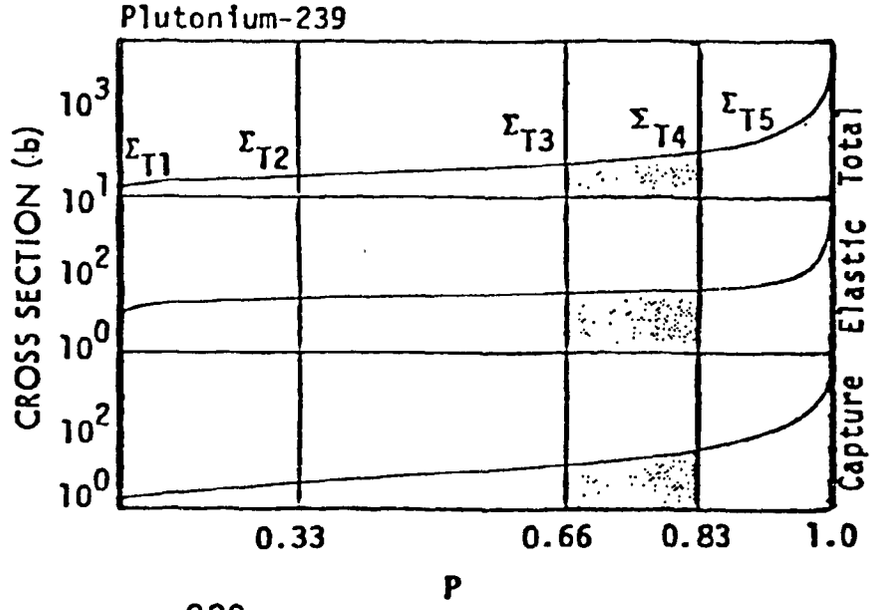

Fig. 2 ^{239}Pu neutron cumulative cross section probability distribution.

predict the unshielded average cross section, determination of the entire distribution of total cross sections can require extremely long ladders. A second problem is that although the probability table method explicitly conserves the unshielded cross section, it does not explicitly conserve the self-shielded cross sections. For example by determining the totally self-shielded cross section ($\Sigma_0 = 0$) using the normal energy integral, Eq. (1) and using Levitt's histogram representation of the probability density in Eq. (4) it is easy to demonstrate that the histogram representation can require extremely large probability tables. As mentioned earlier, in the unresolved resonance region the size of these tables will still be small compared to the number of points required to represent the energy dependent cross sections and as such does not present a problem.[14] However, the size of the tables does preclude extension of Levitt's direct analogue definition of the probability density to the entire energy range.

The multi-group, multi-band method[2,3] was developed in order to use cross section probability tables in all energy groups with minimum size probability tables. In the case of multi-group cross sections we would like to define our self-shielded cross sections using a self-shielding factor that is similar to what we expect to encounter in applications; e.g. $1/(\Sigma_t + \Sigma_0)$, for one Σ_0. Then if in our applications the actual self-shielding is similar to our guess we will obtain an accurate answer. The trouble with multi-group calculations is that at any given time and space point and usually within an entire zone only one weighting function is used. In the multi-band approach we will follow the same procedure as is used in multi-group methods, except that now we have more degrees of freedom or unknowns that may be used to guarantee that we obtain an accurate answer if the actual self-shielding is similar to one of a variety of weighting functions; e.g., $1/(\Sigma_t + \Sigma_0)$, for various values of Σ_0.[15] Since, in actual applications the self-shielding factor will be a function of position, this approach allows the flux in a transport calculation to vary from point to point such that it reproduces the actual spatially dependent self-shielding.

We will define the probability density such that we will exactly reproduce a variety of known self-shielded cross sections produced by using a variety of self-shielding factor that we expect to encounter in applications. For example using the Bonderenko self-shielding model[16] the equation we wish to solve is,

$$\left\langle \Sigma_i(\Sigma_0,N) \right\rangle = \frac{\int \frac{\Sigma_i(\Sigma_t^*)p(\Sigma_t^*)d\Sigma_t^*}{(\Sigma_t^* + \Sigma_0)^N}}{\int \frac{p(\Sigma_t^*)d\Sigma_t^*}{(\Sigma_t^* + \Sigma_0)^N}} = \frac{\left\langle \frac{\Sigma_i}{(\Sigma_t + \Sigma_0)^N} \right\rangle}{\left\langle \frac{1}{(\Sigma_t + \Sigma_0)^N} \right\rangle} \qquad (10)$$

This is a classical moments problem; given $\langle\Sigma_i(\Sigma_0,N)\rangle$, determine $p(\Sigma_t^*)$ and $\Sigma_i(\Sigma_t^*)$. For $\Sigma_0 = 0$, and various values of N this problem reduces to Hausdorff moment problem.[17] For N = 1, and various values of Σ_0 this problem reduces to the Stieltjes-Hilbert moment problem.[17] Both of these problems have been widely studied and only results will be presented here. In the multi-group, multi-band method[2,3] by assuming the probability density $p(\Sigma_t^*)$ is given by a series of Dirac delta functions the integral moments problem is reduced to a coupled set of non-linear algebraic equations,

$$\langle\Sigma_i(\Sigma_0,N)\rangle = \frac{\sum_k \frac{\Sigma_{ik}P_k}{(\Sigma_{tk} + \Sigma_0)^N}}{\sum_k \frac{P_k}{(\Sigma_{tk} + \Sigma_0)^N}} \qquad (11)$$

Starting with the total cross sections $\langle\Sigma_t(\Sigma_0,N)\rangle$,(i = total) for B bands we have 2 × B unknowns; P_k and Σ_{tk}. Therefore given 2 × B self-shielded total cross sections (using different Σ_0 and N combinations) this system can be solved to uniquely define P_k and Σ_{tk}. Given more than 2 × B different self-shielded total cross sections this system can be solved in some "best fit" sense; e.g. least squares or min-max. Once P_k and Σ_{tk} are known, for any given reaction i the equations are linear in the B unknowns Σ_{ik} and starting from known cross sections $\langle\Sigma_i(\Sigma_0,N)\rangle$ the system is easy to solve either uniquely or in a "best fit" sense.

If the multi-band approach is to be applicable to all energy ranges it must be demonstrated that only a small number of bands are required to correctly predict self-shielded cross sections. For example, if we assume the flux in all applications is of the form,

$$w(\Sigma_t) = \frac{1}{\Sigma_t + \Sigma_0} \qquad \Sigma_0 \; \varepsilon(0,\infty) \qquad (12)$$

how many bands are required to adequately reproduce self-shielded cross sections over the entire range of $\Sigma_0 \; \varepsilon(0,\infty)$? In order to more clearly illustrate the dependence of the self-shielded cross section on Σ_0 in the multi-band method setting N = 1 in Eq. (11) and multiplying by the product of terms $[\Sigma_{tk} + \Sigma_0]$; i.e., $\prod_k [\Sigma_{tk} + \Sigma_0]$ it is found that in the multi-band method, Bonderenko self-shielded cross sections[16] are given by a rational approximation in Σ_0,

$$\langle\Sigma_i(\Sigma_0)\rangle = \frac{\langle\Sigma_i(\infty)\rangle \; \Sigma_0^{B-1} + A_{n-1}\Sigma_0^{B-2} + \ldots A_1\Sigma_0 + A_0}{\Sigma_0^{B-1} + B_{n-1}\Sigma_0^{B-2} + \ldots B_1\Sigma_0 + A_0/\langle\Sigma_i(0)\rangle} \qquad (13)$$

where B is the number of bands used.

In this form the equation explicitly defines the $\Sigma_0 \to \infty$ and $\Sigma_0 \to 0$ limits.

The coefficients A_i and B_i can be determined by fitting Eq. (13) to a known set of self-shielded cross sections $\langle\Sigma_i(\Sigma_0)\rangle$. In order to determine the polynomial order required for an accurate fit, a highly underdetermined set of equations involving twenty-three pairs of $\langle\Sigma_t(\Sigma_0)\rangle$ and Σ_0 were used. Instead of the traditional approach of expressing Σ_0 as powers of ten,[16] within each group Σ_0 was defined as multiples of $\langle\Sigma_t(\infty)\rangle$. The values of Σ_0 used were infinity and zero as well as multiples of $\langle\Sigma_t(\infty)\rangle$ from 1 to 1024 in powers of 2, and from 1 to 1/1024 in powers of 1/2.[18] Therefore, within each group, besides the points at zero and infinity, Σ_0 covered a range of over 10^6, centered on $\langle\Sigma_t(\infty)\rangle$. It was found that using only two to four bands allowed the twenty-three known values of $\langle\Sigma_t(\Sigma_0)\rangle$ to be approximated to within 0.1% for all materials in the ENDL[19] library and all energy groups. Table 1 presents for each material the maximum error using two to four bands.

Since highly accurate Bonderenko self-shielded cross sections can be calculated directly from unresolved resonance parameters[20] without recourse to resonance ladders and only two to four bands are required to accurately reproduce self-shielding, the multi-band approach eliminates both problems that are inherent in the probability table method.

What might be considered to be serendipity is the realization that besides the use of multi-band parameters directly in multi-group, multi-band transport calculations the parameters may be used to accurately calculate Bonderenko self-shielded cross sections for use in normal multi-group calculations. As such these parameters can replace tables of Bonderenko self-shielded cross sections normally carried in multi-group libraries. Note from Eq. (14) and Table 1, that not only does this procedure require only a few coefficients (A_i and B_i), but it also has a "natural" interpolation law in Σ_0 that explicitly defines the self-shielded cross section for all $\Sigma_0 \in (0,\infty)$.

SOLUTION OF THE MULTI-BAND EQUATIONS

The solution of the multi-band equations for the case of two bands will be presented. Solution of the equations for more bands is analogous. From the definition of the multi-band equations (Eq. 11) we may see that the major problem of solving these equations is that for the total cross section (i = total) the equations are non-linear. Once P_k and Σ_{tk} are known, for any given reaction i (i = elastic, capture, etc.) the equations are linear and as such are trivial to solve. Therefore, the emphasis here will be on solving for the band weights P_k and total cross sections Σ_{tk}. By inspection of Eq. (11) we may see that the multi-band parameters P_k and Σ_{tk} are not uniquely defined. That is to say we may exchange the parameters for any two bands and still obtain a solution. The parameters

TART 175 GROUP STRUCTURE DERIVED FROM ENDL LIBRARY

MAXIMUM PER-CENT ERROR DURING SIGMA-0 INTERPOLATION

TARGET	1 BAND	2 BAND	3 BAND	4 BAND	TARGET	1 BAND	2 BAND	3 BAND	4 BAND
0-NU-1	0.29	0.00			63-EU-NAT	132.52	0.71	0.01	
1-H -1	0.16	0.00			64-GD-NAT	456.50	2.25	0.05	
1-H -2	0.04	0.00			67-HO-165	1825.96	6.73	0.43	0.02
1-H -3	0.03	0.00			73-TA-181	1807.27	13.12	0.59	0.04
2-HE-3	3.70	0.00			74-W -NAT	2316.44	8.43	0.66	0.03
2-HE-4	1.75	0.00			75-RE-185	1261.69	6.92	0.38	0.02
3-LI-6	8.97	0.01			75-RE-187	2184.84	9.00	0.37	0.06
3-LI-7	14.79	0.02			78-PT-NAT	260.57	2.36	0.05	
4-BE-7	4.01	0.00			79-AU-197	466.07	4.30	0.10	
4-BE-9	0.13	0.00			82-PB-NAT	4.15	0.01		
5-B -10	3.70	0.00			90-TH-231	0.10	0.01		
5-B -11	5.11	0.00			90-TH-232	5658.04	14.09	0.09	0.10
6-C -12	6.00	0.01			90-TH-233	3.69	0.00		
7-N -14	10.03	0.01			92-U -233	152.01	1.22	0.01	
8-O -16	73.31	0.40	0.00		92-U -234	3.42	0.00		
9-F -19	116.90	0.60	0.01		92-U -235	236.94	1.47	0.03	
11-NA-23	66.06	0.40	0.00		92-U -236	2010.67	5.44	0.15	0.01
12-MG-NAT	44.33	0.16	0.00		92-U -237	3.62	0.00		
13-AL-27	60.93	2.32	0.09		92-U -238	2990.51	8.23	0.44	0.03
14-SI-NAT	174.90	0.77	0.01		92-U -239	10.42	0.04		
15-P -31	17.46	0.06			92-U -240	1.44	0.00		
16-S -32	32.72	0.20	0.00		93-NP-237	790.30	7.65	0.25	0.02
17-CL-NAT	89.16	0.93	0.02		94-PU-238	1615.13	8.50	0.41	0.02
18-AR-NAT	17.11	0.01			94-PU-239	623.01	3.57	0.00	
19-K -NAT	165.07	1.53	0.07		94-PU-240	6092.50	10.65	0.50	0.07
20-CA-NAT	89.70	0.54	0.01		94-PU-241	07.37	0.10	0.00	
22-TI-NAT	314.07	3.04	0.11	0.00	94-PU-242	2670.06	7.73	0.51	0.07
23-V -51	606.72	4.20	0.13	0.01	94-PU-243	407.05	2.09	0.00	
24-CR-NAT	131.70	0.92	0.01		95-AM-241	322.40	2.01	0.07	
25-MN-55	1155.01	2.09	0.11	0.01	95-AM-242	61.96	0.25	0.00	
26-FE-NAT	77.36	0.09	0.02		95-AM-243	532.32	2.61	0.06	
27-CO-59	225.10	3.02	0.10		96-CM-242	991.05	6.06	0.30	0.01
28-NI-NAT	105.90	0.91	0.01		96-CM-243	120.77	0.90	0.01	
28-NI-58	190.50	1.10	0.01		96-CM-244	1273.60	7.30	0.40	0.02
29-CU-NAT	19.90	0.06			96-CM-245	132.99	0.95	0.01	
31-GA-NAT	43.36	0.12	0.00		96-CM-246	669.11	3.46	0.13	0.00
40-ZR-NAT	161.00	2.95	0.07		96-CM-247	341.71	2.32	0.06	
41-NB-93	274.00	3.91	0.10		96-CM-248	847.79	5.41	0.15	0.01
42-MO-NAT	00.95	0.26	0.00		97-BK-249	946.69	3.65	0.12	0.01
47-AG-107	029.74	5.97	0.16	0.01	98-CF-249	263.50	1.40	0.04	
47-AG-109	1723.35	0.00	0.31	0.02	98-CF-250	499.59	2.09	0.10	
48-CD-NAT	63.37	0.47	0.01		98-CF-251	102.40	0.44	0.01	
50-SN-NAT	94.49	0.43	0.00		98-CF-252	906.71	4.79	0.16	0.01
56-BA-130	21.23	0.04			FISS.PROD.	4.23	0.00		

1 BAND = UNSHIELDED MULTI-GROUP CROSS SECTIONS

$$\% \text{ Error} = 100^{\%}\left[\frac{\text{Exact} - (\text{multi-band})}{\text{Exact}}\right]$$

TABLE 1. Maximum error in self-shielded cross sections using multi-band parameters.

do not become unique until we introduce an ordering into the parameters, such as $\Sigma_{t1} < \Sigma_{t2} < \ldots < \Sigma_{tB}$. This leads us to believe that the B band parameters will be the B roots of a B-th order polynomial. Since polynomials of order four or less can be solved by changes of variables (which essentially introduce an ordering) we expect that there is an analytic solution defining the multi-band parameters for four or fewer bands. Since polynomials of order five and higher are irreducible only iterative solutions exist for five or more bands.

In the case of two bands if we wish to exactly conserve, $\langle\Sigma_t\rangle$, $\langle 1/\Sigma_t\rangle$, $\langle 1/\Sigma_t^2\rangle$ and the sum of the band probabilities our four equations in four unknowns are,

$$\left.\begin{aligned} 1 &= P_1 + P_2 &&= P_1 + P_2 \\ \langle\Sigma_t\rangle &= P_1\Sigma_{t1} + P_2\Sigma_{t2} &&= \frac{P_1}{X_1} + \frac{P_2}{X_2} \\ \left\langle\frac{1}{\Sigma_t}\right\rangle &= \frac{P_1}{\Sigma_{t1}} + \frac{P_2}{\Sigma_{t2}} &&= P_1X_1 + P_2X_2 \\ \left\langle\frac{1}{\Sigma_t^2}\right\rangle &= \frac{P_1}{\Sigma_{t1}^2} + \frac{P_2}{\Sigma_{t2}^2} &&= P_1X_1^2 + P_2X_2^2 \end{aligned}\right\} X_i = \frac{1}{\Sigma_{ti}} \qquad (14)$$

According to the preceding discussion we expect the two band parameters to be solutions of quadratic equations. The standard change of variables used to solve quadratic equations are,

$$P_1 = 1/2 + \delta \qquad X_1 = A + B \qquad (15)$$

$$P_2 = 1/2 - \delta \qquad X_2 = A - B$$

This change of variables immediately satisfies the first equation and the remaining three equations may be readily solved to find,

$$\delta = \frac{\left\langle\frac{1}{\Sigma_t}\right\rangle - A}{2B} \qquad (16)$$

$$A = \frac{1}{2}\frac{\left\langle\frac{1}{\Sigma_t^2}\right\rangle}{\left\langle\frac{1}{\Sigma_t}\right\rangle}\frac{\left[\langle\Sigma_t\rangle - \left\langle\frac{1}{\Sigma_t}\right\rangle\Big/\left\langle\frac{1}{\Sigma_t^2}\right\rangle\right]}{\left[\langle\Sigma_t\rangle - 1\Big/\left\langle\frac{1}{\Sigma_t}\right\rangle\right]} \qquad (17)$$

$$B^2 = \left[\langle\Sigma_t\rangle A^2 - 2A + \left\langle\frac{1}{\Sigma_t}\right\rangle\right]\Big/\langle\Sigma_t\rangle \qquad (18)$$

As expected, there are two possible solutions for B; the positive and negative roots of the above defintions of B^2. This is a result of the non-uniqueness of the solution without an ordering. From the definition of X_1, X_2 and δ in terms of B it may be seen that choosing the positive or negative value of B yields the same two band weights and total cross sections with the pairs (P_1, Σ_{t1}) and (P_2, Σ_{t2}) exchanged. For definiteness we will always choose the positive root to define B. From the definitions of X_1, X_2 and Σ_{t1}, Σ_{t2} choosing B positive corresponds to introducing an order such that Σ_{t1} is always less than or equal to Σ_{t2}.

All of the required parameters A, B and δ have now been defined. The expression for A has been written in what may appear to be a somewhat strange form only so that it can be written in terms of the data that is normally found in a Bonderenko self-shielded, multi-group library.[18] The terms required are,

$\langle \Sigma_t \rangle$ - the unshielded or infinitely dilute total cross section

$1 \Big/ \left\langle \frac{1}{\Sigma_t} \right\rangle$ - the totally shielded flux weighted total cross section

$\left\langle \frac{1}{\Sigma_t} \right\rangle \Big/ \left\langle \frac{1}{\Sigma_t^2} \right\rangle$ - the totally shielded current weighted total cross section

Once the cross section weights P_k and total cross sections Σ_{tk} are known the two band parameters for each reaction i may be readily solved to simultaneously conserve both the unshielded $\langle \Sigma_i \rangle$ and totally shielded $\langle \Sigma_i / \Sigma_i \rangle$ cross sections. The two equations for each reaction are,

$$\langle \Sigma_i \rangle = P_1 \Sigma_{i1} + P_2 \Sigma_{i2}$$

$$\left\langle \frac{\Sigma_i}{\Sigma_t} \right\rangle = \frac{P_1 \Sigma_{i1}}{\Sigma_{t1}} + \frac{P_2 \Sigma_{i2}}{\Sigma_{t2}} \qquad (19)$$

It is convenient to introduce the change of variables

$$\Sigma_{i1} = \langle \Sigma_i \rangle - \frac{C}{P_1}$$

$$\Sigma_{i2} = \langle \Sigma_i \rangle + \frac{C}{P_2} \qquad (20)$$

This change of variables immediately satisfies the first equation and the remaining equation can be solved to find,

$$C = \frac{\langle \Sigma_i \rangle \left\langle \frac{1}{\Sigma_t} \right\rangle - \left\langle \frac{\Sigma_i}{\Sigma_t} \right\rangle}{\frac{1}{\Sigma_{t1}} - \frac{1}{\Sigma_{t2}}} \tag{21}$$

All parameters for a two band library have now been defined in terms of Bonderenko self-shielded cross sections that are normally available in standard multi-group libraries. In particular it is not necessary to start from energy dependent cross sections or to generate ladders of resonances.

Note how easy it is to implement this two band algorithm. Starting from known group averaged, self-shielded cross sections the two band parameters can be defined using roughly a dozen lines of Fortran coding. Relative to the cost of calculating the self-shielded cross section, this procedure introduces very little additional overhead.

PHYSICALLY ACCEPTABLE PARAMETERS

In defining multi-band parameters it should be realized that since the parameters are being selected by replacing a set of integrals by a set of sums,

$$\left\langle \frac{\Sigma_i}{(\Sigma_t + \Sigma_0)^N} \right\rangle = \int_{\Sigma_{tmin}}^{\Sigma_{tmax}} \frac{\Sigma_i(\Sigma_t) p(\Sigma_t) d\Sigma_t}{(\Sigma_t + \Sigma_0)^N} = \sum_k \frac{\Sigma_{ik} P_k}{(\Sigma_{tk} + \Sigma_0)^N} \tag{22}$$

we are defining a quadrature which imposes additional mathematical and physical constraints on the multi-band parameters. Since $p(\Sigma_t)$ is a normalized probability density all of the band weights P_k should be positive and should sum to unity, as a normalization,

$$0 \leq P_k \leq 1$$

$$1 = \sum_k P_k \quad . \tag{23}$$

In addition for each reaction i (i = total, elastic, etc.) the multi-band cross sections Σ_{ik} should lie in the range between the minimum and maximum values that the cross section reaches within each energy group. This last condition is particularly important. If this criteria is not met, in applications it is possible to obtain erroneous solutions

where the equivalent group averaged cross section for one or more reactions lies outside of the cross section range for those reactions.

The algorithms presented in the preceding sections to define the multi-band parameters will satisfy all of these criteria as long as the cross section moments that are used are consistent. For example in the two band algorithm presented in the preceding section, from Eq. (15) it may be seen that the two band weights will always sum to unity. However, both will be positive only if $|\delta| \leq \frac{1}{2}$.

By substituting for A and B in the definition of δ [Eq. (16)] this condition may be reduced to,

$$\left\langle \frac{1}{\Sigma_t^2} \right\rangle \geq \left\langle \frac{1}{\Sigma_t} \right\rangle^2 \tag{24}$$

which is true for any function and in particular for $1/\Sigma_t$. Therefore in principle this condition should always be satisfied and indeed it has been demonstrated that when the Bonderenko self-shielded cross sections are calculated using analytic integrals this condition is always satisfied.[18] However, when iterative integration is used it is not always satisfied.[21] Obviously if both integrals are performed to within some accuracy $\pm\varepsilon$, if the integrals differ by less than 2ε this inequality may be violated, resulting in physically unacceptable multi-band parameters.

Starting from the definition of the Bonderenko self-shielded total cross section.

$$\left\langle \Sigma_t(\Sigma_0,N) \right\rangle = \frac{\left\langle \frac{\Sigma_t}{(\Sigma_t + \Sigma_0)^N} \right\rangle}{\left\langle \frac{1}{(\Sigma_t + \Sigma_0)^N} \right\rangle} \tag{25}$$

we can find,

$$\frac{\partial}{\partial \Sigma_0}\left\langle \Sigma_t(\Sigma_0,N) \right\rangle = N\left\{ \frac{\left\langle \frac{1}{(\Sigma_t + \Sigma_0)^{N-1}} \right\rangle \left\langle \frac{1}{(\Sigma_t + \Sigma_0)^{N+1}} \right\rangle - \left\langle \frac{1}{(\Sigma_t + \Sigma_0)^N} \right\rangle^2}{\left\langle \frac{1}{(\Sigma_t + \Sigma_0)^N} \right\rangle^2} \right\} \tag{26}$$

$$\langle \Sigma_t(\Sigma_0,N)\rangle - \langle \Sigma_t(\Sigma_0,N+1)\rangle = \left\{ \frac{\left\langle \frac{1}{(\Sigma_t+\Sigma_0)^{N-1}} \right\rangle \left\langle \frac{1}{(\Sigma_t+\Sigma_0)^{N+1}} \right\rangle - \left\langle \frac{1}{(\Sigma_t+\Sigma_0)^{N}} \right\rangle^2}{\left\langle \frac{1}{(\Sigma_t+\Sigma_0)^{N}} \right\rangle \left\langle \frac{1}{(\Sigma_t+\Sigma_0)^{N+1}} \right\rangle} \right\} \tag{27}$$

Note that the numerator of both expressions are identical. By using the Cauchy-Schwarz inequality[22] it can be shown that this numerator is always greater than or equal to zero; with equality only in the case of a constant total cross section across the entire energy group. Therefore for fixed N increasing Σ_0 cannot lead to a smaller self-shielded cross section,

$$\langle \Sigma_t(\Sigma_1,N)\rangle \geq \langle \Sigma_t(\Sigma_2,N)\rangle \quad : \quad \Sigma_1 > \Sigma_2 \quad . \tag{28}$$

Similarly for fixed Σ_0 decreasing N cannot lead to a smaller self-shielded cross section,

$$\langle \Sigma_t(\Sigma_0,M)\rangle \geq \langle \Sigma_t(\Sigma_0,N)\rangle \quad : \quad M < N \quad . \tag{29}$$

These inequalities must be satisfied by any physically acceptable moments of a real total cross section. If a set of moments used to generate multi-band parameters do not satisfy these conditions one should not be surprised to obtain physically unacceptable multi-band parameters. This result is merely indicative of the fact that there is no real cross section distribution corresponding to these moments. Therefore it is recommended that any multi-group processor that generates self-shielded cross sections insure that the above inequalities are satisfied.

As a practical matter these conditions are usually violated by multi-group processors only when there is very little self-shielding, in which case all of the self-shielded cross sections are all nearly equal. This condition may be understood by examining the equations defining the two band parameters [Eq. (14)]. In the limit of no self-shielding,

$$\left\langle \frac{1}{\Sigma_t^2} \right\rangle \to \left\langle \frac{1}{\Sigma_t} \right\rangle^2 \to \frac{1}{\langle \Sigma_t \rangle^2} \tag{30}$$

and the four equations are no longer linearly independent. A solution to these equations is obtained by setting all multi-band total cross sections Σ_{tk} equal to the unshielded average $\langle \Sigma_t \rangle$ and choosing any two arbitrary weights P_k that sum to unity.

In order to avoid this case, in generating multi-group parameters, whenever a self-shielded cross section is close to the unshielded

cross section,

$$\langle \Sigma_t \rangle - 1/\left\langle \frac{1}{\Sigma_t} \right\rangle < \varepsilon \tag{31}$$

it is recommended that all band cross sections be set equal to their unshielded average value, the weight of the first band be set to unity and all other weights to zero.

MULTI-BAND TRANSFER MATRICES AND SOURCES

Starting from G energy groups and using B bands in each group results in a coupled set of G × B multi-group, multi-band equations.[2,3] Mathematically these equations are identical to a set of G × B multi-group equations and may be solved by existing transport codes. Once the multi-band cross sections are defined the only other parameters that a multi-group processor must provide in order to completely describe the multi-group, multi-band equations[2,3] is the transfer matrix and source. Starting from a multi-group transfer matrix,

$$f_\ell(G' \to G) = \sum_i m_i \langle \Sigma \rangle_{iG'} g_\ell(G' \to G) \tag{32}$$

where

$f_\ell(G' \to G)$ - total transfer for Legendre component ℓ from group G' to G

i - reactions; elastic, fission, etc.

m_i - multiplicity for reaction i (m_i = 1-elastic, = ν-fission, = 2-(n,2n))

$\langle \Sigma \rangle_{iG'}$ - group averaged cross section for process i in group G'

$g_\ell(G' \to G)$ - normalized (when summed over G) probability of transfer from group G' to G.

The equivalent multi-band transfer matrix may be derived from this expression by realizing that the multiplicity and probability of transfer from one energy to another is independent of the magnitude of the cross section. Furthermore, the probability of interacting in group G', band B' is merely $\Sigma_{iG'B'}$, instead of $\langle \Sigma \rangle_{iG'}$. Similarly the probability of arriving at group G, band B, in the probability table method is merely the probability of arriving in group G times the probability of being in band B (i.e., P_{GB}). Therefore, the multi-group transfer matrix may be written in the form,[2,3]

$$f_\ell(G'B' \rightarrow GB) = P_{GB} \sum_i m_i \Sigma_{iG'B'} g_\ell(G' \rightarrow G) \tag{33}$$

where m_i and $g_\ell(G' \rightarrow G)$ are the normal multi-group expressions and P_{GB} and $\Sigma_{iG'B'}$ are the multi-band parameters defined earlier. Therefore, starting from a multi-group transfer matrix for G groups in which each reaction is represented separately the multi-band transfer matrix for G × B group, bands may be immediately defined. If only the total transfer elements are available, by following the above arguments an excellent approximation is,[2,3]

$$f_\ell(G'B' \rightarrow GB) = P_{GB} \frac{\Sigma_{tG'B'}}{\langle \Sigma \rangle_{tG'}} f_\ell(G' \rightarrow G) \tag{34}$$

where $\langle \Sigma \rangle_{tG'}$ and $f_\ell(G' \rightarrow G)$ are the normal multi-group expressions and P_{GB} and $\Sigma_{tG'B'}$ are multi-band parameters.

Similarly according to the above arguments the group, band source is merely the group sources times the probability of being in band B (i.e., P_{GB})

$$S_{GB} = P_{GB} S_G \tag{35}$$

where S_G is the normal multi-group source, P_{GB} is the group, band weight and S_{GB} is the group, band source.

INTERMEDIATE RESONANCE EFFECTS

The probability table method uses the narrow resonance approximation by assuming that after a collision neutrons are uniformly distributed in energy; which is equivalent to saying that they are distributed in total cross section according to the total cross section probability density $P(\Sigma_t^*)$. This is reflected in the multi-band transfer matrix since the probability of transferring from one group, band to another group, band is given by a product of two terms,

$\sum_i m_i \Sigma_{iG'B'} g_\ell(G' \rightarrow G)$ - probability of interacting and transfer from group, band G'B' to group G

P_{GB} - probability of arrival in band B of group G.

In extending the multi-band method to the entire energy range R. Goldstein's intermediate resonance treatment[2,3] may be included to eliminate the narrow resonance approximation. In the narrow resonance approximation the probability of elastically scattering from one cross section value to another is merely given by the probability of the final cross section occurring (see Ref. 4)

$$g(\Sigma_t' \rightarrow \Sigma_t) = p(\Sigma_t) \tag{36}$$

In the wide resonance approximation elastically scattered neutrons emerge from collision with the same cross section that they entered collision,

$$g(\Sigma_t' \rightarrow \Sigma_t) = \delta(\Sigma_t' - \Sigma_t) \tag{37}$$

In his intermediate resonance formulation Goldstein combined these two extremes to define,

$$g(\Sigma_t' \rightarrow \Sigma_t) = \lambda p(\Sigma_t) + (1 - \lambda)\delta(\Sigma_t' - \Sigma_t) \quad . \tag{38}$$

In this formulation, following an elastic collision the secondary neutrons are either (1) randomly distributed, with probability λ, or (2) remain in the same band. The equivalent multiband transfer matrix [Eq. (33) or (34)] can be modified to include intermediate resonance effects merely by replacing P_{GB} by $\lambda_G P_{GB} + (1 - \lambda_G)\delta_{B'B}$. In the intermediate resonance formulation the self-shielding factor is assumed to be,[23]

$$\omega(\Sigma_t) = \frac{\langle \Sigma_m \rangle + \lambda_G \langle \Sigma_s \rangle}{\Sigma_m(E) + \Sigma_a(E) + \lambda_G \Sigma_s(E)} \tag{39}$$

where,

Σ_m - moderator cross section

Σ_s - elastic cross section of heavy material

Σ_a - absorption cross section of heavy material.

Within each group the intermediate resonance parameter λ_G may be defined by comparing the self-shielded absorption cross section using the above self-shielding factor and various values of λ_G to experimental measurements, or simple infinite medium calculations.[4]

RESULTS

The magnitude of the importance of correcting for self-shielding effects may be illustrated by examining Figs. 3 and 4 which present plots of the TART-175 group constants and totally shielded f-factors for $^{232}_{90}Th$.[24] Since the f-factors are merely the ratio of the shielded to unshielded cross section, an f-factor close to unity indicates little or no self-shielding. From Fig. 4 it is obvious that even using 175 groups results in a large uncertainty in the cross section due to self-shielding. In this case the minimum f-factor is only 0.025, indicating that the shielded cross section is only 2.5% of the unshielded value. The results presented in Fig. 4 are fairly typical for heavy isotopes and even persist into fairly light isotopes.[24]

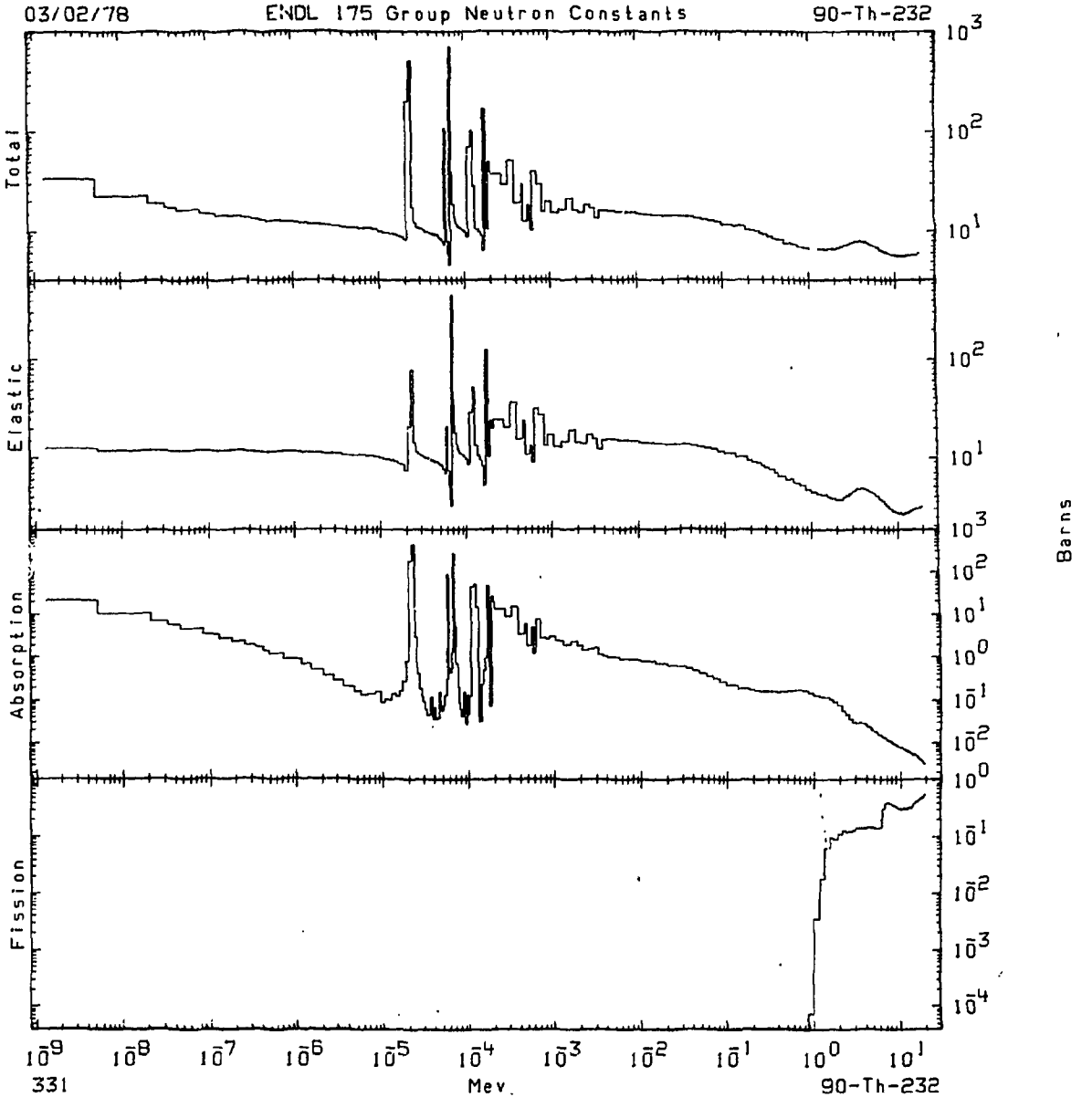

Figure 3. ^{232}Th 175 Group Cross Sections

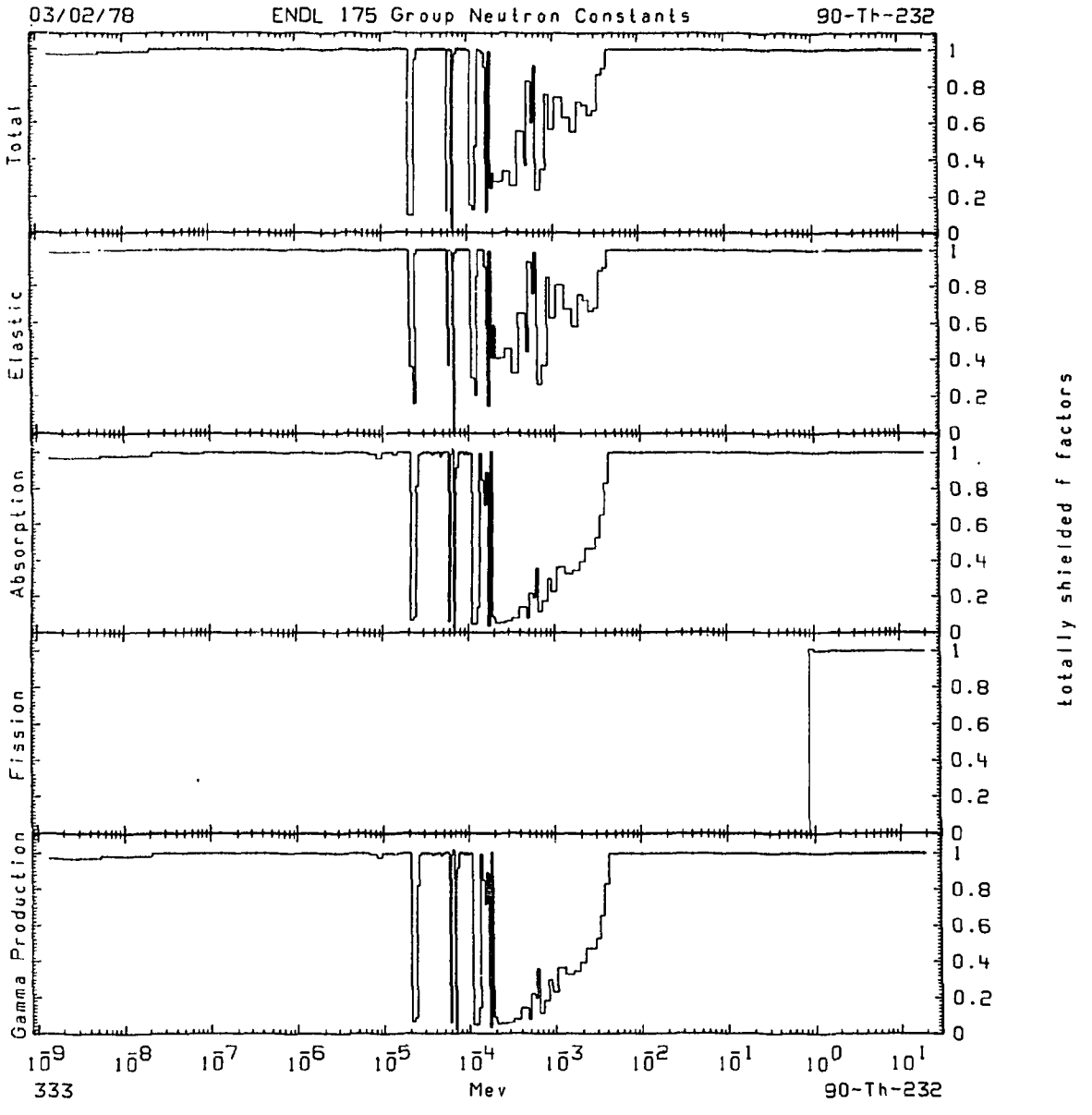

Figure 4. ^{232}Th 175 Group totally shielded f-factors

In using multi-band parameters it is important to compensate for self-shielding effects in the elastic, capture and fission cross sections as well as photon production and energy deposition. Self-shielding effects in all other reactions are relatively minor with the possible exception of (n, charged particle) reactions in light isotopes, if only a few neutron groups are used.

The importance of the multi-band approach can best be illustrated by considering a photon transport problem. Consider a slab of ^{27}Al initially at 1 keV temperature with radiation incident on the slab from the left. We will allow the slab to come to equilibrium and then examine the leakage from the right hand side of the slab. Figure 5 presents the results of a variety of LASNEX[7] calculations using a variable number of groups and Planckian/unshielded, Rosseland/shielded or two band parameters. The results are plotted vs groups × bands used in each of the three methods, which is approximately proportional to running time. The important result to glean from Fig. 5 is that the two band result is approaching the asymptotic value much more rapidly than either of the other two methods. Therefore the two band results are much less sensitive to the number of groups used.

Similar results have been obtained in neutron transport problems by examining the transmission of an incident 1/E spectrum through 30cm of iron. Comparison of the results obtained by the Los Alamos Monte Carlo code MCN[9] which uses energy dependent cross sections to TARTNP[6] results using either 175 groups/2 bands or 2020 groups illustrates that the agreement between the MCN and TARTNP 175 groups/2 band results are as good or better than the 2020 group results.[25]

In fissile materials the multi-band method has been successfully used to calculation the transmission of neutrons through ^{239}Pu and ^{235}U,[26] as well as the self-shielding effects in critical assemblies for various enrichments of uranium in water[27] and uranium hydrides.[28]

STATUS

At present the multi-band method is implemented at Livermore for use with the neutron/photon Monte Carlo code TARTNP[6] as well as in the photon transport code LASNEX.[7] At Oak Ridge the two band method has been implemented in MINX-[21]ANISN[8] as applied to neutron transport calculations.

CONCLUSIONS

In this paper algorithms have been provided to allow one to derive all parameters required for a multi-band calculation from data that is normally available in Bonderenko self-shielded multi-group cross section libraries. In particular one need not start from energy dependent cross sections nor perform expensive ladder calculations in order to define

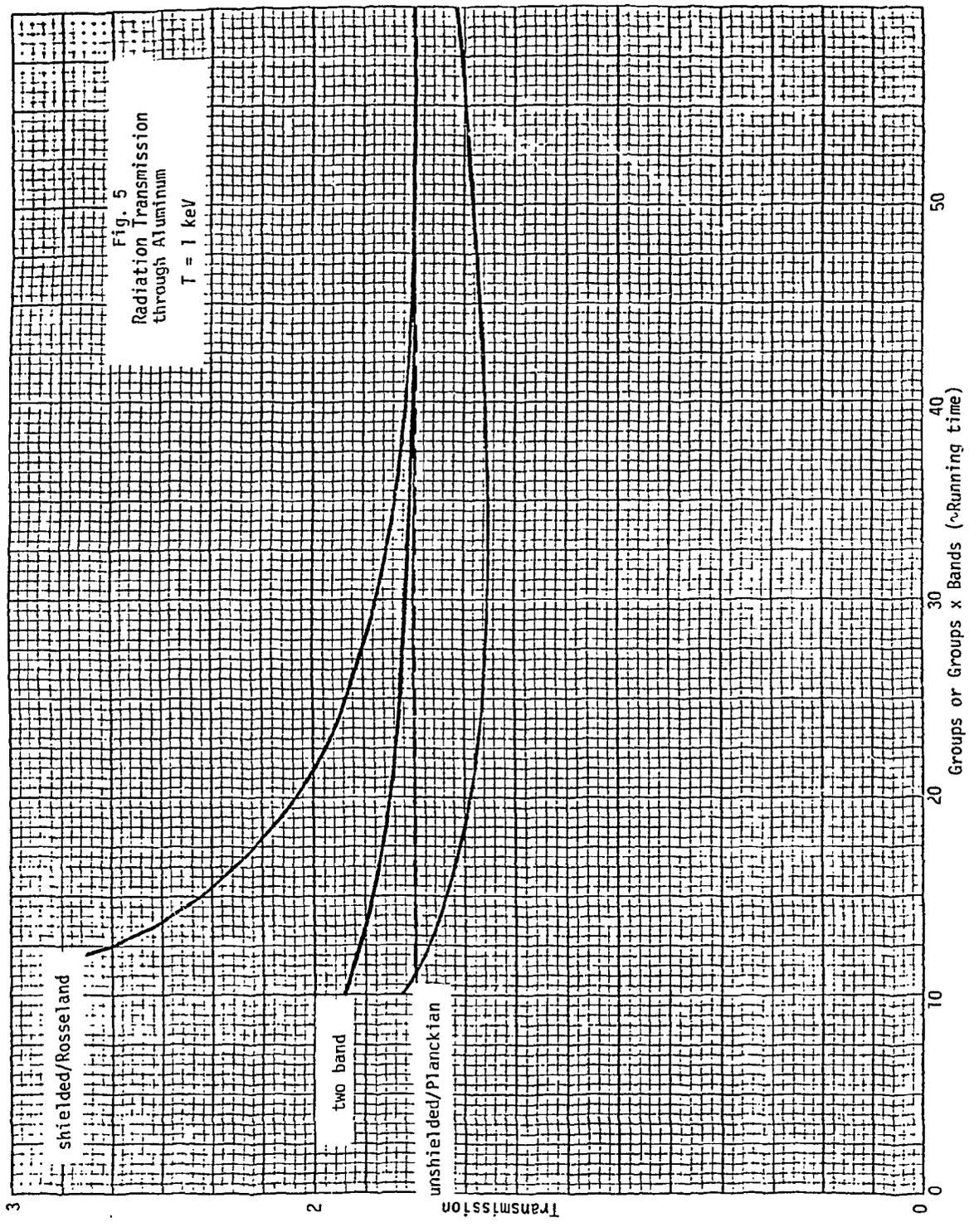
Fig. 5
Radiation Transmission
through Aluminum
T = 1 keV
shielded/Rosseland
two band
unshielded/Planckian
Transmission
3
2
0
0
10
20
30
40
50
Groups or Groups x Bands (~Running time)

probability table parameters.

Application of the multi-band method to a variety of problems indicates that the method is highly accurate compared to more exact calculations by MCN[9] and is rapidly convergent as a function of the number of groups used (see Fig. 5). Recognizing the potential implications of this latter point in computer storage or execution time is extremely important and is an area that still warrants further studies.

REFERENCES

1. L. B. Levitt, Nucl. Sci. Eng. 49, 450 (1972).

2. D. E. Cullen, "Application of the Probability Table Method to Multi-Group Calculations," in Brookhaven National Laboratory's report BNL-50387 (ENDF-187) (1973).

3. D. E. Cullen, Nucl. Sci. Eng. 55, 387 (1974).

4. D. E. Cullen, Calculation of Probability Table Parameters to Include Self-Shielding and Intermediate Resonances, Lawrence Livermore Laboratory report UCRL-79761 (1977).

5. D. E. Cullen, Nucl. Sci. Eng. 58, 261 (1975).

6. E. F. Plechaty, J. R. Kimlinger, TART Monte Carlo Neutron Transport Code, Lawrence Livermore Laboratory report UCIR-522 (1971).

7. G. Zimmerman, Comments Plasma Phys. 2, 51 (1975).

8. W. W. Engle, Jr., "A User's Manual for ANISN, A One-Dimensional Discrete Ordinate Transport Code with Anisotropic Scattering," Computing Technology Center, Union Carbide Corporation report K-1693 (1967).

9. E. D. Cashwell et al., MCN: A Neutron Monte Carlo Code, Los Alamos Scientific Laboratory report LA-4751 (1972).

10. C. R. Weisbin and R. J. LaBauve, Specification of Generally Useful Multi-Group Structure for Neutron Transport, Los Alamos Scientific Laboratory report LA-5277MS (1973).

11. G. C. Pomraning, The Equations of Radiation Hydrodynamics, Pergamon Press, New York (1973).

12. J. M. Otter et al., U3R - A Code to Calculate Unresolved Resonance Cross Section Probability Tables, Atomics International report AI-AEC-13024 (1972).

13. L. B. Levitt and R. C. Lewis, VIM-1, A Non-Multi-Group Monte Carlo Code for Analysis of Fast Critical Assemblies, Atomics International report AI-AEC-12951 (1970).

14. L. B. Levitt, Brookhaven National Laboratory, private communication (1975).

15. D. E. Cullen, A Method for Multi-Group Neutron Calculations in the Unresolved Resonance Energy Region, Lawrence Livermore Laboratory report UCRL-75164 (1973).

16. I. I. Bonderenko, Group Constants for Nuclear Reactor Calculations, Consultants Bureau, New York (1964).

17. P. R. Graves-Morris, ed., Pade Approximants and their Applications, Academic Press, London and New York (1973) pp. 217-240.

18. D. E. Cullen, "Program GROUPIE: Calculation of Bonderenko Self-Shielded Cross Sections and Multi-Band Parameters from Evaluated Data in the ENDF/B Format," Lawrence Livermore Laboratory report UCRL-50400, Vol. 17, Part C (to be published).

19. R. J. Howerton et al., "The LLL Evaluated Nuclear Data Library (ENDL): Graphs of Cross Sections from Library," Lawrence Livermore Laboratory report UCRL-50400, Vol. 15B (1976).

20. H. Henryson et al., MC^2-2: A Code to Calculate Fast Neutron Spectra and Multi-group Cross Sections, Argonne National Laboratory report ANL-8144 (ENDF-239) (1976).

21. C. R. Weisbin et al., MINX: A Multigroup Interpretation of Nuclear X-Sections from ENDF/B, Los Alamos Scientific Laboratory report LA-6486-MS (ENDF-237) (1976).

22. B. Friedman, Principles and Techniques of Applied Mathematics, John Wiley and Sons, Inc., London (1956).

23. R. Goldstein and E. R. Cohen, Nucl. Sci. Eng. 13, 132 (1962).

24. E. F. Plechaty et al., "Tabular and Graphical Presentation of 175 Neutron Group Constants Derived from the LLL Evaluated Nuclear Data Library (ENDL)," Lawrence Livermore Laboratory report UCRL-50400, Vol. 16, Rev. 2 (1978).

25. E. F. Plechaty and D. E. Cullen, Proc. Am. Nucl. Soc. 27, 367 (1977).

26. E. F. Plechaty and D. E. Cullen, Resonance Self-Shielding Calculations Using the Probability Table Method, Lawrence Livermore Laboratory report UCID-17230 (1976).

27. E. F. Plechaty, Monte Carlo Criticality Calculations of Hydrogen Moderated Uranium Sustems Using the Probability Table Method and Multigroup Cross Section Representations, Lawrence Livermore Laboratory report UCID-17455 (1977).

28. F. H. Lewis and P. D. Soran, Calculations of UH_3 Critical Masses for Various Uranium Enrichments, Lawrence Livermore Laboratory report UCRL-80042 (1977).

BLANK PAGE

COMPARISON OF VITAMIN-C MASTER LIBRARY REACTION CROSS SECTIONS FOR IRON WITH MULTIGROUP CROSS SECTIONS GENERATED BY THE VIM MONTE CARLO CODE

N. E. Hertel and B. W. Wehring
University of Illinois
Urbana, Illinois, 61801, USA

R. H. Johnson
Purdue University
West Lafayette, Indiana, 47907, USA

ABSTRACT

Bondarenko-self-shielded and infinitely dilute iron reaction cross sections from the VITAMIN-C master library were compared with multigroup reaction cross sections generated in a continuous-energy Monte Carlo calculation of neutron leakage for a spherical shell of iron containing a neutron source at its center. The specific cross sections compared were (n,2n), elastic scattering, inelastic scattering, and absorption. The self-shielded VITAMIN-C multigroup cross sections obtained with the Bondarenko formalism agree well with the VIM generated cross sections while the infinitely dilute cross sections do not.

INTRODUCTION

The present work is part of a program of integral testing of neutron cross sections being carried on at the University of Illinois.[1-3] The objective of this research is to provide tests of multigroup cross section sets and evaluated nuclear data by comparing calculated and measured neutron and gamma-ray leakage spectra for spherical shells of materials of interest to fusion, fission, and radiotherapy technologies. Measured and calculated neutron leakage spectra have been reported for a Cf-252 fission neutron source in spherical shells of iron, niobium, polyethylene, and beryllium.[1,2] Integral test results have also been reported for a D-T fusion neutron source in an iron spherical shell.[1,2] Recently, coupled calculations for a niobium sphere[3] have been compared to measurements using an NE-213 spectrometry system capable of simultaneous neutron and gamma-ray leakage measurements.[4,5] In these tests, the discrete ordinates code ANISN[6] had been used. To further investigate large discrepancies between calculated and measured neutron leakage spectra for the iron spherical shell,[2] additional calculations were performed with the continuous-energy Monte Carlo code VIM.[7]

The VIM calculations were performed by us at Argonne National Laboratory for the iron sphere for both D-T and Cf-252 fission neutron sources located in the central void of the shell. The VIM Monte Carlo code performs neutron transport calculations between 1 eV and 14.2 MeV using large sets of point microscopic-cross-section data[8] closely representing ENDF/B-IV data. The statistical edit of VIM also provides multigroup reaction cross sections with standard error estimates for specified spatial regions. Since infinitely dilute and self-shielded ANISN calculations had been performed for the iron sphere using a preliminary version of the DCTR fine group cross section library[9] and since it is anticipated that the current version of this library, VITAMIN-C,[10] will be employed in future calculations, the VITAMIN-C 171 group structure was chosen to bin the VIM calculations.

The ANISN calculations for the iron sphere had demonstrated that the neutron leakage spectrum is sensitive to self-shielding.[2] The VITAMIN-C cross section set employs the Bondarenko formalism to provide self-shielded multigroup cross sections. The VIM code performs a continuous-energy calculation with pointwise cross sections. Therefore, the reaction cross sections generated in VIM are not based on a self-shielding approximation. However, the VIM results include statistical errors. Comparison of cross sections from these two sources serves as a test of the adequacy of the Bondarenko self-shielding method for analysis of the iron sphere leakage spectra. The comparison also provides a test of the VITAMIN-C multigroup cross sections such as (n,2n) which are not self-shielded. The comparison of the VIM generated sets with the two VITAMIN-C sets is presented for neutron energies between 1 keV and 14.2 MeV for absorption, inelastic scattering, elastic scattering, and (n,2n) reaction cross sections.

MONTE CARLO TRANSPORT CODE VIM

The VIM code[7,8,11] is a continuous energy Monte Carlo code originally designed for fast reactor criticality calculations. The fixed source option was used for the iron sphere leakage calculations. Cross section definition in VIM is by isotopic microscopic data sets derived from ENDF/B-IV data. Resonance and smooth cross sections (Doppler broadened to 300°K in the resolved resonance region) are specified pointwise and interpolated linearly in energy to provide a continuous energy treatment. To obtain more accurate thinned resonance cross sections both the total and absorption cross sections must meet desired accuracy criteria before the energy grid may be thinned. Neutron trajectories and scattering are continuous in angle. Anisotropic elastic and discrete inelastic scattering are described with probability tables at energies specified in ENDF/B-IV.[12] In the unresolved resonance region, cross sections are described by random linear interpolation in lethargy between unresolved resonance probability tables. The VIM point cross section sets define fission, elastic scattering, discrete level inelastic scattering, inelastic continuum scattering, and the (n,2n) reactions specifically and define the capture reaction to cover the

remaining possibilities. Inelastic continuum and (n,2n) reactions are assumed to be isotropic in the lab system and full ENDF/B energy distributions are utilized where possible.[7]

The VIM code provides both collision and track length estimation of reaction rates by region, group, and/or isotope as well as group- and region-wise integrated fluxes by track length estimation. Track length estimation of reaction rates and volume integrated fluxes are used to provide group microscopic cross sections for user specified spatial edit regions. All output quantities are provided with standard error estimates.

Of particular interest for our comparison is the generation of reaction cross sections by VIM. In the statisitcal edit, neutron flux by region and reaction rates by isotopes, region, and energy group are estimated. The microscopic multigroup reaction cross sections presented are obtained from the ratio of the reaction rate to the flux in a given group and region. These microscopic reaction cross sections are homogenized over the spatial edit region. The components which define the VIM reaction cross sections[7] are: (1) the (n,2n) reaction by MT*=16; (2) the inelastic scattering reaction by MT=51-91; (3) parasitic absorption or "capture" (referred to as absorption in the text) by MT=102-108 and MT=17; and (4) elastic scattering by MT=2.

MULTIGROUP REACTION CROSS SECTIONS

Fine Group Reaction Cross Sections

Infinitely dilute and Bondarenko-self-shielded[14] sets of 171-group iron reaction cross sections were obtained from the Radiation Shielding Information Center at Oak Ridge National Laboratory. The infinitely dilute cross sections were generated from MINX[15] and are for a temperature of 300°K. The self-shielded set was generated in BONAMI[9] using $\sigma_o = 10^{-8}$ (essentially $1/\sigma_t$ weighting). These cross sections are from an AMPX interface library and are identical to the reaction cross sections used in the DLC-41/VITAMIN-C coupled cross section set.[10] This multigroup set was weighted in MINX with a Maxwellian shape from 10^{-5} eV to 0.125 eV, a 1/E shape from 0.125 eV to 820.8 keV, a fission spectrum from 820.8 keV to 10 MeV, a 1/E shape from 10 to 12.57 MeV, a velocity exponential fusion peak from 12.57 to 15.57 MeV, and a 1/E shape above 15.57 MeV.[10] This weighting function was designed to cover a range of applications encompassing fusion, LMFBR, and thermal reactor analyses. The energy structure is intended to be fine enough to minimize the variation between the group data if an actual flux had been employed as a weighting function. A feature of interest in the iron calculations is the detailed representation of the 80 and 24 keV minima. The VIM generated reaction cross sections provide a test of this average cross section philosophy.

*See ref. 13 for further elucidation on MT values.

Iron Sphere

The VIM leakage calculations were done for the iron sphere used for leakage measurements at the University of Illinois. This spherical shell of iron has an outer radius of 38.1 cm and a central void of 7.65-cm radius in which to position a source for leakage measurements. The shell thickness corresponds to approximately 6.6 mean free paths for 14-MeV neutrons and approximately 7.9 mean free paths for 2-MeV neutrons.

VIM Generated Multigroup Reaction Cross Sections

For the VIM calculations the source was located in a 0.25-cm radius sphere in the center of the central void of the iron spherical shell. The neutron source was randomly generated using a 1.43 MeV Maxwellian temperature for the Cf-252 fission neutron source. The D-T neutron source was randomly generated between 13.85 and 14.2 MeV (corresponds to group 6 of the 171 group structure). A 100,000 neutron history calculation was performed for both sources with analog weighting to obtain the desired multigroup reaction cross sections. The resulting group reaction cross sections generally have estimated errors of less than 1% for each group between 1 keV and 14.2 MeV, but the (n,2n) reaction cross sections from the Cf-252 calculation contain larger error estimates.

RESULTS

Multigroup Reaction Cross Section Comparison

Since VIM reaction cross sections were generated using both D-T and Cf-252 neutrons, a comparison of these two sets was performed. The absorption cross sections were identical except in the 9-67 keV region where differences of less than 10% for some groups exist. The elastic cross sections showed no appreciable disagreement although small differences were observed for 3 groups in the 100-200 keV region. The inelastic cross section compares well, but the (n,2n) cross section compares poorly, probably due to the large statistical error in the VIM Cf-252 (n,2n) cross sections. This error results from the low generated Cf-252 source strength above the (n,2n) threshold (11.4 MeV). The similarity of the reaction cross section values generated from VIM for the D-T and Cf-252 leakage spectra indicated that a comparison of the VITAMIN-C master library values with the cross sections generated from the VIM D-T calculation was sufficient.

The (n,2n) and inelastic scattering cross sections are the same for the self-shielded and infinitely dilute sets since the Bondarenko formalism is not applied to these reactions. The (n,2n) cross sections from the VITAMIN-C master library compared with the values resulting

from the VIM D-T calculations are shown in Fig. 1. The discrepancies are within 13%. The comparison of the inelastic scattering cross sections is shown in Fig. 2. Again the discrepancies are small, but steadily increase to 52% at the inelastic scattering threshold (861 keV) where the VIM estimated statistical error is only 7%. For the other energies, the VIM statistical error is <1%.

The VIM generated elastic scattering cross sections are compared to the infinitely dilute and self-shielded VITAMIN-C cross section in Fig. 3(a) and 3(b), respectively. Using the self-shielding correction results in significant improvement over the infinitely dilute set. The self-shielded values agree well from 1 to 24 keV and from 700 keV up. The 24 keV minima is defined well. Discrepancies occur in minima between 70 and 700 keV although only 4 groups in this region exhibit a difference of greater than 10%. It is of interest to note in this region of disagreement, the self-shielded set seems to be overcorrected.

The absorption cross sections are compared in Fig. 4(a) and 4(b). Once again the groups with large disagreement seem to be sufficiently corrected using the self-shielding formalism. From 70 keV up the values for the cross sections are in good agreement even with no self-shielding correction. The differences in the VIM generated values and the self-shielded values are all below 10% with the larger differences occuring at resonance peaks. Except for a few perhaps insignificant differences, the self-shielded values represent a good "average" cross section approximation to the group reaction cross sections needed to perform a calculation on the 78.2-cm diameter iron sphere.

SUMMARY

The comparisons performed have demonstrated that the Bondarenko self-shielded cross section set provides an improvement over infinitely dilute cross section sets. In general this self-shielding formalism tends to appropriately adjust the cross section values. However, the self-shielding formalism tends to overcorrect in some cases. For instance, between 135.69 and 142.67 keV, the infinitely dilute elastic cross section was a factor of 5.3 higher than the VIM value while the self-shielded value was 0.8 of the VIM value. The general agreement of the self-shielded and the VIM cross sections is good. The errors inherent in the use of multigroup cross section sets with self-shielding approximations are small and do not explain the differences between our leakage calculations and measurements.[1,2]

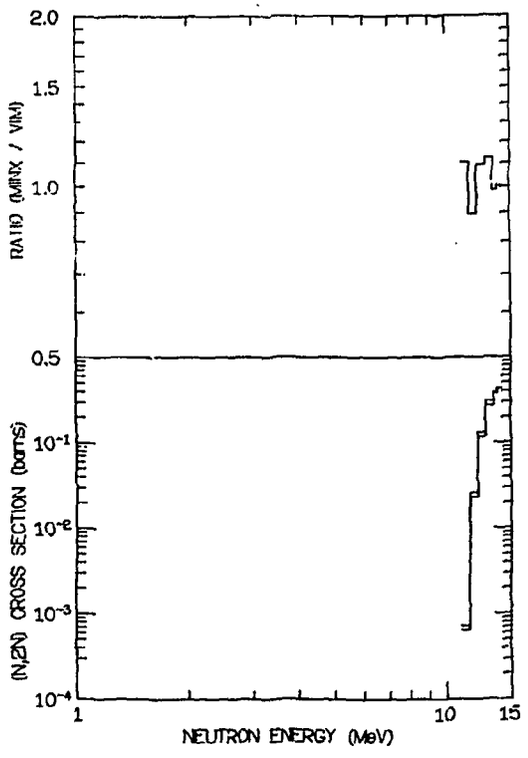

Fig. 1. The (n,2n) Cross Sections. In the lower graph, the VITAMIN-C infinitely dilute values are shown by the solid line and the VIM values by the dashed line. The upper graph gives the ratio of the VITAMIN-C and VIM cross-section values.

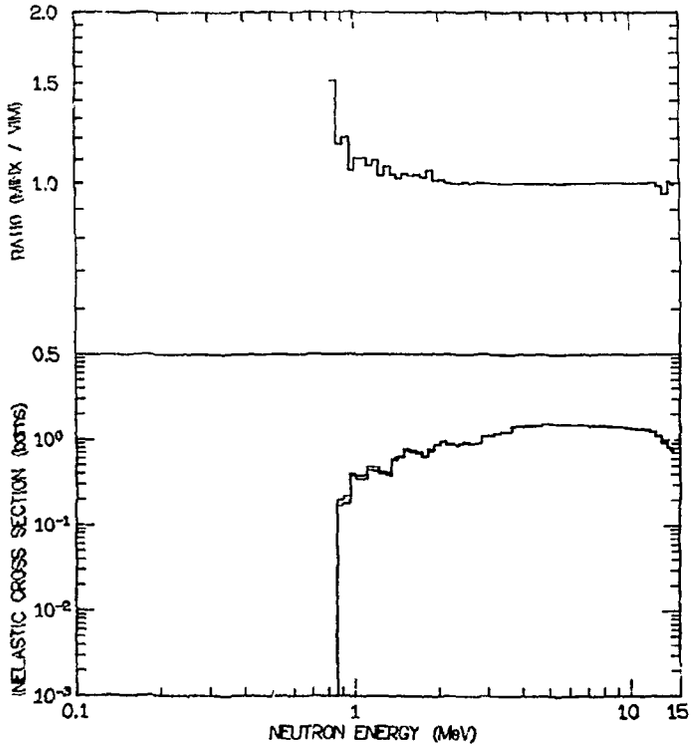

Fig. 2. The Inelastic Scattering Cross Sections. In the lower graph, the VITAMIN-C infinitely dilute values are shown by the solid line and the VIM values by the dashed line. The upper graph gives the ratio of the VITAMIN-C and VIM cross-section values.

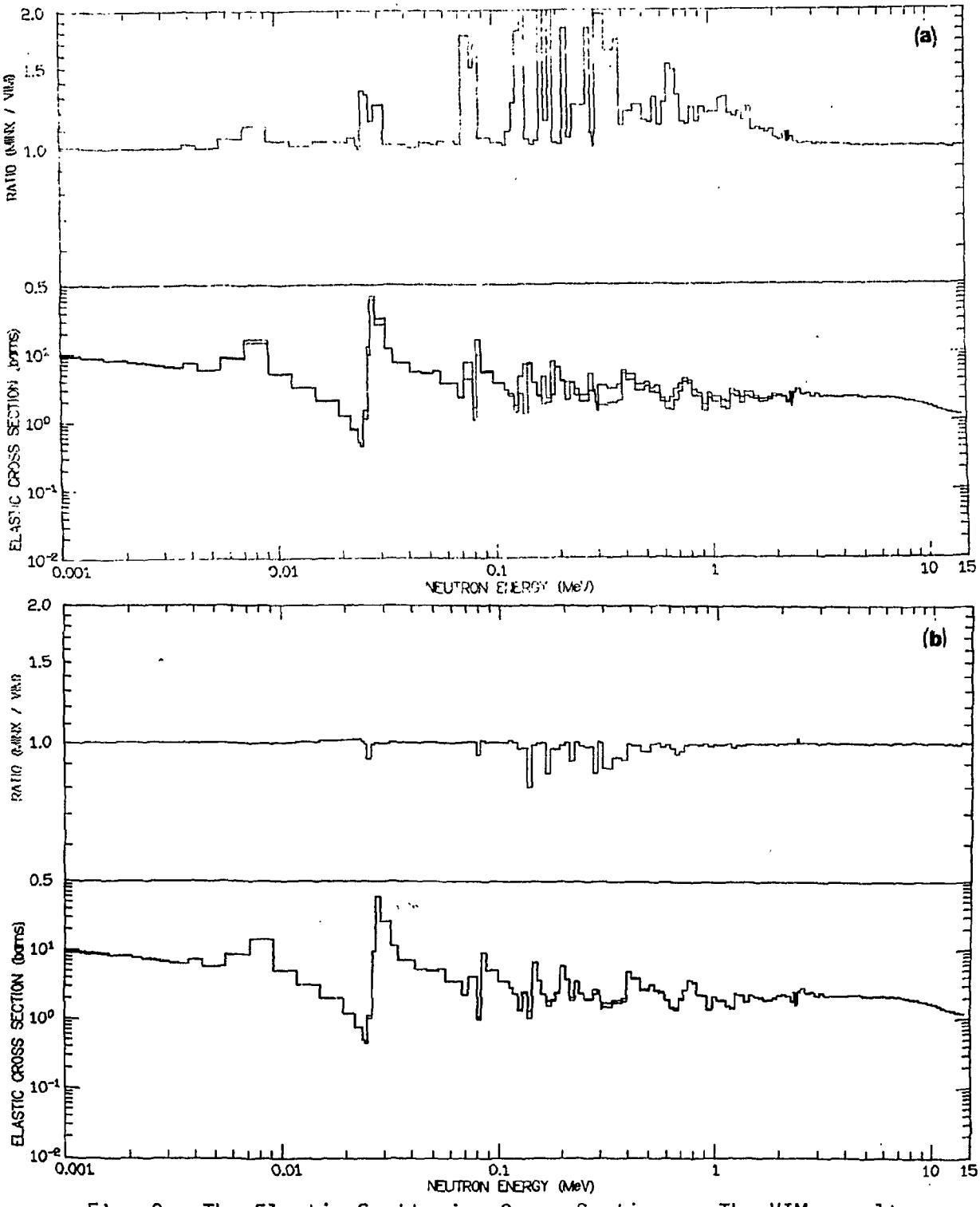

Fig. 3. The Elastic Scattering Cross Sections. The VIM results (dashed lines) are compared in (a) with the infinitely dilute and in (b) with the self-shield VITAMIN-C values (solid lines). The corresponding ratios are given above the cross-section graphs.

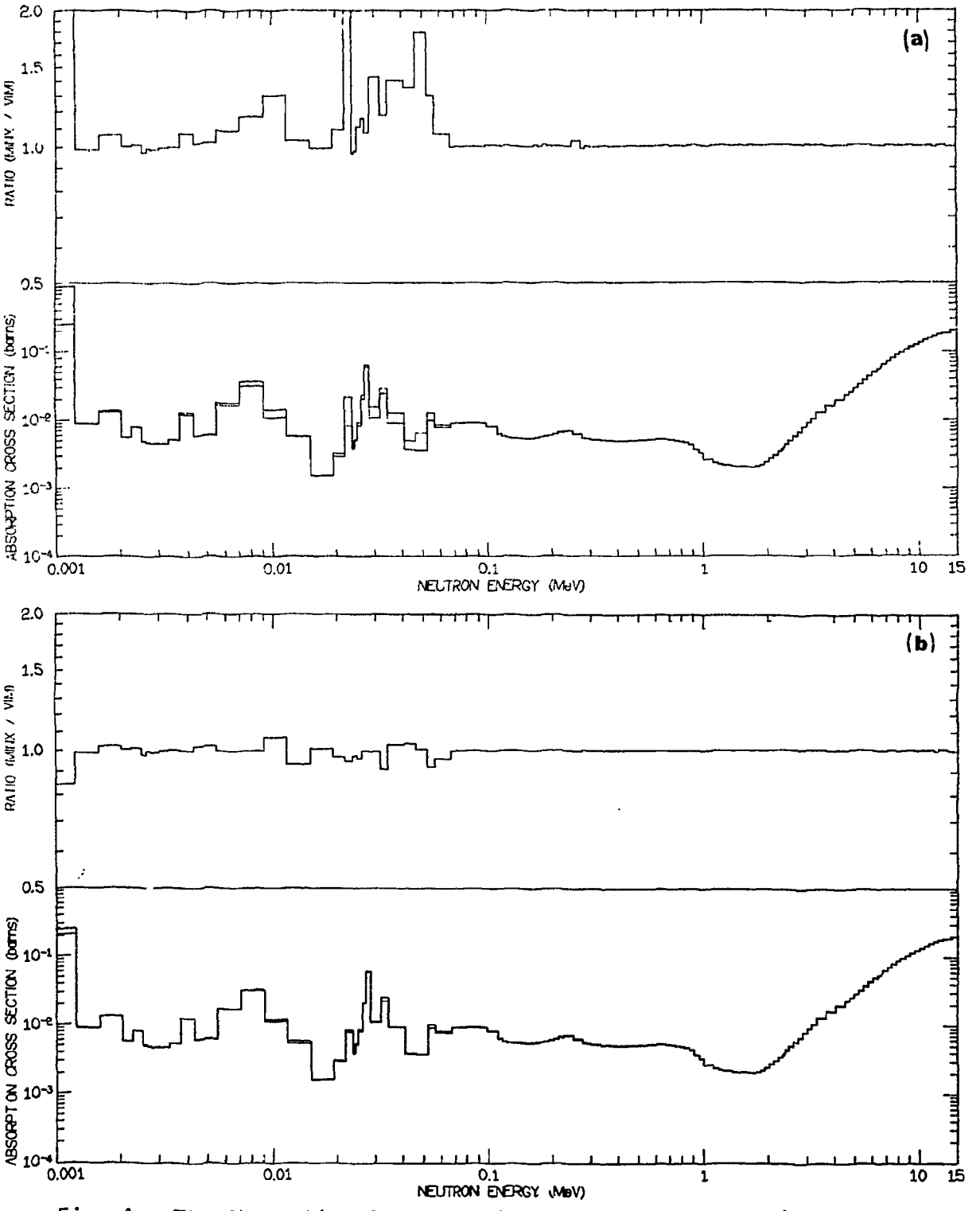

Fig. 4. The Absorption Cross Sections. The VIM values (dashed lines) are compared in (a) with the infinitely dilute and in (b) with the self-shielded VITAMIN-C (solid Lines). The corresponding ratios are given above the cross-section graphs.

ACKNOWLEDGEMENT

The VIM calculations were performed at Argonne National Laboratory in conjunction with an Argonne Center for Educational Affairs thesis parts appointment supervised by David Wade of the Applied Physics Division. Special thanks go to R. W. Roussin at RSIC for supplying us with the infinitely dilute and self-shielded cross section. This work was partially supported under HEW PHS CA09067.

REFERENCES

1. R. H. Johnson, J. J. Dorning, and B. W. Wehring, "Integral Test of Cross Sections Using Neutron Leakage Spectra from Spheres of Iron, Niobium, Beryllium, and Polyethylene," Proc. Conf. on Nuclear Cross Sections and Technology, Washington, D.C., March 3-7, 1975, NBS Special Publication 425, 169 (1975).

2. R. H. Johnson, J. J. Dorning, and B. W. Wehring, "Integral Tests of Neutron Cross Sections for Iron above 1.0 MeV," Trans. Am. Nucl. Soc. 22, 799 (1975).

3. D. T. Ingersoll, B. W. Wehring, and J. J. Dorning, "Integral Tests of Niobium Cross Sections Through Simultaneous Measurements of Neutron and Gamma-Ray Leakage Spectra," Proceedings of the Fifth International Conference on Reactor Shielding, April 17-23, 1977, Knoxville, Tennessee, 841 (1977).

4. R. H. Johnson, D. T. Ingersoll, B. W. Wehring, and J. J. Dorning, "NE-213 Neutron Spectrometry System for Measurements from 1.0 to 20 MeV," Nucl. Inst. Meth. 145, 337 (1977).

5. D. T. Ingersoll and B. W. Wehring, "Gamma-Ray Pulse-Height Response of an NE-213 Scintillation Detector," Nucl. Inst. Meth. 147, 551 (1977).

6. W. W. Engle, Jr., A User's Manual for ANISN, K-1693, Union Carbide Corp., (1967).

7. R. E. Prael and L. J. Milton, A User's Manual for the Monte Carlo Code VIM, Argonne National Laboratory FRA-TM-84 (1976).

8. R. L. Prael, "Cross Section Preparation for the Continuous-Energy Monte Carlo Code VIM," Proc. Conf. on Nuclear Cross Sections and Technology, Washington, D.C., March 3-7, 1975, NBS Special Publication 425, 447 (1975).

9. R. W. Roussin, C. R. Weisbin, J. E. White, N. M. Green and R. H. Johnson "Development, Generation, and Testing of the DCTR Fine-Group Cross-Section Library," Trans. Am. Nucl. Soc. 22, 820 (1975).

10. C. R. Weisbin, R. W. Roussin, E. M. Oblow, D. E. Cullen, J. E. White, and R. W. White, "The Role of 'Standard' Fine-Group Cross Section Libraries in Shielding Analysis," Proceedings of the Fifth International Conference on Reactor Shielding, April 17-23, 1977, Knoxville, Tennessee, 742 (1977).

11. R. E. Prael and H. Henryson II, "A Comparison of VIM and MC^2-2-Two Detailed Solutions of the Neutron Slowing-Down Problem," Proc. Conf. on Nuclear Cross Sections and Technology, Washington, D.C., March 3-7, 1975, NBS Special Publication 425, 451 (1975).

12. D. J. Garber and C. Brewster, ENDF/B Cross Sections, BNL17100 (ENDF-200), 2 ed. (1975).

13. D. Garber, C. Dunford, and S. Pearlstein, Data Formats and Procedures for the Evaluated Nuclear Data File, ENDF, BNL-NSC50496 (ENDF-102), Appendix B (1975).

14. I. I. Bondarenko, Editor, Group Constants For Nuclear Reactor Calculations, Consultants Bureau, New York, 1964.

15. C. R. Weisbin, P. D. Soran, D. R. Harris, R. J. LaBauve, and D. Hendricks, "MINX - A Multigroup Interpretation of Nuclear X-Sections," Trans. Am. Nucl. Soc. 16, 127 (1973).

EXPERIENCE WITH THE DLC-37/EPR CROSS SECTION LIBRARY FOR PRELIMINARY GAMMA-RAY HEATING ANALYSIS OF THE PURDUE UNIVERSITY FAST BREEDER BLANKET FACILITY

R.H. Johnson and J.H. Paczolt
Purdue University
West Lafayette, Indiana 47907

ABSTRACT

A subcritical facility for testing fast breeder blanket mock-ups has recently been constructed at Purdue University. Preliminary calculations of gamma-ray heating rates and fission rates in the first blanket loading were performed using the one-dimensional discrete ordinates code ANISN-W and the coupled multigroup cross section set DLC-37/EPR. Group collapsing of the cross section set and modification of ANISN-W were necessary. Proper self-shielding of the cross sections was found to be important. Fission rates are given for uranium-235 and uranium-238; these fission rates are compared with results from a two-dimensional diffusion calculation. Calculated gamma-ray heating rates for lead and UO_2 are presented.

INTRODUCTION

A subcritical facility for testing fast breeder reactor blanket mock-ups has recently been constructed at Purdue University. Preliminary gamma-ray heating calculations have been performed for the purpose of planning thermoluminescence dosimetry (TLD) measurements of gamma-ray heating rates in the first blanket mock-up. These preliminary calculations will also serve to guide the planning of the final analysis of gamma-ray heating rates.

Gamma-ray heating is a significant contribution to the power generated in the blanket region of a fast breeder reactor. An accurate prediction of the power distribution in the blanket is important for proper blanket design. Overheating of fuel must be avoided. However, overcooling of the blanket should be minimized; overcooling leads to a lower coolant outlet temperature and, as a result, a decrease in the thermal efficiency of the power plant.

The coupled 100N-21G* cross section library DLC-37/EPR was used for the preliminary calculations. Infinite medium ANISN-W calculations were

*Read as 100 neutron groups, 21 gamma-ray groups.

used to collapse macroscopic cross sections for the various radial zones of the facility into a 23N-21G group structure. Several modifications of ANISN-W and auxiliary programs were necessary for use in this collapsing process. ANISN-W was then used with the collapsed cross sections to calculate gamma-ray heating rates. Fission rates were also calculated for comparison with results from the two-dimensional diffusion code 2DB.

DESCRIPTION OF THE FAST BREEDER BLANKET FACILITY

The Fast Breeder Blanket Facility (FBBF) is a subcritical facility designed to test mock-ups of blankets for fast breeder reactors.[1] Experiments planned for the blanket region of the facility are neutron spectrum measurements, fission rate measurements, a variety of capture rate measurements, and gamma-ray heating measurements. These experiments will be analyzed using both diffusion and transport codes. Comparisons of the measurements and calculations will serve as integral tests of both the calculational methods used and the cross sections used. A major goal of this project is to eliminate much of the large uncertainty currently present in the design of fast breeder reactor blankets. Reaction rates in blankets are much more sensitive to errors in cross sections than are the same reaction rates in a fast reactor core.[2]

A view of the FBBF is shown in Fig. 1. At the center of this cylindrical subcritical facility are four californium-252 spontaneous fission neutron sources. Each source contains approximately 1 mg of californium-252; the total neutron emission rate of all sources is approximately 10^{10} neutrons per second. The four sources are equally spaced in a source rod. When the facility is not in operation, the source rod is lowered into a concrete storage cask below the facility.

Surrounding the source region are inner and outer transformer regions with an active (fueled) height of 92 cm. The inner transformer contains closely-packed, stainless steel clad, 4.8%-enriched UO_2 fuel rods. The spaces between fuel rods are filled with boron carbide powder. The inner transformer has an inner radius of 3.5 cm and an outer radius of 16 cm. The outer transformer contains the same type of fuel rods, but with a wider hexagonal pitch. Sodium-filled stainless steel cans (with an approximately hexagonal cross section) are placed between the fuel rods; remaining spaces are filled with boron carbide powder. The outer transformer has an outer radius of 22 cm.

The transformer regions were designed to achieve two main goals. First, the calculated energy spectrum at the transformer-blanket interface closely matches the energy spectrum at the core-blanket interface of the proposed Clinch River Breeder Reactor (CRBR). Second the

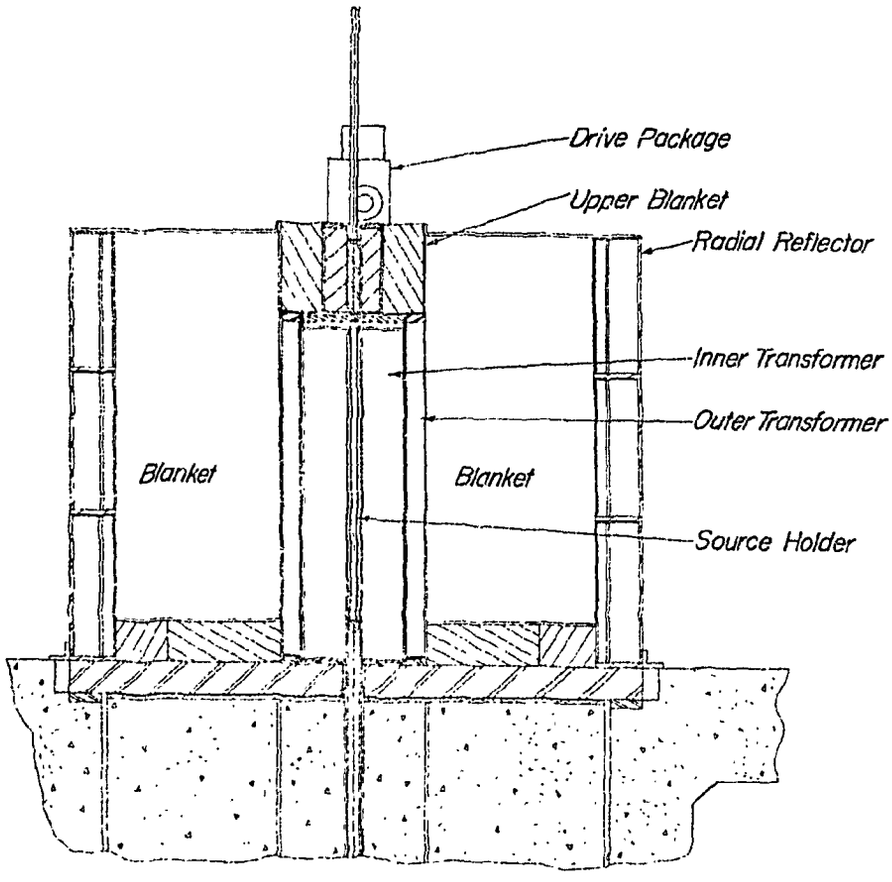

Figure 1: Cross-sectional view of the Purdue University Fast Breeder Blanket Facility.

axial flux distribution at the transformer-blanket interface closely matches that which would be produced by a continuous, chopped-cosine source. (That is, the use of point sources instead of a continuous source results in negligible flux distortions in the blanket region.)

The blanket region surrounds the transformer regions. The mock-up used in the first FBBF loading is a two-region blanket. The fuel used for the first loading is aluminum-clad natural UO_2. (1.3%-enriched UO_2 fuel rods are also available and will be used in later loadings.) Aluminum serves to mock-up sodium in the blanket; the actual use of sodium is not currently planned for any of the blanket mock-ups. In the inner blanket (outer radius of 57 cm) each fuel rod is placed in a stainless steel tube; in the outer blanket (outer radius of 74 cm) each fuel rod is placed in an aluminum tube. The same pitch is used for both the inner and outer blankets; the hexagonal pitch was chosen so that the stainless steel and aluminum tubes are closely packed. The inner blanket has number densities comparable to those of current blanket designs for liquid metal fast breeder reactors (with aluminum substituted for sodium). The outer blanket contains only aluminum and natural UO_2, permitting somewhat cleaner experiments.

The blanket region is surrounded by a reflector region (outer radius of 89 cm) composed of sodium chloride and carbon steel. Future blanket loadings with a smaller blanket thickness are planned; a new reflector region will be fabricated for those loadings. A more detailed description of the FBBF is given in Ref. 3. The FBBF laboratory, experimental equipment, and experimental plans are also discussed in Ref. 3.

GAMMA-RAY HEATING CALCULATIONS

The gamma-ray heating calculations were performed using the DLC-37/EPR cross section set[4,5] and the discrete ordinates code ANISN-W[6], a CDC version of ANISN.[7] DLC-37/EPR is based on ENDF/B-IV data and contains coupled (100N-21G) multigroup cross sections of the important nuclides for the first FBBF loading. DLC-37/EPR also includes neutron and gamma-ray kerma factors for many of the elements in the cross section set. The coupled neutron and gamma-ray transport calculations were also used to give radially-dependent fission rates for comparison with the two-dimensional diffusion calculations discussed in Ref. 8.

The block diagram in Fig. 2 shows the calculations initially performed. A tape containing the DLC-37/EPR cross sections in the form of BCD card images was obtained from the Radiation Shielding Information Center (RSIC). The LIBGEN[9] code was modified for use on the Purdue dual CDC-6500 system; LIBGEN was used to generate a binary tape of those nuclides in the calculational model of the FBBF; the binary tape also included the response matrix containing the kerma factors.

The TAPEMAKER[10] code was used to form macroscopic mixtures for each of the 11 radial zones in the one-dimensional model used for the FBBF.

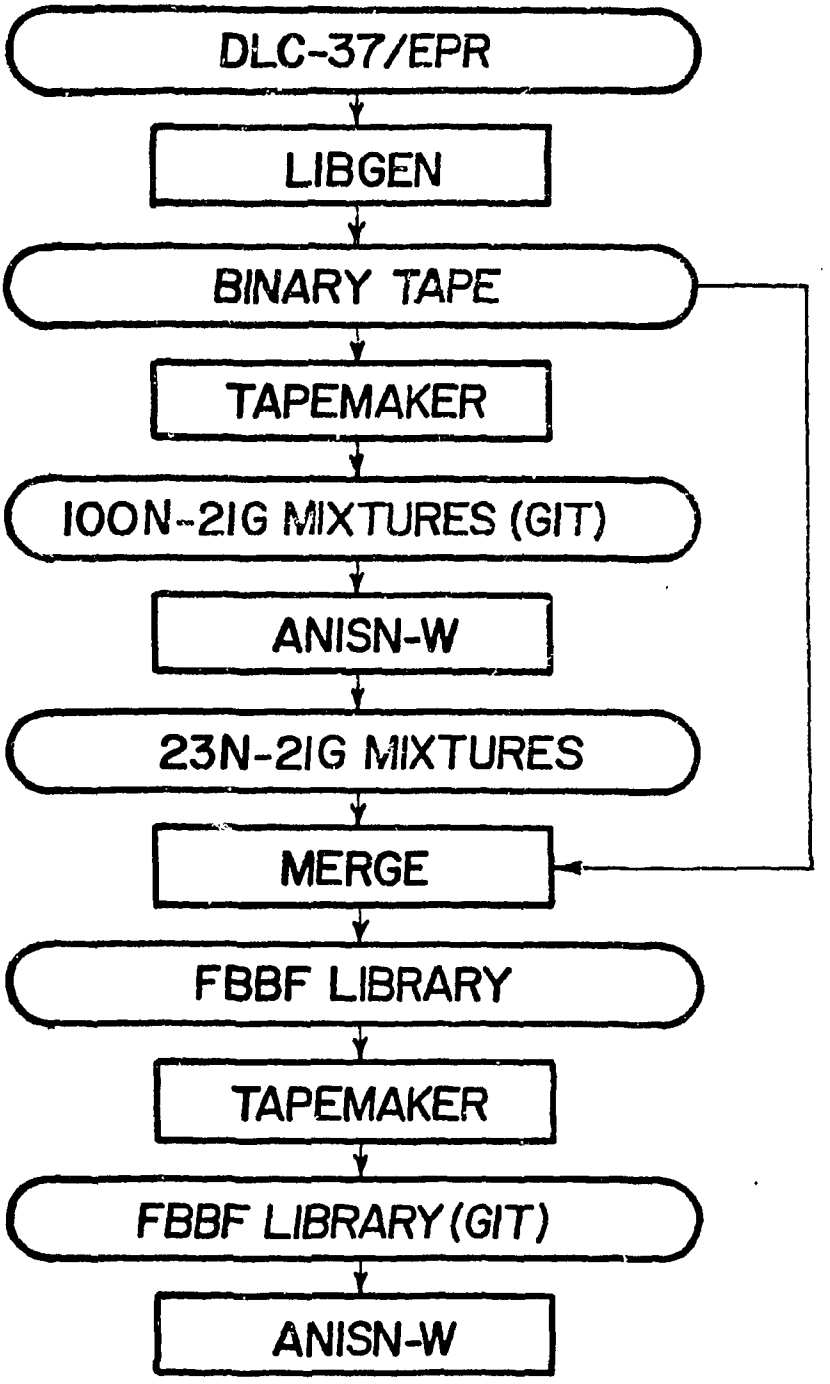

Figure 2: Block diagram of ANISN-W calculation using the DLC-37/EPR cross section library.

Detailed specifications of the model are given in Ref. 8. The macroscopic library produced by TAPEMAKER has a group-independent tape (GIT) format which allows the cross sections to be stored out of core for the ANISN-W calculations.

Insufficient core memory was available to do the FBBF calculations using the 100N-21G cross sections, even with the use of the GIT format. Therefore, ANISN-W was used to perform infinite medium calculations to collapse P_3 cross sections for each mixture to a 23N-21G group structure. The procedure outlined in Ref. 11 was followed for group collapsing.

A modification of ANISN-W was found to be necessary for proper group collapsing. In the original version of ANISN-W, group collapsing was performed by using the total flux as a weighting function for all cross sections except the self-scattering cross section $\sigma_{g\to g}$ of the P_0 cross sections for group g. The self-scattering P_0 cross section was then calculated as

$$\sigma_{g\to g} = \sigma_t^g - \sigma_a^g - \sum_{g'=g+1}^{N} \sigma_{g\to g'} \qquad (1)$$

where N is the total number of neutron (or gamma-ray) groups. This approach forces a neutron (or gamma-ray) balance for group g and is appropriate if multiplication is negligible for all reactions other than fission. This approach is not appropriate for high energy gamma-rays because pair production is significant. ANISN-W used this approach for both neutron and gamma-ray cross sections, even for energy groups not being collapsed. The gamma-ray groups of DLC-37/EPR were not collapsed in the infinite medium calculations. However, ANISN-W still applied the above procedure to the self-scattering P_0 cross sections, giving negative results for high energy gamma-ray groups. To correct this error, ANISN-W was modified to apply the above procedure only to neutron groups.

The neutron group structure for the collapsed cross section set was based on a 21-group set used for diffusion calculations. (This set is discussed below.) The two additional groups are a thermal neutron group and a group above 10 MeV. Infinite medium calculations for group collapsing were performed for each of the 11 radial zones. Neutron energy spectra obtained in preliminary diffusion calculations were used as fixed sources for the collapsing runs; transverse leakage corrections were made to approximate axial and radial leakage for the various zones.

The results of these 11 infinite medium calculations were 11 files containing 23N-21G cross sections for the radial zones. A program shown as MERGE in the block diagram in Fig. 2 was written to further process these collapsed macroscopic cross sections. MERGE took P_0 cross sections for uranium-235 and uranium-238 and collapsed the absorption and fission ($\nu\sigma_f$) cross sections to the 23N-21G group structure. MERGE took the response matrix containing the kerma factors, removed the kerma factors for neutron groups, and collapsed the response matrix to the 23N-21G group structure. Finally, MERGE combined these three matrices (containing uranium-235 and uranium-238 microscopic cross sections and gamma-ray kerma factors) with the P_3 cross sections for the 11 mixtures. This

process resulted in a single file referred to in the block diagram as the FBBF Library. TAPEMAKER was then used to form a GIT version of the FBBF library.

Finally, ANISN-W was used to calculate radially-dependent gamma-ray heating rates and fission rates for uranium-235 and uranium-238. The fixed source for the calculation was a californium-252 source distributed along the center line of the FBBF. The californium-252 neutron and gamma-ray spectra used were based on recent measurements made at the University of Illinois.[13,14] A transverse leakage correction was made using the extrapolated blanket height of 160 cm. The fixed source was normalized so that the calculation would correspond to the axial midplane of the FBBF for a neutron source strength of 10^{10} neutrons per second (for a chopped-cosine axial source distribution). An S_4 angular quadrature set was used which satisfied both even moment and rotational invariance conditions.[6] Good convergence was obtained after 7 outer iterations; the diffusion approximation was used in the first 4 outer iterations. The calculation required approximately 1000 seconds and $150{,}000_8$ words of core memory on the Purdue dual CDC-6500 system.

The ANISN-W calculations of fission rates were compared with results from two-dimensional diffusion calculations[8] made using the code 2DB.[15] A comparison of the calculated uranium-235 fission rates along the axial midplane is shown in Fig. 3; agreement is poor. The two-dimensional model for the 2DB calculations used the four point sources rather than a line source; therefore, the large discrepancies for radii less than 10 cm are to be expected because the axial midplane is actually some distance from either of the middle two point sources. The large discrepancies for radii greater than 20 cm (i.e., the blanket and reflector regions) could not be attributed simply to differences in the geometrical models.

Differences in the cross section sets used were examined next. DLC-37/EPR contains infinitely dilute cross sections; a 1/E weighting spectrum was used in the fast groups. The 21-group cross section set used for the 2DB calculations, however, was generated using the MC^2-2 code[16,17] and was self-shielded. The weighting spectra used were fine group spectra calculated for various regions of the proposed CRBR. The 21-group cross section set was self-shielded for a temperature of 1000°K. Macroscopic mixtures were formed using the one-dimensional diffusion code LAZARUS.[18]

The major difference between the two cross section sets appeared to be self-shielding. Resonance self-shielding in uranium is quite important for the blanket region (containing natural uranium) and differences of approximately a factor of two were found in the macroscopic absorption cross sections for some energy groups. A simple approach was taken to incorporate the effects of self-shielding into the 23N-21G cross section set collapsed from DLC-37/EPR. Macroscopic absorption and fission cross sections for groups 4 through 21 of the 21-group cross section set for the 2DB calculations were substituted into the corresponding groups 5 through 22 of the 23N-21G FBBF Library (GIT). The macroscopic total

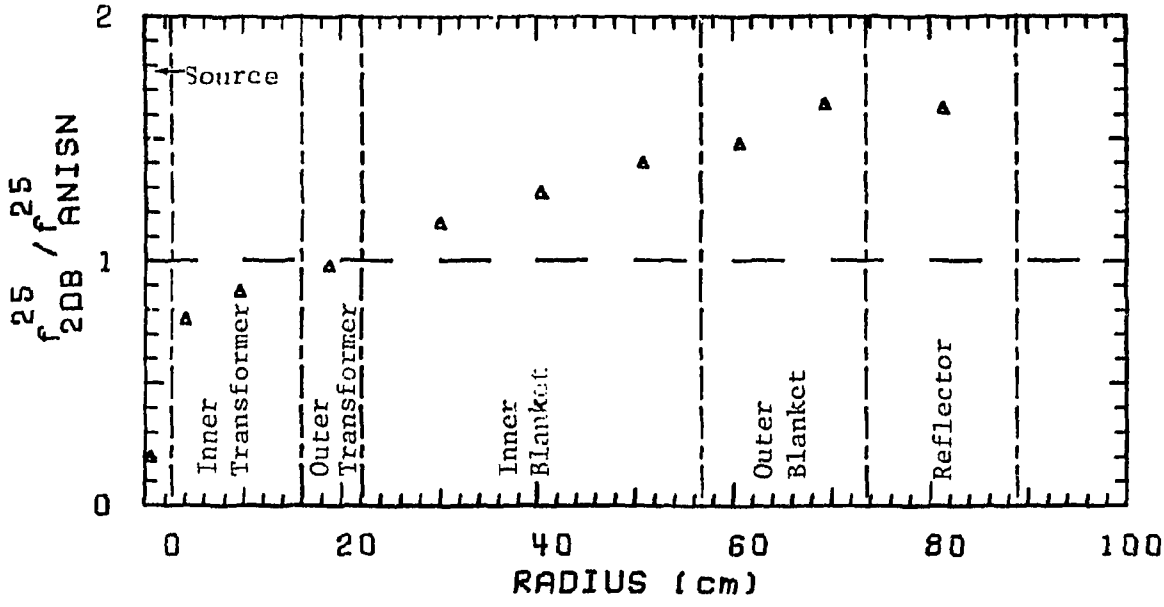

Figure 3: Ratio of 2DB calculation to initial ANISN-W calculation for ^{235}U fission rate.

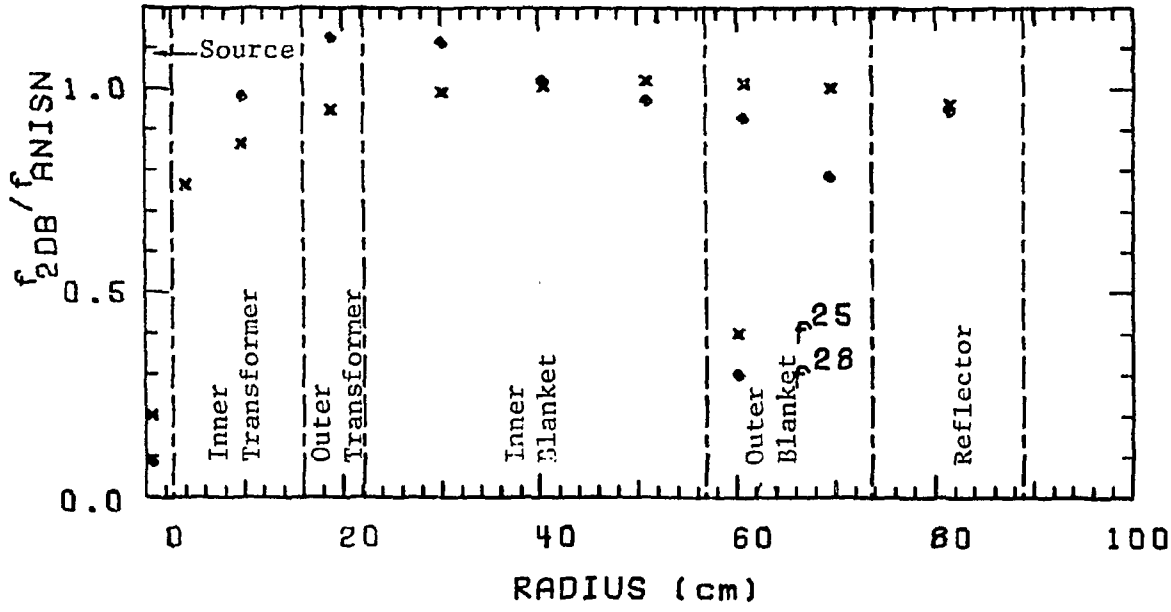

Figure 4: Ratio of 2DB calculation to ANISN-W calculation using self-shielded cross sections.

cross sections were reduced by the same amount as the absorption cross section; the scattering cross sections were not changed. The energy groups modified are those for neutron energies below 1 MeV.

The self-shielded FBBF Library (GIT) was used with ANISN-W to recalculate the fission rates and gamma-ray heating rates. A comparison of the resulting fission rates with those calculated by 2DB are shown in Fig. 4. The 2DB and ANISN-W calculations for uranium-235 agree within several percent in the blanket regions. The uranium-235 fission rates calculated by ANISN-W are shown in Fig. 5. Agreement of 2DB and ANISN-W for uranium-238 is seen in Fig. 4 to be fair, although not nearly as good as for uranium-235. The uranium-238 fission rates calculated by ANISN-W are shown in Fig. 6.

Gamma-ray heating rates are calculated by ANISN-W by folding a response matrix containing gamma-ray kerma factors with the calculated gamma-ray flux. Gamma-ray heating rates in the FBBF were calculated for each element in the kerma factor response matrix. The resulting heating rates are output by ANISN-W as activities by spatial interval. Kerma factors for uranium were not included with DLC-37/EPR. Rather than attempt to extrapolate the kerma factors, the calculated gamma-ray heating rates were plotted as a function of atomic number and extrapolated to obtain gamma-ray heating rates in uranium. Lead was the highest-Z material for which kerma factors were included in the response matrix included in the DLC-37/EPR library. Gamma-ray heating rates obtained using the self-shielded FBBF Library are shown for UO_2 in Fig. 7 and for lead in Fig. 8.

CONCLUSIONS

Several conclusions have been made on requirements for a multigroup cross section set for further analysis of the gamma-ray heating rates in the FBBF. These conclusions are partially based on the results of the preanalysis calculations discussed in this paper.

Resonance self-shielding is vital. The amount of self-shielding will vary from region to region as well as from one blanket loading to the next; therefore, a self-shielding method such as that of Bondarenko[19] should be used to allow changes to be easily made. Self-shielding should be performed for room temperature.

An alternative method of performing gamma-ray heating calculations may be worth investigation. Neutron transport can be calculated first, giving neutron flux as a function of radius. Next, the neutron flux can be multiplied by the gamma-ray production cross sections to give a distributed gamma-ray source throughout the facility. Finally, the gamma-ray transport can be calculated separately. This approach was used, for example, in gamma-ray heating calculations for the Gas-Cooled Fast Reactor.[20] Coupled multigroup cross section sets such as DLC-37/EPR

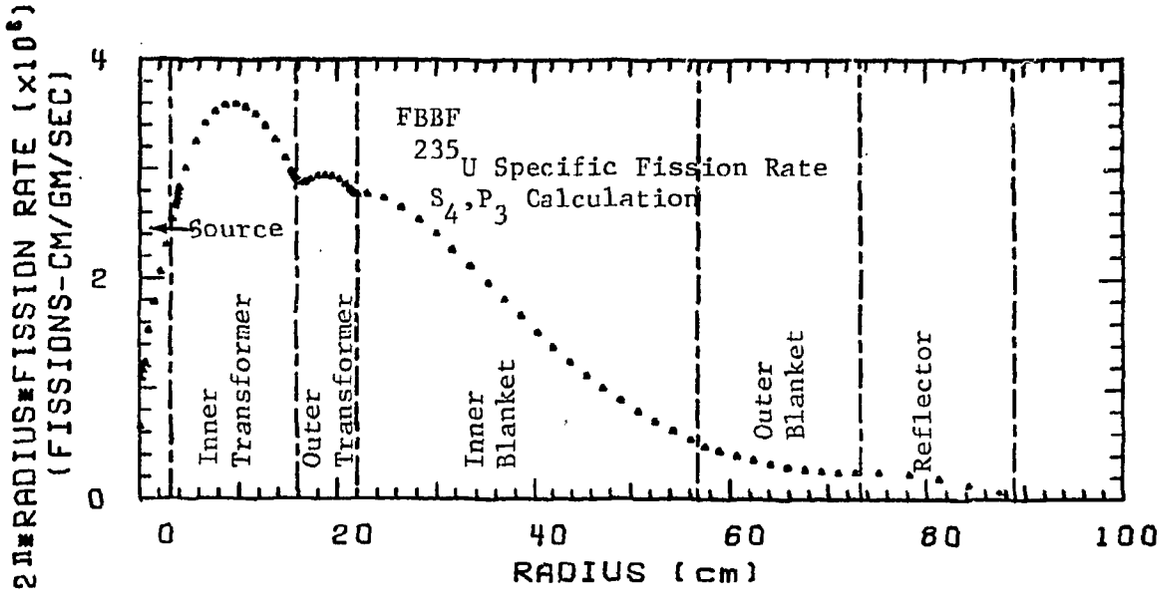

Figure 5: ANISN-W calculation of ^{235}U fission rate using self-shielded cross sections.

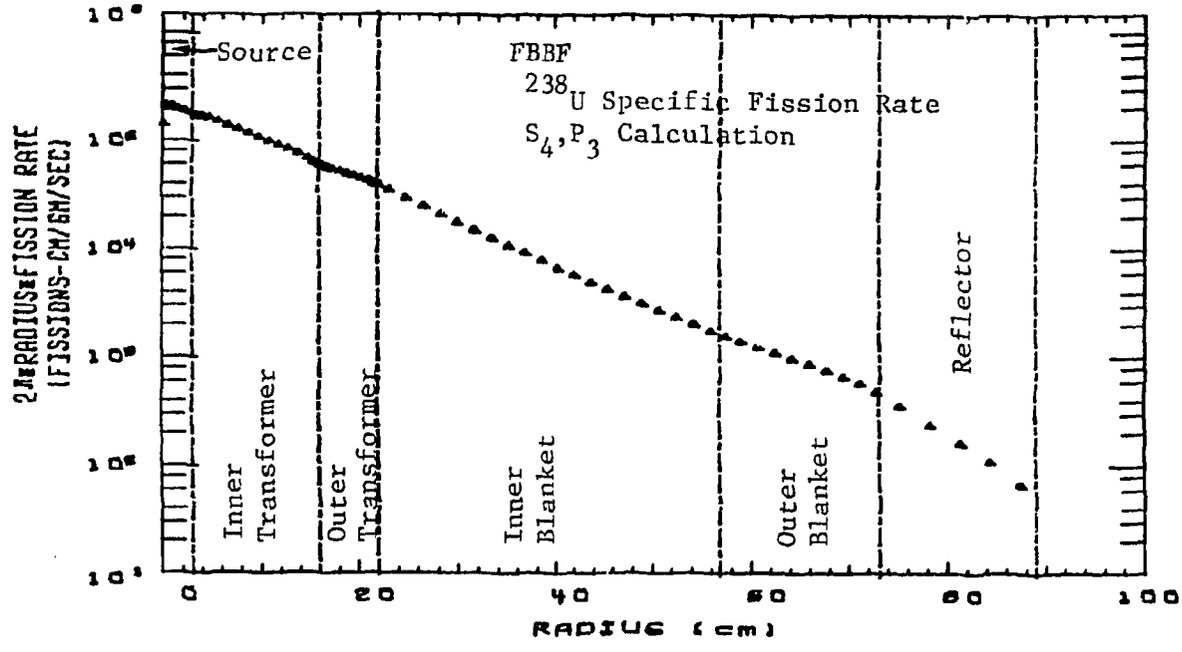

Figure 6: ANISN-W calculation of ^{238}U fission rate using self-shielded cross sections.

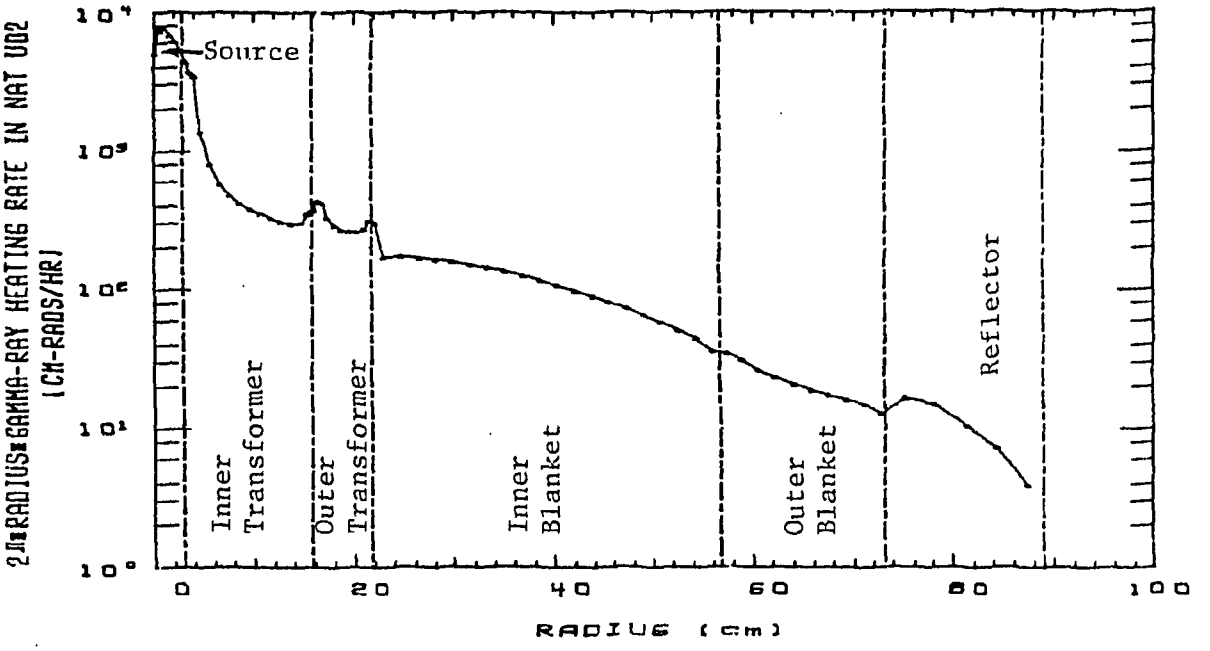

Figure 7: Calcuated gamma-ray heating rate in UO_2.

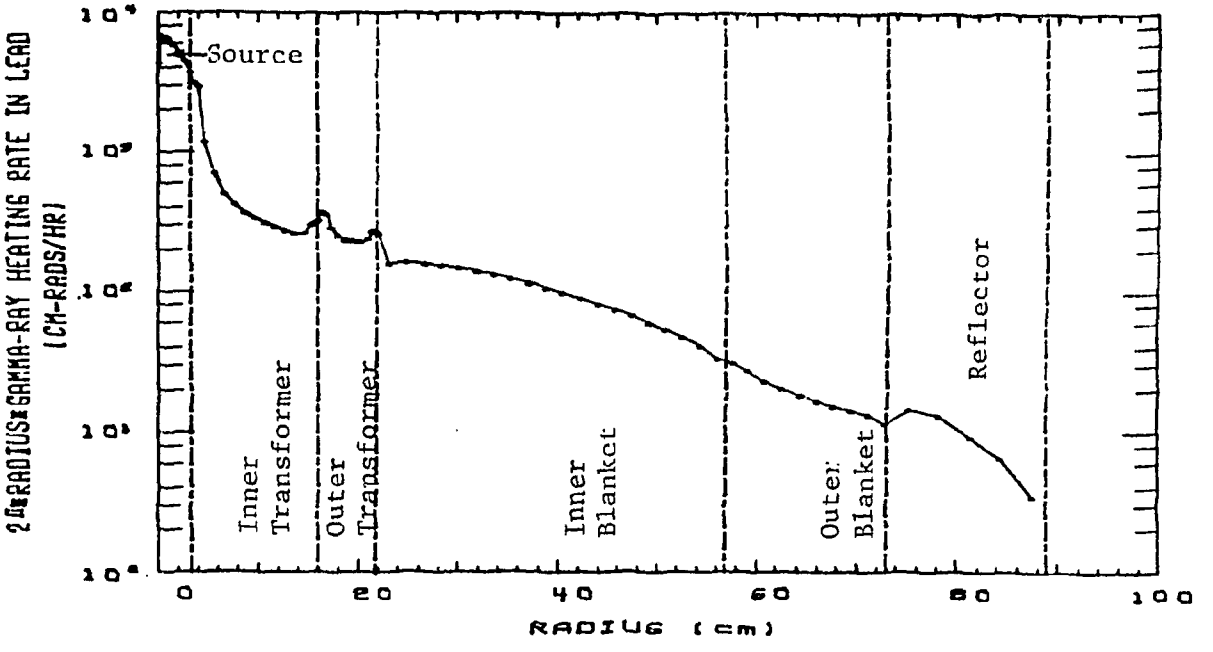

Figure 8: Calculated gamma-ray heating rate in lead.

could be split into three parts: neutron cross sections, gamma-ray production cross sections, and gamma-ray cross sections. This procedure would result in more efficient usage of computer memory, but would possibly lead to a longer total running time.

The main advantage of the three-step gamma-ray heating calculation outlined above, however, would be to allow more efficient investigations involving modified gamma-ray production cross sections. The gamma-ray production cross sections in DLC-37/EPR, for example, contain prompt gamma rays from fission but do not include decay gamma rays from fission products.[21] Some experiments in the FBBF may involve irradiations of several weeks, and decay gamma rays from fission products may increase the gamma-ray heating rate by several percent.

Neutron kerma factors will be used in the final analysis to calculate the neutron energy deposition rate in the TLD material. The calculated neutron response in the TLD material should be subtracted from the total measured response in the gamma-ray heating rate experiments.

Overall, the self-shielded ANISN-W calculations agree reasonably well with the two-dimensional diffusion calculations and have been useful in the preanalysis of the gamma-ray heating rate measurements in the FBBF. The DLC-37/EPR library was used for this preanalysis. However, a more suitable cross section library (with user-adjustable self-shielding) is desirable for the final analysis of these planned experiments.

ACKNOWLEDGEMENTS

This investigation was jointly supported by the Electric Power Research Institute and the Department of Energy.

REFERENCES

1. F.G. Krauss, K.O. Ott and F.M. Clikeman, "The Conceptual Design of a Fast Subcritical Blanket Facility", Nucl. Tech. 25, 429, (1975).

2. K.O. Ott, K.R. Boldt and F.M. Clikeman, "Review of Nuclear Physics Uncertainties in Fast Reactor Blankets," Department of Nuclear Engineering, Purdue University, PNE-75-103, (1975).

3. "FBBF Annual Progress Report for the Period of January 1, 1977 - December 31, 1977," School of Nuclear Engineering, Purdue University, PNE-78-127, COO-2826-7, (1978).

4. "DLC-37/EPR, Coupled 100-Group Neutron 21-Group Gamma-Ray Cross Sections for EPR Neutronics," Radiation Shielding Information Center, Oak Ridge National Laboratory.

5. W.E. Ford, III, R.T. Santoro, R.W. Roussin and D.M. Plaster, "Modification Number One to the Coupled 100n21γ Cross Section Library for EPR Calculations", Oak Ridge National Laboratory, ORNL/TM-5249, (1976).

6. R.G. Soltesz and R.K. Disney, "Nuclear Rocket Shielding Methods, Modification, Updating, and Input Data Preparation, Volume 4 -- One-Dimensional, Discrete Ordinates Transport Technique", Westinghouse Astronuclear Laboratory, WANL-PR-(LL)-034, (1970).

7. W.W. Engle, Jr., "A User's Manual for ANISN, A One Dimensional Discrete Ordinates Transport Code with Anisotropic Scattering", Union Carbide Corporation, K-1693, (1967).

8. "FBBF Quarterly Progress Report for the Period July 1, 1977 - September 30, 1977", pp. 2-23, School of Nuclear Engineering, Purdue University, PNE-77-120, COO-2826-5, (1977).

9. L.R. Williams, "Instructions for LIBGEN, a Code to Convert from Card Image to Binary ANISN Format", Oak Ridge National Laboratory, Informal Notes, (1972).

10. "TAPEMAKER, A Routine to Prepare a 'Group Independent' Cross-Section Tape for ANISN", Oak Ridge National Laboratory, Informal Notes.

11. R.W. Roussin, "Using ANISN to Reduce the DLC-2/100-Group Cross-Section Data to a Smaller Number of Groups", Oak Ridge National Laboratory, ORNL-TM-3049, (1969).

12. "FBBF Quarterly Progress Report for the Period July 1, 1977 - September 30, 1977", pp. 24-43, School of Nuclear Engineering, Purdue University, PNE-77-120, COO-2826-5, (1977).

13. R.H. Johnson, B.W. Wehring, J.J. Dorning and D.T. Ingersoll, "^{252}Cf Fast-Neutron Spectrum Measured to 15 MeV", Trans. Am. Nucl. Soc. 22, 727, (1975).

14. D.T. Ingersoll, "Integral Testing of Neutron Cross Sections Using Simultaneous Neutron and Gamma-Ray Measurements", Ph.D. Thesis, University of Illinois, (1977).

15. W.W. Little, Jr. and R.W. Hardie, "2DB User's Manual", Pacific Northwest Laboratory, BNWL-831, (July, 1968).

16. B.J. Toppel, "The Multigroup Cross Section Code MC^2-2", Proc. Conf. New Developments in Reactor Mathematics and Applications, March 29-31, 1971, Idaho Falls, Idaho, CONF-710302, (1971).

17. J. Cahalan, Argonne National Laboratory, Personal Communication, (1975).

18. D.J. Malloy, L.B. Luck and G.A. Terpstra, "LAZARUS, A One-Dimensional Diffusion Code for Fast Reactor Calculations", Department of Nuclear Engineering, Purdue University, PNE-76-112, (1976).

19. I.I. Bondarenko, Ed., "Group Constants for Nuclear Reactor Calculations", Consultants Bureau, New York, (1964).

20. A. Razani, M. Nagel, C.A. Rouse, R.G. Perkins and R.J. Cerbone, "Gamma Ray Heating in a 300-MW(e) Gas-Cooled Breeder Reactor," Ann. Nucl. Energy 4, 51, (1977).

21. D.K. Trubey, Oak Ridge National Laboratory, Personal Communication, (1977).

AN ANALYTIC ANGULAR INTEGRATION TECHNIQUE FOR GENERATING MULTIGROUP TRANSFER MATRICES

J. A. Bucholz
Union Carbide Corporation Nuclear Division
at Oak Ridge National Laboratory
Oak Ridge, Tennessee USA

ABSTRACT

Many detailed multigroup transport calculations require group-to-group Legendre transfer coefficients to represent scattering processes in various nuclides. These (fine group) constants must first be generated from the basic data. This paper outlines an alternative technique for generating such data, given the total scattering cross section of a particular nuclide on a pointwise energy basis, $\sigma(E')$, and some information regarding the angular scattering distribution for each initial energy point.

The evaluation of generalized multigroup transfer matrices for transport calculations requires a double integration extending over the primary and secondary energy groups where, for a given initial energy, the integration over the secondary energy group may be replaced by an integral over the possible scattering angles. In the present work, analytic expressions for these angular integrals are derived which are free of truncation error. Differences between the present method (as implemented in ROLAIDS) and other methods (as implemented in MINX and NEWXLACS) will be explored. Of particular interest is the fact that, for hydrogen, the angular integration is shown to simplify to the point that, for many weight functions, the integration over the primary energy group might also be performed analytically. This completely analytic treatment for hydrogen has recently been implemented in NEWXLACS.

Given the Legendre coefficients of the scattering cross section on a point-wise basis, $\sigma_\ell(E' \to E)$, the group-to-group Legendre transfer coefficients are defined as:

$$\sigma_\ell(g' \to g) \equiv (1/\phi_\ell^{g'}) \int_{E^g}^{E^{g-1}} \int_{E^{g'}}^{E^{g'-1}} \phi_\ell(E')\, \sigma_\ell(E' \to E)\, dE'\, dE \qquad (1)$$

where the spatial dependence of each term is understood and $\phi_\ell(E')$ represents the Legendre coefficients of the angular flux distribution at each spatial point. In practice, the higher order terms, $\phi_\ell(E')$, are replaced by an energy dependent weight function $\phi(E')$. In ROLAIDS[1], for example, this would be the (zone averaged) scalar flux resulting from the solution of the integral slowing down equation on a point-wise basis. In other codes, such as XLACS,[2,3] the weight function may be specified by the user. The Legendre coefficients of the point-to-point angular scattering cross section are formally defined as

$$\sigma_\ell(E'\to E) \equiv 2\pi \int_{-1}^{+1} \sigma(E'\to E,\mu_L)\ P_\ell(\mu_L)\ d\mu_L \qquad (2)$$

In the fast and epithermal range, however, there is a unique relationship between the initial and final energies, the exitation energy (Q), the mass of the target nuclide (A), and the cosine of the angle of scatter in the lab system:

$$\mu_L(E',E,Q,A) = \frac{1}{2}\left[(A+1)\sqrt{\frac{E}{E'}} - (A-1)\sqrt{\frac{E'}{E}} + \frac{AQ}{\sqrt{E'E}}\right] \qquad (3)$$

Representing this as a delta function in Eq. (2) yields

$$\sigma_\ell(E'\to E) = \sigma(E'\to E)\ P_\ell[\mu_L(E',E,Q,A)] \qquad (4)$$

and

$$\sigma_\ell(g'\to g) = (1/\phi^{g'}) \int_{E^{g'}}^{E^{g'-1}} \phi(E') \left[\int_{E^{g}}^{E^{g-1}} P_\ell[\mu_L(E',E,Q,A)]\ \sigma(E'\to E)\ dE\right] dE' \ . \qquad (5)$$

The accurate evaluation of this expression represents a severe computational burden which must be addressed by any cross section processing code. The present method differs from previous approaches in that it yields an analytic solution for the integral on dE which is free of

truncation error when the scattering function is given by a Legendre expansion in either the center-of-mass (C) or the lab (L) system.

The scattering function, $\sigma(E'\rightarrow E)$, represents a distribution over the secondary energy (E) and hence over the scattering angle. Thus,

$$\sigma(E'\rightarrow E)\, dE = \sigma(E')\, f(E',\mu_c)\, 2\pi d\mu_c \tag{6}$$

where μ_c is the cosine of the scattering angle in the center-of-mass system and $f(E',\mu_c)$ is the angular distribution function in that system. A similar expression could certainly have been written for the lab system. Because all scattering processes appear more isotropic in the C system and because most scattering involving the formation of a compound nucleus is in fact isotropic in the C system, the present choice was made. While the present method can easily accomodate anisotropic scattering, it is most easily introduced assuming isotropic elastic scattering in the C system [$f(E',\mu_c) = 1/4\pi$, $Q = 0$]. The integral on dE can then be written as

$$\int_{E^g}^{E^{g-1}} P_\ell[\mu_L(E',E,Q,A)]\, \sigma(E'\rightarrow E)\, dE =$$

$$= \frac{1}{2}\sigma(E') \int_{\mu_c(E',E_L,Q,A)}^{\mu_c(E',E_U,Q,A)} P_\ell[\mu_L(E',E(\mu_c),Q,A)]\, d\mu_c \tag{7a}$$

$$= \frac{1}{2}\sigma(E') \int_{\mu_L(E',E_L,Q,A)}^{\mu_L(E',E_U,Q,A)} P_\ell[\mu_L(E',E,Q,A)] \left|\frac{d\mu_c}{d\mu_L}\right| d\mu_L \tag{7b}$$

$$= \frac{\sigma(E')}{2A} \int_{\mu_L(E',E_L,Q,A)}^{\mu_L(E',E_U,Q,A)} \left\{2\mu_L + \sqrt{a^2+\mu_L^2} + \frac{\mu_L^2}{\sqrt{a^2+\mu_L^2}}\right\} P_\ell(\mu_L)\, d\mu_L \tag{7c}$$

where E_U and E_L depend on the location of the secondary energy group relative to E' as shown in Fig. 1, and the relationship between μ_c and μ_L is given by

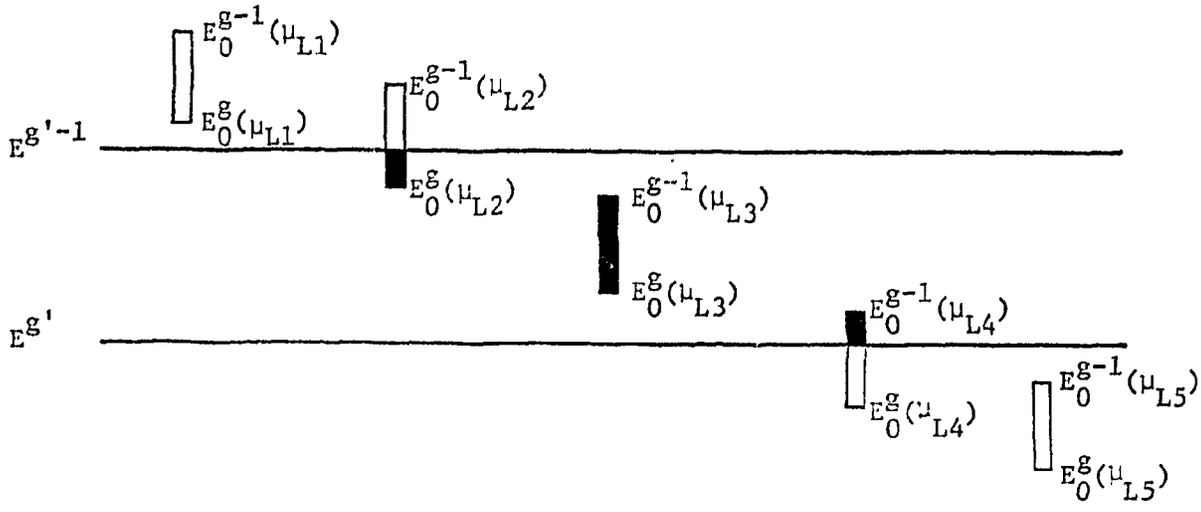

$E_{high}=0$	$E_{high}=E^{g'-1}$	$E_{high}=E_0^{g-1}$	$E_{high}=E_0^{g-1}$	$E_{high}=0$
$E_{low}=0$	$E_{low}=E_0^g$	$E_{low}=E_0^g$	$E_{low}=E^{g'}$	$E_{low}=0$

Fig. 1. Possible Location of an Arbitrary Secondary Energy Group Relative to the Range of Possible Secondary Energies $E' \rightarrow \alpha E'$ and the Limits of Integration that Should be Used in Each Case.

$$\mu_c = \left(\frac{1}{A}\right)\left[\mu_L^2 - 1 + \mu_L\sqrt{a^2 + \mu_L^2}\right], \qquad a^2 = A^2 - 1 \tag{8}$$

Since $P_\ell(\mu_L)$ is simply a polynomial in μ_L, it is necessary only to evaluate integrals of the form:

$$f_n(x) = \int x^n\, dx \qquad n=1,2,3,4,5, \ldots, (\ell+1) \tag{9}$$

$$g_n(x) = \int x^n \sqrt{a^2+x^2}\, dx \qquad n=0,1,2,3,4, \ldots, \ell \tag{10}$$

$$h_n(x) = \int \frac{x^n}{\sqrt{a^2+x^2}}\, dx \qquad n=2,4,5,6,7, \ldots, (\ell+2) \tag{11}$$

The integrals represented by $g_n(x)$ and $h_n(x)$ are less obvious than those represented by $f_n(x)$. They can, however, be evaluated analytically by setting $x = a \tan\theta = a\sqrt{\sec^2\theta - 1}$, using the Binomial theorem to expand integer powers of $(\sec^2\theta - 1)$, and applying a standard reduction formula to integrate powers of $(\sec\theta)$. Defining $r = \sqrt{a^2 + x^2}$ and letting $m = n/2$ for n = even and $m = (n-1)/2$ for n = odd, the results may be written as:

$$g_n(x) = a^{n+2}\sum_{i=0}^{m}(-1)^i\binom{m}{i}\rho_{2(m-i)+3}(x) \qquad n=0,2,4, \ldots, \tag{12}$$

$$g_n(x) = a^{n+2}\sum_{i=0}^{m}\left[\frac{(-1)^i}{2(m-i)+3}\right]\binom{m}{i}\left[\frac{r}{a}\right]^{2(m-i)+3} \qquad n=1,3,5, \ldots, \tag{13}$$

$$h_n(x) = a^n \sum_{i=0}^{m} (-1)^i \binom{m}{i} \rho_{2(m-i)+1}(x) \qquad n=2,4,6, \ldots, \quad (14)$$

$$h_n(x) = a^n \sum_{i=0}^{m} \left[\frac{(-1)^i}{2(m-i)+1}\right] \binom{m}{i} \left[\frac{r}{a}\right]^{2(m-i)+1} \qquad n=3,5,7, \ldots, \quad (15)$$

where

$$\rho_j(x) = \left(\frac{1}{j-1}\right)\left(\frac{r}{a}\right)^{j-2}\left(\frac{x}{a}\right) + \left(\frac{j-2}{j-1}\right)\rho_{j-2}(x) \qquad (16)$$

$$\rho_1(x) = \ell n(x+r), \qquad \text{and} \quad \binom{m}{i} = \frac{m!}{(m-i)!\,i!} \qquad (17a,b)$$

Despite their appearance, these expressions are generally quite simple. For example:

$$\int_{E^g}^{E^{g-1}} P_0(\mu_L)\sigma(E' \to E)\, dE = \frac{\sigma(E')}{2A}\left[x(1+r) + (1-a^2)\ell n(x+r)\right]\Bigg|_{x=\mu_L^L}^{x=\mu_L^U} \qquad (18)$$

$$\int_{E^g}^{E^{g-1}} P_l(\mu_L)\sigma(E'\rightarrow E)\,dE = \frac{\sigma(E')}{2A}\left[\frac{2}{3}(x^3 + r^3) - a^2 r\right]\Bigg|_{x=\mu_L^L}^{x=\mu_L^U} \tag{19}$$

Note that these analytic expressions are in closed form, and do not simply represent the first few terms of an infinite series. It is for this reason that the present method has been incorporated in the ROLAIDS cross section processing code.[1]

For anisotropic scattering in the C-system, the angular distribution function $f(E',\mu_c)$ would look like:

$$f(E',\mu_c) = \sum_{k=0}^{ISCT(CM)} \frac{2k+1}{4\pi} f_k(E')\ P_k(\mu_c) \tag{20}$$

and $P_\ell(\mu_L)$ in Eq. (7c) would be replaced by the product $P_k(\mu_c)P_\ell(\mu_L)$. Using Eq. (8) to represent each power of μ_c in $P_k(\mu_c)$, Eq. (7c) could still be written in terms of $f_n(x)$, $g_n(x)$ and $h_n(x)$. Thus, the resulting expressions could again be written in closed form with no truncation error.

The present method as described above is to be advocated whenever the angular scattering function is known in the C-system. If, on the other hand, it is specified as an expansion in the L-system such that

$$\tilde{f}(E',\mu_L) = \sum_{k=0}^{ISCT(LAB)} \frac{2k+1}{4\pi} \tilde{f}_k(E')\ P_k(\mu_L) \tag{21}$$

it would be more expedient to write the scattering function as

$$\sigma(E'\rightarrow E)\,dE = \sigma(E')\ \tilde{f}(E',\mu_L)\ 2\pi d\mu_L \tag{22}$$

and substitute Eqs. (21) and (22) directly into Eq. (5) where the integration in the L-system would involve only the product $P_k(\mu_L)P_\ell(\mu_L)$. Such terms represent simple polynominals in μ_L and are easily integrated.[4] To take advantage of this simplicity, the MINX code[5] uses Amster's transformation[6] to convert C-system expansions to L-system expansions prior to performing the integration. Note, however, that even the simplist function in the C-system [$f(E',\mu_C) = 1/4\pi$] requires an infinite number of Legendre terms in the L-system. In practice, the L-system expansion must be truncated, leaving some residual error not found in the present method.

For comparison purposes, it should be noted that NEWXLACS[7] uses a numerical quadrature to perform the angular integration in the evaluation of $\sigma_\ell(g'\to g)$.[8,9,10] To be more precise, it calculates $\sigma_\ell(g'\to g)$ as

$$\sigma_\ell(g'\to g) \doteq (2\pi/\phi^{g'}) \sum_{n=1}^{N} w_n P_\ell(\mu_{Ln}) \int_{E^{g'}}^{E^{g'-1}} \phi(E')\,\sigma(E')\,\tilde{f}(E',\mu_{Ln})\,\varepsilon(\mu_{Ln})\,dE' \qquad (23)$$

where $\varepsilon(\mu_{Ln}) = 1$ if $\mu_L(E',E_L,Q,A) \le \mu_{Ln} \le \mu_L(E',E_U,Q,A)$ for $E^{g'} \le E' \le E^{g'-1}$, and $\varepsilon(\mu_{Ln}) = 0$ otherwise. The integration over E' is then done semi-analytically. The power of the method is that it is extremely fast and reasonably accurate in most cases. It is, however, an approximate method. Its chief weakness is that one must use higher order quadratures to obtain fairly accurate results as the group structure becomes finer. For light nuclides this method may also leave holes in the multigroup transfer matrices which should physically not be present. Numerical experiments do, however, indicate the approximation to be quite good for heavy nuclides, and adequate for all nuclides but hydrogen. In all cases, the accuracy of the approximation may be increased by increasing N.

To be perfectly rigorous in the case of hydrogen, one should account for the fact that the atomic mass ratio (A) is less than unity. The radicals in Eq. (7c) would then become $\sqrt{\mu_L^2 - b^2}$ where $b^2 = 1 - A^2$. A substitution of the form $\mu_L = b \sec\theta$ would then allow Eq. (7c) to be written in terms of $\rho_j(x)$. This exact treatment, however, would represent an unnecessary degree of accuracy in most cases.

A most interesting and extremely useful simplification of Eq. (7c) results in the case of hydrogen where one is willing to make the A = 1 approximation. In that case, the bracketted quantity in Eq. (7c) simplifies to $4\mu_L$, Eq. (3) simplifies to $\mu_L = \sqrt{E/E'}$, and Eq. (5) becomes

$$\sigma_\ell(g'\to g) = \left(\frac{2}{\phi^{g'}}\right) \int_{E^{g'}}^{E^{g'-1}} \phi(E')\sigma(E') \left[\int_{\mu_L=\sqrt{E_L/E'}}^{\mu_L=\sqrt{E_U/E'}} \mu_L\, P_\ell(\mu_L)\, d\mu_L \right] dE' \qquad (24)$$

Defining $a_{\ell,n}$ as the coefficients of μ_L^n in $P_\ell(\mu_L)$, it becomes convenient to describe $\sigma_\ell(g' \to g)$ as

$$\sigma_\ell(g' \to g) = \sum_{n=0}^{\ell} a_{\ell,n}\, \sigma_{\ell,n}\,(g' \to g) \tag{25}$$

The terms $\sigma_{\ell,n}(g' \to g)$ can then be written as

$$\sigma_{\ell,n}\,(g' \to g) = \left(\frac{1}{p\phi^{g'}}\right)\left[\left(E^{g-1}\right)^p - \left(E^g\right)^p\right]\beta_p^{g'} \qquad \text{for } g' < g \tag{26}$$

$$\sigma_{\ell,n}(g' \to g) = \left(\frac{1}{p\phi^{g'}}\right)\left[\beta_0^{g'} - \left(E^g\right)^p\,\beta_p^{g'}\right] \qquad \text{for } g' = g \tag{27}$$

where $p = (n+2)/2$ and

$$\beta_p^{g'} = \int_{E^{g'}}^{E^{g'-1}} \phi(E')\sigma(E')[E']^{-p}\,dE' \tag{28}$$

In the case of hydrogen, the piecewise continuous ENDF specification for $\sigma(E')$ is always of the form

$$\sigma(E') = a\,[E']^b \tag{29}$$

for 10^{-5} ev $\leq E' \leq$ 20 Mev. As long as $\phi(E')$ is represented in a piecewise continuous fashion by one of the five ENDF interpolation formulas, the integral in Eq. (28) may be evaluated analytically. Assuming, for example, that the weight function is $1/E'$, Eq. (28) yields

$$\beta_p^{g'} = \int_{E^{g'}}^{E^{g'-1}} a[E']^{b-p-1}\,dE' = \left(\frac{a}{b-p}\right)[E']^{b-p}\,\Bigg|_{E^{g'}}^{E^{g'-1}} \tag{30}$$

This completely analytic treatment for hydrogen has recently been implemented in NEWXLACS.[11] Because of the analytic treatment and the A = 1 approximation, a full down-scattering matrix is generated with no holes.

REFERENCES

1. R. M. Westfall, "Theory and Validation of ROLAIDS: AMPX Module for Treating Resonance Shielding in Multiregion Geometries," UCCND/CSD/INF-65 (to be published).

2. N. M. Greene et. al., "XLACS: A Program to Produce Weighted Multigroup Cross Sections from ENDF/B Data," ORNL/TM-3646 (1972).

3. N. M. Greene et. al., "AMPX: A Modular Code System for Generating Coupled Multigroup Neutron-Gamma Libraries from ENDF/B," ORNL/TM-3706 (1976).

4. C. R. Weisbin et. al., "A New Procedure for the Determination of Neutron Multigroup Transfer Matrices," Nucl. Sci. & Eng. 45, pp. 329 (1974).

5. D. R. Harris et. al., "MINX, A Modular Code System for Processing Multigroup Cross Sections from Nuclear Data in ENDF/B Format," LA-UR-1766 (1973).

6. H. J. Amster, "Slowing Down in a Uniform Medium," Naval Research Physics Handbook, Vol I (1964).

7. W. E. Ford, III and B. R. Diggs, "AMPX Newsletter - No. 2," UCC-ND Internal Correspondence, December 16, 1977.

8. N. M. Greene, "Anisotropic Inelastic Scattering Matrices from ENDF Data," Trans. Am. Nucl. Soc., 17 (2), 549 (1973).

9. N. M. Greene and J. L. Lucius, "Simple and Efficient Schemes for Processing ENDF/B Scattering Data," Trans. Am. Nucl. Soc., 27, (2), 395 (1977).

10. J. A. Bucholz, "A Method of Generating Multigroup Transfer Matricies Using an Analytic Angular Integration Free of Truncation Error," ORNL/NUREG/CSD-8 (1978).

11. J. A. Bucholz, "A Completely Analytic Scattering Treatment for Hydrogen Presently Available in NEWXLACS," UCC-ND Internal Correspondence, February 28, 1978.

CODE IMPLEMENTATION OF PARTIAL-RANGE ANGULAR SCATTERING CROSS SECTIONS: GAMMER AND MORSE

J. T. Ward, Jr.
University of Virginia
Charlottesville, Virginia, USA

ABSTRACT

A partial-range (finite element) method has been previously developed for representing multigroup angular scattering in Monte Carlo photon transport. Here we discuss computer application of the method, with preliminary quantitative results. A multigroup photon cross section processing code, GAMMER, has been written, which utilizes ENDF File 23 point data and the Klein-Nishina formula for Compton scattering. The cross section module of MORSE, along with several execution routines, were rewritten to permit use of the method with photon transport. Both conventional and partial-range techniques were applied for comparison to calculating angular and spectral penetration of 6 MeV photons through a six-inch iron slab. GAMMER was found to run 90% faster than SMUG, with further improvement evident for multiple-media situations; MORSE cross section storage was reduced by one-third, cross section processing greatly simplified, and execution time reduced by 15%. Particle penetration was clearly more forward peaked, as moment accuracy is retained to extremely high order. This method of cross section treatment offers potential savings in both storage and handling, as well as improving accuracy and running time in the actual execution phase.

INTRODUCTION

Truncated Legendre polynomial expansions are commonly used to approximate angular scattering distributions in multigroup Monte Carlo transport codes. Although adapted from discrete ordinates usage as a matter of convenience and familiarity, these representations have long been known to produce at times negative and oscillatory amplitudes[1,2] (Figure 1). Several investigators have recently proposed theoretical models for improved representations by means of finite element, or "partial-range" methods. Suggested as a potential remedy for both neutron elastic scatter[3,4] and photon Compton scatter[5,6], the approach has met with some degree of skepticism, the feeling being that no palatable alternative to conventional techniques exists. Be that as it may, we discuss implementation of the method, from formulation for encoding to comparative numerical testing. The following aspects are considered:

1. GAMMER--a multigroup photon cross-section generating code, which produces data for input to modified versions of MORSE;
2. Modification of the MORSE cross-section module to accept GAMMER-formatted input;
3. Modification of those MORSE execution routines using angular scattering cross sections;
4. Comparison of numerical MORSE results between conventional and partial-range cross sections.

CROSS SECTION GENERATION: SMUG AND GAMMER

Angle-dependent group-to-group scattering cross sections are typically generated and transferred to transport codes as full-range Legendre coefficients $f_\ell^{g\to g'}$, from which polar angular scattering densities are reconstructed in the form of truncated L'th order series:

$$f^{g\to g'}(\mu) \sim f_L^{g\to g'}(\mu) = \sum_{\ell=0}^{L} \left(\frac{2\ell+1}{2}\right) f_\ell^{g\to g'} P_\ell(\mu) \quad , \tag{1}$$

where $P_\ell(\mu)$ is the ℓ'th order Legendre polynomial in μ, the polar scatter cosine. Here g and g' denote, respectively, incident and outscatter group indices for a given transfer mode. The SMUG[7] code employs a flux-weighted double integral relation to compute the coefficients:

$$f_\ell^{g\to g'} = \int_{E_{g+1}}^{E_g} \Phi(E) \int_{E_{g'+1}}^{E_{g'}} \sigma_s(E\to E',\mu)\, P_\ell(\mu)\, dE'\, dE \,/\, \int_{E_{g+1}}^{E_g} \Phi(E)\, dE \ . \tag{2}$$

For Compton scattering, as given by the Klein-Nishina formula,

$$\sigma_s(E\to E',\mu) = \frac{d\sigma}{dE'd\Omega} = \frac{r^2mc^2}{2E^2}\left(\frac{E}{E'} + \frac{E'}{E} + \mu^2 - 1\right)\delta\left(1 - \mu + \frac{mc^2}{E} - \frac{mc^2}{E'}\right) \tag{3}$$

with r being the classical electron radius and mc^2 the electron rest energy, assuming azimuthal symmetry, i.e., $d\Omega = 2\pi\, d\mu$. Here the Dirac delta function embodies the governing relation (scattering law) among E, E', and μ, by considering conservation of energy and momentum. SMUG treats pair production by adding appropriate magnitudes to zero'th order coefficients for corresponding transfers on an element-dependent basis. Then, specifying a fixed maximum number of downscatters for all incident energy groups, the user receives ANISN-formatted data for each atomic element desired.

One obvious characteristic of the partial-range technique is that cross sections cannot be generated and transferred in a conventionally formatted structure, which necessitates the development of a new one. Given a particular choice of energy group boundaries, GAMMER first

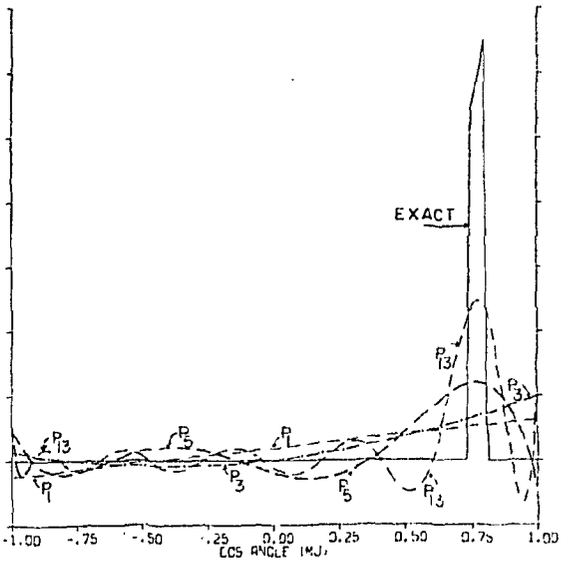

Fig. 1. Exact Compton scattering amplitude for (10-8 → 2-1.6 MeV) transfer with several truncated full-range representations.

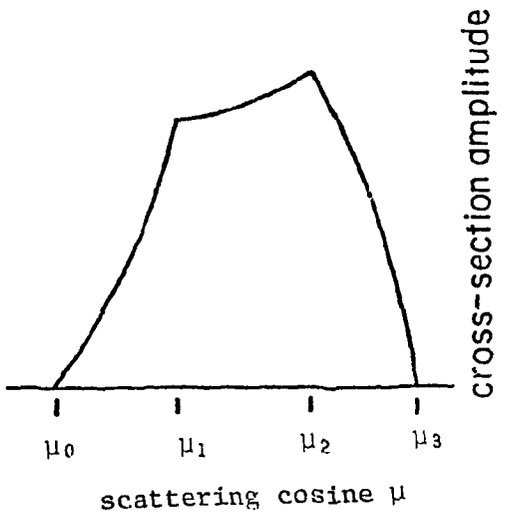

Fig. 2. A typical three-segment multigroup angular scattering amplitude $f^{g\to g'}(\mu)$.

determines the number of physically permissible scattering modes for each incident group by examining values of the nodal or "break" points (Figure 2):

$$\begin{aligned}
\mu_0 &= 1 + mc^2(1/E_g - 1/E_{g'+1}) \\
\mu_1 &= 1 + mc^2(1/E_{g+1} - 1/E_{g'+1}) \\
\mu_2 &= 1 + mc^2(1/E_g - 1/E_{g'}) \\
\mu_3 &= 1 + mc^2(1/E_{g+1} - 1/E_{g'}) \ .
\end{aligned} \tag{4}$$

Since upscatter is precluded, the test for admissibility of a possible mode ($g \to g'$) is that $\mu_3 > -1$. In this manner computation is performed and storage allocated only for non-vacuous scattering modes. Within a particular mode the μ-range is redefined for each segment:

$$\mu_n^* = \frac{2\mu - (\mu_n + \mu_{n-1})}{\mu_n - \mu_{n-1}} \quad , \quad -1 \le \mu_n^* \le +1 \quad , \tag{5}$$

where μ_n and μ_{n-1} ($\mu_n > \mu_{n-1}$) are the nodes or end points of that segment. If, from Eq. 4, $\mu_1 > \mu_2$, GAMMER reorders the values to preserve positive segment lengths. All $|\mu_n| > 1$ are translated to the appropriate boundary, ±1 . Then, partial-range coefficients are constructed by taking

$$f_{n,\ell}^{g\to g'} = \int_{\mu_{n-1}}^{\mu_n} f^{g\to g'}(\mu)\, P_\ell(\mu_n^*)\, d\mu \quad . \tag{6}$$

As many as three distinct series - one for each smooth positive segment $f_n^{g\to g'}(\mu)$ - are required to represent fully a single transfer mode. The flux-weighted angular transfer density is usually defined as

$$f^{g\to g'}(\mu) = \int_{E_{g'+1}}^{E_{g'}} dE' \int_{E_{g+1}}^{E_g} dE\, \sigma_s(E\to E',\mu)\, \Phi(E) \;/\; \int_{E_{g+1}}^{E_g} dE\, \Phi(E) \quad . \tag{7}$$

Integration over outscattered energy E' yields

$$f^{g\to g'}(\mu) = \int_{E_{low}(\mu)}^{E_{high}(\mu)} dE\, \frac{d\sigma}{d\mu}(E,\mu)\, \Phi(E) \;/\; \int_{E_{g+1}}^{E_g} dE\, \Phi(E) \quad , \tag{8}$$

where E_{high} is the maximum energy in group g from which a photon can be scattered through the polar cosine μ into group g'; similarly, E_{low} is the minimum incident energy in g permitting μ and g'. This integral can be expressed <u>analytically</u> for two frequently-used spectral weighting functions $\Phi(E)$.

Letting $\beta(E) = 1 + (1 - \mu)\, E/mc^2$, we have:

(a). Flat flux: $$f^{g\to g'}(\mu) = \frac{\pi\, r^2 mc^2}{(1-\mu)(E_g - E_{g+1})}\left[\ln\beta + \frac{1-\mu^2-1/2\beta}{\beta}\right]_{\beta(E_{low})}^{\beta(E_{high})} \tag{9}$$

(b). 1/E flux: $$f^{g\to g'}(\mu) = \frac{\pi\, r^2}{\ln(E_g/E_{g+1})}\left[(1+\mu^2)\ln\frac{\beta-1}{\beta} + \frac{\mu^2}{\beta} + 1/2\beta^2\right]_{\beta(E_{low})}^{\beta(E_{high})} \tag{10}$$

Now, μ_n and μ_{n-1} are known explicitly, as is $f^{g\to g'}(\mu)$, which is smooth over $\mu_{n-1} \le \mu \le \mu_n$; therefore, the $f_{n,\ell}^{g\to g'}$ can be obtained directly from integration of Eq. 6 by Gaussian quadrature, eliminating the double integral of Eq. 7 . Further, by representing Eq. 6 as

$$\overline{f_n^{g\to g'}} = \int_{\mu_{n-1}}^{\mu_n} f^{g\to g'}(\mu)\, \bar{P}(\mu_n^*)\, d\mu \quad , \tag{11}$$

$$\text{with} \quad \overline{f^{g\to g'}} = \begin{pmatrix} f^{g\to g'}_{n,0} \\ \vdots \\ f^{g\to g'}_{n,L} \end{pmatrix} \quad \text{and} \quad \overline{P}(\mu_n^*) = \begin{pmatrix} P_0(\mu_n^*) \\ \vdots \\ P_L(\mu_n^*) \end{pmatrix} , \tag{12}$$

computation for all values of ℓ, $0 < \ell < L$, within an individual segment is greatly compacted and simplified. Next, downscatter probabilities $P(g\to g')$ are determined and normalized so that

$$P(g\to g') = \int_{-1}^{+1} f^{g\to g'}(\mu)\, d\mu \;/\; \sum_{g'} \int_{-1}^{+1} f^{g\to g'}(\mu)\, d\mu \; . \tag{13}$$

Hence, $\sum_{g'} P(g\to g') = 1$. This in turn permits normalization of the angular density shape functions:

$$\int_{-1}^{+1} f^{g\to g'}(\mu)\, d\mu = 1 \; . \tag{14}$$

Scattering magnitudes have now been externalized to the downscatter probability table and, ultimately, to the atomic number densities in mixed material media. In short, we have posited spatial separability as a characteristic of the collision kernel. With Klein-Nishina (free electron) scattering, possible material-dependent corrections due to coherent-incoherent (bound electron) effects are ignored[8]; the electron density $N_e(\underline{r})$ rests as the sole measure or index of spatial (viz. "material") dependence, thus rendering the collision kernel spatially separable. Note that the scattering tableau - that is, the nodal points, downscatter probabilities, and coefficients, which determine angular density shapes - becomes independent of element or isotope ; as such, calculation and storage need be performed only once, regardless of the total number of materials and mixtures present.

GAMMER then computes values of the microscopic Compton, photoelectric, and pair production cross sections in each energy group for each element specified, the latter two quantities being group-averaged from ENDF File 23 point data. Thus for N elements and G groups, this entails evaluation of 3*N*G entries in addition to the basic Compton tableau. Typically, low-order P_1 or P_2 partial-range expansions yield excellent agreement with exact amplitudes (Figure 3). A summary of SMUG and GAMMER punched output formats appears in Table 1.

Parallel runs were made on the University of Virginia CDC CYBER 172 with GAMMER and SMUG to generate 16-group (Table 2) photon cross sections for a single element. Surprisingly, GAMMER required only 9 CPU seconds for this task, as compared to 91 seconds for SMUG; for three elements, GAMMER ran in 21 seconds, since the Compton tableau did not have to be repeated, while SMUG tripled in time. Apparently then, for this group structure, GAMMER computes the Compton tableau in about three seconds, while 6 seconds are needed for the tape reads and computation associated

with each additional atomic element.

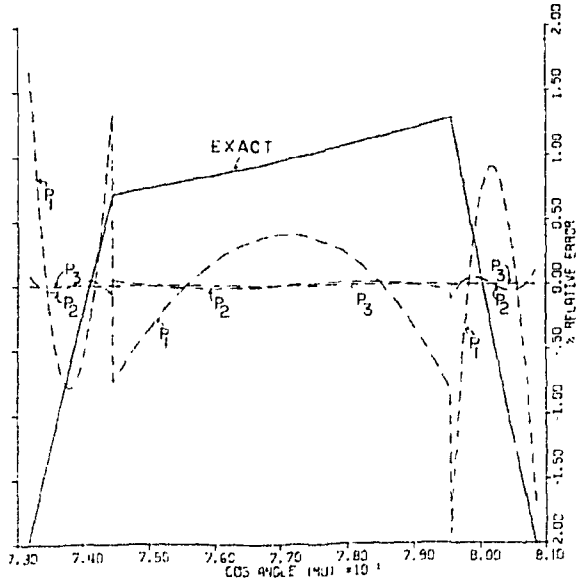

Fig. 3. Exact Compton scattering amplitude for (10-8 → 2-1.6 MeV) transfer with percent relative error of several low-order partial range expansions. These are given since the expansions themselves would not differ visibly from the exact shape.

THE MORSE CROSS SECTION MODULE

The familiar "Coveyou technique"[9], first applied to O5R[10], was subsequently adapted for selecting outscatter or post-collisional angles in MORSE[11]. A clever method using Gaussian quadrature is employed to establish a set of discrete angles and weights [probabilities] amenable to rapid Monte Carlo selection. In addition, D. C. Irving, et.al.[12] introduced a method to detect "bad" or "impossible" coefficients in generated sets - "bad" in the sense that they cannot represent any physically meaningful angular distribution $f(\mu) \geq 0$, $-1 \geq \mu \geq +1$. Rejection tests are applied to eliminate these anomalies; but when coefficients are thrown out, truncations of order less than the desired level are produced. This scheme was also incorporated into the MORSE cross-section module. Thus, after reading ANISN or DTF-IV formatted data and setting up storage location parameters, MORSE performs the above two processes. Original input coefficients are themselves saved ane re-stored only if the user requests point detectors to register next-flight flux or dose rate estimates.

This entire module was rewritten to accommodate GAMMER-type input and, in the process, greatly simplified and shortened. Data is read and stored directly. Macroscopic cross sections are then constructed via the usual mixing table, but manipulation is limited to element-dependent entries - the entire Compton tableau remains intact - and preparation is complete; i.e., no further handling is necessary.

Table 1. Output Array for SMUG and GAMMER

SMUG: Standard ANISN format: σ_t, $\nu\sigma_f$, σ_a, $\sigma_{g,g}$, $\sigma_{g-1,g}$, etc. for each group, first element.

Repeat for each element, P_0 through P_L.

GAMMER:

1. Cumulative number of downscatters for each incident group:

   g'th entry = $\sum_{i=1}^{g}$[NDS(i)] ; G entries.

2. Four nodal values (μ_n's) for each mode ($g \rightarrow g'$); 4*NGN entries, where NGN = total number of modes--NGN = last entry in (1) above.

3. Downscatter probabilities $P(g \rightarrow g')$; NGN entries.

4. Normalized $f_0^{g \rightarrow g'}$'s; 3 values per mode, 3* NGN entries.

5. Normalized $f_1^{g \rightarrow g'}$'s; 3*NGN entries.

6. Repeat until desired f_L's; usually L = 1,2.

7. Microscopic σ_c, σ_{pe}, σ_{pp} for each group; first element, 3*G entries.

8. Repeat (7) for each successive element.

MORSE PHOTON TRANSPORT-THE SCATTERING KERNEL AND EXECUTION ROUTINES

In the execution phase, as particle histories are generated and results scored, the kernels are utilized in two complementary ways:

1. To pick μ at random from a particular distribution $f^{g \rightarrow g}(\mu)$, once the mode ($g \rightarrow g'$) has been selected; and
2. To compute the proper value of $f^{g \rightarrow g}(\mu)$, given a fixed scattering cosine μ.

One disadvantage of the conventional method of selecting outscattered angles is that, aside from computing and storing discrete angles and weights, the continuous range of scattering angles is discretized, causing angular distortion through ray effects during the first few collisions of a particle's history.[1]

Table 2. The 16 group energy structure

g	E_g(MeV)
1	6.05
2	5.95
3	5.
4	4.
5	3.
6	2.
7	1.
8	.8
9	.65
10	.52
11	.5
12	.4
13	.3
14	.21
15	.12
16	.07
	.01

By contrast, an ad hoc Monte Carlo rejection technique of reasonably high efficiency[13] has been incorporated into the partial-range modifications (subroutine ANGLER) to choose polar scattering cosines directly from the appropriate partial range expansion, thereby eliminating ray effects.

Several additional routines involved with angular scattering mechanics, among them being COLISN, PTHETA, NSIGTA, RELCOL, and SGAM, were modified. Otherwise, particle transport remains unaffected in all other respects.

MORSE PHOTON TRANSPORT-COMPARATIVE CALCULATIONS

Parallel multigroup Monte Carlo photon transport computations were performed with MORSE, alternately using conventional and partial-range cross sections, to compare the two methods in regard to computational accuracy and efficiency. In each case a monodirectional 5.95-6.05 MeV photon beam was directed perpendicularly onto a flat six-inch thick iron slab surrounded by vacuum. Thirteen point detectors were positioned at various angles from the incident beam direction to measure angular transmission characteristics of the slab; all were located at a ten-foot distance from the point of intersection of the beam and slab. Weight-adjusted photons were allowed to scatter until either escaping the slab or reaching an 0.07 MeV energy cutoff. Insofar as transport is concerned, the two runs differed solely in the handling of group-to-group angular scattering probabilities, as treated by the two methods: a conventional full-range P_{11} expansion was employed on the one hand and a P_2 partial-range expansion on the other. A comment in this regard may be appropriate: although expansions to P_{11} were requested in the conventional run, unavoidable cross-sectional roundoff to five-digit accuracy resulted in numerous "bad moments" being generated and rejected, particularly for transfers originating in high-energy groups whose exact scattering amplitudes exhibit limited angular support; hence the calculation of discrete angles and probabilities for certain transfer modes employed less than the full complement of twelve coefficients, as shown in Table 3.

Table 3. Number of moments accepted for each mode (g→g') in the sixteen-group energy structure

Outscatter Group g'	Inscatter Group g															
	1	2	3	4	5	6	7	8	9	10	11	12	13	14	15	16
1	1															
2	1	3														
3	3	2	2													
4	2	2	3	3												
5	3	6	3	3	2				X = full complement							
6	4	6	6	3	10	X										
7	X	5	X	10	9	4	3									
8	3	3	3	10	10	4	3	6								
9	3	8	4	7	5	5	4	3	8							
10	X	X	X	X	X	X	3	3	7	2						
11	X	X	5	X	X	5	5	6	X	3	6					
12	5	5	X	X	5	10	7	5	X	5	5	X				
13	X	4	7	X	X	5	X	7	8	7	X	X	7			
14						4	3	3	X	X	X	9	X	X		
15													3	X	X	
16															X	X

A comparison of detector flux estimates and corresponding statistical variances is presented in Table 4 for runs of 1000 particles by each method. Several observations can be made on the basis of these sample runs:

Partial-range fluxes are clearly more forward-peaked than counterpart conventional fluxes, scoring consistently 15-20 percent higher for narrow angle directions, but uniformly lower at angles above 30^0. This effect distinguishes the ability of the partial-range method to retain full-range moment accuracy to extremely high order[6] as compared with the dispersive nature of full-range expansions. Variances are tighter at smaller angles of interest with the new method; some conventional variances, particularly those at large-angle detectors, may actually be greater than the values indicated, since conventional ray effects would tend to be at least self-consistent to an unwarranted extent.

Although nearly equal numbers of particles escaped the slab before reaching the energy cutoff in the two cases (213 versus 210), there were fewer total scatters with the new method (8930 vs. 9174). While photon transmission may be affected to some small extent, judgment on this matter would be premature due to the sample size.

In terms of computing efficiency, cost savings were effected both in execution time and field length requirements. First, the calculation of discrete angles and probabilities was bypassed by the new method, saving a net 38 CPU seconds for one material medium. Moreover, the actual particle transport phase ran about 15 percent more quickly with the new method: 517 versus 605 CPU seconds on the University of Virginia CDC CYBER 172.

Table 4. A comparison of point flux estimates in photons/cm^2-sec per source photon/sec for conventional and partial-range calculations

Angle From Incident Beam (Degrees)	Conventional		Partial-Range	
	Flux	Variance	Flux	Variance
0	1.1022E-06	0.05145	1.3343E-06	0.03133
1/4	1.1773E-06	0.05154	1.3339E-06	0.03162
1/2	1.1613E-06	0.04722	1.3349E-06	0.03152
1	1.1723E-06	0.05874	1.3272E-06	0.03200
2	1.1616E-06	0.05846	1.3036E-06	0.03258
4	1.0792E-06	0.05152	1.2361E-06	0.03418
8	9.1795E-07	0.05280	1.0741E-06	0.03811
15	6.0761E-07	0.06168	6.9759E-07	0.05203
30	2.3519E-07	0.09105	2.3658E-07	0.08571
45	1.1594E-07	0.10315	8.8021E-08	0.12285
60	5.5098E-08	0.15362	3.8232E-08	0.18556
75	1.9377E-08	0.25782	1.1686E-08	0.35038
85	1.1792E-09	0.41122	8.9881E-10	0.67529

The partial-range method permits storage of Legendre coefficients directly into blank common; they are not required to first compute and store moments, then to be themselves re-stored in new locations when point detectors are used, as in the conventional procedure. For these runs, in which only one material medium appears, a blank common allocation of 5300 in the conventional treatment was reduced to 3400 for the partial-range application. When multiple media appear, only electron densities need be added. By contrast, MORSE conventionally stores a complete downscatter (cross section) set for each separate material. The storage advantage then becomes even greater for multi-media computations.

RESULTS AND CONCLUSIONS

In summary, the partial-range angular scattering technique has been incorporated into the MORSE framework for photon transport, in effect replacing or modifying all subroutines dealing with cross sections. A multigroup photon cross section generating code, GAMMER, has been written to supply convenient input to the transport code. The method is computationally accurate, to the extent that can be shown by these brief runs, and it is computationally more efficient than the conventional MORSE. Further investigation of resulting angular distributions is warranted, however, particularly in deep-penetration situations with sharply anisotropic scattering and complicated geometry, where retention of extremely high-order moments may be desired.

REFERENCES

1. L. L. Carter and C. A. Forest,"Transfer Matrix Treatments for Multigroup Monte Carlo Calculations--The Elimination of Ray Effects," Nucl. Sci. Eng. 59, 27 (1976).

2. L. L. Carter and E. D. Cashwell, Particle Transport Simulation With The Monte Carlo Method, TID-26607, U. S. Energy Research and Development Administration (1975).

3. E. A. Attia and A. A. Harms,"A New Expansion for Highly Anisotropic Neutron-Nucleus Scattering," Nucl. Sci. Eng. 59, 319 (1976).

4. W. J. Mikols and J. K. Shultis,"A Low-Order Approximation for Highly Anisotropic Multigroup Transport Cross Sections," Nucl. Sci. Eng. 62, 738 (1977).

5. J. T. Ward, Jr.,"An Improved Multigroup Representation of Differential Compton Scattering Cross Sections," Trans. Am. Nuc. Soc. 21, 529 (1975).

6. J. T. Ward, Jr. and M. B. Scudiere,"A Partial-Range Expansion For Multigroup Monte Carlo Photon Transport," CONF-770401, Fifth International Conference on Reactor Shielding, Knoxville, Tennessee, April 1977.

7. J. L. Lucius and W. E. Ford, III, SMUG-Multigroup Photon Cross Section Generator, PSR-51, Oak Ridge National Laboratory (1973).

8. W. A. Woolson, W. H. Scott, Jr., and N. E. Banks,"Resolution of the Importance of Coherent-Incoherent Scattering in Photon Transport in Air," Trans. Am. Nuc. Soc. 18, 374 (1974).

9. R. R. Coveyou,"A Monte Carlo Technique for Selecting Neutron Scattering Angles from Anisotropic Distributions," Nucl. Sci. Eng. 21, 260 (1965).

10. D. C. Irving, R. M. Freestone, and F. B. K. Kam, O5R, A General-Purpose Monte Carlo Neutron Transport Code, ORNL-3622, Oak Ridge National Laboratory (1965).

11. M. B. Emmett, The MORSE Monte Carlo Radiation Transport Code System, ORNL-4972 (1972).

12. D. C. Irving, R. R. Coveyou, and R. D. MacPherson,"Impossible Legendre Coefficients," CONF-660303 (1966).

13. J. T. Ward, Jr.,"A Rejection Technique for Selecting Photon Scattering Angles in MORSE," Trans. Am. Nuc. Soc. 26, 497 (1977).

BLANK PAGE

ANALYTICAL INEQUALITIES SATISFIED BY THE CROSS-SECTION SELF-SHIELDING FACTORS

Dan G. Cacuci
Engineering Physics Division
Oak Ridge National Laboratory

and

M. A. Bjerke
Computer Science Division
Union Carbide Corporation, Nuclear Division

ABSTRACT

Recently, questions have arisen concerning the limits of the range of values within which a cross-section self-shielding factor (f-factor) is restricted. In this study, best upper and lower bounds for the range of values of an arbitrary f-factor have been derived analytically starting from the definitions which form the basis for the computer codes currently employing the self-shielding method. A fundamental assumption used in the present derivation is that the fluxes and cross-sections be elements of a Hilbert Space. The strict upper and lower bounds for the f-factors have been obtained by applying well-known inequalities from the theory of functions. In particular, it is shown that total and partial reaction f-factors can exceed unity. The conditions leading to such a situation are discussed from both a mathematical and a physical point of view.

Due to its ease of application, it is planned to implement the results of this study in a routine checking procedure in codes employing the self-shielding method.

I. INTRODUCTION

One of the most important methods for calculating effective multigroup cross-sections is the shielding factor method. In this method, the group cross-sections are obtained form the precalculated self-shielding factors as a function of the temperature T and the "total cross-section per atom" σ_0.

Questions have arisen concerning the limits of the range of values within which a cross-section self-shielding factor (f-factor) is restricted, and, in particular, whether values of f exceeding unity are physically meaningful.

Clearly, the computed values of the f-factors depend rather acutely on the computational models used to reconstruct the cross-sections from the ENDF/B tapes, on the assumed behavior of the neutron flux and on the boundaries of the chosen energy groups. Thus, in principle, one can readily construct situations where, indeed, some self-shielding factors can greatly exceed unity (e.g., by choosing a group boundary that "cuts through" a resonance, or one that is located in the wing of a resonance, etc.).

It was therefore the purpose of this study to investigate analytically the possible ranges of values of an arbitrary self-shielding factor. Best upper and lower bounds for these ranges have been derived, starting from the definitions which form the basis for the computer codes currently employing the self-shielding method. These strict upper and lower bounds have been obtained by applying well-known inequalities from the theory of functions. These bounds will depend, as could be expected, on the upper and/or lower bounds of the fluxes and cross-sections considered within that group. Our derivations, however, are independent of the computational model employed in reconstructing the pointwise cross sections.

The material presented in this study is structured as follows: in the next chapter, we shall analyze the "current-weighted" "total" self-shielding factor, for both the resolved and unresolved energy regions. This will then be followed by an analysis of the partial reaction self-shielding factors. Some numerical results will be presented next as illustrations of the practical consequences of our investigation. Finally, some conclusions that may be drawn from this work will be offered in the last chapter.

II. BEST BOUNDS FOR THE TOTAL SELF-SHIELDING FACTOR $f_t(\sigma_0,T)$

We recall the customary definition[1-3] of the total self-shielding factor $f_t(\sigma_0,T)$, for one isotope, for energy group g, at temperature T, in a mixture of dilution σ_0:

$$f_t(\sigma_0,T) \equiv \frac{\langle \sigma_t^g(\sigma_0,T)\rangle_1}{\langle \sigma_t^g(\infty,0)\rangle_1} \tag{1}$$

Here, $\langle \sigma_t^g(\sigma_0,T)\rangle_1$ represents a special "total" group-averaged cross-section which is related to the "transport" cross-section employed in diffusion-theory type calculations. Moreover, as will be seen shortly, the form of $\langle \sigma_t^g(\sigma_0,T)\rangle_1$ employed throughout the resolved energy range differs from that employed in the unresolved energy range. The investigation of the bounds for $f_t(\sigma_0,T)$ will therefore have to be carried out separately, first for the resolved energy region and then for the unresolved energy region.

II.A. Resolved Energy Region

According to the Bondarenko method[1-3], the definition $\langle \sigma_t^g(\sigma_0,T)\rangle_1$ within this energy range is

$$\langle \sigma_t^g(\sigma_0,T)\rangle_1 \equiv \frac{\int_g \frac{\sigma_t(E,T)}{[\sigma_t(E,T)+\sigma_0]^2}\,C(E)dE}{\int_g \frac{1}{[\sigma_t(E,T)+\sigma_0]^2}\,C(E)dE} \tag{2}$$

reflecting the "current weighting" appropriate to its role in the transport equation. All of the quantities in Eq. (2) have their usual meaning,[3] i.e.

$C(E)$: represents the broad energy behavior of the spectrum [e.g., 1/E, fission spectrum, etc.]

$\sigma_t(E,T)$: is the energy-dependent total cross section at temperature T for the isotope of interest

σ_0: is the macroscopic total cross section per atom of the isotope of interest (spatial and lattice effects are subsequently deduced by incorporation of equivalence principles through σ_0 parameters).

The infinitely dilute group cross section $\langle\sigma_t^g(\infty,0)\rangle_1$ is readily seen to be

$$\langle\sigma_t^g(\infty,0)\rangle_1 = \frac{1}{K_g} \int_g \sigma_t(E,0)C(E)dE \tag{3}$$

where the (group-dependent) constant K_g is defined as

$$K_g \equiv \int_g C(E)dE \tag{4}$$

In view of (2) and (3), the expression (1) for $f_t(\sigma_0,T)$ becomes:

$$f_t(\sigma_0,T) = \frac{K_g}{\int_g \sigma_t(E,0)C(E)dE} \cdot \frac{\int_g \frac{\sigma_t(E,T)}{[\sigma_t(E,T)+\sigma_0]^2} C(E)dE}{\int_g \frac{1}{[\sigma_t(E,T)+\sigma_0]^2} C(E)dE} \tag{5}$$

A strict lower bound for $f_t(\sigma_0,T)$ will be derived next. For this purpose, we introduce two auxiliary functions $a_1(E,T)$ and $b_1(E,T)$ defined as:

$$a_1(E,T) \equiv [\sigma_t(E,T)C(E)]^{1/2} \tag{6}$$

and

$$b_1(E,T) \equiv \frac{\sqrt{C(E)}}{\sigma_t(E,T) + \sigma_0} \tag{7}$$

The case of finite dilution (i.e., $\sigma_0 \neq \infty$) will be considered first. We readily observe that, for $E \in g$, functions $a_1(E,T)$ and $b_1(E,T)$ will satisfy the inequalities

$$0 < m_1 \leq a_1(E,T) \leq M_1 < \infty \tag{8}$$

and

$$0 < m_2 \leq b_1(E,T) \leq M_2 < \infty \tag{9}$$

where

$$m_1 = \inf_{E \in g} a_1(E,T) \tag{10}$$

$$M_1 = \sup_{E \in g} a_1(E,T) \tag{11}$$

$$m_2 = \inf_{E \in g} b_1(E,T) \tag{12}$$

$$M_2 = \sup_{E \in g} b_1(E,T) \tag{13}$$

We can therefore apply the Diaz-Goldman-Metcalf Inequality[4] to the pair of functions a_1 and b_1, to obtain:

$$\frac{1}{\int_g \frac{C(E)dE}{[\sigma_t(E,T)+\sigma_0]^2}} \geq \frac{1}{C_1^2} \frac{\int_g \sigma_t(E,T)C(E)dE}{\left[\int_g \frac{\sqrt{\sigma_t(E,T)}}{\sigma_t(E,T)+\sigma_0} C(E)dE\right]^2} \tag{14}$$

where the constant C_1 is

$$C_1 = \frac{1}{2} \left[\left(\frac{M_1 M_2}{m_1 m_2} \right)^{1/2} + \left(\frac{m_1 m_2}{M_1 M_2} \right)^{1/2} \right] \tag{15}$$

Next, defining the quantities

$$\phi_1 \equiv \inf_{E \varepsilon g} \sqrt{C(E)} \tag{16}$$

$$\phi_2 \equiv \sup_{E \varepsilon g} \sqrt{C(E)} \tag{17}$$

$$\sigma_1 \equiv \inf_{E \varepsilon g} \sigma_t(E,T) \tag{18}$$

$$\Sigma_1 \equiv \sup_{E \varepsilon g} \sigma_t(E,T) \tag{19}$$

we can easily show that

$$\left(\frac{M_1 M_2}{m_1 m_2} \right)^{1/2} \leq A \tag{20}$$

where

$$A \equiv \frac{\phi_2}{\phi_1} \left(\frac{\sigma_0 + \Sigma_1}{\sigma_0 + \sigma_1} \right)^{1/2} \left(\frac{\Sigma_1}{\sigma_1} \right)^{1/4} \tag{21}$$

is a constant greater than unity.

It therefore follows that

$$C_1 \leq K_1 \tag{22}$$

where

$$K_1 \equiv \frac{1}{2} \left(A + \frac{1}{A} \right) \tag{23}$$

Thus, in view of (22), the inequality (14) leads to:

$$\frac{1}{\int_g \frac{C(E)dE}{\left[\sigma_t(E,T)+\sigma_0\right]^2}} \geq \frac{1}{K_1^2} \frac{\int_g \sigma_t(E,T)C(E)dE}{\left[\int_g \frac{\sqrt{\sigma_t(E,T)}}{\sigma_t(E,T)+\sigma_0} C(E)dE\right]^2} \tag{24}$$

Using inequality (24) in (5) gives:

$$f_t(\sigma_0,T) \geq \frac{K_g}{K_1^2} \frac{\int_g \sigma_t(E,T)C(E)dE}{\int_g \sigma_t(E,0)C(E)dE} \cdot \frac{\int_g \frac{\sigma_t(E,T)}{\left[\sigma_t(E,T)+\sigma_0\right]^2} C(E)dE}{\left[\int_g \frac{\sqrt{\sigma_t(E,T)}}{\sigma_t(E,T)+\sigma_0} C(E)dE\right]^2} \tag{25}$$

We now consider the pair of functions $a_2(E,T)$ and $b_2(E,T)$, defined as

$$a_2(E,T) \equiv \sqrt{C(E)} \tag{26}$$

$$b_2(E,T) \equiv \frac{\sqrt{\sigma_t(E,T)C(E)}}{\sigma_t(E,T)+\sigma_0} \tag{27}$$

Taking again into consideration that $\sigma_0 \neq \infty$, we can apply Schwartz' Inequality[4] to the pair a_2 and b_2, to obtain

$$\frac{1}{\left[\int_g \frac{\sqrt{\sigma_t(E,T)}}{\sigma_t+\sigma_0} C(E)dE\right]^2} \geq \frac{1}{K_g} \cdot \frac{1}{\int_g \frac{\sigma_t(E,T)}{\left[\sigma_t(E,T)+\sigma_0\right]^2} C(E)dE} \tag{28}$$

Combining the inequalities (25) and (28) yields the following (strict) lower bound for f_t:

$$f_t(\sigma_0,T) \geq \frac{1}{K_1^2} \cdot \frac{\int_g \sigma_t(E,T)C(E)dE}{\int_g \sigma_t(E,0)C(E)dE} \tag{29}$$

The strict upper bound for $f_t(\sigma_0,T)$ can be readily determined by a straightforward application of Tschebycheff's Theorem[4] to the functions:

$$C(E),\ \sigma_t(E,T) \text{ and } [\sigma_t(E,T) + \sigma_0]^{-2} \tag{30}$$

Since $\sigma_t(E,T)$ and $[\sigma_T(E,T) + \sigma_0]^{-2}$ are always monotone in the opposite sense for a fixed value of σ_0, we obtain the following best upper bound for $f_t(\sigma_0,T)$:

$$f_t(\sigma_0,T) \leq \frac{\int_g \sigma_t(E,T)C(E)dE}{\int_g \sigma_t(E,0)C(E)dE} \tag{31}$$

So far, we have assumed in our derivations that $\sigma_0 \neq \infty$. However, it is a simple matter to show that for the case of infinite dilution

$$f_t(\infty,T) = \frac{\int_g \sigma_t(E,T)C(E)dE}{\int_g \sigma_t(E,0)C(E)dE} \tag{32}$$

by passing to the limit as $\sigma_0 \to \infty$ directly in Eq. (5). We can therefore conclude that for any value of σ_0 and T, $f_t(\sigma_0,T)$ obeys the double inequality

$$\frac{1}{K_1^2} \frac{\int_g \sigma_t(E,T)C(E)dE}{\int_g \sigma_t(E,0)C(E)dE} \leq f_t(\sigma_0,T) \leq \frac{\int_g \sigma_t(E,T)C(E)dE}{\int_g \sigma_t(E,0)C(E)dE} \tag{33}$$

for any energy group g contained within the resolved energy region.

Several rather obvious conclusions concerning the behavior of $f_t(\sigma_0,T)$ can be drawn from the double inequality (33). Thus, while for most practical cases

$$\frac{\int_g \sigma_t(E,T)C(E)dE}{\int_g \sigma_t(E,0)C(E)dE} \leq 1 , \tag{34}$$

there are physical situations when the above ratio can be substantially larger than unity. Such situations occur, for example, in the case of narrow groups contained within the interference minima, for groups at very low energies, or for groups whose boundaries cut through a resonance, etc. It is therefore quite clear that in such cases the inequality (34) is reversed, i.e., $f_t(\sigma_0,T) > 1$, and this effect is more pronounced the higher the temperature T in question. Notice also that since the upper bound for $f_t(\sigma_0,T)$ in (33) does not depend on σ_0, even $f_t(\infty,T)$ (i.e., at infinite dilution) would exceed unity for the above mentioned examples. We would therefore like to point out that the practice of setting the limiting value of $f_t(\sigma_0,T)$ to unity[1,2] is not justified, and could lead to serious errors.

II.B. Unresolved Energy Region

The expression of the special "total" group cross section employed in the unresolved region is:[3]

$$\langle \sigma_t^g(\sigma_0,T) \rangle_1 \equiv \frac{\int_g \frac{\bar{\sigma}_{t_1}(E,\sigma_0,T)}{\sigma_0 + \bar{\sigma}_{t_1}(E,\sigma_0,T)} \cdot \frac{C(E)dE}{\sigma_0 + \bar{\sigma}_{t_0}(E,\sigma_0,T)}}{\int_g \frac{1}{\sigma_0 + \bar{\sigma}_{t_1}(E,\sigma_0,T)} \cdot \frac{C(E)dE}{\sigma_0 + \bar{\sigma}_{t_0}(E,\sigma_0,T)}} \tag{35}$$

where the quantities $\bar{\sigma}_{t_1}(E^*,\sigma_0,T)$ and $\bar{\sigma}_{t_0}(E^*,\sigma_0,T)$ represent effective self-shielded point cross-sections generated at discrete points E^* in the unresolved energy region, according to the well-known prescriptions[1-3]

$$\bar{\sigma}_{t_1}(E^*,\sigma_0,T) \equiv \frac{\dfrac{1}{E_2 - E_1}\displaystyle\int_{E_1}^{E_2} \frac{dE}{[\sigma_t(E,E^*,T) + \sigma_0]}}{\dfrac{1}{E_2 - E_1}\displaystyle\int_{E_1}^{E_2} \frac{dE}{[\sigma_t(E,E^*,T) + \sigma_0]^2}} - \sigma_0 \tag{36}$$

and

$$\bar{\sigma}_{t_0}(E^*,\sigma_0,T) \equiv \frac{\dfrac{1}{E_2 - E_1}\displaystyle\int_{E_1}^{E_2} \frac{\sigma_t(E,E^*,T)}{\sigma_t(E,E^*,T) + \sigma_0}\, dE}{\dfrac{1}{E_2 - E_1}\displaystyle\int_{E_1}^{E_2} \frac{dE}{\sigma_t(E,E^*,T) + \sigma_0}} \tag{37}$$

We recall[1-3] that E^* is some energy point in the range (E_1,E_2) which is assumed to contain many narrow resonances, and the integrals of the form $1/(E_2 - E_1)\int_{E_1}^{E_2} g(E)dE$ appearing in (36) and (37) are treated within the narrow resonance approximation formalism and evaluated by performing the respective statistical averages over the reduced widths and spacings.

It can be readily seen from (36) and (37) that at infinite dilution we have:

$$\lim_{\sigma_0\to\infty} \bar{\sigma}_{t_1}(E^*,\sigma_0,T) = \lim_{\sigma_0\to\infty} \bar{\sigma}_{t_0}(E^*,\sigma_0,T) = \sigma_t^{\infty}(E^*) \tag{38}$$

where $\sigma_t^{\infty}(E^*)$ represents the infinitely dilute effective total cross-section at the discrete energy point E^*. Note the important fact, that $\sigma_t^{\infty}(E^*)$ is independent of the temperature T. This result enables us to determine the expression of the infinitely dilute total group cross-section from Eq. (35) as:

$$\langle \sigma_t^{g}(\infty,T) \rangle_1 = \frac{1}{K_g} \int_g \sigma_t^{\infty}(E) C(E) dE \tag{39}$$

Using Eqs. (1), (35) and (39) we can write the explicit expression for the total self-shielding factor $f_t(\sigma_0,T)$ in the unresolved region as:

$$f_t(\sigma_0,T) = \frac{K_g}{\int_g \sigma_t^{\infty}(E) C(E) dE} \cdot \frac{\int_g \frac{\bar{\sigma}_{t_1}(E,\sigma_0,T)}{\sigma_0 + \bar{\sigma}_{t_1}(E,\sigma_0,T)} \cdot \frac{C(E)dE}{\sigma_0 + \bar{\sigma}_{t_0}(E,\sigma_0,T)}}{\int_g \frac{1}{\sigma_0 + \bar{\sigma}_{t_1}(E,\sigma_0,T)} \cdot \frac{C(E)dE}{\sigma_0 + \bar{\sigma}_{t_0}(E,\sigma_0,T)}} \tag{40}$$

Based on Eq. (40), we can now determine the best lower and upper bounds for $f_t(\sigma_0,T)$ along exactly the same lines as for the resolved energy range. For this purpose, we need to define the quantities:

$$s_0 \equiv \inf_{E \epsilon g} \bar{\sigma}_{t_0}(E,\sigma_0,T) \tag{41}$$

$$S_0 \equiv \sup_{E \epsilon g} \bar{\sigma}_{t_0}(E,\sigma_0,T) \tag{42}$$

$$s_1 \equiv \inf_{E \epsilon g} \bar{\sigma}_{t_1}(E,\sigma_0,T) \tag{43}$$

$$S_1 \equiv \sup_{E \epsilon g} \bar{\sigma}_{t_1}(E,\sigma_0,T) \tag{44}$$

and consider the functions

$$a_3(E,\sigma_0,T) \equiv [\bar{\sigma}_{t_1}(E,\sigma_0,T)C(E)]^{1/2} \tag{45}$$

$$b_3(E,\sigma_0,T) \equiv \left[\frac{1}{\sigma_0 + \bar{\sigma}_{t_1}(E,\sigma_0,T)} \cdot \frac{C(E)}{\sigma_0 + \bar{\sigma}_{t_0}(E,\sigma_0,T)}\right]^{1/2} \tag{46}$$

$$a_4(E) \equiv \sqrt{C(E)} \tag{47}$$

$$b_4(E,\sigma_0,T) \equiv \left[\frac{\bar{\sigma}_{t_1}(E,\sigma_0,T)}{\sigma_0 + \bar{\sigma}_{t_1}(E,\sigma_0,T)} \cdot \frac{C(E)}{\sigma_0 + \bar{\sigma}_{t_0}(E,\sigma_0,T)}\right]^{1/2} \tag{48}$$

By repeating the sequence of manipulations (i.e., apply the Diaz-Goldman-Metcalf, and Hölder's inequalities) in a manner analogous to that for the resolved region calculations [cf. Eqs. (8–33)], with the pair of functions (a_3, b_3) playing the same role as previously played by (a_1, b_1), and the pair (a_4, b_4) playing the role of (a_2, b_2), we can finally show that

$$\frac{1}{K_2^2} \frac{\int_g \bar{\sigma}_{t_1}(E,\sigma_0,T)C(E)dE}{\int_g \sigma_t^{\infty}(E)C(E)dE} \leq f_t(\sigma_0,T) \leq \frac{\int_g \bar{\sigma}_{t_1}(E,\sigma_0,T)C(E)dE}{\int_g \sigma_t^{\infty}(E)C(E)dE} \tag{49}$$

The quantity K_2 in (49) is defined as

$$K_2 = \frac{1}{2}(B + \frac{1}{B}) \tag{50}$$

with

$$B \equiv \frac{\phi_2}{\phi_1}\left(\frac{S_1}{s_1}\right)^{1/4}\left[\frac{(\sigma_0 + S_0)(\sigma_0 + S_1)}{(\sigma_0 + s_0)(\sigma_0 + s_1)}\right]^{1/4} \tag{51}$$

The double inequality (49) is the counterpart of (33), for energy groups contained within the unresolved range. However, there are some rather obvious differences between (49) and (33), perhaps the most important being the fact that the upper bound $f_t(\sigma_0,T)$ in (49) depends on σ_0. For a particular group g in the unresolved range, and at a fixed temperature T, it can be readily shown that $f_t(\sigma_0,T)$ attains its largest value for the case of infinite dilution, when

$$f_t(\infty,T) = \frac{\int_g \sigma_t^{\infty}(E)C(E)dE}{\int_g \sigma_t^{\infty}(E)C(E)dE} = 1 \tag{52}$$

III. ANALYSIS OF THE PARTIAL REACTION SELF-SHIELDING FACTORS $f_x(\sigma_0,T)$

We recall[1-3] that the definition of the partial reaction self-shielding factor $f_x(\sigma_0,T)$, for reaction x, energy group g, at temperature T, and in a mixture of dilution σ_0 is:

$$f_x(\sigma_0,T) \equiv \frac{\sigma_x^{g}(\sigma_0,T)}{\sigma_x^{g}(\infty,0)} \tag{53}$$

where $\sigma_x^{g}(\sigma_0,T)$ represents the group-averaged cross-section for reaction of type x.

The task of obtaining best bounds for the reaction self-shielding factor is somewhat less straightforward than that for $f_t(\sigma_0,T)$. As will be seen shortly, the complication arises from the well-known fact that the sum of the partial reaction cross sections is equal to the total cross section. The analysis of the reaction self-shielding factors $f_x(\sigma_0,T)$ will be carried out separately for the two energy regions (resolved and unresolved) due to differences in the expressions of the group-averaged cross-sections used in these two regions.

III.A. Resolved Resonance Region

According to the Bondarenko model for the energy-dependent flux[1-3], the expression for the group cross section for reaction of type x in this energy region is

$$\sigma_x^g(\sigma_0,T) \equiv \frac{\int_g \frac{\sigma_x(E,T)}{\sigma_t(E,T)+\sigma_0}\,C(E)dE}{\int_g \frac{1}{\sigma_t(E,T)+\sigma_0}\,C(E)dE} \tag{54}$$

where $\sigma_x(E,T)$ is the Doppler-broadened smooth cross-section of type x and the other quantities have the same meaning as before. Thus, in view of (53) and (54), the explicit expression of $f_x(\sigma_0,T)$ for an energy group contained within the resolved range becomes:

$$f_x(\sigma_0,T) \equiv \frac{K_g}{\int_g \sigma_x(E,0)C(E)dE} \cdot \frac{\int_g \frac{\sigma_x(E,T)}{\sigma_t(E,T)+\sigma_0}\,C(E)dE}{\int_g \frac{1}{\sigma_t(E,T)+\sigma_0}\,C(E)dE} \tag{55}$$

The qualitative behavior of $f_x(\sigma_0,T)$ can be studied by applying Tschebycheff's Theorem[4] to the functions $C(E)$, $\sigma_x(E,T)$, $\frac{1}{\sigma_t(E,T)+\sigma_0}$, for $E \in g$, to obtain

$$\frac{\int_g \frac{\sigma_x(E,T)}{\sigma_t(E,T)+\sigma_0}\,C(E)dE}{\int_g \frac{1}{\sigma_t(E,T)+\sigma_0}\,C(E)dE} \geq \frac{1}{K_g}\int_g \sigma_x(E,T)C(E)dE \tag{56}$$

whenever $\sigma_x(E,T)$ and $\frac{1}{\sigma_t(E,T)+\sigma_0}$ are monotone in the same sense; the

inequality in (56) reverses if $\sigma_x(E,T)$ and $\frac{1}{\sigma_t(E,T) + \sigma_0}$ are monotone in the opposite sense. Making use of this result and Eq. (55), we conclude that

$$f_x(\sigma_0,T) \geq \frac{\int_g \sigma_x(E,T)C(E)dE}{\int_g \sigma_x(E,0)C(E)dE} \quad , \tag{57a}$$

if $\sigma_x(E,T)$ and $\frac{1}{\sigma_t(E,T) + \sigma_0}$ are monotone in the same sense

or

$$f_x(\sigma_0,T) \leq \frac{\int_g \sigma_x(E,T)C(E)dE}{\int_g \sigma_x(E,0)C(E)dE} \tag{57b}$$

if $\sigma_x(E,T)$ and $\frac{1}{\sigma_t(E,T) + \sigma_0}$ are monotone in the opposite sense.

The equality in (57) is attained at infinite dilution, when, as can also be seen directly from (55),

$$f_x(\infty,T) = \frac{\int_g \sigma_x(E,T)C(E)dE}{\int_g \sigma_x(E,0)C(E)dE} \tag{58}$$

Relations (57) and (58) clearly outline the fact that the value of a reaction self-shielding factor does not necessarily have to be less than unity. Indeed, we can easily envisage situaitons when $f_x(\sigma_0,T)$ can substantially exceed unity, especially if we happen to deal with some narrow group contained within the wings of a giant resonance.

We next wish to derive an interesting and useful relationship showing the interdependence among the self-shielding factors for the various reaction cross-sections x. For this purpose, we sum Eq. (55) over the reactions x, to obtain

$$\sum_x \left(f_x(\sigma_0,T) \int_g \sigma_x(E,0)C(E)dE \right) = K_g \cdot \frac{\int_g \frac{\sigma_t(E,T)}{\sigma_t(E,T)+\sigma_0} C(E)dE}{\int_g \frac{1}{\sigma_t(E,T)+\sigma_0} C(E)dE} \tag{59}$$

We can now proceed to derive strict lower and upper bounds for the expression on the left-hand side of Eq. (59) by following essentially the same procedure as described in section II.A. For the sake of brevity, we shall omit the details, and give here the final result only:

$$\begin{aligned} \frac{1}{K_3^2} \cdot \int_g \sigma_t(E,T)C(E)dE \;&\le \sum_x \left(f_x(\sigma_0,T) \cdot \int_g \sigma_x(E,0)C(E)dE \right) \\ &\le \int_g \sigma_t(E,T)C(E)dE \end{aligned} \tag{60}$$

where

$$K_3 \equiv \frac{1}{2}\left(D + \frac{1}{D}\right) \tag{61}$$

with

$$D \equiv \frac{\phi_2}{\phi_1}\left[\frac{\Sigma_1}{\sigma_1} \bullet \frac{\sigma_0 + \Sigma_1}{\sigma_0 + \sigma_1}\right]^{1/4} \tag{62}$$

III.B. Unresolved Resonance Region

The expression of the group cross section for reaction x, in the unresolved region is[3]:

$$\sigma_x^{\,g}(\sigma_0,T) \equiv \frac{\int_g \frac{\bar{\sigma}_x(\sigma_0,E,T)}{\bar{\sigma}_{t_0}(\sigma_0,E,T) + \sigma_0} C(E)dE}{\int_g \frac{1}{\bar{\sigma}_{t_0}(\sigma_0,E,T) + \sigma_0} C(E)dE} \tag{63}$$

where $\sigma_{t_0}(\sigma_0,E^*,T)$ is the same as in Eq. (37), and where the self-shielded effective point reaction cross section $\bar{\sigma}_x(\sigma_0,E^*,T)$ is generated at discrete energy points E* employing well-known procedures[1-3] whose starting point is the definition:

$$\bar{\sigma}_x(\sigma_0,E^*,T) \equiv \frac{\frac{1}{E_2 - E_1}\int_{E_1}^{E_2} \frac{\sigma_x(E,E^*,T)}{\sigma_t(E,E^*,T) + \sigma_0} dE}{\frac{1}{E_2 - E_1}\int_{E_1}^{E_2} \frac{1}{\sigma_t(E,E^*,T) + \sigma_0} dE} \tag{64}$$

We readily see that, at infinite dilution

$$\lim_{\sigma_0 \to \infty} \bar{\sigma}_x(\sigma_0,T,E^*) \equiv \sigma_x^{\infty}(E^*) \tag{65}$$

is independent of temperature[1-3]; therefore, the infinitely dilute group cross section for reaction x becomes

$$\sigma_x^g(\infty,0) = \frac{1}{K_g}\int_g \sigma_x^\infty(E)C(E)dE \tag{66}$$

The expression of the reaction self-shielding factor f_x defined by (53) can be now written explicitly for this energy region by means of (64) and (66) as

$$f_x(\sigma_0,T) = \frac{K_g}{\int_g \sigma_x^\infty(E)C(E)dE} \cdot \frac{\int_g \frac{\bar{\sigma}_x(E,\sigma_0,T)}{\bar{\sigma}_{t_0}(E,\sigma_0,T)+\sigma_0}C(E)dE}{\int_g \frac{1}{\bar{\sigma}_{t_0}(E,\sigma_0,T)+\sigma_0}C(E)dE} \tag{67}$$

The behavior of $f_x(\sigma_0,T)$ in the unresolved region can once again be studied by means of the same procedures used for the resolved region. Thus, we can employ Tschebycheff's Theorem[4] to Eq. (67) to obtain

$$f_x(\sigma_0,T) \leq \frac{\int_g \bar{\sigma}_x(\sigma_0,E,T)C(E)dE}{\int_g \sigma_x^\infty(E)C(E)dE} \tag{68}$$

whenever $\bar{\sigma}_x$ and $\frac{1}{\bar{\sigma}_{t_0}+\sigma_0}$ are monotone in the opposite sense. As before, the inequality in (68) is reversed for the rare situations when $\bar{\sigma}_x$ and $[\bar{\sigma}_{t_0}+\sigma_0]^{-1}$ are monotone in the same sense over the energy group g.

The behavior of the reaction self-shielding factor in the unresolved region at infinite dilution can be obtained by passing directly to the limit as $\sigma_0 \to \infty$ in Eq. (67); the result is simply

$$f_x(\infty,T) = 1 \tag{69}$$

Finally, we shall give the analogue of the double inequality (60), for energy groups within the unresolved region, i.e.

$$\frac{1}{K_4^2}\int_g \bar{\sigma}_{t_0}(\sigma_0,E,T)C(E)dE \leq \sum_x\left(f_x(\sigma_0,T)\int_g \sigma_x^{\infty}(E)C(E)dE\right)$$

$$\leq \int_g \bar{\sigma}_{t_0}(\sigma_0,E,T)C(E)dE \tag{70}$$

where

$$K_4 = \frac{1}{2}(F + \frac{1}{F}) \tag{71}$$

with

$$F \equiv \frac{\phi_2}{\phi_1}\left(\frac{S_0}{s_0}\cdot\frac{\sigma_0 + S_0}{\sigma_0 + s_0}\right)^{1/4} \tag{72}$$

We wish to remark that the double inequality (70) was derived by making use of the obvious relationship

$$\sum_x \bar{\sigma}_x(\sigma_0,E,T) = \bar{\sigma}_{t_0}(\sigma_0,E,T) \tag{73}$$

and by subsequently employing the Diaz-Goldman-Metcalf and Holder inequalities. Moreover, all of the quantities in (70)–(73) retain their meaning as defined in the previous sections of this study.

IV. PRACTICAL APPLICATIONS

In the preceeding chapters we have derived upper and lower bounds on the "current-weighted total" self-shielding factors (Chapter II) and on the

sum of the "flux-weighted" reaction cross sections (Chapter III). Separate inequalities have been presented for the resolved and unresolved resonance ranges because of the difference in the methods used in the two ranges for calculating group-averaged cross sections. In this chapter we will summarize the important conclusions and give several examples to illustrate the practical application of this work.

In the resolved resonance range, we have shown that the total f-factor can exceed unity for some physical situations. These situations include groups in the wings of a broad resonance, within the interference minima and at very low energies. As will be seen in the examples of the next section, this effect is more pronounced at higher temperatures.

In the unresolved range, however, we have shown that unity is indeed an upper bound on the total f-factor, although not necessarily the least upper bound. The physical reason for this is that any group in this range must span many resonances, and Doppler broadening does not significantly change the area under a resonance. Another important difference in these two regions is that the upper bound on the resolved range is <u>not</u> dependent on σ_0, whereas it is in the unresolved range. As with the total f-factor, we saw that the upper bound for the sum of the reaction cross sections was <u>not</u> dependent on σ_0 in the resolved range, but was dependent on σ_0 in the unresolved range.

We shall next present a few numerical examples of total f-factors calculated with the ORNL version of the MINX[3] code. The official preliminary ENDF/B-V data files were the source of data for ^{240}Pu and Na, while ENDF/B-IV was used for ^{239}Pu.

For ^{240}Pu, the following table gives f_t for various temperatures, at $\sigma_0 = 10^5$ b, in a group whose energy range is 1.13 eV to 2.38 eV.

Temperature (°K)	$f_t(\sigma_0 = 10^5, T)$	(Eq. 31) Upper bound
300	.990	1.058
900	1.119	1.233
2100	1.424	1.670

As we can see in Reference 5, this group lies in the upper wing of a broad resonance at 1.06 eV. As the temperature is raised, Doppler broadening lowers the peak of the resonance, but raises the wings, thus increasing the cross section over most of the group.

If one processes cross sections at temperatures found in CTR work, this effect is even more evident. The following table gives f_t at temperatures of 300, 900, 2100 and 10^6 °K, σ_0 = 100 b for ^{239}Pu. Note the increase in going to very high temperatures.

Energy Range (eV)	f_t	T = 300 °K Upper Bound (Eq. 31)	f_t	T = 900 °k Upper Bound (Eq. 31)	f_t	T = 2100 °K Upper Bound (Eq. 31)	f_t	T = 10^6 °K Upper Bound (Eq. 31)
5.04-6.48	1.005	1.005	1.007	1.007	1.009	1.009	4.571	4.656
3.93-5.04	1.002	1.003	1.004	1.004	1.006	1.006	2.792	2.825
3.06-3.93	1.007	1.007	1.009	1.010	1.013	1.013	1.821	1.825

The final example shows the effect of Doppler broadening on a group at very low energies. The material is Na, the energy group extends from 10^{-5} eV to 0.414 eV and $\sigma_0 = 10^3$ b. The temperature dependence of f_t is illustrated in the following table.

Temperature (°K)	$f_t(\sigma_0 = 10^3, T)$	Upper bound (Eq. 31)
300	1.017	1.018
900	1.046	1.046
2100	1.099	1.100

All of these f-factors are larger than unity, but are still below the computed upper bound.

The inequalities satisfied by the total f-factors [equations (33) and (49)] and by the sum of the reaction cross sections [equations (60) and (70)] are being programmed into a set of routines to be used in conjunction with the MINX and NJOY codes at ORNL, providing, thus, the capability of automatically checking the "reasonability" of these f-factors. The unphysical f-factors, if any, will henceforth be flagged based on the above mentioned analytical constraints rather than on intuitive reasoning.

REFERENCES

1. R. E. Schenter, J. L. Baker, and R. B. Kidman, "ETOX, A Code to Calculate Group Constants for Nuclear Reactor Calculations," BNWL-1002, Battelle Northwest Laboratory (1969).

2. B. A. Hutchins and L. N. Price,"ENDRUN-1, A Computer Code to Generate a Generalized Multigroup Data File from ENDF/B," GEAP-13592, General Electric Co. (1970).

3. C. R. Weisbin, et al., "MINX, A Multigroup Interpretation of Nuclear X-Sections from ENDF/B," LA-6486-MS (1976).

4. D. S. Mitrinonic, "Analytic Inequalities," Springer-Verlag, New York (1970).

5. S. D. Garber, C. Dunford, and S. Pearlstein, ENDF-200, October 1975.

APPENDIX A

Calculation of ϕ_1/ϕ_2

The ratio ϕ_1/ϕ_2, used in evaluating the lower bound on the f-factors, can be calculated explicitly for each of the four analytical weight functions allowed in MINX. The following definitions apply to the calculation of this ratio for energy group g.

$C(E)$ = Weighting function
ϕ_1 = $\min\sqrt{C(E)}$ over group g
ϕ_2 = $\max\sqrt{C(E)}$ over group g
E_g = Lower energy boundary of group g
E_{g+1} = Upper energy boundary of group g

I. C(E) = constant

$$\text{Obviously, } \frac{\phi_1}{\phi_2} = 1 \tag{A-1}$$

II. C(E) = 1/E

$$\frac{\phi_1}{\phi_2} = \left(\frac{E_g}{E_{g+1}}\right)^{1/2} \tag{A-2}$$

III. C(E) = Maxwellian + 1/E + fission spectrum

Region 1: $C_1(E) = S_1 E e^{-E/kT}$ for $E<E_1$ $S_1 = E_1^{-2} e^{E_1/kT}$
Region 2: $C_2(E) = 1/E$ for $E_1<E<E_2$
Region 3: $C_3(E) = S_2 E^{1/2} e^{-E/\theta}$ for $E>E_2$ $S_2 = E_2^{-3/2} e^{E_2/\theta}$

Region 1: The Maxwellian peaks at $E_{max} = kT$, so that there are three cases to consider.

$$\text{For } E_{g+1} \leq kT, \frac{\phi_1}{\phi_2} = \left(\frac{E_g}{E_{g+1}}\right)^{1/2} e^{\frac{E_{g+1} - E_g}{2kT}} \tag{A-3}$$

$$\text{For } E_g \geq kT, \quad \frac{\phi_1}{\phi_2} = \left(\frac{E_{g+1}}{E_g}\right)^{1/2} e^{\frac{E_g - E_{g+1}}{2kT}} \tag{A-4}$$

$$\text{For } E_g \leq kT, \; E_{g+1} \geq kT, \quad \frac{\phi_1}{\phi_2} = \left(\frac{e}{kT}\right)^{1/2} \min\left\{E_g^{1/2} e^{-E_g/2kT}, \; E_{g+1}^{1/2} e^{-E_{g+1}/2kT}\right\} \tag{A-5}$$

Now, suppose the energy group in question spans the boundary at E_1, with $E_g \geq kT$ and $E_{g+1} \leq E_2$. Other possible ways of spanning this boundary exist, of course, and must be accounted for, but this is the most likely situation. In this case,

$$\frac{\phi_1}{\phi_2} = (s_1 E_g E_{g+1})^{-1/2} e^{E_g/2kT} \tag{A-6}$$

$$\text{Region 2:} \quad \frac{\phi_1}{\phi_2} = \left(\frac{E_g}{E_{g+1}}\right)^{1/2} \tag{A-7}$$

Region 3: This function peaks at $E_{max} = \frac{\theta}{2}$.

$$\text{For } E_{g+1} \leq \frac{\theta}{2}, \quad \frac{\phi_1}{\phi_2} = \left(\frac{E_g}{E_{g+1}}\right)^{1/4} e^{\frac{E_{g+1} - E_g}{2\theta}} \tag{A-8}$$

$$\text{For } E_g \geq \frac{\theta}{2}, \quad \frac{\phi_1}{\phi_2} = \left(\frac{E_{g+1}}{E_g}\right)^{1/4} e^{\frac{E_g - E_{g+1}}{2\theta}} \tag{A-9}$$

$$\text{For } E_g \leq \frac{\theta}{2}, \; E_{g+1} \geq \frac{\theta}{2}, \quad \frac{\phi_1}{\phi_2} = \left(\frac{2e}{\theta}\right)^{1/4} \min\left\{E_g^{1/4} e^{-E_g/2\theta}, \; E_{g+1}^{1/4} e^{-E_{g+1}/2\theta}\right\} \tag{A-10}$$

For $E_g \leq E_2$, $E_{g+1} \geq E_2$, $E_{g+1} \leq \frac{\theta}{2}$,

$$\frac{\phi_1}{\phi_2} = \frac{E_2^{-1/2}}{\max\left\{E_g^{-1/2}, S_2^{1/2} E_{g+1}^{1/4} e^{-E_{g+1}/2\theta}\right\}} \qquad \text{(A-11)}$$

IV. C(E) = CTR-CRBR combined weight function

Region 1:	$C_1(E) = S_1 E e^{-E/kT}$	for $E<E_1$
Region 2:	$C_2(E) = 1/E$	for $E_1<E<E_2$
Region 3:	$C_3(E) = S_3 E^{1/2} e^{-E/\theta}$	for $E_2<E<E_3$
Region 4:	$C_4(E) = S_4/E$	for $E_3<E<E_4$
Region 5:	$C_5(E) = S_5 \exp\left[-\frac{5}{\theta_f}\left(E^{1/2} - E_p^{1/2}\right)^2\right]$	for $E_4<E<E_5$
Region 6:	$C_6(E) = S_6/E$	for $E>E_5$

The normalization constants are

$$S_1 = E_1^{-2} e^{E_1/kT} \qquad S_3 = E_2^{-3/2} e^{E_2/\theta}$$

$$S_4 = S_3 E_3^{3/2} e^{-E_3/\theta} \qquad S_5 = \frac{S_4}{E_4} \exp\left[\frac{5}{\theta_f}\left(E_4^{1/2} - E_p^{1/2}\right)^2\right]$$

$$S_6 = S_5 E_5 \exp\left[-\frac{5}{\theta_f}\left(E_5^{1/2} - E_p^{1/2}\right)^2\right]$$

Regions 1, 2 and 3: These three regions are identical to the weight function described in section III above, and equations A-3 through A-11 can be used. The boundary at E_3 is evaluated next.

$$\text{For } E_g \leq E_3,\ E_{g+1} \geq E_3,\ \frac{\phi_1}{\phi_2} = \left(\frac{S_4}{S_3 E_g E_{g+1}^{1/2}}\right)^{1/2} e^{E_g/2\theta} \qquad \text{(A-12)}$$

$$\text{Region 4:}\quad \frac{\phi_1}{\phi_2} = \left(\frac{E_g}{E_{g+1}}\right)^{1/2} \qquad \text{(A-13)}$$

Region 5: This function peaks at $E_{max} = E_p$.

$$\text{For } E_{g+1} \leq E_p,\ \frac{\phi_1}{\phi_2} = \exp\left\{\frac{5}{2\theta_f}\left[\left(E_{g+1}^{1/2} - E_p^{1/2}\right)^2 - \left(E_g^{1/2} - E_p^{1/2}\right)^2\right]\right\} \tag{A-14}$$

$$\text{For } E_g \geq E_p,\ \frac{\phi_1}{\phi_2} = \exp\left\{\frac{5}{2\theta_f}\left[\left(E_g^{1/2} - E_p^{1/2}\right)^2 - \left(E_{g+1}^{1/2} - E_p^{1/2}\right)^2\right]\right\} \tag{A-15}$$

$$\text{For } E_g \leq E_p,\ E_{g+1} \geq E_p,\ \frac{\phi_1}{\phi_2} = \min\left\{\exp\left[-\frac{5}{2\theta_f}\left(E_g^{1/2} - E_p^{1/2}\right)^2\right], \exp\left[-\frac{5}{2\theta_f}\left(E_{g+1}^{1/2} - E_p^{1/2}\right)^2\right]\right\} \tag{A-16}$$

$$\text{For } E_g \leq E_4,\ E_{g+1} \geq E_4,\ E_{g+1} \leq E_p$$

$$\frac{\phi_1}{\phi_2} = \frac{\left(S_4/E_4\right)^{1/2}}{\max\left\{\left(\frac{S_4}{E_g}\right)^{1/2},\ S_5^{1/2}\exp\left[-\frac{5}{2\theta_f}\left(E_{g+1}^{1/2} - E_p^{1/2}\right)^2\right]\right\}} \tag{A-17}$$

$$\text{For } E_g \leq E_5,\ E_{g+1} \geq E_5,\ \frac{\phi_1}{\phi_2} = \left(\frac{S_6}{S_5 E_{g+1}}\right)^{1/2}\exp\left[\frac{5}{2\theta_f}\left(E_g^{1/2} - E_p^{1/2}\right)^2\right] \tag{A-18}$$

Region 6: $$\frac{\phi_1}{\phi_2} = \left(\frac{E_g}{E_{g+1}}\right)^{1/2} \tag{A-19}$$